LCH Laboratoire de Constructions Hydrauliques
Laboratory of Hydraulic Constructions

ÉCOLE POLYTECHNIQUE
FÉDÉRALE DE LAUSANNE

Communication 46

Influence of tributary widening on confluence morphodynamics

Marcelo Leite Ribeiro

Editeur : Prof. Dr A. Schleiss

Lausanne, 2011

Communications du Laboratoire de Constructions Hydrauliques ISSN 1661-1179
Ecole Polytechnique Fédérale de Lausanne
Editeur: Prof. Dr A. Schleiss

Preface

Confluences are the nodes of the fluvial network. They are typically characterized by highly heterogeneous conditions that are favorable for a sound fluvial ecosystem, and play a key role in the connectivity of the river system. During the past centuries, many rivers and their tributaries have been channelized and regulated, often resulting in quasi-homogeneous flow and morphologic conditions, deficient flood safety, reduced natural dynamics, impoverished ecological value, and reduced connectivity.

Marcelo Leite Ribeiro's PhD research investigated the potential of river rehabilitation by means of a local widening in the tributary of channelized confluences in an alpine environment. Such confluences are characterized by a dominant discharge in the low-gradient main channel, a dominant supply of poorly graded sediment in the steep tributary, and a pronounced bed discordance at the tributary mouth. Due to considerably different confluence characteristics, none of the existing conceptual models can represent the hydro-morpho-sedimentary processes in this type of confluences.

Dr. Leite Ribeiro's research was performed in a laboratory set-up that is representative of the 20 major confluences on the Rhône River upstream of Lake Geneva, Switzerland. Measurements of the three-dimensional velocity field, turbulence, sediment transport, morphology and bed material characteristics in a wide range of configurations of the local tributary widening and under various hydraulic conditions provided the following results:

- A conceptual model has been proposed for the hydro-morpho-sedimentary processes in the investigated type of channelized alpine confluences. This conceptual model explains the adaptation to changing hydraulic conditions and to the local widening of the tributary.

- Without having adverse effects on flood safety, the local widening of the tributary was found to considerably enhance the hydraulic and morphologic heterogeneity, which enhances the ecological value.

- The validity of this result for all investigated widening configurations indicates that relatively small interventions conditioned by local constraints can considerably contribute to the rehabilitation of confluences in strongly anthropologized environements.

We would like to thank Prof. André Roy (University of Montreal, Canada) for his support and guidance during the project as academic guest and for his valuable comments as member of

the PhD committee. We also thank the other members of the committee, Prof. Stuart Lane (Durham University, UK) and Prof. Christophe Ancey (LHE-EPFL) as well as Prof. Antonio Cardoso (IST Lisbon, Portugal) as visiting professor for their helpful suggestions. Finally we also gratefully thank the Swiss Federal Office for the Environment (FOEN) for financial support in the framework of the project “Integrated River Basin Management”.

Prof. Dr. Anton Schleiss Dr. Koen Blanckaert

Esse trabalho é dedicado ao meu pai Manoel,
à minha mãe Neuza, às minhas irmãs Helena e
Regina, à minha querida Montsita e ...

Abstract

In alpine regions of Europe, river training works were typically the reason for the transformation of wide and braided rivers into linear river systems with a lack of structural diversity, i.e. gravel banks, islands, woody debris, riffles or pools. These interventions considerably impoverished river ecosystems. From the end of the 20th century, "river rehabilitation" has been a concept commonly used by environmental professionals and river management authorities. The rehabilitation purpose is to recover the vital space required for the rivers that were degraded by human interventions and to link the sustainable use of rivers and wetlands with human well-being. Furthermore the flood safety has to be adapted to the higher hydrological risk resulting from increased urbanization. A good understanding of the flow dynamics, sediment transport patterns and of the development of the bed morphology is essential to successfully accomplish river rehabilitation projects.

Alpine confluences are typically characterized by steep gravel-bed streams carrying large sediment loads, which often connect asymmetrically at large angles with the main river. Such zones present important challenges, not only for flood protection but also for rehabilitation works. Current knowledge of river channel confluences, mainly based on lowland confluences is not applicable to alpine conditions.

The morphodynamics of confluences have been experimentally investigated with special attention to the potential of local tributary widening in the framework of confluence rehabilitation projects. Local widening of the tributary in the confluence zone aims to increase the heterogeneity in sediment substrate, flow depth and flow velocity, which is favourable for in-stream habitat (e.g. aquatic invertebrates, fish, and vegetation) and for the connectivity between the main river and the tributary. Zones of quiescent water (flow stagnation or flow recirculation zones) may play an important role as refuges during flood events. Moreover, a local tributary widening can create a riparian zone which favours the diversity of plants and animals (e.g. birds, mammals, insects, amphibians). Obviously, river rehabilitation by means of local tributary widening is only feasible if it has negligible adverse effects on the flood safety of the confluence zones.

The experimental set-up and the test configurations are based on the analysis of the Upper Rhone River, in Switzerland, which can be considered as representative of regulated

alpine river confluences. Systematic laboratory experiments were performed in a confluence flume where the main channel is 8.5 m long and 0.50 m wide. A 4.9 m long and 0.15 m wide tributary channel is connected at an angle of 90°. Three discharge scenarios were tested for four different geometrical configurations: a reference case (without widening) and three different tributary widenings: the "Small" configuration, (B_w = 0.30 m and L_w = 0.45 m, the "Medium" configuration (B_w = 0.45 m and L_w = 0.45 m) and the "Large" configuration (B_w= 0.45 m and L_w = 0.60 m). Each experiment was conducted under steady flow conditions in the main and tributary channels and with a steady supply of poorly sorted sediments (d_{50}=0.82 mm and d_{90} = 5.7 mm) at the tributary. There is no sediment transport in the main channel upstream of the confluence. All experiments were conducted until the equilibrium conditions were reached. The duration of the tests varied between 22 and 24 hours.

Measurements of the three-dimensional velocity field, turbulence, bed material grain size distribution and morphology as well as observations of the sediment transport in the confluence flume for the reference case revealed that the hydro-morpho-sedimentary processes occurring in alpine confluences differ fundamentally from existing conceptual models of confluence morphodynamics. Therefore, a conceptual model for the main hydraulic and morphological processes occurring in confluences with characteristics similar to those found in alpine environments is proposed. Bed morphology in alpine confluences is characterized by the presence of a significant deposition bar downstream of the confluence. Differences between the water depths in the tributary and in the main channel induce the formation of large bed discordance between the confluent channels. Moreover, no considerable scour hole is observed. Regarding the flow, the tributary momentum input, associated with the presence of the deposition bar resulted in a considerable mass redistribution in the confluence zone as the main flow is deviated towards the outer bank. The main channel flow moves beneath the tributary in the lower part of the water column, giving rise to a two-layer flow structure at the tributary mouth. The two-layer flow plays an important role in dampening the formation of a flow recirculation zone downstream of the confluence. The deposition bar downstream from the confluence reduces the flow area and causes flow acceleration. The sediment supplied by the tributary is mainly sorted and transported on the face of the deposition bar. The sediment transport capacity is further increased by the three-dimensionality of the flow. It is characterized by maximum velocities occurring near the bed and by a considerable increase in turbulent kinetic energy generated in

the shear layer at the interface of the flows originating from the main channel and the tributary.

Laboratory experiments revealed that the local widening of tributaries creates a pronounced heterogeneity in the sediment substrate, flow velocities and flow depths, without having any adverse effects on flood safety in the confluence zone. Although the local tributary widening allows a reduction in the confluence angle, it locally amplifies the hydro-morpho-sedimentary processes in the confluence zone. This is due to the reduction of the effective flow area in the local tributary widening, resulting in locally increased tributary velocities and momentum flux. This reduction of the effective flow area occurs due to a general rise of the bed elevation and by a lateral constriction of the flow induced by a zone of flow stagnation at the upstream confluence corner. Flow coming from the tributary remains in the upper part of the water column in the main river and it is considerably more directed outwards than flow in the lower part of the water column coming from the main channel. The increased tributary velocities lead to increased bed discordance and a higher tributary penetration in the confluence zone.

Despite the different morphodynamic responses at the widened zones depending on the geometry and the discharge ratio, the local tributary widening always enhance the variability of flow depths, bed constitution and flow velocities without causing adverse effects on the morphodynamics of the tributary and main channels in equilibrium conditions. Furthermore, the lateral freedom obtained by the local widening associated to the different combinations of the main and tributary discharge events further allows the formation of different bed forms, which contributes to the improvement the lateral connectivity of regulated networks.

Therefore, local tributary widening can be considered as an efficient solution for increasing the ecological potential of fluvial systems without reducing the conveyance capacity of a given network.

Keywords: Alpine river confluences, experimental investigation, morphodynamics, sediment transport, river rehabilitation.

Résumé

Dans les régions alpines d'Europe, les aménagements des cours d'eau ont généralement transformé les larges rivières en tresse en systèmes linéaires caractérisés par un manque de diversité structurale, à savoir de bancs de graviers, d'îles, de rapides et de zones calmes. Ces interventions ont considérablement appauvri les valeurs écologiques. A partir de la fin du 20ème siècle, "la réhabilitation des cours d'eau" est devenue un concept couramment utilisé par les professionnels dans le domaine de l'environnement et par les autorités responsables de la gestion des cours d'eau. Le but de la réhabilitation est de reconstituer l'espace vital nécessaire au cours d'eau qui a été fortement dégradé par les interventions humaines. Ce concept associe une utilisation durable des cours d'eaux avec le bien-être des communautés riveraines. En plus, les protections contre les crues doivent être adaptées aux risques hydrologiques liés à l'urbanisation croissante. La compréhension de la dynamique de l'écoulement, du transport des sédiments et de l'évolution morphologique est essentielle pour accomplir avec succès les projets de réhabilitation des cours d'eaux.

Les confluences alpines sont généralement caractérisées par des petits cours d'eaux à forte pente dont le lit est formé par des graviers qui se connectent asymétriquement à la rivière principale avec des grands angles. Pendant les crues, les petits affluents transportent des quantités importantes de sédiments. Ces zones présentent des défis importants, non seulement pour la protection contre les crues, mais aussi pour les travaux de réhabilitation. Les connaissances actuelles sur les confluences sont principalement basées sur les régions de plaine et ne sont pas applicables aux confluences alpines.

La morphodynamique des confluences est étudiée expérimentalement avec une attention particulière sur le potentiel de l'élargissement local de l'affluent dans le cadre de projets de réhabilitation des confluences. L'élargissement vise à augmenter la variabilité des sédiments dans le substrat, de la profondeur d'écoulement et de la vitesse d'écoulement, ce qui est favorable pour le développement des habitats (par exemple, des invertébrés aquatiques, des poissons et de la végétation) et pour la connectivité latérale des réseaux fluviaux. Les zones d'eau calmes (stagnation et/ou recirculation) présentes dans les zones élargies peuvent jouer un rôle important en tant que refuges en cas de crues. En outre, un élargissement local de l'affluent peut créer une zone riveraine qui favorise la diversité des plantes et des animaux (oiseaux, mammifères, insectes, amphibiens). De toute évidence, la réhabilitation des cours

d'eau par le biais d'un élargissement de l'affluent n'est possible que si elle a des effets négatifs négligeables sur la protection contre les crues dans les zones des confluences.

L'installation expérimentale et les configurations testées sont basées sur le Rhône en Suisse et sont représentatives des confluences aménagés trouvées en zone alpine. Les essais systématiques ont été effectués dans une confluence où le canal principal a une longueur de 8.5 m et une largeur de 0.50 m. L'affluent, d'une longueur de 4.9 m et d'une largeur de 0.15 m, se connecte au canal principal avec un angle de 90°. Trois scénarios de débit ont été testés dans quatre configurations différentes de la confluence : une configuration de référence (sans élargissement) et trois élargissements. Chaque essai a été réalisé avec des conditions stationnaires de débit dans l'affluent et dans le canal principal et un débit solide constant constitué par des sédiments avec une granulométrie étendue (d_{50} = 0.82 mm et d_{90} = 5.7 mm) dans l'affluent. Il n'y a pas de transport de sédiments dans le canal principal en amont de la confluence. Tous les essais ont été menés jusqu'à ce que les conditions d'équilibre soient atteintes, ce qui durait entre 22 et 24 heures.

Les mesures du champ de vitesse en trois dimensions, de la turbulence, de la granulométrie des matériaux déposés et de la morphologie ainsi que les observations du transport de sédiments pour la configuration de référence ont révélé que les processus hydro-morpho-sédimentaires agissant sur les confluences alpines sont fondamentalement différents de ceux décrits par des modèles existants sur la morphodynamique des confluences.

Par conséquent, un modèle conceptuel expliquant les principaux processus hydrauliques et morphologiques dans les zones de confluences avec caractéristiques similaires à celles trouvées dans les environnements alpins est proposé. Le modèle est validé par les trois essais expérimentaux menés dans la configuration de référence avec différents rapports de débit ainsi que par des observations sur les confluences du Rhône. La morphologie des confluences alpines est caractérisée par la présence d'un banc important en aval de la confluence. Les différences entre les profondeurs de l'écoulement dans l'affluent et dans le canal principal conduisent à la formation d'une discordance entre les lits. De plus, aucune zone d'érosion significative n'est créée. En ce qui concerne l'hydrodynamique, la quantité de mouvement introduite par l'affluent, associée à la présence du banc, provoque une redistribution des masses considérable dans la zone de confluence, induisant une déviation de l'écoulement principal vers la rive externe. L'écoulement principal près du fond est peu obstrué par l'affluent, donnant naissance à une structure de l'écoulement à deux couches dans l'embouchure de l'affluent. L'écoulement à deux couches joue un rôle important en

empêchant la formation d'une zone de recirculation en aval de la confluence. Le banc en aval de la confluence réduit la surface d'écoulement et provoque son accélération. Les sédiments transportés par l'affluent sont triés et transportés sur le parement du banc. La capacité de transport des sédiments est accrue par la tridimensionnalité de l'écoulement, qui se caractérise par des vitesses maximales près du fond et par une augmentation considérable de l'énergie cinétique turbulente générée dans la zone de cisaillement à l'interface des écoulements confluents.

Les essais en laboratoire indiquent que l'élargissement local des affluents conduit à une variabilité importante des substrats du lit, des vitesses d'écoulement et aussi des profondeurs d'écoulement. Cette augmentation de variabilité n'est par contre pas associée à des effets adverses concernant la sécurité contre les crues dans la zone de la confluence. Bien que l'élargissement local de l'affluent permette une réduction de l'angle de confluence, il amplifie localement les processus hydro-morpho-sédimentaire dans la zone de confluence. Cela est dû à la réduction de la surface de l'écoulement dans la zone élargie, ce qui entraine une augmentation de vitesse de l'écoulement. La réduction de la surface de l'écoulement est due à l'élévation générale du niveau du fond et par une constriction latérale de l'écoulement induite par une zone de stagnation d'écoulement dans le coin à l'amont de la confluence. L'augmentation de vitesse dans la zone élargie conduit à l'augmentation de la discordance du fond et à une plus grande pénétration de l'affluent dans la zone de confluence.

Même si la morphodynamique des zones élargies répond différemment aux scénarios de débit et à la forme de l'élargissement, un élargissement local de l'affluent améliore toujours l'hétérogénéité morphodynamique de la zone de confluence, sans toutefois provoquer d'effets négatifs sur la protection contre les crues dans des conditions d'équilibre. En plus, le degré de liberté spatial donné par l'élargissement, associé aux différentes combinaisons de débits dans le cours d'eau principal et dans le tributaire peut conduire à la formation des différentes formes du lit, ce qui est favorable à l'amélioration de la connectivité latérale. Ainsi, un élargissement local de l'affluent peut être considéré comme une solution efficace pour augmenter le potentiel écologique des systèmes fluviaux sans réduire leur capacité de transport.

Mots-clé: Confluences alpines, investigation expérimentale, morphodynamique, transport de sédiments, réhabilitation.

Resumo

Na região dos Alpes Europeus, as obras de regularização de rios foram responsáveis pela transformação de leitos largos e trançados em leitos lineares com ausência de diversidade estrutural, como por exemplo bancos de cascalho, ilhas, corredeiras e piscinas. Essas alterações empobreceram consideravelmente os ecosistemas fluviais. A partir do final do século 20, o conceito de "revitalização fluvial" passou a ser amplamente utilisado por profissionais e autoridades de gestão fluvio-ambiental. O objetivo é a recuperação dos espaços vitais degradados pela atividade humana e a associação da utilização sustentável dos rios com o bem-estar humano. Além disso, a proteção contra as cheias também tem de ser adaptada devido ao aumento do risco hidrológico resultante da crescente urbanização. Um bom entendimento da dinâmica do escoamento, do transporte de sedimentos e do desenvolvimento morfológico do leito é essencial para o sucesso dos projetos de revitalização fluvial.

As confluências alpinas são geralmente caracterizadas pelo encontro de pequenos rios com declive acentuado e que transportam grandes quantidades de materiais não uniformes durante suas cheias, com um rio principal com grandes ângulos em planta. Esse tipo de confluência representa desafios importantes, não somente no que diz respeito à proteção contra as cheias mas também pelo seu grande potencial de revitalização. O conhecimento atual relativo às confluências é, em grande parte, resultado de medidas de campo em confluências de planície e por isso não pode ser diretamente aplicado a esse tipo de configuração.

No presente trabalho, a morfodinâmica de confluências alpinas regularizadas é estudada experimentalmente com uma atenção especial ao alargamento do afluente na zona da confluência no âmbito de projetos de revitalização. O alargamento local do afluente tem como objetivo o aumento da heterogenidade do seu substrato e também das velocidades e alturas do escoamento. Essas características são essênciais para a criação de habitats. Além disso, o alargamento pode ajudar na criação de uma zona ripária que favorece a diversidade de plantas e animais. Essas mudanças são extremamente favoráveis pra o o aumento da conectividade lateral dos sistemas fluviais atualmente regularizados. Obviamente, projetos de revitalização fluvial somente são viáveis com a ausência de efeitos negativos em termos de proteção contra as cheias.

A instalação experimental e o programa de ensaios foram projetados com base na parte suíça do rio Ródano. Esse rio sofreu duas importantes obras de regularização do seu leito e atualmente sua bacia hidrográfica encontra-se em uma situação ecológica crítica. Foram realizados ensaios sistemáticos em uma confluência onde o canal principal tem 8.50 m de comprimento e 0.50 m de largura. Um afluente de 4.90 m de comprimento e 0.15 m de largura é conectado com um ângulo de 90° em planta. Três cenários de vazão foram testados em 4 configurações diferentes da confluência: a configuração de referência (sem alargamento) e três alargamentos simétricos com diferentes tamanhos. Cada ensaio foi realizado com condições permanentes de vazão no canal principal e no afluente, e uma vazão sólida permanente introduzida no afluente. Em nenhum dos casos houve introdução de sedimentos no canal principal à montante da confluência. Todos os ensaios foram conduzidos até a condição de equilíbrio e a duração de cada um foi entre 22 e 24 horas.

Medidas do campo de velocidade em três dimensões, da turbulência, da morfologia e da constituição do fundo, além de observações do transporte de sedimentos para o caso de referência mostraram que os processos hidro-morfo-sedimentológicos relativos ao tipo de confluência estudada são fundamentalmente diferentes dos apresentados nos modelos morfológicos existentes, mais adaptados a confluência em planície. Os resultados permitiram o desenvolvimento de um modelo conceitual que considera os principais processos morfodinâmicos relativos à confluências semelhantes às encontradas nas regiões alpinas. Nos casos estudados, a morfologia é caracterizada pela presença de um importante depósito a jusante da confluência. A diferença entre as profundidades dos escoamentos é responsável pela formação de uma grande discordância dos fundos entre o canal principal e o afluente. Além disso, as erosões do fundo, geralmente presentes nos modelos existentes são bem menores ou mesmo inexistente nesses casos.

No que diz respeito ao campo de escoamento, a quantidade de movimento introduzida pelo afluente, associada com a presença do depósito à jusante leva à uma redistribuição de massa, onde o escoamento principal é desviado para lado externo da confluência. A parte inferior do escoamento principal na parte interior do canal principal não é afetada pelo afluente e isso leva à formação de um escoamento em duas camadas. Esse fenômeno impede a formação de uma zona de recirculação à jusante da confluência. A presença da zona de depósito leva à uma redução da área do escoamento e consequentemente à uma aceleração do escoamento. No canal principal, os sedimentos sofrem uma triagem natural. Os sedimentos mais finos são transportados no topo enquanto os sedimentos mais grosseiros são

principalmente transportados nas encostas do depósito.. A capacidade do transporte de sedimentos é aumentada pela tri-dimensionalidade do escoamento, que é caracterizada por velocidades máximas ocorrendo perto do fundo e por um aumento considerável da energia turbulenta do escoamento.

Os ensaios em laboratório revelaram que o alargamento local dos afluentes conduz à uma grande heterogeneidade do leito, das velocidades e das profundidades do escoamento do fluxo, sem quaisquer efeitos que prejudiquem às cheias na zona da confluência. Embora o alargamento local do afluente permita uma redução no ângulo da junção, verifica-se localmente uma amplificação dos processos hidro-morfo-sedimentológicos na zona da confluência. Isto ocorre devido à redução da área efetiva do escoamento na zona alargada, resultando em uma aceleração do escoamento e em um aumento da quantidade de movimento do afluente. Esta redução de área efetiva ocorre devido à sobrelevação do leito e da constrição lateral do escoamento do afluente induzido pela zona de estagnação formada no canto à montante da confluência. A aceleração do escoamento do afluente na zona de confluência leva ao aumento da discordância dos fundos e à uma maior penetração do afluente na zona da confluência.

Apesar das diferentes respostas morfodinâmicas nas zonas alargadas dependendo da geometria do alargamento e da relação de vazões entre o afluente e o canal principal, o alargamento local do afluente sempre aumenta a variabilidade dos parâmetros necessários para a revitalização, sem causar efeitos negativos em condições de equilíbrio de transporte de sedimentos, como as consideradas nessa pesquisa. Além disso, a liberdade lateral obtida pelo alargamento associada à diferentes combinações des cheias naturais do canal principal e do afluente permite ainda a formação de diferentes formas de fundo, o que contribui para o aumento da conectividade lateral de sistemas fluviais regularizados.

Sendo assim, o alargando local do afluente pode ser considerado como uma solução eficiente para aumentar o potencial ecológico dos sistemas fluviais, sem reduzir sua capacidade de transporte.

Palavras-chave: Confluências alpinas, investigação experimental, morfodinâmica, transporte de sedimentos, revitalização fluvial.

Acknowledgments

First of all, I would like to thank my thesis advisor Prof. Anton Schleiss for giving me the opportunity to join the LCH team and for trusting me during all those years, at the beginning as a MAS student and then, since 2006 as a PhD student. I would like also to thank him for the guidance and for all the support. I also wish to express my gratitude to my thesis co-advisor, Dr. Koen Blanckaert for all his help during these last 3 years. Thank you, Koen, for all the discussions (including the "Chinese evening endless skype calls"). Your contribution was essential for the success of my work.

My research project was funded by the Swiss Federal Office for the Environment (FOEN). I would like to express my gratitude to the FOEN for the financial support of my work.

I also acknowledge the members of the jury, Prof. Andrew Barry (president) from EPFL, Prof. Christophe Ancey from EPFL, Prof. Stuart Lane from Durham University (UK) and Prof. André Roy from the University of Montreal (Canada) for having accepted to evaluate this work. I really appreciated the exciting discussion during the exam, theirs comments, advices and valuable insights.

Un grand merci également à Jean-Louis Boillat, qui en plus de m'avoir beaucoup aidé pour ma thèse, a été également très présent dans ma vie pendant tout mon séjour au LCH. Il a été fondamental pour ma formation en hydraulique et aussi (et comme pour la majorité des doctorants étrangers au LCH) pour mon apprentissage du français. C'était vraiment un plaisir pour moi d'avoir travaillé avec toi Jean-Louis.

Un merci spécial à Louis Schneiter et à Cédric Bron pour tout le support informatique et les appuis pour la halle. Merci également aux membres de l'atelier qui m'ont beaucoup aidé pour la construction et modifications du modèle: Michel, Panpam, Jean-Marc, Virgile, Shawna, Laurent, Grégory. Merci aux frères Mattias et Jonathan pour le montage du modèle et pour les divers coups de main dans la halle. J'aimerais également remercier Jean-Wilfrid Fils-Aimé pour m'avoir gentiment prêté les tamis pour les analyses granulométriques.

Je profite également pour remercier le Prof. António Cardoso de l'IST (Portugal), pour son aide au début de la construction du modèle et pour toutes les discussions qui ont été (et sont toujours) très fructueuses. Merci également à la Prof. Márcia Coelho de l'UFMG

(Brésil), pour l'aide pendant une partie de mes essais ainsi que pour sa collaboration pour les simulations numériques. Dans la dernière ligne droite de ma thèse, j'ai eu la chance d'avoir connu le Prof. André Roy. Je profite des ces petits mots pour le remercier de toute sa gentillesse et pour l'aide pendant la dernière année de mon doctorat. Son expérience dans le domaine des confluences a été très importante pour la validation de mon projet. La collaboration avec lui a été exceptionnelle et j'espère avoir encore beaucoup d'autres opportunités de le rencontrer. Merci André.

J'ai eu le plaisir de passer un peu plus de sept ans au LCH et pendant tout ce temps, j'ai connu des très bon collègues et amis. Tout d'abord, un merci spécial à Giovanni et Martine pour toute aide dès mon arrivée en Suisse et aussi pour toutes les conversations toujours très intéressantes pendant le MAS et aussi pendant le doctorat. J'aimerais encore remercier Caroline, Sonia et Scarlett pour le support administratif. Je profite pour remercier l'ancienne génération des doctorants et stagiaires: Alex Duarte, Azin, Burkhard, Fréd, Islam, Mattias, Olivier, Paul, Joan, Pedro, Peyman, Philippe, Remi, Mathilde, Sabrina, Sameh, Selim, Stéphanie et Tobias pour tous les moments partagés et les discussions pendant la période que j'ai passé comme stagiaire au LCH pendant le MAS et également au début de mon doctorat.

Un merci très chaleureux à la génération actuelle du LCH: Martin, Javier, Fadi, Michael, Jolanda, Milad, Tamara, Matteo, Rafael, Violaine, José Pedro, Ana Margarida, Walter, Jean-Marc Ribi, Michael Pfister, et bien sure à ma très chère collège du bureau Théodora, pour toutes les moments professionnels et privés (sorties, bières au SAT, barbecues, etc…) qu'on a passé ensemble. Vous êtes superbes et j'ai beaucoup apprécié de faire parti de votre groupe.

Merci aussi à tous les étudiants que j'ai eu la chance d'assister pendant ces dernières années et spécialement à Simon Wampfler et Lucien Bidaud.

Une vie sans des amitiés n'est jamais possible, surtout quand on n'est pas chez soi. Pour cette raison, je tiens à remercier tous les très grands amis que j'ai rencontrés depuis mon arrivée en Suisse. Ils sont très nombreux et je peux dire que suis vraiment chanceux de vous avoir connu. Parmi tous, j'aimerais faire mention spéciale à la « velha guarda », soit ceux qui ont arrivé en 2003 comme moi et qui ont suivi tout mon chemin jusqu'ici: Sami, Paulo, Lucas, Pietro, Mark, Wellerson, Islam, Henri et Kristijan. Merci également à tous les amis avec lesquels j'ai partagé des moments inoubliables à Lausanne: Alexandre Dal Fabbro, Joana, Simone, Rosy, Alê, Reni, Fanny, Maria, Sandy, David Ingram, Rafael, Laurence,

Eduardo, Kristina, Pedrão, Antônio Conselheiro, Leandro, Tuca, Schubert, Milene, Janina, Bruno, Intan, Luis Borges, Daniel Mocibob, Stéph, Predrag, Rumiana, Danilo, Laetitia, Sitaram, Lucie, Alexis et Marine, Fernando Cruz, Juan Martinez, David et Cecilia, Ruben Sandiano, Davide Malatesta, Song Hao, Paula, Victor, Luis Panicelli, Nadège, Daniel Grogg, Didier, Giovanni Polito, Davor, Andrés, Robin, Francesco, Peter, Reto, Benoît Desgraz, Gilbeto et Nicole.

Un remerciement spécial à Pedro, un grand ami que j'ai eu l'honneur de connaitre ici et qui sans lequel ma vie en Suisse aurait été beaucoup plus dure. Muito obrigado Pedro, do fundo do meu coração! Merci aussi à Juliano, pour l'amitié et fraternité depuis très longtemps. Valeu meu velho !

J'aimerais également remercier toute l'équipe du Water Polo de Lausanne que m'a servi comme calmant. Je suis très content de faire toujours partie de ce groupe : tout d'abord comme joueur, après comme entraineur et maintenant comme touriste et supporteur ! Allez Lausanne!

Gostaria também de agradecer toda a equipe do Departamento de Hidráulica da UFMG que me apoiou bastante na preparação para a vinda para a Suiça e em especial ao Prof. Nilo Nascimento, que me ajudou muito na organização dos documentos para a inscrição no mestrado na EPFL.

Agradeço também à minha adorável familia Sevilhana: meus sogros Ricardo e Montse, minha cunhada Clara e meu concunhado Alejandro.

Finalmente, eu gostaria de agradecer aos meus pais Manoel e Neuza e às minhas irmãs Helena e Regina pelo amor incondicional e por todo o apoio emocional durante toda minha vida pra que eu pudesse chegar até aqui. Um agradecimento mais do que especial também à minha querida Montsita por todos esses anos ao meu lado e pelo amor sincero e verdadeiro.

Table of contents

List of Figures

1. Introduction

1.1 Alpine river confluences

During the past centuries, rivers have been trained in many countries in order to improve flood protection of cultivated and urban land. In alpine regions, river training typically transformed wide braided rivers into relatively narrow straight channels with monotonous linear profiles with a lack of structural diversity, i.e. gravel banks, islands, woody debris, riffles or pools. The results impoverished river ecosystems. Currently, only about 10% of the most important rivers of the entire Alpine region are still in a "near-natural" condition (Rohde et al., 2005).

In fluvial networks, stream channel confluences produce significant changes in flow, sediment transport and morphology. Moreover, confluences are important for example for the ecological connectivity, flood control and water quality. Alpine confluences are typically characterized by steep gravel-bed streams carrying large sediment loads, which often connect asymmetrically at large angles with the main river at the valley bottom. Such zones present important challenges, not only for flood protection but also for rehabilitation works. A good understanding of the flow patterns, sediment transport as well as bed morphology is essential to successfully design river rehabilitation project for confluence zones.

Bourgeois (2006) has performed an analysis of the ecological value of the Rhone basin in the Valais Canton, Switzerland, as well as the potential to improve the ecological value by means of an optimal connection of its tributaries. The methodology was based on the analyses of four different criteria: ecomorphology, flow, water quality and connectivity and it was applied to the 21 main confluences of the Upper Rhone River. The analysis revealed that the river's ecological quality is currently poor, a situation that is mainly due to past river training works. However, a considerable improvement of the ecological quality can be obtained by means of relatively low-cost measures at the confluences.

From the end of the 20th century, rehabilitation of rivers that were previously degraded by human interventions has been commonly applied by environmental professionals and authorities (Bernhardt et al., 2005; Reichert et al., 2007). The purpose is to recover the vital space required for the rivers, linking the sustainable use of rivers and wetlands with human well-being (Nakamura et al., 2006). The vital space is required to maintain the quantity and quality of the water in the natural water system in order to safeguard its role in the ecosystem over time (Havinga et al., 2005). Rehabilitation projects can therefore be considered as

complex processes in which fluvial dynamics, environment and flood protection play an important role (Peter, 2006). The insufficient understanding of natural conditions may be responsible for the fact that a high proportion of rehabilitation projects fail (Lockwood and Pimm, 1999).

1.2 Research project "Integrated River Basin Management"

River rehabilitation projects commonly include experiments in scale models. Over the last years, the Laboratory of Hydraulic Constructions (LCH), at the École Polytechnique Fédérale de Lausanne (EPFL), has participated in a large number of rehabilitation projects in Switzerland (Boillat et al., 2006; Meile, 2006; Schleiss, 2006; Jenzer et al., 2008). Moreover, LCH is a partner in the interdisciplinary research project "Integrated River Basin Project" (*Integrales Flussgebiestmanagement*) which has the objective of understanding the ecological and socio-economical consequences of river training works and providing advice for future interventions on river systems. The main focus is on "biodiversity and flood protection measures" as well as "lateral and longitudinal connectivity of rivers". The research project is funded by the Federal Office for the Environment (FOEN) and the project partners are EAWAG, WSL and VAW-ETH Zurich. In the LCH, the following topics are investigated:

A) Flood protection measures and habitat quality ("*Konstructiver Hochwasserschutz und Lebensraumvielfalt"*)

B) Improvement of habitat conditions in case of hydropeaking ("*Verbesserung der Habitatsbedingungen bei Schwall und Sunk")*

C) Morphology of restored river confluences ("*Morphologie von naturnah gestalteten Einmündungen von Seitengewässern")*

D) Stability and connectivity of block ramps *("Stabilität und Durchgängigkeit von Blockrampen")*

A diagram illustrating the other projects with their respective leaders and the connection between all the projects is shown in Figure 1-1.

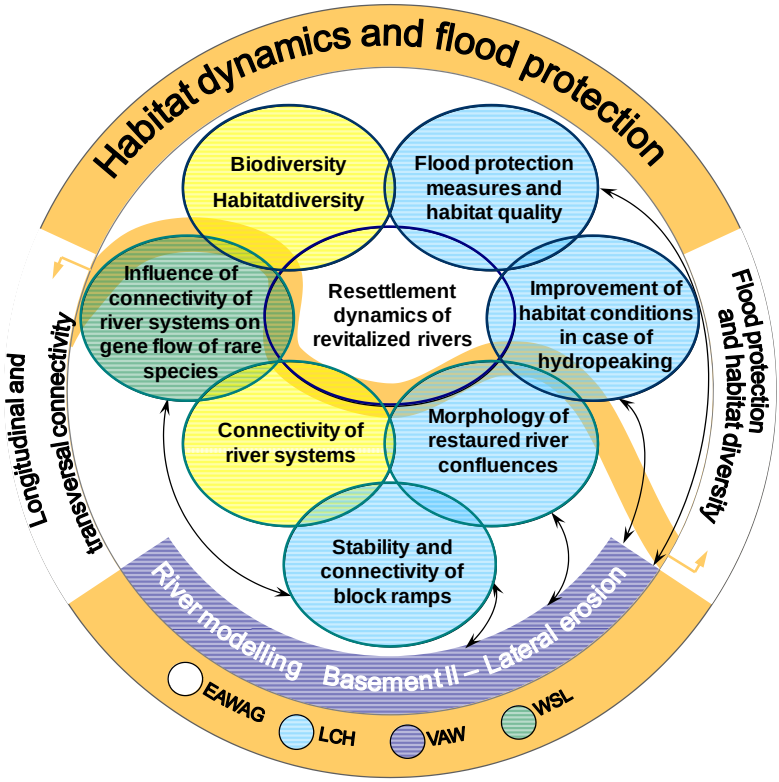

Figure 1-1: Diagram of the Integrated River Basin Management research project.

1.3 Purpose of the research project

The present Ph.D. project corresponds to topic C of the Integrated River Basin Management project. The aim is to gain insight in the flow structure and morphological development in alpine confluences in the framework of river rehabilitation projects. Special attention is given to the local widening of the tributary channel and its influence on the hydro-morpho-sedimentary processes in the confluence zone. Results are obtained by means of systematic experimental investigation carried out in a confluence flume at EPFL. The experimental set-up and conditions are based on the Upper Rhone River confluences, in Switzerland.

The main objectives of the present research project are:

- To observe, measure and quantify the hydro-morpho-sedimentary processes in controlled laboratory settings that are representative of alpine confluences;
- To gain insight in the interactions and feedback mechanisms between these hydro-morpho-sedimentary processes;
- To investigate the influence of the discharge and momentum flux ratios on the morphology of channelized alpine confluences;
- To investigate the influence of the local widening of the tributary channel on the flow dynamics, sediment transport and bed morphology;
- To qualitatively examine the ecological potential of a local tributary widening;
- To provide detailed data on the three-dimensional flow field, the morphology and the sediment characteristics that is essential for the validation of numerical models.

1.4 Structure of the report

This report is divided into eight chapters. Each chapter is self-contained, which unavoidably leads to some redundancy, especially in the chapters concerning the data analyses (Chapters 5, 6 and 7) that are written as scientific papers.

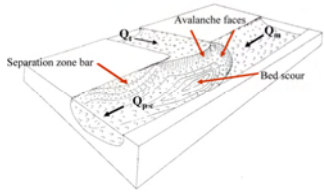

Chapter 2 presents a review of the existing literature on confluences, which leads to the conclusion that there is a lack of information regarding studies on sediment transport and the morphology in natural and laboratory confluences. Furthermore, alpine confluences have not yet been studied and no investigation has been done on the potential of local tributary widening for rehabilitation projects.

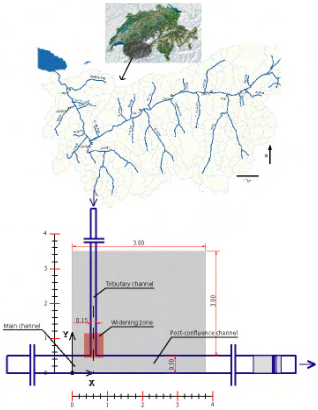

Chapter 3 presents the design of the experiments based on an analysis of river confluences located in the Upper Rhone basin. The choice of this basin for designing the experimental set-up is justified by its representativeness of regulated alpine river systems. The experimental procedures and techniques are presented.

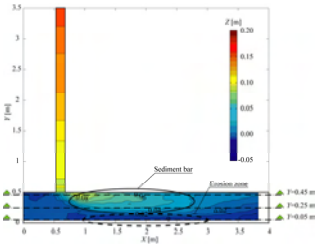

Chapter 4 reports the main hydro-morpho features that are common for all experiments. Moreover, it presents the appendixes where all the data are documented systematically.

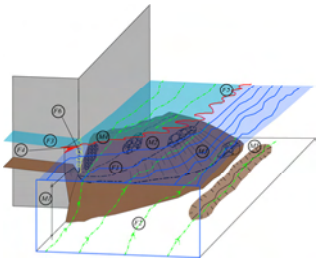

Chapter 5 discusses the test results performed in a reference configuration (without tributary widening) for one discharge scenario. The analyses of the hydro-morpho-sedimentary processes in the confluence zone revealed that the existing knowledge on channel confluences is not applicable for the investigated conditions. Therefore, a conceptual framework for hydro-morpho-sedimentary processes in confluences with characteristics similar to those found in alpine environments is proposed.

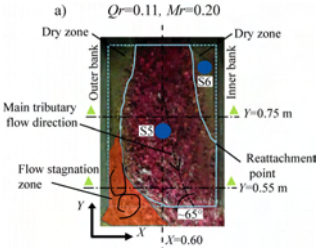

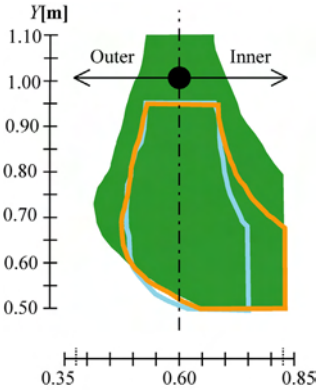

Chapter 6 discusses the influence of the local tributary widening on the hydro-morpho-sedimentary processes for one discharge scenario. The hydraulic and sedimentary conditions of the test presented in this chapter are the same as those discussed in chapter V. The analyses reveal that a local tributary widening in the confluence zone creates a zone of important variability of flow depths, bed constitution and flow velocities without adverse impacts on the conveyance capacity. Therefore, local tributary widening is a potential measure for river rehabilitation projects.

Chapter 7 discusses the ensemble of the experimental database including three discharge scenarios and four tributary configurations (reference configuration and three tributary widening). The results confirm the findings presented in Chapters 5 and 6 regarding the hydro-morpho-sedimentary processes in alpine confluences and the influence of a local tributary widening. Moreover they confirm that local tributary widening has no adverse effects on the conveyance capacity and the flood safety of the confluence zone. The ecological potential of a local tributary widening is highlighted.

Finally, Chapter 8 gives the general conclusions of the research project and highlights the main original contributions. Furthermore, it gives some suggestions and guidelines for future research.

2. Literature review

2.1 General

Confluence is the hydraulic singularity where two or more channels (or rivers) converge in a single channel downstream. Mosley (1976) defines two types of river channel confluence planform: (*i*) asymmetric confluences, where the main channel downstream of the confluence is an extension of the main channel upstream (Figure 2-1a) and (*ii*) symmetric confluences, where the two confluents join and form a new channel, i.e. Y-shaped, (Figure 2-1b).

Over the last 30 years, the synergy between laboratory tests, field measurements and computational dynamic models has provided valuable information about the complex hydro-morpho-sedimentary processes acting in river confluence zones. Recently, Biron and Lane (2008) and Best and Rhoads (2008) present a complete bibliographic review which discusses the most significant works regarding river confluences.

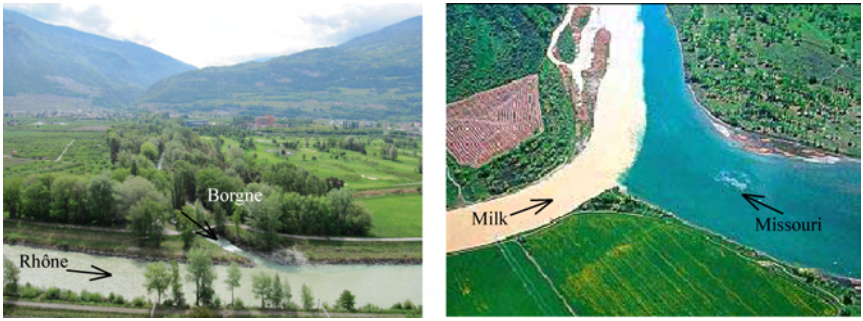

Figure 2-1: Examples of different confluence planforms. a) asymmetric confluence of the Borgne (tributary) and the Rhone (main channel) rivers, in Switzerland and b) symmetric confluence of the Milk and Missouri Rivers, in USA (By courtesy of Jim Wark, www.airphotona.com).

2.2 Flow behaviour at river confluences

Taylor (1944) is probably the first researcher to perform theoretical and experimental analyses in channel confluences in subcritical regimes, considering junction angles of 45° and 135° in an asymmetrical planform. He proposes a one-dimensional approach based on the momentum and mass conservation equations to calculate the ratio between the upstream and the downstream water depths, neglecting boundary friction effects and assuming the upstream depth equal to both upstream channels. Following the same assumption, Webber and Greated (1966) carried out experiments with 30°, 60° and 90° confluence angles, suggesting an empirical correction for Taylor's model.

Subsequent to the works of Taylor and Webber and Greated, several authors proposed one-dimensional approaches to estimate the water depths upstream of the confluences for different angles, discharge ratios, channel widths, slope and flow regimes (Milano and Sassoli, 1977; Ramamurthy et al., 1988; Hager, 1989; Gurram et al., 1997; Hsu et al., 1998; Shabayek et al., 2002; Coelho, 2003). The applicability of these one-dimensional approaches may, however, be limited by the strong three-dimensional hydrodynamic behaviour of confluences.

The first detailed description of the flow dynamics is presented by Best (1987). By means of an experimental investigation in a small asymmetric confluence flume, he proposes a descriptive hydrodynamic model (Figure 2-2). His model describes six different regions in confluence zones: flow deflection, flow stagnation, flow separation, maximum velocity, shear layer and flow recovery.

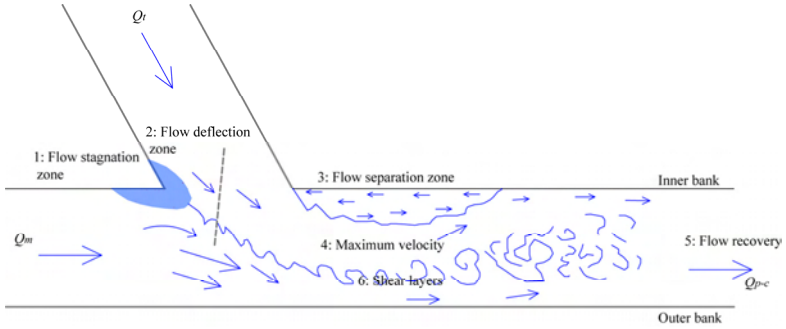

Figure 2-2: Descriptive model of flow dynamics at channel confluence proposed by Best (1987).

The flow stagnation zone is created by the deflection of both streams at the junction and is associated firstly, with an increase of pressure and flow depth and secondly, with a decrease of flow velocities and shear stresses. The change of the tributary direction creates a separation zone due to the flow detachment from the inner wall in the post confluence and its reattachment further downstream (Best and Reid, 1984; Fujita and Komura, 1989; Hager, 1989; Qing-Yuan et al., 2009; Shakibainia et al., 2010). The geometry of the separation zone is of special interest because it delimits the width of the post-confluence channel, reducing the effective flow sectional area. Additionally, it is a region of low pressure and recirculating flows, commonly associated with the accumulation of fine sediments (Modi et al., 1981; Best and Reid, 1984). The dimensions of the flow separation zone increase with the increase of the confluence angle and of the discharge ratio between the tributary and the main channel (Best

and Reid, 1984; Weber et al., 2001b). The maximum velocity zone occurs after the junction of the flows at the contracted cross section besides the separation zone. It is generally associated with the increase of bed shear stresses and consequently with the presence of a scour.

Shear layers are formed along the contact of the stagnated areas of the fluid and the flow outside. They are characterized by high turbulence intensities and shear stresses and also by the presence of well-organized flow structures (Nezu and Nakagawa, 1993; Nezu et al., 1993; Rhoads and Sukhodolov, 2001; Sukhodolov and Rhoads, 2001; Rhoads and Sukhodolov, 2004). This turbulence intensity enhances the mixing processes downstream of the confluences (Biron et al., 1996a; Biron et al., 1996b; Bryan and Kuhn, 2002).

The presence of two helical cells driven by the confluence converging at the surface downstream of the junction (Figure 2-3) was first described by Mosley (1976) and has been the subject of a large scientific debate. Their existence is confirmed by the experimental results of Fujita and Komura (1989) and the field measurements performed in a small bed concordant confluence discussed by Rhoads and Kenworthy (1998).

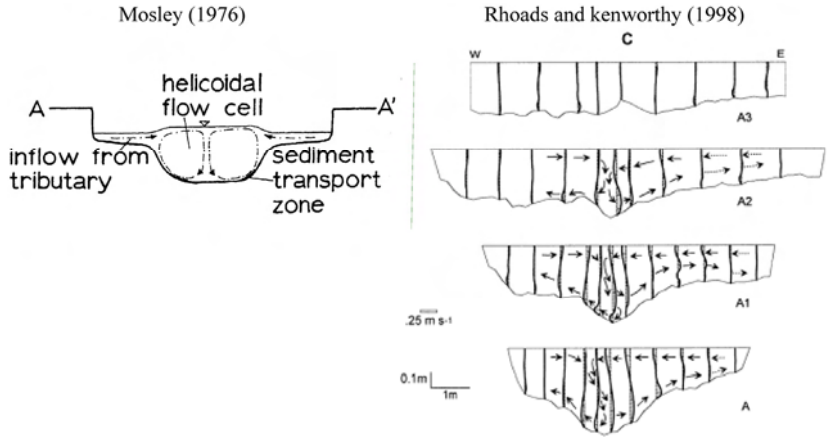

Figure 2-3: Two helical cells as described by (Mosley, 1976) and measured by (Rhoads and Kenworthy, 1998).

Bradbrook et al. (1998) demonstrate numerically that secondary circulation can be developed at a channel junction in the absence of planform curvature (parallel channels), under a wide range of combinations of depth and velocity ratios. Then, a large number of numerical simulations confirms that bed concordance and planform curvature are extremely important in

the formation of the secondary flows in confluence zones (Lane et al., 1999b; Bradbrook et al., 2000a; Bradbrook et al., 2000b; Bradbrook et al., 2001; Biron et al., 2002).

Weber et al. (2001a) provides important experimental data and a description of the flow in a confluence by means of 3D velocities and turbulence measurements in a horizontal fixed bed laboratory flume with a junction of 90° and channel widths of 0.91 cm. The study comprises the surface velocity, the cross sectional velocity and the turbulent kinetic energy analysis. They propose a three-dimensional model of the flow behaviour, illustrated in Figure 2-4. The model highlights the three-dimensionality of the flow separation zone (larger at the surface) and the shear plane (not vertical). It also reports the presence of one large helical cell, instead of two.

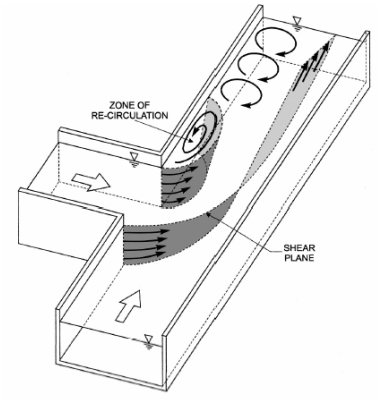

Figure 2-4 : Three-dimensional of flow structure at a confluence (Weber et al., 2001a).

The presence of helical cells is however, not reported in all studies. A recent investigation in a large confluence in the Paraná River, Argentina (Parsons et al., 2007) reveals that in reaches with large width-to-depth ratios, the magnitude of the water super-elevation due to the junction is much lower than the channel width. Therefore, the magnitude of the driving component of the curvature-driven circulation is quite small, which explains the absence of the secondary circulation.

A good agreement between two-dimensional numerical simulations and laboratory tests and/or field measurements is described by several authors either for research objectives (Lane, 1995; Lane and Richards, 1998; Ghostine et al., 2007) or for case studies (Khan et al., 2000; Duan and Schwar, 2003; Masujin et al., 2005; D'Oria and Tanda, 2007; Guo, 2007). Lane et al. (1999b) perform an extensive comparison between two and three-dimensional models

validated by experimental data with bed discordance (Biron et al., 1996a), parallel channels with bed discordance (Bradbrook et al., 1998) and field measurements (Lane and Richards, 1998). They suggest that there is a significant advantage in moving towards three-dimensional modelling for confluence studies. Therefore, the use of three-dimensional numerical models considering fixed bed to describe flow patterns in confluences has become more frequent over the last years.

Baranya and Józsa (2007b; 2007a) carried out a case study in a symmetrical confluence of two rivers in the Northwest of Hungary with the SSIIM program (Olsen, 2006) without bed changes. They found good agreement between the numerical model and experimental data in a distorted scale model upstream of the confluence but less concordance in the downstream of it. The authors advise that the steady turbulence closure is not able to fully reproduce the three-dimensionality of the river turbulence. This suggestion confirms the assumption of Lane et al. (2000) and Parsons (2003) who suggest that the application of an unsteady turbulence model is the only way to fully capture the intermittent or periodic flow structures, which are present in flows with shear layers.

2.3 Morphodynamics of river confluences

The confluence of two channels, each of them having independent flow and sediment discharge regimes creates complex erosional and depositional conditions. Changing these input conditions (eg. river training works, dam construction, urbanization) can promote important changes in channel morphology at the confluence (Wampfler, 2008). The acquired knowledge of confluence streams over the last years has been extremely important to understand the complexity of the flow. Despite these advances, there are comparatively still few studies of bed morphology at channel confluences. Furthermore, the nature of sediment transport within the junction is not yet completely understood.

A large number of natural confluences have been studied over the last years. Among the natural sites, the confluences of the Kaskaskia and Cooper Slough Rivers in the USA (Kenworthy and Rhoads, 1995; Rhoads and Kenworthy, 1995; Rhoads, 1996; Rhoads and Kenworthy, 1998; Rhoads and Sukhodolov, 2001; Sukhodolov and Rhoads, 2001; Rhoads and Sukhodolov, 2004; , 2008; Rhoads et al., 2009) and of the Bayonne-Berthier rivers in Canada (Biron et al., 1993; Biron et al., 1996a; Leclair and Roy, 1997; De Serres et al., 1999; Biron et al., 2002; Boyer et al., 2006) have been analysed extensively. These two confluences

are the main source of the existing knowledge concerning the morphodynamics of river confluences.

The discharge ratio between the tributaries (Q_r), the confluence planform and the confluence angles were first defined as the most important parameters controlling the morphodynamics behaviour of river confluences (Mosley, 1976; Best and Reid, 1984; Best, 1987; Best, 1988). However, the momentum flux ratio (Mr) between the tributary and the main channels has also been identified as an important parameter because of its influence on the bed morphology of small confluences (Biron et al., 1993; Rhoads and Kenworthy, 1995; Rhoads and Kenworthy, 1998; Biron et al., 2002; Boyer et al., 2006). The momentum flux ratio (Mr) is defined as:

$$Mr = \frac{\rho Q_t U_t}{\rho Q_m U_m} \qquad \text{Eq. 2.1}$$

where ρ is the water density [kgm^{-3}], Q the discharge [m^{3}s^{-1}], U the mean velocity [ms^{-1}] and the subscripts t and m represent the tributary and the main channels respectively.

In Figure 2-5, the momentum flux ratios (Mr) are presented as a function of the discharge ratios (Qr) for the most important studies concerning the morphodynamics of river confluences. With the exception of Best's work, all other studies have been performed in the field.

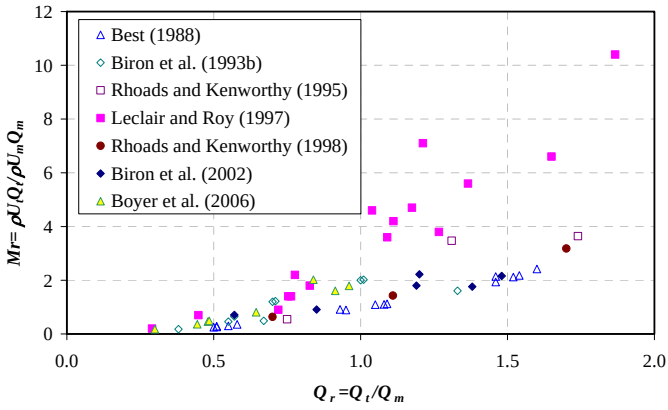

Figure 2-5: Momentum flux ratio (Mr) as a function of the discharge ratio (Qr) for the most relevant investigations concerning the morphodynamics of river confluences. With the exception of Best's work (performed in laboratory), all other studies have been carried out on natural confluences.

Only a few experimental studies can be found in the literature which have been carried out under active bed conditions, i.e. with consideration of sediment transport. After Roy and Bergeron (1990), the lack of laboratory studies on flow and sediment transport at confluences can be explained by the difficulty of implementing adequate experimental procedures.

Mosley (1976) performed a laboratory study in a wide flume (1.3 m) with mobile bed for symmetrical and asymmetrical planforms and sediment discharge input. In his study, small confluent channels were cut in erodible material. The morphology of the confluence zone including the scour depth, confluence angle and the post-confluence width were free to adjust to the imposed flow conditions. Ashmore and Parker (1983) extended their analyses to self formed confluences representative of braided rivers based on experimental tests in two wide channels (1.3 m and 2.3 m).

Best (1988) was the first researcher to present a conceptual model of the bed morphology, which is based on systematic experimental tests performed under live bed conditions in asymmetrical confluences with equal channel widths (0.15 m) and concordant beds. Several discharge ratios (around 0.5 to around 1.5) and different confluence angles between the tributaries (15° to 105°) were considered. Well-sorted sand was used for the bed constitution and sediment supply. Among the other results, the estimation of the maximum bed scour (Figure 2-6a) and scour orientation (Figure 2-6b) as a function of the discharge ratio (Q_r) and the confluence angle (α) can be mentioned.

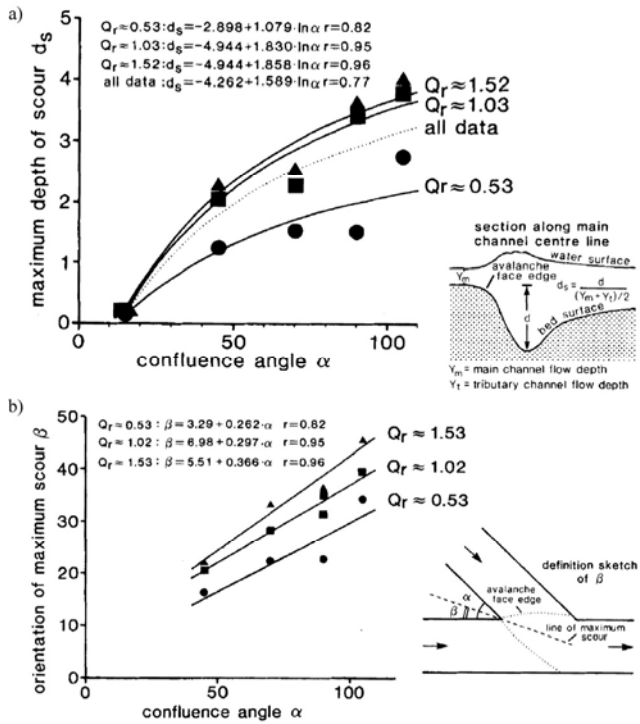

Figure 2-6 : a) Scour depth (d_s) as a function of confluence angle (α) and discharge ratio Qr and b) orientation of maximum scour as a function of α and Qr (Best, 1988).

Best's (1988) conceptual model was further refined by Best and Rhoads (2008) who describes the bed morphology of river confluences by five main features influencing directly the flow dynamics discussed in the section 2.2 (Figure 2-2):

1) Scour hole due to the increase of flow velocity and turbulence within the confluence zone. The scour hole is also linked to the helical cells;
2) Tributary mouth bars with the associated avalanche faces formed at the mouth of one or both tributaries and often sloping into the scour hole;
3) Mid-channel bar;
4) Bank-attached lateral bars, associated with regions of flow deceleration and/or flow separation and

5) A region of sediment accumulation near the upstream corner, probably associated with the flow stagnation zone. In Figure 2-7, the first, second and fourth features are illustrated.

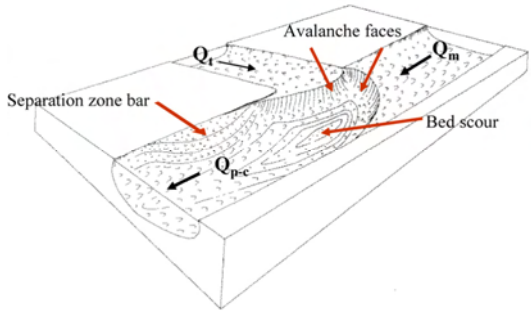

Figure 2-7: Morphologic descriptive model proposed by (Best, 1988).

The consideration of confluences with discordant beds is relatively recent even if this characteristic morphology is common in nature (Kennedy, 1984). Contrary to bed concordant confluences discussed above, the tributary and main channels mouth elevations are not the same in confluences with bed discordance. Field measurements (Biron et al., 1993; Biron et al., 1996a) demonstrate that the presence of a bed discordance between the confluent channels modifies considerably the flow in the confluence zone, affecting the sediment transport and the bed morphology. In addition, it can increase the turbulence intensity in the shear layer and consequently increase flow mixing downstream of the confluence (Gaudet and Roy, 1995; Biron et al., 2004). By means of field measurements, Leclair and Roy (1997) propose different models of the hydro-morpho-sedimentary dynamics at a confluence with discordant beds during low flow and high momentum flux ratio, $Mr \geq 1$. They relate the variations of the tributary mouth bar to changes in *Mr*. Furthermore, they distinguish between a phase of bar erosion for $Mr \sim 1$ and a phase of bar construction and full bar extension for $Mr >> 1$. The most complete study concerning bed discordant confluences is presented by (Boyer et al., 2006). They describe in detail the flow structure and its interaction with sediment transport and bed morphology at the Bayonne-Berthier confluence. Two conceptual models of sediment transport and morphological changes are proposed, one for $Mr > 1$ and the other for $Mr < 1$ (Figure 2-8).

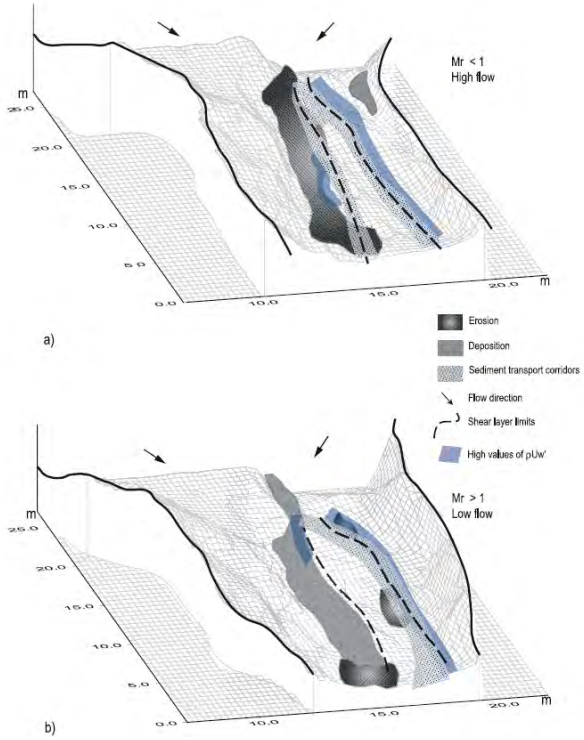

Figure 2-8: Conceptual models for flow and sediment dynamics at discordant bed confluences during a) high (Mr<1) and b) low flows (Mr>1) proposed by (Boyer et al., 2006).

Recently, experimental studies performed under clear water conditions focused on confluence scour. Ghobadian and Bajestan (2007) presents dimensionless relationships for predicting scour hole and point bar dimensions as a function of the discharge ratio between the post-confluence and tributary channels ($Q_{p\text{-}c}/Q_t$), the confluence angle (α), the Densimetric Froude Number (F_g) downstream of the confluence and the post-confluence water depth. The Densimetric Froude Number is defined as:

$$Fg = \frac{U_{p-c}}{\sqrt{g*(G_s-1)*d_{50}}} \qquad \text{Eq. 2.2}$$

where $U_{p\text{-}c}$ denotes the flow velocity downstream of the river confluence, g is the gravitational acceleration, G_s the specific gravity of sediment and d_{50} the median particle size.

The results are derived from experimental investigations performed in an asymmetrical confluence where the main channel is 0.35 m and the tributary 0.25 m wide. Three different confluence angles (60°, 75° and 90°) and several discharge ratios were considered. The same approach has been presented by Borghei and Sahebari (2010). A one-dimensional equation is given for the estimation of the scour hole depth based on the confluence angle, downstream water depth and the ratios of channel widths, discharges and flow velocities.

Bajestan and Hemmati (2008) investigated the influence of the bed discordance on the scour depth in a confluence flume where the main channel is 0.35 m wide. Two tributary widths, 0.25 and 0.35 m were considered for a confluence angle of 60°. It was shown that for a same hydraulic condition, the presence of the bed discordance can reduce the magnitude of the scour hole. These results are confirmed by the absence of an important scour hole in the bed discordant confluence of the Bayonne and Berthier Rivers (Leclair and Roy, 1997; Boyer et al., 2006).

2.4 Concluding remarks

From the review of the existing literature on confluence studies, the following conclusions can be drawn:

- Hydraulic and sedimentary processes in confluences involve several variables such as the number of adjoining channels, intersection angles, planform of the confluence, channel sizes and slopes, water and solid discharges.
- The hydro-sedimentary-processes of confluences are extremely complex. However, hydrodynamics in confluence zones are quite well understood. The influence of the most important parameters controlling the hydrodynamic features as the planform of the confluence, the confluence angle, the bed concordance, the ratios between the channels width, flow discharge and flow velocity are well recognized. The remaining open discussion mainly concerns:
  - the presence, the number and the intensity of the secondary circulation driven by the confluence;
  - the processes of flow mixing downstream of the confluences;
  - the characteristics of the shear layers;
  - the behaviour of the flow separation zones.

- The database of flow measurements performed in both natural confluences and laboratory flumes is considerable. These data have been used for the validation of three-dimensional models. They are crucial for gaining better insight into the hydrodynamics of the confluence zone as a function of the different controlling parameters.
- No systematic laboratory experiments have been performed under active bed conditions except Mosley (1976), who has performed experiments in bank erodible channels and Best (1988), who has investigated asymmetric confluences in a small laboratory flume. Thus, there is a considerable lack of morphodynamic studies under systematic controlled laboratory conditions.
- Most of the current knowledge regarding morphodynamics in river confluences is based on the analyses of two small scale confluences: (i) the asymmetric bed concordant confluence between the Kaskaskia and the Copper Slough Rivers in USA and (ii) the asymmetric bed discordant confluence between the Bayonne and Berthier Rivers in Canada. Both confluences are characterized by a low sediment transport activity.
- In spite of the advances in the understanding of the dynamics of confluences, no attention has been devoted to steep river channel confluences with coarse bed material as can be found in alpine environments.
- Finally, no tributary widening and its influence on the morphology of confluence zones has been investigated.

3. Design of the experiments

3.1 Characteristics of Alpine confluences. The Upper Rhone Basin

In order to design the experimental set-up and the conditions for the research project, a detailed analysis of the Upper Rhone River catchment (Switzerland) and its twenty main confluences between Brig and Lake Geneva was performed. The analysis is based on the last reach of the tributaries in the floodplain before their junction with the Rhone. The river basin was chosen because it is representative for regulated alpine river systems, which is the focus of the present research project.

The Upper Rhone basin is located in the south-western part of Switzerland (Figure 3-1) and covers an area of 5220 km^2. The catchment area is comprised of 38% of rocks and glaciers, and 62% of pastures, forest and agricultural lands according to Loizeau and Dominik (2000). The main river, the Rhone has a length of approximately 166 km from its source at the Gletsch Glacier (~1800 m asl) to Lake Geneva (~372 m asl).

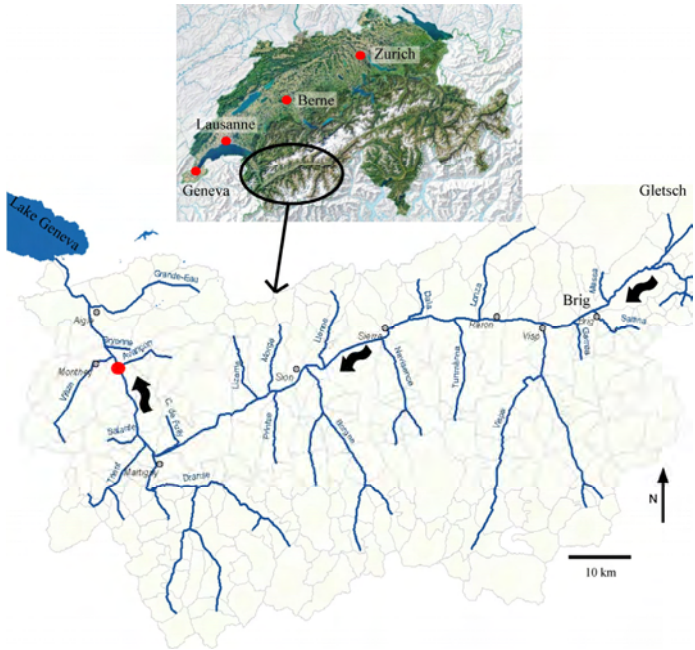

Figure 3-1: Upper Rhone River basin showing the main confluences downstream of Brig. The red circle in the Rhone basin indicates the location of the confluence between the Rhone and Avançon River shown in Figure 3-5.

3.1.1 Historical evolution

Originally, the Rhone River was a natural alpine braided river with a powerful dynamics (Figure 3-2). The bed of the main channel could laterally extend over hundreds of meters and was in strong interaction with wetlands. From the middle of the 19th century, the Rhone river training works started and they were mainly motivated by flood protection of cultivated and urban land. Human activities (agriculture, industry and urbanization) extended more and more into the flood plains. These river training works changed considerably the hydro-morpho-sedimentological structure of the Rhone (Brauchli, 2009).

Figure 3-2: Image extracted from the Napoleonic maps drawn in 1802 showing the braided Rhone (SRCE, 2008).

The so-called 1st Rhone River Correction started in 1863 and took about 30 years. The main objective was to fix the main channel, ensuring the flood safety of the floodplain required for agricultural development. However, the sediment transport capacity of the new Rhone was not sufficient to transport the huge quantity of gravel carried by its tributaries. Consequently, the bed rose by sediment deposition endangering again the flood safety.

For that reason, the 2nd Rhone River Correction began in 1930 and was completed in 1960. The main goal was to increase the sediment transport capacity. Thus, the main channel was further narrowed by filling the space between the perpendicular groynes of the 1st Rhone River Correction with continuous rip-raps. Furthermore, the flood dykes (levees) were heightened. Figure 3-3 illustrates the 1st and 2nd Rhone River Corrections.

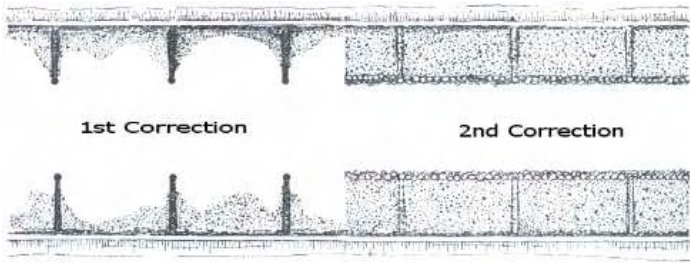

Figure 3-3: Plan view of a typical reach of the 1st and 2nd Rhone River Corrections (SRCE, 2008).

Presently, less than 1% of the Rhone can be considered as truly natural. The main channel is fixed and its width varies between 30 and 60 m.. The morphological characteristic of the river can be summarized by a monotonous linear prismatic profile and a lack of structural diversity (i.e. gravel banks, islands, woody debris, riffles or pools), as illustrated in Figure 3-4. Furthermore, today, the Rhone River has an important deficit of discharge capacity, revealed during the three recent major floods (1987, 1993 and 2000). These safety problems combined with the low ecological value motivated the ongoing 3rd Rhone correction, mainly based on river widening.

Figure 3-4: Typical reach of the Upper Rhone River in 2008.

3.1.2 Upper Rhone River confluences

As already mentioned in Chapter 2, the hydrodynamic processes in confluences involve several parameters, such as the number of adjoining channels, intersection angles, shape and

slope of the channels, discharge ratios, sediment transport, the rounding of the corners. (Gurram et al., 1997; Weber et al., 2001b; Huang et al., 2002; Shakibaeinia et al., 2007). For this reason, the different confluences are difficult to categorize.

In spite of the many different parameters that characterize river confluences, the analysis of the main confluences of the Upper Rhone has revealed some important similarities. All tributaries are channelized, a result of the past river training works. The bed elevations of the tributaries and the main channel are discordant as illustrated by the confluence of the Rhone with the Avançon River (Figure 3-5).

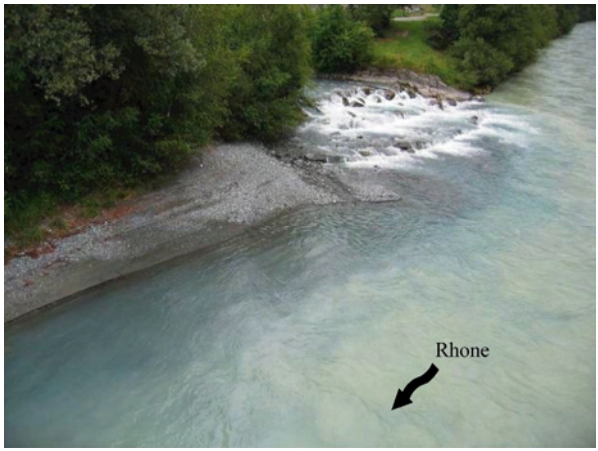

Figure 3-5: Picture of the confluences of the Rhone with the Avançon Rivers showing the bed discordance (see Figure 3-1 for the location).

Bourgeois (2006) performed an extensive analysis of the increase of the "ecological potential" of the Upper Rhone River by an optimal connection of its tributaries. The methodology is based on the analyses of four different domains, i.e., ecomorphology, flow regime, water quality and connectivity and was applied to the main Rhone confluences (Figure 3-6). It was concluded that the Rhone catchment is currently in an ecologically poor state mainly because of the channelization of the Rhone's tributaries as well as the presence of fixed weirs in some confluence zones. However, the ecological value of the major part of the confluences can be increased with a relatively small investment.

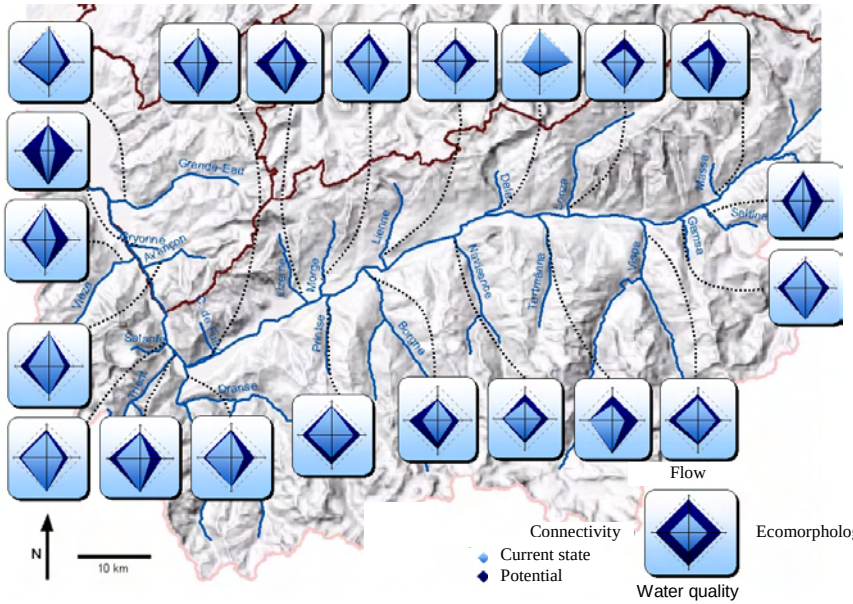

Figure 3-6: Graphical representation of the current state and the ecological potential of the Upper Rhone River confluences in Switzerland (Bourgeois, 2006).

A more detailed analysis of the main parameters discussed in Chapter 2 was performed concerning the hydraulic and morphological behavior of river confluences in the Rhone basin. In fluvial systems, there are progressive changes in a river from its source to downstream. Discharge increases with the increase of the drainage areas. As a response, channel size increases whereas bed slope and bed-material grain sizes decreases (Lodina and Chalov, 1971; Knighton, 1980; Richards, 1980; Roy et al., 1988).

From the analysis of the drainage areas it can be seen that the size of the tributary basins compared to that of the Rhone at the confluence node decreases considerably downstream, as illustrated in Figure 3-7. As described by Benda et al. (2004), this behaviour is characteristic of rectangular shaped basins.

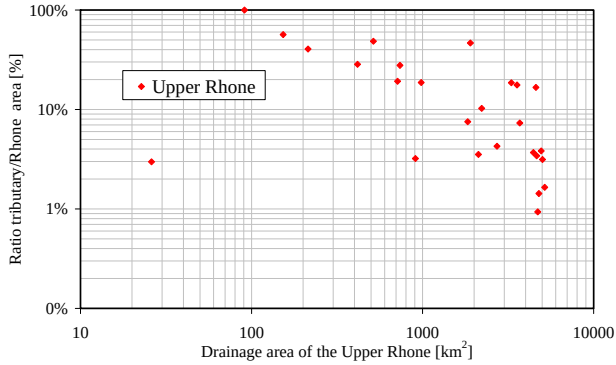

Figure 3-7: Comparison between the drainage area of the Rhone and the ratio between the drainage areas of the tributaries and Rhone for the different confluences.

Concerning the grain size distribution of the Rhone basin, an important grain sampling campaign has been carried out in the Upper Rhone basin, downstream of Brig (about 120 km upstream of Lake Geneva, Figure 3-8) in the framework of the 3rd Rhone Correction (Rovina+Partner-AG, 2008). Twelve locations (Figure 3-8a) have been sampled and, for each location, different bed layers have been analysed (Figure 3-8b). The analysis of the grain size distributions of the bed surface confirms that the Upper Rhone is characterized by poorly sorted sediments with gradation coefficients ($\sigma = 0.5*(d_{84}/d_{50} + d_{50}/d_{16}$) varying from 3 to 9. One of the most remarkable features of natural rivers is the fining of the bed-composed sediments in the downstream direction (Seal et al., 1997; Toro-Escobar et al., 2000). The analysis of the different particle size distributions in five of the twelve locations (e.g. Naters, Chablais, Bramois, Branson and Vouvry), depicted in Figure 3-8c, reveals that such a downstream fining process can be observed in the Upper Rhone Basin. The median diameter (d_{50}) passes from 128 mm in Naters to 15 mm in Vouvry, near the Lake Geneva. Abrasion and grain sorting are the two determinant processes responsible for the changes in the sediment size along the river (Knighton, 1980).

a)

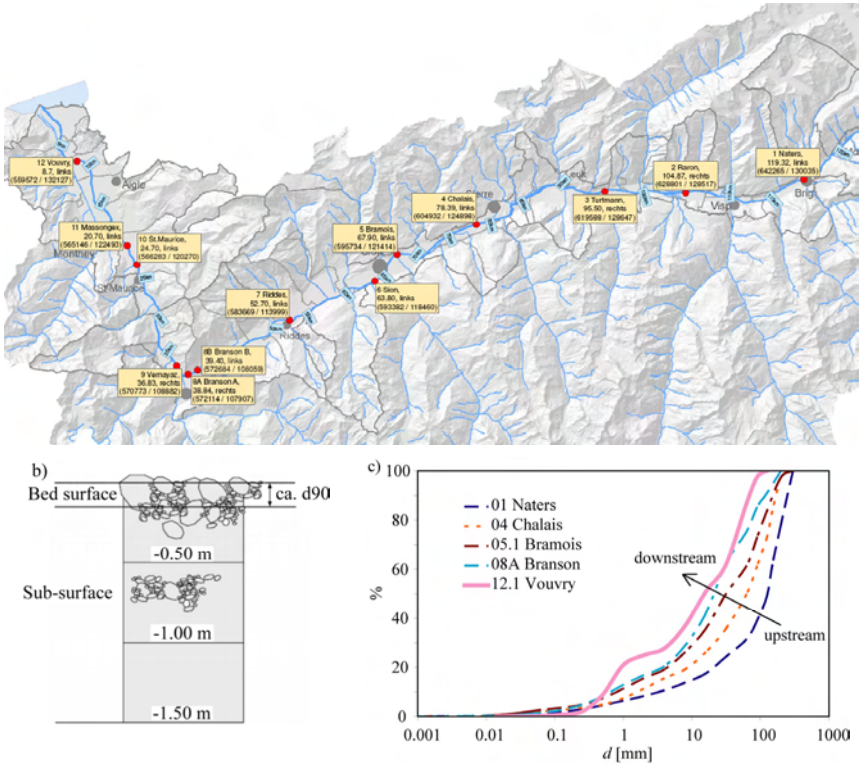

Figure 3-8: a)Position of the 12 bed surface sample locations performed in the framework of the 3rd Rhone Correction, b) Scheme of the sampling procedure and c) Grain size distribution of the bed surface in Naters, Chablais, Bramois, Branson and Vouvry.

Due to the addition of the water and sediment discharges by the tributary, the channel downstream of a river confluence naturally tends to widen. Lane (1955) proposes that channel width scales with the square root of the discharge ($B \sim Q^{0.5}$). This proposition is consistent with the results of a detailed study of discontinuities in width performed by Richards (1980), where the increase of the width is proportional to the discharge to the power 0.6. The water discharges and the main channel widths do not increase gradually. The increase occurs by steps downstream of confluences (Ferguson and Hoey, 2008). As described above, most reaches of the Upper Rhone have been channelized and consequently the channel width has been reduced. The current Rhone's channel shapes are not regime channels, i.e. "the channels

that the river would like to have" (Yalin and da Silva, 2001). Therefore, the analysis based on Lane's (1955) formulae is not appropriate for the present case.

Figure 3-9 illustrates the ratio between upstream and downstream channel width (B_m/B_{p-c}) and the ratio between the tributaries and Rhone width upstream of the confluence (B_t/B_m). Due to channelization, the Rhone River width remains more or less the same downstream of the confluences. Thus, the ratio between the widths is around 1. This is not surprising since most of the tributaries are small (Figure 3-7) and the additional discharge is not important. Thus, the required increase in width in the main channel remains mostly insignificant. The most important increase of width occurs downstream of the Vispa River, which is its major tributary and where the catchment area is almost doubles at this confluence. Considering the relation with the tributaries, Figure 3-9 clearly shows that except for the Vispa River (B_t/B_m = 0.54), the variation of the ratio B_t/B_m is below 0.32.

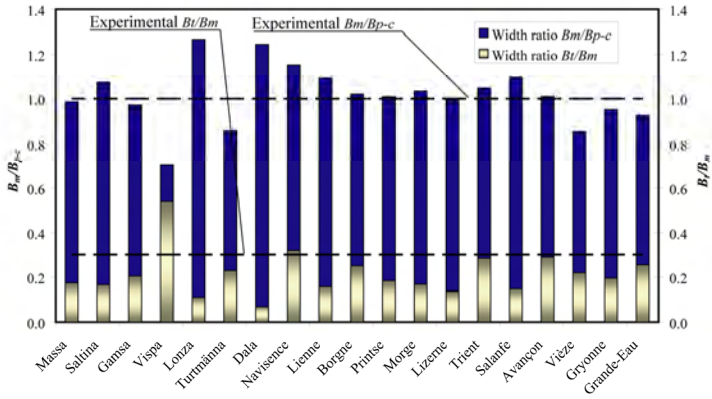

Figure 3-9: Ratio between the main and post-confluence channel widths of the main confluences of the Upper Rhone River and values adopted for the experimental investigation.

The rectangular shape of the Rhone basin is typical for mountainous areas with a main alluvial valley and several steep torrents that reach the valley bottom almost perpendicularly (Figure 3-1). However, in the vicinity of the confluence zones, the connection angle between the channels is sometimes reduced. The final confluence angle is formed naturally due to the adjustment of fluvial and geomorphologic conditions. In the Rhone basin, however, it has been frozen by the river training works. Figure 3-10 illustrates the angles measured nearby the confluences by means of aerial photography (www.maps.google.com).

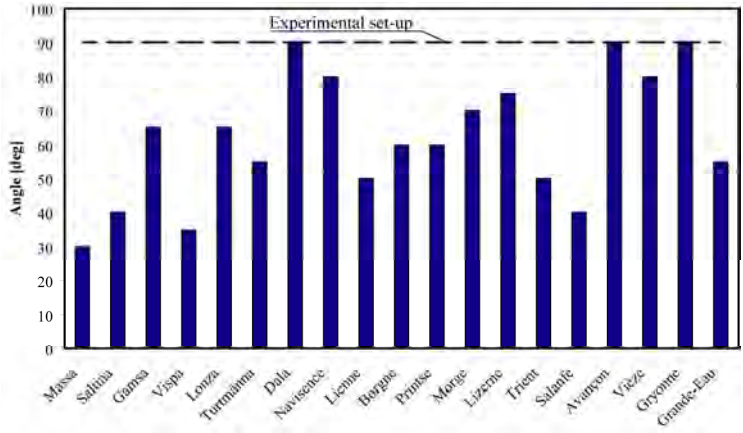

Figure 3-10: Angle of the main confluences in the Upper Rhone basin compared with the chosen angle of 90° in the confluence flume.

As illustrated in Figure 3-11, the Upper Rhone basin is generally characterized by steep small tributaries (source: "Valais river's database", "BD-Eaux"). However, some tributaries cross the flood plain of the Rhone and are characterized by low slopes, as is the case of the Turtmanna, Dala, Morge and Grand-Eau River.

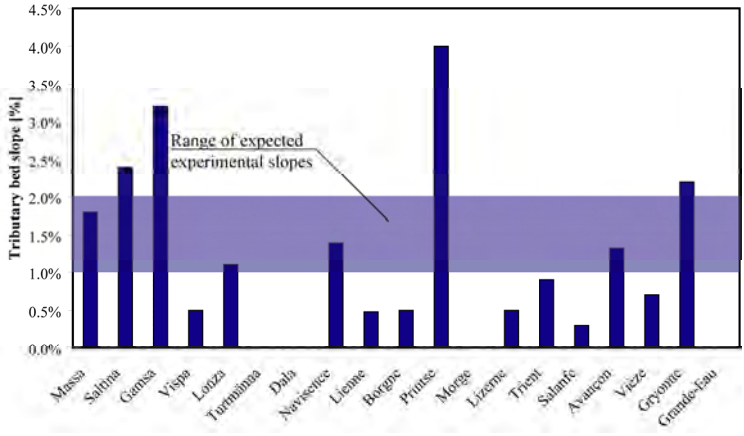

Figure 3-11: Tributary channel slopes of the downstream reach before the confluence with the Rhone and range of self-forming slopes during the experimental investigation.

The hydrologic regime of the Rhone River is strongly influenced by glaciers and can be divided into two flow regimes. Low flows occur during the winter, where precipitation falls as

snow and accumulates in the mountains. High flows start in May and is generally influenced by snow and ice melt. It continues until the beginning of the high altitude freeze up in October (Brauchli, 2009). The flow regime in the lower part of the Rhone River is also strongly influenced by hydropeaking (Meile et al., 2010). During the winter, the electricity demand and the peak energy production are high whereas during the summer, the electricity demand is lower and consequently the power generation is reduced. Therefore, discharges are generally higher during the winter and lower during the summer compared to the natural regimes.

River geomorphologists are particularly interested in the concept of channel-forming discharge which is considered to be the morphogenic agent. The correct identification of channel-forming discharges is difficult and quite subjective (Knighton, 1998). Generally, flood events between 2 and 5 years return period (Q_2 and Q_5 respectively) can be assumed as determinant for the size and shape of a river channel, being also responsible for the main morphological and ecological development of fluvial systems over very long time-scales. In natural systems, the channel-forming stage is around the connection level between the channel and adjacent floodplain at a river reach (Wu et al., 2008; Xia et al., 2010).

For the present research, based on the above considerations, flood discharges with a return period of 2 to 5 years (Q_2 and Q_5 respectively) were considered. Several gauging stations operated by the Swiss Federal Office for the Environment (FOEN) record continuously the discharges of the Rhone. As the same information is missing for most of the tributaries, their discharges have been calculated by the difference between the downstream and upstream discharges of the Rhone during the given flood events. Figure 3-12 presents the ratio between the flow discharges of the tributaries and Rhone River, showing values between 0.2 and 0.3 for the confluences in the upper part of the basin. Values around 0.10 and 0.15 occur for the confluences at the middle reach of the basin and very low values (less than 0.05) for the confluences near the Lake Geneva. Discharge values of the Dala, Printse, Morge, Lizerne and Salanfe are missing.

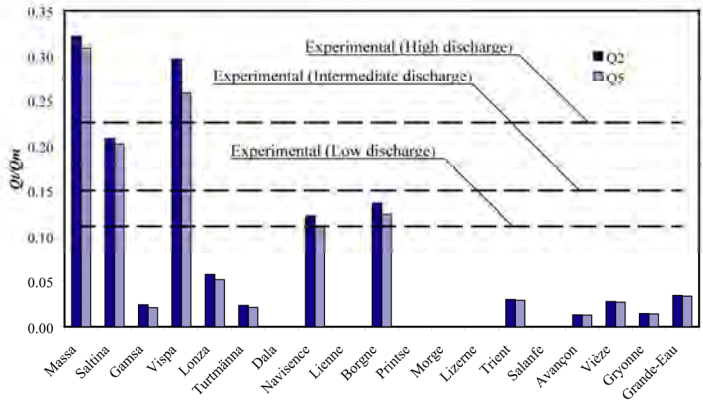

Figure 3-12: Ratio between the discharge of the tributaries and the Rhone during flood events with a return period of 2 and 5 years in the Rhone and discharges ratios chosen for the experimental tests.

In order to analyse the flow regime of the different tributaries, the Froude Number ($Fr = \frac{U}{\sqrt{2g}}$) of the different reaches have been calculated for the 2 years flood as shown in Figure 3-12. A uniform flow was assumed and no backwater effects due to the confluence were considered. In order to calculate the normal depth (h) of the flow, the Manning-Strickler equation has been used:

$$U = \frac{1}{n} * R_h^{\frac{2}{3}} * \sqrt{E_s} \qquad \text{Eq. 3.1}$$

Here, U is the average flow velocity [ms^{-1}], n is the Manning coefficient [$sm^{-1/3}$] and R_h is the hydraulic radius. For uniform flows, the energy gradient E_s [-] is equal to the bed slope. A constant Manning coefficient equal to 0.03 (d_{90} of the tributary bed surfaces is around 0.10 m) was adopted and the cross-section has been considered rectangular. Figure 3-13 reveals that generally the flow at the tributaries is transcritical (Fr~1), with some rivers flowing in supercritical conditions (Fr>1, Saltina, Gamsa, Navisance and Gryonne) and others in subcritical conditions (Fr<1, Vispa, Lonza, Borge, Trient and Vièze). Turtmanna and Grande-Eau have extremely low Froude Numbers because of their low bed slopes (~0).

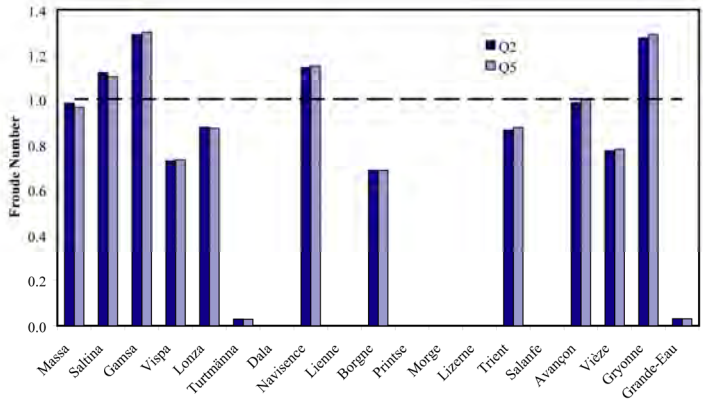

Figure 3-13: Froude Numbers of the main tributaries of the Rhone and line corresponding to Fr=1, which denotes transcritical regimes.

For the Upper Rhone River, the momentum flux ratios (*Mr*) between the tributaries and the main channels were estimated. Water depths and mean flow velocities in the Rhone River were calculated with the one-dimensional hydraulic model HEC-RAS while simple calculations using the Manning-Strickler equation were applied for the tributaries. Figure 3-14 shows that the Upper Rhone basin is characterized by low momentum flux ratios (maximum 0.45) compared to those presented in most of the field investigations in bed concordant confluences (Rhoads and Kenworthy, 1995; Rhoads and Kenworthy, 1998; Rhoads and Sukhodolov, 2001; Sukhodolov and Rhoads, 2001; Rhoads and Sukhodolov, 2004) and bed discordant confluences (Biron et al., 1993; Biron et al., 1996a; Leclair and Roy, 1997; Biron et al., 2002; Boyer et al., 2006). As expected, the downstream reduction of the momentum flux ratio between the tributaries and the Rhone is correlated with the reduction of the discharge ratios presented in Figure 3-12. This behaviour is directly linked to the important reduction of the tributaries drainage areas compared to those of the Rhone River (Figure 3-7).

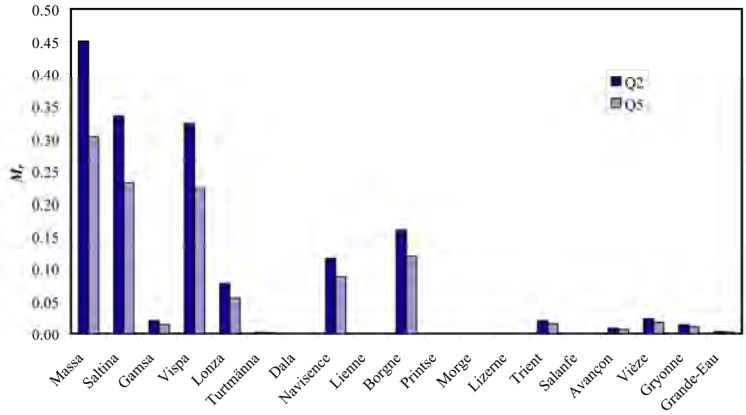

Figure 3-14: Momentum flux ratios between the tributaries and the Rhone for the 2 and 5 years return period floods.

3.2 Experimental set-up

From the analyses performed in section 3.1, it can be concluded that the confluences of the Upper Rhone River (representative of a regulated alpine basin) are characterized by relatively small steep tributaries joining the main channel at large angles. During the channel-forming events, the tributaries generally flow in transcritical regimes (Fr~1) and carry important quantities of poorly-sorted sediments. Discharge ratios as well as the resulting momentum flux ratios between the tributaries and the main channel are quite small. An important morphological feature is the always observed important bed discordance between the confluent channels. The main characteristics used for designing the experimental set-up and the experimental conditions are summarized in Table 3-1. Tributaries where some data are missing were not considered here.

As described in Chapter 2, these characteristics have not yet been considered in previous studies concerning confluences. Therefore, the design of a new facility is required. It is important to mention that the experimental set-up is not a scale of a particular confluence, but a schematized configuration with main parameters representative of the Rhone. The aim is to reproduce the dominant hydro-morpho-sedimentary processes.

Table 3-1: Geometrical characteristics of the main confluences in the Upper Rhone basin.

	Angle [°]	B_t/B_m	$B_m/B_{p\text{-}c}$	*Tributary bed slope [%]*	$Q2_t/Q2_m$	$Q5_t/Q5_m$	Fr_{tQ2}	Fr_{tQ5}	M_r_Q2	M_r_Q5
Average	62	0.22	1.02	1.1%	0.10	0.09	0.83	0.83	0.12	0.08
Max	90	0.54	1.27	4.0%	0.32	0.31	1.29	1.30	0.45	0.30
Min	30	0.07	0.71	0.0%	0.01	0.01	0.03	0.03	0.00	0.00

The experimental facility was built using existing straight glass sided flume 8.5 m long and 0.50 m wide located at the EPFL. The width of this channel, assumed as the main channel ($B_m/B_{p\text{-}c}$ = 1), was used to determine the width of the tributary channel, which was made in PVC. From Table 3-1, the average value of B_t/B_m is equal to 0.22 for the Rhone River. It would result in quite a small tributary (~0.10 cm). In order to avoid wall effects, the tributary width was chosen equal to 0.15 cm, that corresponds to a ratio B_t/B_m = 0.30. This value is a little higher than the average found in the Rhone basin but is still representative for the studied zone (Figure 3-9).

The tributary (4.9 m long) and the main channel are connected with an angle of 90°, at a distance of 3.60 m downstream of the inlet of the main channel. The angle corresponds to the maximum value measured in the studied zone (Figure 3-10). In the confluence zone, a widening region has been defined and allows the study of the three different configurations of local tributary widening: the Small (B_w=0.30 m and L_w=0.45 m), the Medium (B_w=0.45 m and L_w=0.45 m) and the Large configuration (B_w=0.45 m and L_w=0.60 m). Here, B_w and L_w denotes the width and the length of the widening respectively. More details about the widened configurations are given in section 3.3.3. The choice of 90° confluence angle is based on the fact that the lateral valleys of the basin are almost perpendicular. The present state of the Rhone confluences zones is the result of the river training works. Consequently the current angles are not truly natural. In addition, with the local widening, a self-natural dynamic is expected in the confluence zone, which includes the adjustment of a natural angle.

The experimental set-up is schematically shown in Figure 3-15. All the results presented in this document are related to the reference axes (*X, Y, Z).*

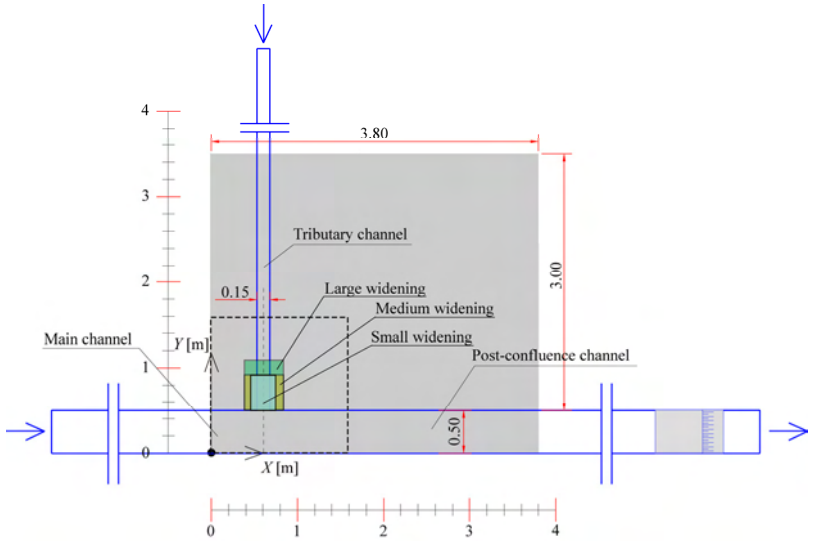

Figure 3-15: Experimental set-up. The dashed rectangle showing the zoom of the confluence zone is presented separately in Figure 3-18.

3.3 Laboratory tests

3.3.1 Water discharge scenarios

In the present investigation, the long-term averaged state of a dynamic equilibrium is investigated and therefore, an approach based on constant flows and sediment discharge was adopted. The definition of the discharge scenarios was primarily based on the analyses of width-to-depth ratios (B/h). The first criterion was to have $B/h \geq 5$ in the main and post-confluence channels in order to avoid wall effects (Yalin, 1971). Preliminary flow calculations using the one-dimensional model HEC-RAS, limited the total discharge, $Q_{p\text{-}c}$ to 20 l/s. Three discharge scenarios were then chosen in the range of the discharge ratios Q_t/Q_m presented in Figure 3-12 and summarized in Table 3-1: so-called "low discharge scenario", where Q_t=2 l/s and Q_m=18 l/s (Q_t/Q_m=0.11), "intermediate discharge scenario" with Q_t=2.6 l/s and Q_m=17.4 l/s (Q_t/Q_m=0.15) and "high discharge scenario" where Q_t=3.7 l/s and Q_m=16.3 l/s (Q_t/Q_m=0.23).

3.3.2 Sediment characteristics and solid discharge

For the experiments, poorly-sorted sediments with d_{50} = 0.82 mm, d_m = 2.3 mm and d_{90} = 5.7 mm were chosen for the bed material and the sediment supply. Sediments are only introduced in the tributary and there is no sediment transport in the main channel upstream of the confluence. This procedure aims at reproducing the typical situation river confluences during tributary flood events where the amount of the tributary solid discharge is relatively more important than that of the main channel.

Figure 3-16a shows the particle size distribution of the used sediments, which are constituted by a mixture of 80% sand (0 - 4 mm) and 20% gravel (4-8 mm). A picture of the mixture is depicted in Figure 3-16b.

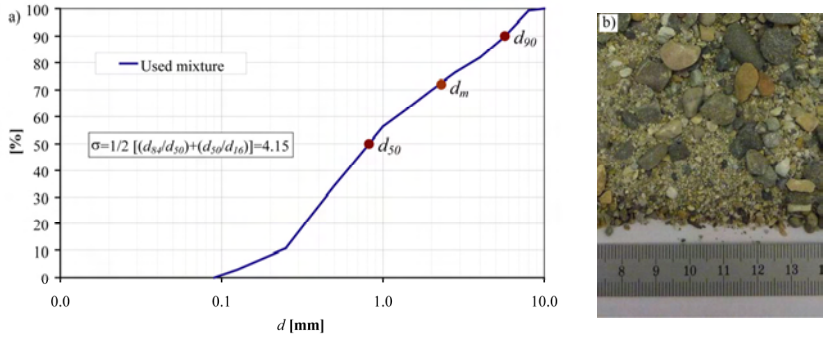

Figure 3-16: a) Grain size distribution of the sediments used for the experiments and b) a picture of the mixture of sediments.

The sediment characteristics and the solid discharge adopted for all experiments satisfy two requirements:

- The grain size distribution, characterized by the dimensionless grain size distribution with respect to the average diameter (d_m) is representative of the Upper Rhone River. The gradation coefficient of the used mixture is σ = 4.15, which is representative of the grain size distributions found in the Rhone (Figure 3-17). The density of the sediments (ρ_s) is 2.650 kg/m^3;
- The solid discharge produces longitudinal slopes in the tributary that are representative of those found in the Upper Rhone basin (Table 3-1). Preliminary one-dimensional calculations were performed using the Meyer-Peter and Mueller (1948) sediment transport formula. The formula was applied for the three tributary discharges (Q_t=2.0,

2.6 and 3.7 l/s) and the average sediment diameter (d_m=2.3 mm). For the preliminary calculations, armouring effects were not considered. Results show that a constant solid discharge of 0.3 kg/min leads to theoretical equilibrium bed slopes in the tributary between 1.0 and 2.0%. Froude Numbers are close to 1. Therefore, it was decided to run all the experiments with 0.3 kg/min.

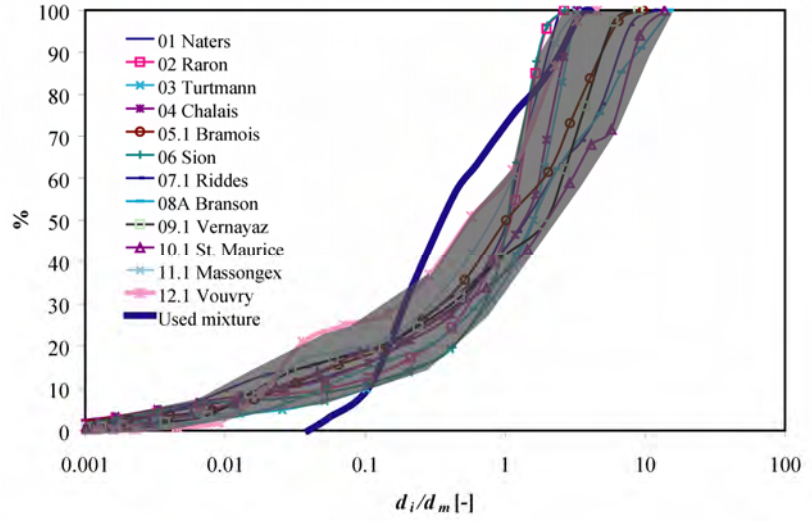

Figure 3-17: Dimensionless grain size distribution of the bed surface of the Rhone River at different locations (see Figure 3-8) and that of the sediment mixture used for the experiments.

A simplified analysis for the similarity in sediment transport (Yalin, 1971) with respect to the Rhone conditions was performed. Results shown that the size of the adopted sediment (Figure 3-16) is in the range of those found in the Upper Rhone basin (Figure 3-8). For these calculations, a geometric scale of 1/70 was adopted.

3.3.3 Tributary configurations

Four geometric configurations of the tributary in the confluence zone have been investigated (Figure 3-18). In the "Reference" configuration, the tributary has a constant width of 0.15 m. Three local tributary widenings were studied. For the "Small" configuration, the tributary width has been symmetrically doubled (B_w = 0.30 m) over a length (L_w) of 0.45 m while the "Medium" configuration considers a tributary three times wider (B_w = 0.45 m) within the

same length (L_w = 0.45 m). The "Large" configuration is composed by a tributary also three times wider (B_w = 0.45 m) over a length L_w = 0.60 m.

The choice of the widening shape was based on two criteria: (*i*) the aim of the project is to study a tributary widening. Therefore, the maximum width of the enlarged zone was limited by the width of the main channel, as wider configurations would result in a local main channel widening, and (*ii*) the length of the tributary was limited by the fact that for longer widening, flow reattachment downstream of the entrance of the enlarged zone would occur symmetrically and thus the effect of a local widening would be lost. In addition, the small widening should neither lead to adverse upstream impacts regarding the flood safety nor to considerable morphologic changes in the post-confluence channel.

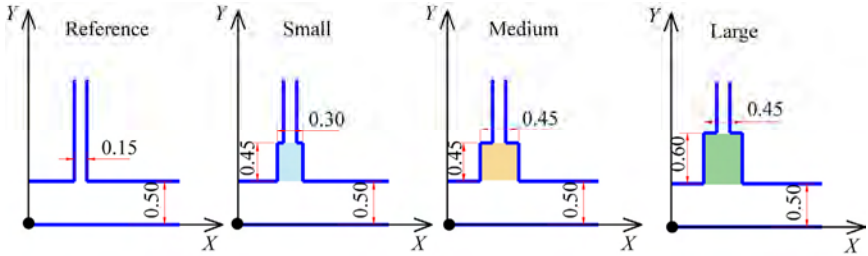

Figure 3-18: Configurations of the confluence zone (same reference axis as presented in Figure 3-15).

3.4 Tests procedure, instrumentation and measurements

For each test, a systematic procedure was followed. Before each experiment, a movable bed composed of the sediment material described in section 3.3.2 was put in place. The main and post-confluence channel beds are horizontal (Figure 3-19). In order to accelerate the development of the bed discordance, a step of 0.03 m is placed at the mouth of the tributary and the initial bed slope of the tributary is around 0.5%. The step and the slope are lower than the expected discordance and the theoretical slope calculated by means of the Meyer-Peter Formula (section 3.3.2). Hence, it forces a process of aggradation due to overloading in the tributary (Ribberink and Van der Sande, 1985; Seal et al., 1997).

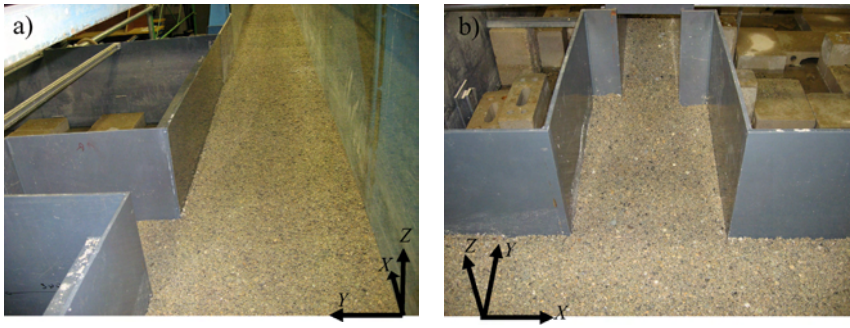

Figure 3-19: Example of the initial bed at the post-confluence channel and at the widened zones. The axes of the coordinate systems are not placed at the origin.

The constant water discharges are supplied by two independent pumps, connected upstream of each channel. The discharge in the main channel (Q_m) is measured by a calibrated V-notch weir, installed upstream of the inlet of the channel (Figure 3-20a) whereas the discharge of the tributary channel (Q_t) is measured by an electromagnetic flowmeter (Figure 3-20b). An adjustable tailgate at the end of the post-confluence channel is used to control flow depths within the flume (Figure 3-20c).

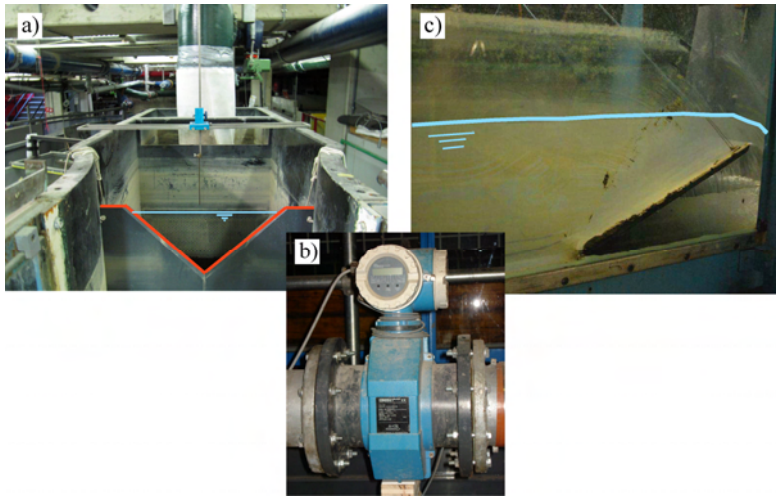

Figure 3-20: Instrumentation for controlling water discharges and downstream water elevation in the confluence flume. a) V-notch weir installed at the entrance of the main channel. b) Electromagnetic flowmeter installed at the entrance of the tributary channel. c) Adjustable tailgate placed downstream of the post-confluence channel to control water levels.

The sediment management system comprises four parts:

- Sediments are automatically supplied at the tributary by a conveyor belt 5 m long and 0.50 m wide installed upstream of the channel (Figure 3-21a).
- A timer, coupled with a velocity regulator device (Figure 3-21b), allows quite slow constant belt displacements (0.5 m/h).
- At the exit of the post-confluence channel, a sediment trap removes the sediment transported by the experiment (Figure 3-21c).
- A weighting scale, placed beside the sediment trap allows the control of the sediment volume feed and removed from the flume (Figure 3-21d).

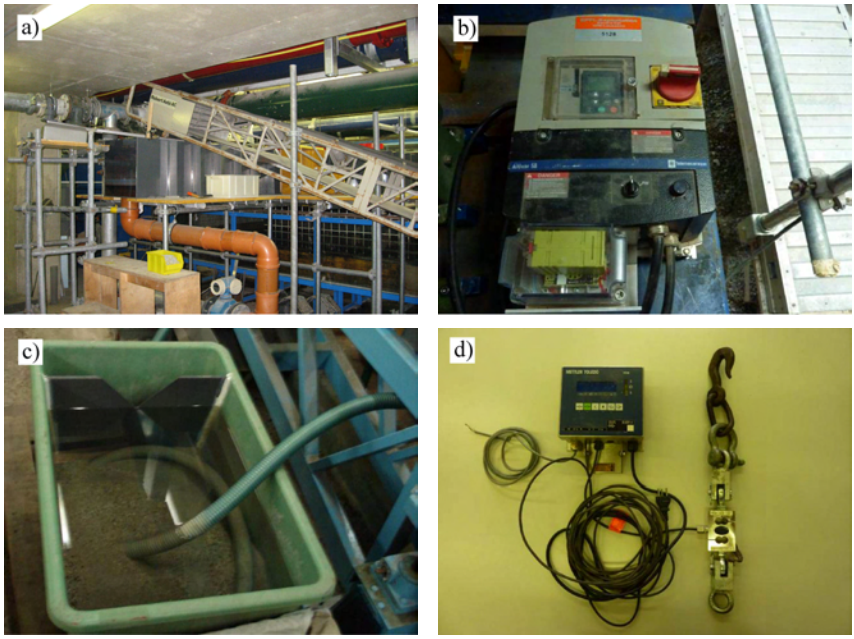

Figure 3-21: Instrumentation for sediment management during the experiments. a) Conveyor belt for the sediment feed, b) Velocity regulator for the conveyor belt. c) Sediment trap for removing the transported sediments. d) Scale used for the control of the sediment balance.

Before the beginning of each experiment, the flume is slowly filled in order to avoid sediment transport during this stage of the test. Once the system is full (water depth around 20 cm), both main and tributary discharges are adjusted to the required values. After that, the downstream tailgate is slowly lowered until the downstream water depth reaches 7 cm, which corresponds to the approximated normal depth of the flow, calculated interactively using

Manning-Strickler and the Meyer-Peter formulas for the given conditions (Q = 20 l/s, B = 0.50 m, Q_s = 0.30 kg/min and d_m = 2.3 mm).

Several campaigns of topographic surveys are performed during a run. Bed elevations are measured using a Mini EchoSounder probe (UltraLab UWS) that works with an ultrasonic-impulse-run time procedure with a precision of ±1 mm (Kantoush et al., 2008). The instrumentation is installed on a movable frame that covers part of the experimental set-up, 3.80 m in the main and post-confluence channels and 3.00 m in the tributary (Figure 3-15). The frame allows automatic movements in the X direction. For each series of measurement, 12 longitudinal profiles (ΔX= 9 mm) laterally spaced by 0.04 m are measured in the main and post-confluence channels. On the tributary, measurements are done in cross-sections spaced by 0.05 m near the tributary mouth (0.50 m<Y<0.95 m) and by 0.20 m in the upstream reach. For the reference configuration, the cross-sections of the tributary are rectangular and for this reason, only one point at the middle of the section is measured. In the enlarged zones, several cross sections in the X-direction spaced by 0.05 m are measured. As for the main and post-confluence channels, the distance of the measured points in each cross-section is 9 mm.

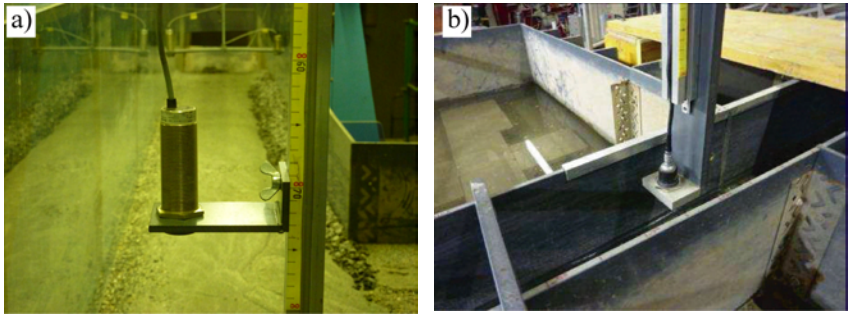

Figure 3-22: a) Ultrasonic limnimeter water level measurements and b) mini Echosounder for measuring the bed elevations.

As the MiniEchoSounder is an intrusive device, the sediment discharge is stopped and the water level in the confluence flume is slowly raised with the downstream tailgate before starting a bed topography survey. Water levels in the confluence flume are increased until the total halt of bed load transport. After obtaining the measurements, the contrary procedure is launched. The downstream tailgate is lowered and the solid discharge restarts. The increase/decrease of the water levels should be done carefully in order to avoid high velocity gradients and consequently sediment transport in the system that is not correlated to operational conditions.

Before starting the bed topography measurements, water levels in several cross-sections (depending on the configuration) on the tributary, main and post-confluence channels are recorded. Measurements are performed using automatic ultrasonic limnimeters (precision ±1 mm, Figure 3-22) during 10 s with a frequency of 128 Hz. For each point, an average value is considered for the analyses.

Each experiment was conducted until equilibrium conditions were reached. The achievement of equilibrium in each run is mainly assessed on the basis of the bed evolution between two times steps and takes between 22 and 24 hours. Sediment volume entering and leaving the flume are weighed and helps the decision of stopping the experiment.

Once the equilibrium is reached, flow visualization techniques relying on colour dye and video camera are used to help the identification of the interactions between flow, sediment transport and bed morphology. After that, the solid discharge is stopped and the water level is raised again. Both supply pumps are turned off and the confluence flume is slowly emptied. Subsequently, pictures of the final morphology are taken and different samples of the bed surface material (~200 g) are collected at different locations, depending on the configuration that is studied. A grain size analysis by means of a hand sieving is performed. The objective of the grain size analyses is to identity qualitatively the behaviour of the sediment deposition and sediment sorting in response to the flow conditions.

Previous to the beginning of a new run, the deposed sediments are removed and the bed is reconstructed with new sediments. Furthermore, in order to avoid the influence of the grain size segregation due to the run, sediments are not recycled.

For two of the runs, the low discharge with the reference configuration, so-called *Low-Reference* and low discharge with the small widening, so-called *Low-Small*, velocity measurements were performed once equilibrium conditions had been attained. For the entire duration of the measurements, the main and tributaries discharges, as well as the solid discharge were maintained constant. Non-intrusive measurements of velocity profiles were made with an Acoustic Doppler Velocity Profiler (ADVP) developed at EPFL. The working principle of the ADVP has been reported by Lemmin and Rolland (1997), Hurther and Lemmin (1998), Blanckaert and Graf (2001) and Blanckaert and Lemmin (2006). The ADVP consists of a central emitter surrounded by four receivers, placed in a water filled box that touches the water surface by means of an acoustically transparent mylar film. It measures profiles of the quasi-instantaneous velocity vector, $\vec{v}(t)=(u,v,w)(t)$, from which the time-

averaged velocity vector, $\bar{\bar{v}} = (\bar{u},\bar{v},\bar{w})$, the Reynolds stresses, $-\rho\overline{v_i'v_j'}$ $(i,j = x,y,z)$ and higher order turbulent correlations can be computed. Henceforward overbars on the time-averaged velocities will be dropped. Measurements were recorded with a sampling frequency of 31.25 Hz during a period of 180 s. Several cross sections were measured in the main and post-confluence channels. More details about the velocity measurements can be found in Chapters 5 (*Low-Reference* test) and 6 (*Low-Small* test).

A summary of the experimental runs is presented in Table 3-2. It shows the characteristics of each water discharge scenario and the confluence configurations, as well as the duration of each test and the time schedule where water levels and bed topography measurements were made. Time steps adopted for the water level and bed topography measurement campaign are not regularly spaced.

Table 3-2: Summary of the tested confluence configurations and discharge scenarios.

				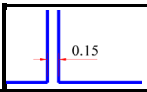				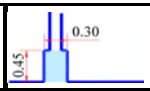				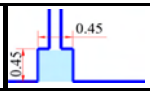				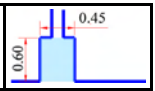			
Description				**Reference**				**Small**				**Medium**				**Large**			
Run	Q_m [ls^{-1}]	Q_t [ls^{-1}]	Qs_t [Kg/min]	**1**	**2**	**3**	**4**	**1**	**2**	**3**	**4**	**1**	**2**	**3**	**4**	**1**	**2**	**3**	**4**
Low discharge	18.0	2.0	0.30	23	23	1; 18; 21; 23	yes	22	22	1; 13; 17; 20; 22	yes	22	22	1; 16; 20; 22	no	22	22	1; 16; 20; 22	no
Intermediate discharge	17.4	2.6	0.30	23	1; 3; 11; 15; 19; 23	1; 3; 11; 15; 19; 23	no	23	23	1; 16; 20; 22; 24	no	22	22	1; 16; 20; 22	no	22	22	1; 16; 20; 22	no
High discharge	16.3	3.7	0.30	24	0; 24	1; 8; 17; 21; 24	no	22	22	1; 7; 16; 20; 22	no	22	22	1; 16; 20; 22	no	22	22	1; 16; 20; 22	no

Legend: 1) Test duration [h]
2) Time of water level measurements [h]
3) Time of bed elevation measurements [h]
4) Velocity measurements with ADVP [yes/no]

4. Test results

4.1 General observations

In this chapter, the results of the test *Low-Reference* (see Table 3-2) are used to illustrate the common hydro-morphological features observed in all experiments. For the widening tests, there is an important variability of the morphological responses in the widened zones which depends on the discharge ratio and the widening shape. Therefore, it is not discussed in this chapter. The analyses of the complete database, including the interaction between the hydro-morpho-sedimentary features at equilibrium are reported in Chapters 5, 6 and 7.

The main common morphological features at equilibrium can be described as follows:

- Deposition bar: For all experiments, there is formation of a deposition bar along the inner bank downstream of the confluence. The bar reaches its maximum elevation near the inner bank just downstream of the confluence. Hence, bar height decreases downstream. Figure 4-1 shows the equilibrium topography of the entire measurement domain ($0<X<3.8$ m and $0<Y<3.5$ m) for the test *Low-Reference*. Figure 4-2a shows an upper view of the main and post-confluence channels where the sediment bar developed for the same test can be recognized.
- Bed discordance: As illustrated by Figure 4-2b, significant bed discordance between the mouth of the tributary and the main channel is observed.
- Absence of marked scour hole: In all tests no important scour hole at equilibrium was observed, which differs considerably from the existing morphologic models of confluences (Best, 1988). There is only a slight erosion that occurs along the sediment bar near the outer bank of the post-confluence channel (Figure 4-2).
- Grain sorting: In the confluence zones, there is an important grain sorting of the sediments forming the bed surface. The differences of the sediment characteristics can bed observed in the pictures shown in Figure 4-2b and in the grain size distributions depicted in Figure 4-3.

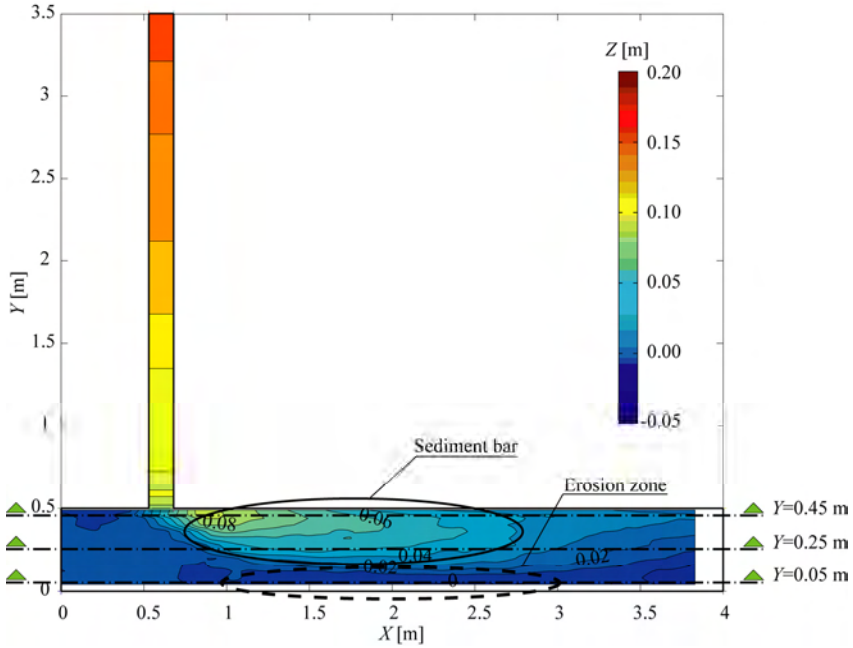

Figure 4-1: Bed elevations of the entire measurement domain 0<X<3.8 m and 0<Y<3.5 m for the test Low-Reference (Qr = 0.11). The locations of the longitudinal profiles presented in Figure 4-4 are indicated by the dashed lines. Sediment bar is delimitated by the full ellipse whereas the erosion zone is indicated by the dashed ellipse.

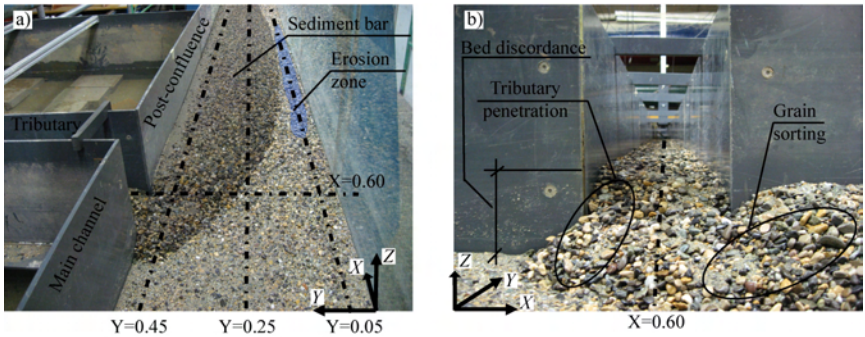

Figure 4-2: a) Upper view of the main and post-confluence channels for the test Low-Reference (Qr=0.11) showing the sediment bar, the erosion zone and the positions of the cross-sections shown in Figure 4-4 and b) upstream view of the tributary channel showing the bed discordance and the grain sorting.

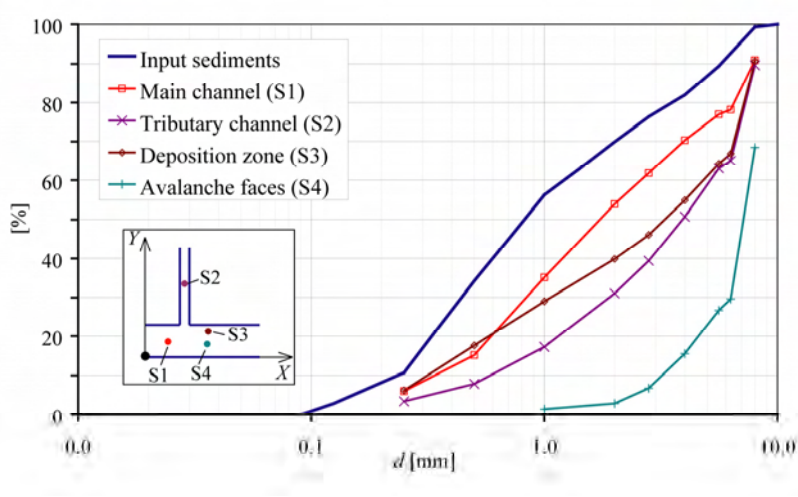

Figure 4-3: Sample locations at the confluence zone and their respective grain size distributions for the test Low-Reference.

Concerning the common flow features, the following behaviours can be highlighted:

- Flow stagnation zone: The deflection of both confluents creates a flow stagnation zone at the upstream corner of the confluence (Figure 4-4a and Figure 4-5). It can be recognized by the increase in the flow depth.
- Backwater effects on the main channel: The presence of the deposition bar reduces the flow sectional area immediately downstream of the confluence. It produces an increase of the upstream flow energy that is followed by a water level raise and a decrease of the energy gradient (Figure 4-4b, c). The decrease of the energy gradient can be noticed by the steadiness in the water levels upstream of the confluence.
- Flow acceleration: The reduction of the flow sectional area induces flow acceleration along the sediment bar (Figure 4-4).
- Shear layer zone: For all experiments, shear layers are developed in the contact of the confluent flows. Figure 4-5 illustrates an upper view showing the shear layer zone at the surface of the flow for the run *Low-Reference*.

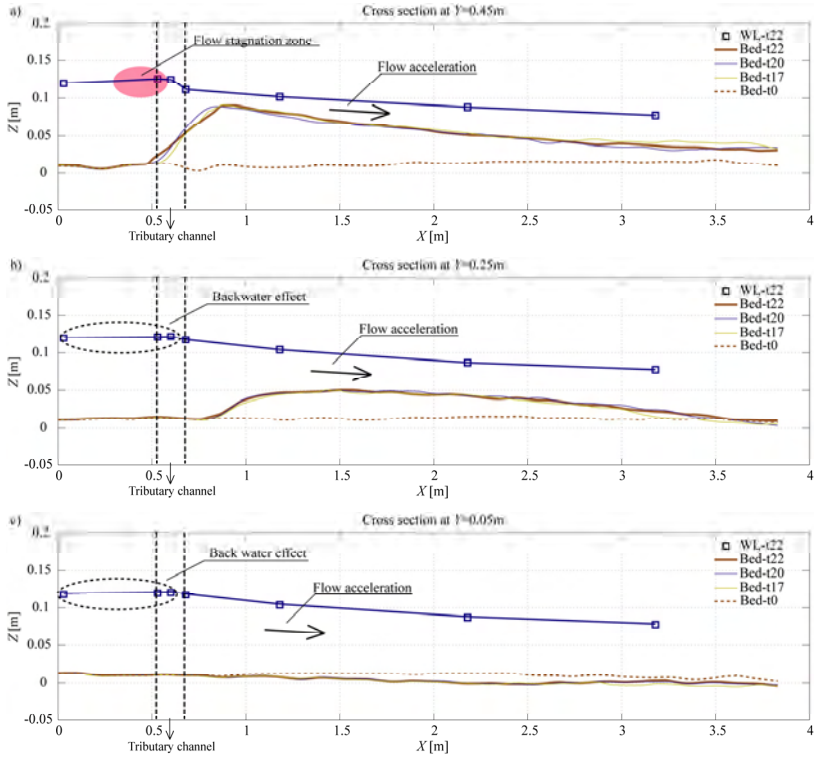

Figure 4-4: Longitudinal profiles of the water surface elevation and the equilibrium bed elevation measured in different time-steps at Y= 0.45 m (near the outer bank), Y = 0.25 m (axis of the channel) and Y = 0.05 m (near the inner bank). The initial bed elevations are indicated by the dashed lines. The flow stagnation zone (shadow ellipse), the backwater effects (dashed ellipses) and the flow acceleration (arrow) are indicated in the longitudinal profiles.

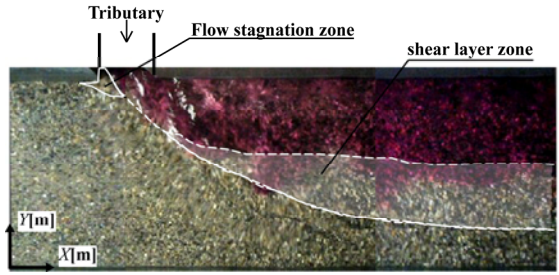

Figure 4-5: Flow visualization of the main and post-confluence channels for the run Low-Reference. Colour dye is only injected in the tributary.

4.2 Systematic documentation of all tests. Description of the Appendixes

The results of each test are systematically presented in the Appendixes at the end of the report. Each Appendix is structured in a standard form and corresponds to a certain test. The twelve appendixes are listed in Table 4-1.

Table 4-1 : List of the Appendixes

			Windening		
Appendix	**Test**	***Qr***	B_w	L_w	
A	*Low-Reference*	0.11	-	-	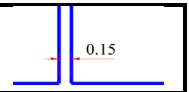
B	*Intermediate-Reference*	0.15			
C	*High-Reference*	0.20			
D	*Low-Small*	0.11	0.30	0.45	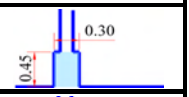
E	*Intermediate-Small*	0.15			
F	*High-Small*	0.20			
G	*Low-Medium*	0.11	0.45	0.45	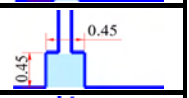
H	*Intermediate-Medium*	0.15			
I	*High-Medium*	0.20			
J	*Low-Large*	0.11	0.45	0.60	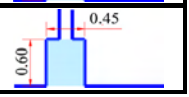
K	*Intermediate-Large*	0.15			
L	*High-Large*	0.20			

Each Appendix (*[1])is divided in the following sections:

- *.1: Summary of the test including the initial hydro-sedimentary conditions (sub-section *.1.1), the equilibrium flow depths measured at different points in the flume (sub-section *.1.2) and the main morphological features including the bed discordance (measured at the mouth of the tributary at X=0.60 m), the maximum elevation of the bar and the volume of sediments deposed above the elevation curve Z=0.02 m. (sub-section *.1.3). This elevation is considered as reference for the calculation of the deposited sediment volumes for all experiments;
- *.2: Bed topography maps of the entire measurement domain ($0<X<3.8$ m and $0<Y<3.5$ m) measured at different time-steps;
- *.3: Longitudinal and cross-sections showing the bed elevations and water levels measured in different locations at different time-steps. The longitudinal profiles along the main and post-confluence channels at Y=0.05 m, Y=0.25 m and Y=0.45 m and

[1] Is a placeholder for the Appendix's name: *A* to *L* (see Table 4-1).

longitudinal profile along the axis of the tributary (X=0.60 m) are presented in the sub-section *.3.1. The sub-section *.3.2 illustrates four cross-sections of the widened zone, two along the Y-direction (X=0.50 m and X=0.72 m for the Small tests and X=0.44 m and X=0.76 m for the Medium and Large tests) and two along the X-direction at the tributary mouth (Y=0.54 m and Y=0.64 m). This section is only presented for the widened tests (Appendixes *D-L*);

- *.4: Pictures showing the surface flow in the main and post-confluence channels at the equilibrium conditions. Colour dye is injected in the tributary;
- *.5: Pictures of the confluence zone showing the equilibrium bed morphology;
- *.6: Grain size distributions of the different bed samples.

This systematic documentation of all tests is beside the analyses of the following chapters, a ride and useful database for validation and calibration of morphodynamic numerical models.

5. Flow and sediment dynamics in channel confluences*

* This chapter has been submitted for publication in the Journal of Geophysical Research – Earth Surface.

5.1 Introduction

In fluvial networks, confluences are associated with significant changes in flow dynamics, sediment transport and bed morphology. Understanding the hydro-morpho-sedimentary processes at confluences is important in river management and engineering, and relevant with respect to hazard mitigation, ecological diversity, river training and/or rehabilitation projects. The hydrodynamics as well as the sedimentological and morphological processes in confluence zones involve several variables (Gurram et al., 1997, Huang et al., 2002), such as the number of adjoining channels, the confluence angles, the shape and slope of the channels, the discharge and momentum flux ratios, the bed material, the sediment supply, the planform of the confluent channels etc. Laboratory experiments are commonly carried out in simplified schematized configurations that allow isolating and/or accentuating certain parameters and processes under controlled conditions.

Best (1987) presented a descriptive model of the flow dynamics at confluences based on laboratory experiments conducted in a small flume with two 0.15 m adjoining channels of rectangular cross-section. These experiments were performed with several confluence angles and discharge ratios under fixed horizontal bed conditions without sediment transport. The tributary and main channels were bed concordant, i.e., the tributary and main channels' mouth elevations were the same. His model distinguished six different zones in confluence channels: flow deflection, flow stagnation, flow separation, maximum velocity, shear layer and flow recovery (Figure 5-1). The flow stagnation zone is created by a deflection of both streams at their junction and is associated with an increase of pressure and flow depth and a decrease of flow velocities and shear stresses. The directional change of the tributary creates a zone of flow separation with horizontal recirculation due to the flow detachment from the inner wall in the post-confluence channel and its reattachment further downstream (Best and Reid, 1984). The geometry of the separation zone is important because it delimits the effective width of the post-confluence channel and is an area of reduced pressure and recirculating flow where sediment tends to accumulate. The maximum velocity zone appears downstream of the junction of the flows at the contracted cross-section besides the separation zone. Shear layers are formed along the contact of the zones of flow separation and of maximum velocity, and they are characterized by high turbulence intensities and shear stresses and also the presence of well-organized flow structures (Biron et al., 1993, De Serres et al., 1999, Sukhodolov and Rhoads, 2001, Rhoads and Sukhodolov, 2004, Boyer et al., 2006). As the shear layer expands

laterally and dissipates, the flow recovers towards a straight shear flow in the post-confluence channel.

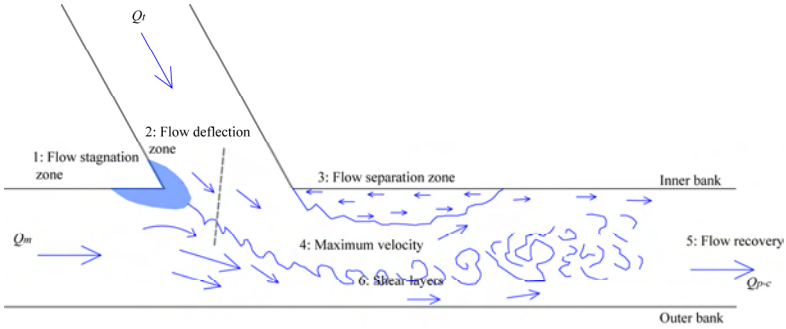

Figure 5-1: Descriptive model of flow dynamics at a channel confluence with concordant beds (slightly modified from Best, 1987).

Flow at river confluences is highly three-dimensional and often characterized by the presence of helical flow cells. The nature and characteristics of these cells have been the subject of a long-standing debate (Mosley, 1976; Ashmore and Parker, 1983; Fujita and Komura, 1989; Rhoads and Kenworthy, 1995; McLelland et al., 1996; Bradbrook et al., 1998; Bradbrook et al., 2000a; Bradbrook et al., 2000b; Lane et al., 2000; Rhoads and Sukhodolov, 2001; Weber et al., 2001b; Parsons et al., 2007; Biron and Lane, 2008). Their presence/absence, the number of cells as well as their intensity depend on many parameters, such as the confluence angle, the water discharge ratio between the tributary and main channels and the bed discordance between the tributary and main channels mouths. Mosley (1976) was the first to observe and describe the helical cells based on experiments in a laboratory flume. In his set-up, the post-confluence channel had been cut in erodible material and was free to adjust to the experimental solicitations. He described two “back to back” helical cells which converge at the surface in the centre of the channel and diverge near the bed and are often associated with the confluence scour. Rhoads and Sukhodolov (2001) support the fact that helical cells can be present in a confluence zone, but claim that they are not characteristic features of all confluences. Bradbrook et al. (2001) have investigated by means of three-dimensional numerical simulations the roles of channel planform curvature and bed discordance in the formation of helical cells. They have shown that in some cases, a single helical cell forms as the flows join, which is consistent with laboratory measurements by Weber et al. (2001b). The majority of foregoing experimental research on confluences uniquely considered the flow field over fixed and flat bed topography. The few existing laboratory studies on bed

morphology at channel confluences include Ashmore and Parker (1983), Best, (1988) and Mosley (1976). Best (1988) was the first to present a conceptual model of the bed morphology, based on systematic experimental tests performed in asymmetrical confluences with equal channel widths (0.15 m) and concordant beds. Several discharge ratios (around 0.5 to around 1.5) and different confluence angles between the tributaries (15° to 105°) were considered. Well-sorted sand was used for the bed constitution and sediment supply. Best's (1988) conceptual model was further refined by Best and Rhoads (2008), who described the bed morphology of river confluences by five main features that are directly linked to the flow dynamics discussed above: 1) a scour hole, associated to the increase of flow velocity and turbulence within the confluence zone; 2) tributary mouth bars with associated avalanche faces formed at the mouth of one or both tributaries and often sloping into the scour hole; 3) a mid-channel bar; 4) bank-attached lateral bars, associated with regions of flow deceleration and/or flow separation and 5) a region of sediment accumulation near the upstream corner, probably associated with the flow stagnation zone. Figure 5-2 illustrates the first, second and fourth features. Best (1988) suggested that the major controls of these features are the junction angle and the discharge ratio, while for Rhoads and Kenworthy (1995) the bed morphology of small confluences is highly responsive to changes in the momentum flux ratio $Mr=\rho QU_t/\rho QU_m$ between the main *(*subscript *m*) and the tributary (subscript *t*) channels where ρ is the water density (kgm^{-3}), Q the discharge (m^3s^{-1}) and U the mean velocity (ms^{-1}).

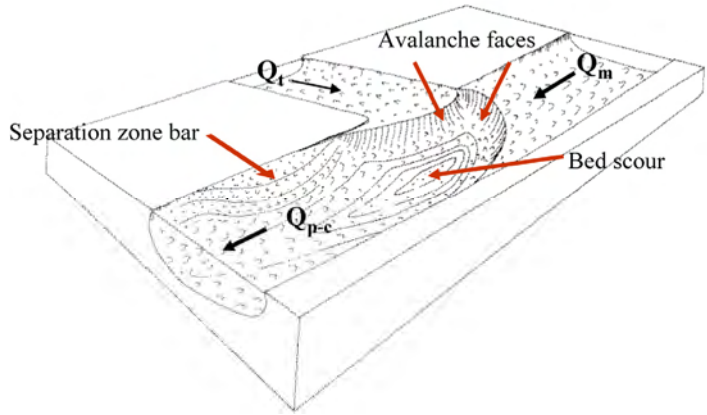

Figure 5-2: Schematic bed morphology of an asymmetric confluence with bed concordance proposed by Best (1988).

The consideration of confluences with discordant beds is relatively recent, even if this characteristic morphology is common in nature (Kennedy, 1984). Different from the bed concordant confluences discussed above, bed discordant confluences are those where the tributary and main channels mouth elevations are not the same. Field measurements (Biron et al., 1993; Gaudet and Roy, 1995; De Serres et al., 1999), laboratory experiments (Best and Roy, 1991; Biron et al., 1996a; Ghobadian and Bajestan, 2007), and numerical modelling (Bradbrook et al., 2001; Biron et al., 2004) have demonstrated that the presence of a bed discordance between the confluent channels modifies considerably the flow in a confluence zone, affecting the sediment transport and the bed morphology. In addition, it can increase the turbulence intensity in the shear layer and consequently increase flow mixing downstream of the confluence (Gaudet and Roy, 1995; Biron et al., 2004). By means of field measurements, Leclair and Roy (1997) proposed different models of the hydro-morpho-sedimentary dynamics at a confluence with discordant beds during low flow and high momentum flux ratio, $Mr \geq 1$. Their models relate variations of the tributary mouth bar to changes in Mr and distinguishes between a phase of bar erosion for $Mr \sim 1$ and a phase of bar construction and full bar extension for $Mr >> 1$. Recently, Boyer et al. (2006) analysed in detail the flow structure and its interaction with sediment transport and bed morphology at the same river confluence and proposed two conceptual models of sediment transport and morphological changes, one for $Mr > 1$ and the other for $Mr < 1$.

In spite of these advances in the understanding of the dynamics of confluences, very little attention has been devoted to steep river channel confluences with coarse bed material that can be found in alpine environments. Mountain torrents carrying large sediment loads often meet asymmetrically the main channel at the valley bottom at a large angle. These characteristics, associated to the relative low discharge and momentum flux ratios present important challenges, most notably for flood protection, hazard mitigation and river rehabilitation. Current knowledge on river channel confluences may not be applicable to these situations. Therefore, the objectives of this paper are:

- To observe, measure and quantify the morphologic, sediment transport and flow processes in controlled laboratory settings that are representative of confluences such as those found in alpine environments;
- To gain insight in the interacting hydro-morpho-sedimentary dynamics channel confluences.

5.2 The experiment

The experimental design, the sediment characteristics and the flow and sediment discharges are representative of the main confluences of the Upper Rhone River, upstream of the Lake Geneva in Switzerland. Because the banks of the Upper Rhone River are stabilized and the bed is armoured, the main sediment supply is provided by the steep tributaries at high flows. A summary of the geometric as well as the discharges characteristics of the Upper Rhone's 20 main confluences is presented in Table 5-1, where *B* is the channel width, *Q2* and *Q5* represent the two and five year return period floods, respectively and the subscripts *t*, *m* and *p-c* represents the tributary, main and post-confluence channels respectively (Figure 5-3). The Froude numbers at the tributary (Fr_t) and the momentum flux ratios (*Mr*) between the tributary and the main channels estimated for *Q2* and *Q5* are also shown in Table 5-1.

Table 5-1 : Geometrical and hydraulic characteristics of the main confluences of the Upper Rhone River in Switzerland.

	Angle [°]	B_t/B_m	B_m/B_{p-c}	*Tributary bed slope [%]*	$Q2_t/Q2_m$	$Q5_t/Q5_m$	Fr_{tQ2}	Fr_{tQ5}	M_r_Q2	M_r_Q5
Average	62	0.22	1.02	1.1%	0.10	0.09	0.83	0.83	0.11	0.08
Max	90	0.54	1.27	4.0%	0.32	0.31	1.29	1.30	0.45	0.30
Min	30	0.07	0.71	0.0%	0.01	0.01	0.03	0.03	0.01	0.01

The experimental facility consists of a confluence flume with smooth vertical banks where the main channel is 8.5 m long and 0.50 m wide. The 4.9 m long and 0.15 m wide tributary channel is connected at an angle of 90° to the main channel 3.60 m downstream of the inlet (Figure 5-3). The results discussed in this paper are related to the reference axes (*X*, *Y*, *Z*) represented in Figure 5-3.

The intersection angles of the tributaries with the upper Rhone River are highly variable (Table 5-1). For the present project, the maximum value of 90° has been adopted. The ratio of the tributary width to the main channel width of $B_t/B_m = 0.3$ and of the main channel width to the post-confluence channel width of $B_m/B_{p-c} = 1$ are representative of the confluences in the Upper Rhone River.

Sediment characteristics and the flow and sediment discharges were also chosen such that conditions were as close as possible to those encountered in the confluences of the upper Rhone River. Flow discharges in the main channel and the tributary were $Q_m = 18$ ls^{-1} and $Q_t = 2$ ls^{-1}, respectively, leading to a discharge ratio of $Q_t/Q_m = 0.11$, width-to-depth ratios in the main channel, the post-confluence channel and the tributary of 5, 7 and 9, respectively (Table 5-2), and a momentum flux ratio of $Mr = 0.20$. Flow was rough turbulent,

$Re_*=u_*k_s/\nu>70$, in the main, tributary and post-confluence channels. Re_* represents the particle Reynolds number, u_* the shear velocity [m/s] defined as $u_* = \sqrt{gHE_s}$ where H and E_s are the average flow depth and the energy gradient, k_s is the characteristic particle size [m] and ν is the kinematic viscosity [m^2s^{-1}].

The sediment characteristics satisfy two requirements: (*i*) they yield a longitudinal slope in the tributary that can be found in the Upper Rhone basin; (*ii*) their grain size distribution is representative of alpine environments. Poorly-sorted sediments with d_{50} = 0.82 mm, d_{90} = 5.7 mm and a sorting coefficient of σ = 0.5 ($d_{84}/d_{50} + d_{50}/d_{16}$) = 4.15, were used for the bed material and the solid discharge. The particle size distribution of the sediment is shown in Figure 3. The ratio between flow depth and median grain diameter of the bed (h/d_m) varies from 5 (tributary) to 48 (main channel). These values are representative of those found in the Upper Rhone basin.

Table 5-2 : Characteristics of the experiment

Q_m [ls^{-1}]	Q_t [ls^{-1}]	Q_t/Q_m	Qs_t [kg/min]	Fr_m	Fr_t	$Fr_{p\text{-}c}$	M_r	h/d_m			B/h		
								Main	Trib.	Post-confl.	Main	Trib.	Post-confl.
18.0	2.0	0.11	0.3	0.32	1.30	0.70	0.2	48	5	19	5	9	7

The bed was initially covered with the poorly sorted sediment mixture in the main channel and the tributary. Before the beginning of the run, the bed was flattened in the main and post-confluence channels and had an initial longitudinal slope of around 0.05% in the tributary near its mouth. Constant water discharges of 18 ls^{-1} and 2 ls^{-1} were provided to the main channel and the tributary, respectively, and a constant solid discharge of 0.3 kg/min was fed to the tributary only. An adjustable tailgate at the end of the post-confluence channel controlled the flow depth within the entire flume. The water level at the end of this channel was kept constant at 0.07 m. During the experiment, sediment volumes entering and leaving the flume were weighed. Achievement of equilibrium was assessed on the basis of changes in the bed morphology and of the sediment budget. Equilibrium conditions occurred 22 hours after the beginning of the experiment.

The flow, sediment dynamics and topography in confluences vary in time in a continuous adaptation to intermittent floods in the main and tributary channels. Their variations can be interpreted as fluctuations superimposed on a dynamic state of equilibrium that corresponds to a long-term average. The adoption of constant flow and sediment

discharges in the experiments is intended to investigate this long-term averaged state of dynamic equilibrium.

Water levels and bed topography were respectively measured during the experiments with ultrasonic gauges and a Mini EchoSounder (Kantoush et al., 2008). Instruments were installed on a movable frame that covered a region of 3.80 m by 3.00 m in the confluence zone as shown in Figure 5-3. Upstream flow discharges were accurately measured by means of a calibrated V-notch weir on the main channel and a digital flow meter on the tributary channel, respectively. At the end of the experiment, samples of the surface bed material were collected at four different locations (S1, S2, S3 and S4 shown in Figure 5-3). Grain size analysis by means of hand sieving was carried out.

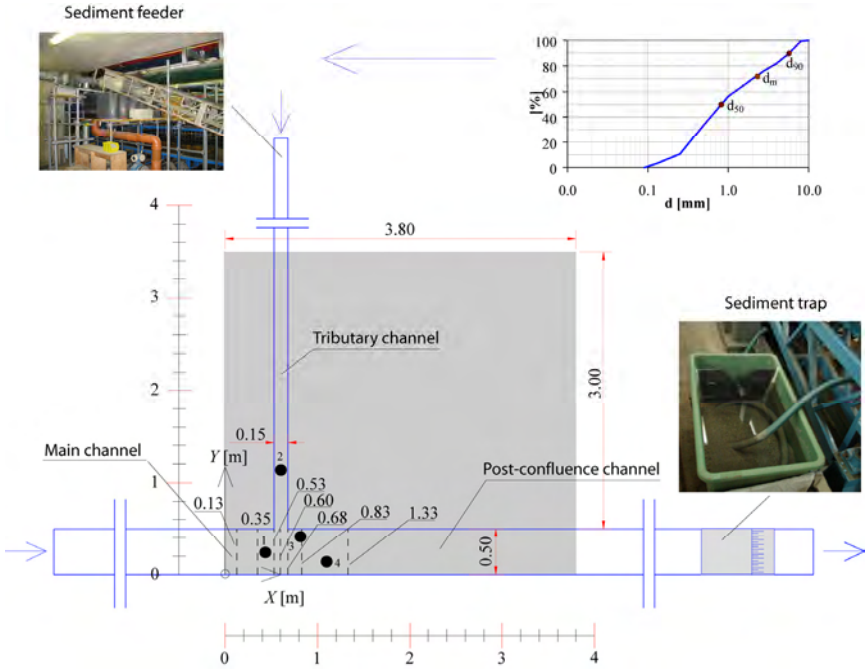

Figure 5-3: Experimental facility and sieving curve of the sediment. The locations of the cross sections where velocity measurements were performed are indicated by the dashed lines and the locations of the bed samples by the dark circles. The limit between the main channel and the post-confluence channel is the tributary axis at X = 0.60 m.

Velocity measurements were performed once equilibrium conditions had been attained. For the entire duration of the measurements, the main and tributary discharges, as well as the solid

discharge were maintained constant. Non-intrusive measurements of velocity profiles were made with an Acoustic Doppler Velocity Profiler (ADVP) developed at École Polytechnique Fédérale Lausanne (Switzerland). The working principle of the ADVP has been reported by Lemmin and Rolland (1997), Hurther and Lemmin (1998), Blanckaert and Graf (2001) and Blanckaert and Lemmin (2006). The ADVP consists of a central emitter surrounded by four receivers, placed in a water filled box that touches the water surface by means of an acoustically transparent mylar film. It measures profiles of the quasi-instantaneous velocity vector, $\vec{v}(t) = (u,v,w)(t)$, from which the time-averaged velocity vector, $\vec{\bar{v}} = (\bar{u}_x, \overline{u_y}, \overline{u_z})$, the Reynolds stresses, $-\rho\overline{u'_i u'_j}$ (i,j = x,y,z) and higher order turbulent correlations can be computed. Henceforward overbars on the time-averaged velocities will be dropped. Measurements were recorded with a sampling frequency of 31.25 Hz during a period of 180 s. Seven cross-sections were measured: three in the main channel (X = 0.13 m, X = 0.35 m and X = 0.53 m), one in the axis of the tributary (X = 0.60 m) and three in the post-confluence channel (X = 0.68 m, X = 0.83 m and X = 1.33 m). Their locations are presented in the Figure 5-3. The transverse spacing of the measured profiles was 1.5 cm (Figure 5-4).

Blanckaert and Lemmin (2006) have shown that a configuration with a central emitter symmetrically surrounded by four receivers at an angle of 45° with respect to the principal flow direction gives redundant information in all three velocity components and is optimal with respect to noise reduction and temporal resolution. This symmetrical configuration, however, only allows us to measure in the central region of the channel (0.16 m<Y<0.35 m). Near the outer (0.06 <Y<0.16 m) and the inner (0.35 m<Y<0.45 m) banks, measurements were made with an asymmetrical configuration of the ADVP (Figure 5-4). The asymmetrical configuration, however, only gives redundant information in the streamwise velocity component and is characterized by a higher noise level than the symmetrical one. This noise does not affect the time-averaged velocities, but it significantly biases the turbulent normal stresses and the estimation of the turbulent kinetic energy (*tke*), as described by Blanckaert and Lemmin (2006).

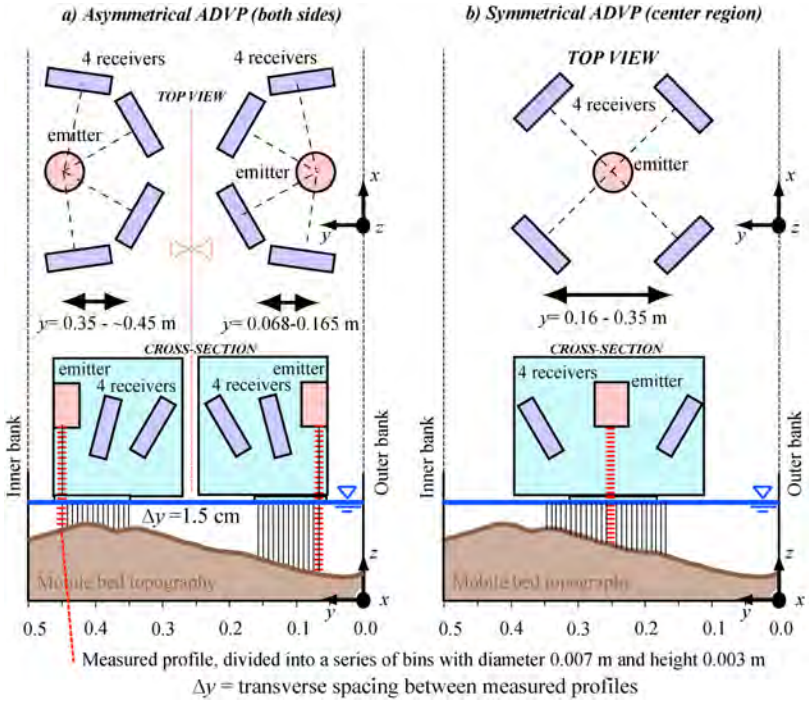

Figure 5-4: Top views and cross-sections showing the asymmetrical (a) and symmetrical (b) configurations of the ADVP and the correspondent measurements grids.

Therefore, results on the turbulence properties of the flow reported in the present paper will uniquely be based on measurements with the symmetrical ADVP configuration in the central zone of the cross-section. Blanckaert (2010) describes in detail the working principle as well as the data treatment procedures for measurements with both ADVP configurations. He quantified the uncertainty in the measurement of the mean flow and turbulent flow quantities, which can be summarized as follows: about 4% in the time-averaged longitudinal velocity u_x, about 10 % in the cross-stream velocities (u_y,u_z), about 20% in the turbulent normal stresses and the *tke*. The uncertainty in turbulence measurements increases progressively towards the bottom in the lower 20% of the water column. The uncertainty in depth-averaged mean velocities is estimated at less than 10%.

5.3 Bed morphology, water surface topography and sediment transport at equilibrium

Figure 5-5a shows a view on the equilibrium bed morphology in the main and post-confluence channels as well as part of the tributary channel. The installed longitudinal slope of 0.5% and the water discharge of 2 ls^{-1} in the tributary were initially unable to transport the supplied sediment. As a result, the longitudinal slope in the tributary increased to an equilibrium value of about 1.9% which was able to transport the sediment discharge. At equilibrium, the flow in the tributary is uniform and supercritical (Fr = 1.30) with a flow depth of about 0.02 m (Figure 5-5b) and velocities of about 0.6 ms^{-1}. Flow in the main and post-confluence channels is subcritical, with Fr = 0.35 and 0.9, respectively. This leads to a change of flow regime at the tributary mouth by means of a weak undulated hydraulic jump (Chow, 1959) that only induces a very small difference in water level elevations at the confluence mouth.

During the slope adjustment from the initial to the equilibrium bed slope, the tributary severely aggraded resulting in a pronounced discordance of about 0.09 m between the bed levels of the tributary and the main channel, which corresponds to 80 % of the flow depth in the main channel upstream of the confluence and to more than four times the flow depth in the tributary. This bed discordance, which is clearly illustrated by the longitudinal profiles in the axis of the tributary (Figure 5-5b) is one of the most characteristic features of the bed morphology in alpine confluences. This characteristic has not yet been observed or documented in foregoing laboratory studies on the morphology of river confluences (Mosley, 1976; Ashmore, 1982; Ashmore and Parker, 1983; Best, 1988), which uniquely concerned concordant beds.

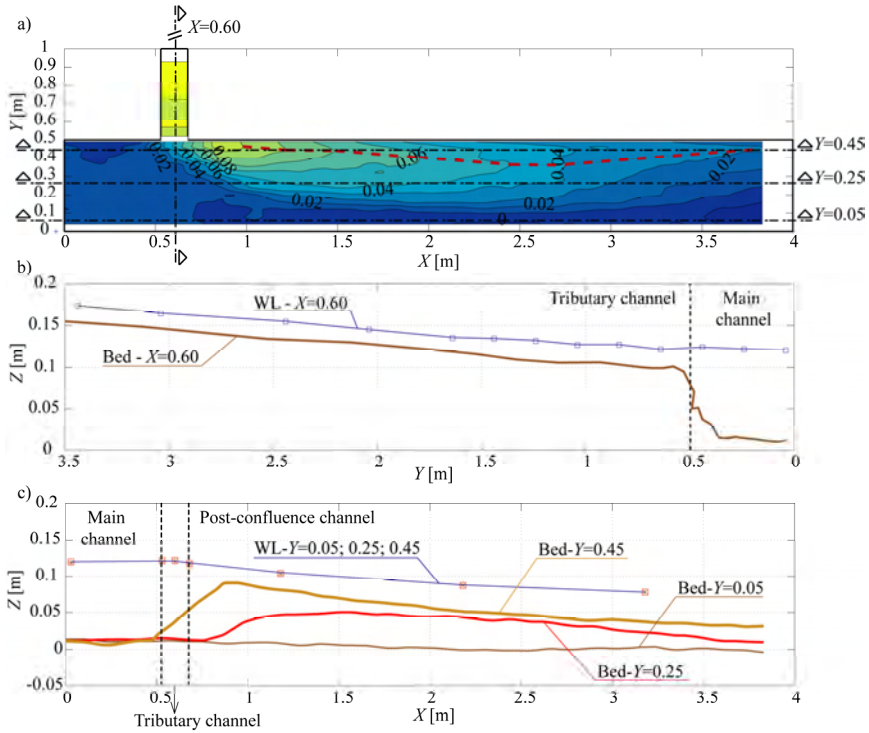

Figure 5-5: Equilibrium bed topography (t22) at the main and post-confluence channels (a). Longitudinal profiles of the water surface elevation and the equilibrium bed elevation at X = 0.60 m (axis of the tributary) (b) and Y= 0.05 m (near the outer bank), Y = 0.25 m (axis of the channel) and Y = 0.45 m (near the inner bank) (c). The initial level is indicated by the dashed line.

Longitudinal profiles in the main and post-confluence channels near the outer bank (Y = 0.05 m), at the centre (Y = 0.25 m) and near the inner bank (Y = 0.45 m) illustrate the evolution of the morphology from the initial to the final state, as well as the equilibrium water level (Figure 5-5c). For the present experiment, no scour occurs in the confluence zone and only a very slight depression occurs near the outer bank in the post-confluence channel. The sediment discharge provided by the tributary builds up an important sediment deposition bar near the inner bank. Just downstream of the tributary mouth ($X \approx 0.85$ m), this bar reaches its maximum height at the inner bank of about 0.09 m, which is comparable to the discordance step height (Figure 5-5b). At the location of its maximum height, the bar (level > 0.02 m) occupies about half of the width of the post-confluence channel. Further downstream, the maximum height of the bar decreases and it is found at some distance from the inner bank,

thereby creating a small depression adjacent to the inner bank that corresponds to a corridor of fine sediment transport, as indicated by the red dashed line at the crest of the bar. Moreover, the bar widens from the confluence mouth to reach its maximum width at about X = 2.6 m. Downstream of this cross-section, the morphology recovers towards a flat bed. Pronounced transverse slopes occur on the faces of the bar, especially in the confluence zone. At the axis of the tributary (X = 0.60 m) the slope of the face is around 47% (~25°) while at the cross-section of maximum bar height the slope of the avalanche face is around 36% (20°). These slopes are slightly lower than the angle of repose of gravel (~40°). The lateral slopes and the volume of the deposited material decrease considerably downstream.

Figure 5-6 illustrates the preferential corridors of sediment transport based on visual observations. In the absence of a scour hole, sediment is transferred on the face of the bar near the downstream apex of the confluence (Figure 5-6a). The corridor of sediment transport widens in the downstream direction and occupies the entire width of the post-confluence channel from the cross-section at X = 2.6 m. Pathways correspond to those of Best (1988) for high-angle confluence. Visual observations (Figure 5-6) clearly show a segregation of the transported sediment in the confluence zone. The face of the bar is covered by the coarse fraction of the sediment mixture. But this coarse sediment is segregated and its diameter increases from the top towards the toe of the deposition bar face. This grain sorting can be explained by the balance of the upslope drag force and of the downslope gravitational force on the grains: the former scales with the square of the sediment particle diameter whereas the latter scales with the cube of the sediment particle diameter (Sekine and Parker, 1992). Both forces are in equilibrium for the average particle diameter found on the bar face, whereas the downslope/upslope forces are dominant for larger/smaller particles.

The morphological depression at the inner bank in the post-confluence channel coincides with a corridor of transport of fine sediment shown in Figure 5-6b. Visual observations shows that these fine sediments are lifted to the upper part of the water column by vertical spiral vortices that are locally generated at the downstream corner of the confluence. This corridor of fine-sediment transport is much narrower than the bank-attached lateral bar that is often associated with a region of flow recirculation in Best's (1988) conceptual model. We did not observe flow recirculation in this zone during the present experiment.

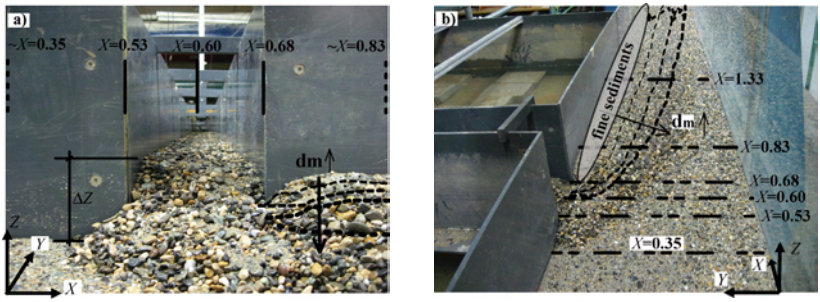

Figure 5-6: View upstream into the tributary from the confluence zone (a) and view downstream into the post-confluence channel (b) showing the preferential corridors of sediment transport.

Grain sorting in the confluence zone is further illustrated by means of some grain size distributions (Figure 5-7) sampled at the bed surface (see Figure 5-3 for locations), in the main channel (S1), in the tributary (S2), on the top of the sediment deposition bar (S3) and on the face of the sediment deposition bar (S4). All of the sampled grain size distributions are coarser than the input sediment mixture, which is due to the transport of the fine sediment with a diameter of less than about 0.15 mm. With the exception of some deposition in the inner-bank corridor (Figure 6b), these fine sediments are washed out of the flume. As aforementioned, the bed in the main channel upstream of the confluence is armoured, with a d_{50}≈1.8 mm at the surface that is considerably larger than the one of the input sediment mixture, d_{50}≈0.8 mm. The bed surface in the tributary (S2) is constituted by a coarse armour layer where d_{50} ~ 4 mm and d_{90} ~ 8 mm. Sediment sorting is illustrated by the sediment on top of the bar (S3: d_{50}~3 mm) that is finer than the tributary sediment, whereas the sediment on the face of the deposition bar is coarser (S4: d_{50}~7 mm).

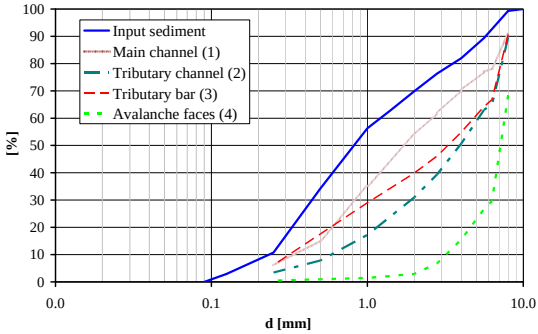

Figure 5-7: Grain size distribution of the input sediment and the different samples. The sampling sites are localized in Figure 5-3.

5.4 Flow dynamics

5.4.1 The depth-averaged flow field

The presence of the confluence causes considerable redistribution of the main channel flow. Figure 5-8 shows the patterns of the depth-averaged unit discharge (U_xh,U_yh) and the depth-averaged velocities (U_x,U_y), plotted over the bed topography in the confluence zone. Here h represents the local flow depth. Upstream of the confluence, the flow distribution is about symmetrical and typical for flow in rather narrow open-channels (see further details in section 5.4.2). The confluence globally causes a gradual outwards redistribution of the discharge. In the cross-section at X = 1.33 m the unit discharge at the outer bank is more than three times higher than at the inner bank.

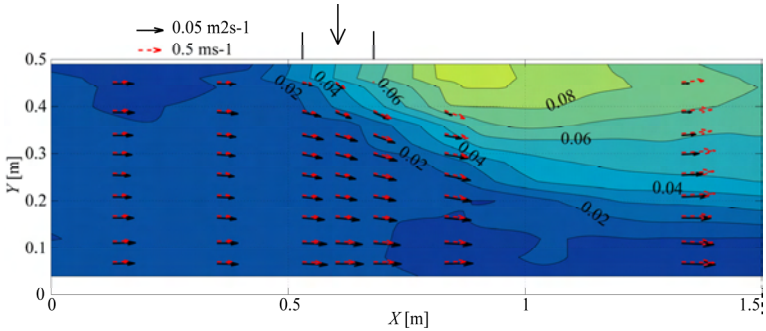

Figure 5-8: Contours of the bed topography and vector representations of the depth-averaged unit discharge (U_xh,U_yh) (full vectors) and the depth-averaged velocities (U_x,U_y) (dashed vectors).

There is a clear relation between bed topography on the one hand and the magnitude and direction of the unit discharges on the other hand. The flow goes around the shallow deposition bar at the inner bank and the major part of the discharge concentrates over the deepest zone near the outer bank. These topographic effects, also called topographic steering can largely be attributed to mass redistribution required by the principle of mass conservation, which can be written as:

$$\frac{\partial U_x h}{\partial X} + \frac{\partial U_y h}{\partial Y} = 0 \Rightarrow U_y h = -\int_0^Y \frac{\partial U_x h}{\partial X} dY \qquad \text{Eq. 5.1}$$

The major contribution in this mass conservation equation is due to the streamwise changes in the bed topography and correspondingly in the flow depth, $\partial h/\partial X$.

According to the majority of models, sediment transport is not primarily determined by the unit discharge, but rather by the local magnitude of bed shear stress $|\vec{\tau}_b|$, which is in first approximation (assuming a constant dimensionless Chézy friction coefficient C_f) proportional to the square of the magnitude of the local depth-average velocity $|\vec{\tau}_b| = C_f \sqrt{U_x^2 + U_y^2}$. The momentum input by the tributary flow is clearly visible in the pronounced increase of the velocitiy magnitudes near the inner bank from the upstream (X = 0.53 m) to the downstream (X = 0.68 m) corner of the tributary mouth (Figure 5-8). These increased velocities play an important role with respect to the transport of sediment originating from the tributary, as indicated by their coincidence with the observed corridors of sediment transport (Figure 5-6; see further in section 5.5).

5.4.2 The three-dimensional flow field

The transverse input of mass and momentum by the tributary as quantified by the discharge ratio and the momentum flux ratio creates a zone characterized by a highly 3D flow field that includes skew-induced cross-sectional flow, turbulence-induced helical flow, unsteady shear layers etc. The three-dimensionality of the flow field is readily illustrated by flow visualization using colour tracer introduced only in the tributary (Figure 5-9a) and only in the main channel (Figure 5-9b). This flow visualization clearly delineates the shear layer where flows from the main channel and the tributary join. There is a clear relation between this shear layer on the one hand, and the sediment transport and morphology on the other. The preferential corridors of sediment transport coincide approximately with the shear layer (Figure 5-6 and Figure 5-9) and the outer limit of the shear layer coincides closely with the toe of the avalanche faces (Figure 5-8 and Figure 5-9).

Flow from the tributary protrudes into the confluence zone and post-confluence channel and thereby changes its direction in a zone of about 1 m long. Ultimately, it occupies about half of the width of the post-confluence channel. Flow from the tributary mainly remains near the water surface, which is due to the bed discordance of about 0.09 m (Figure 5-5b). At the upstream corner of the confluence (X = 0.53 m), the transverse inflow from the tributary is so strong that it blocks the flow coming from the main channel. This leads to the formation of a stagnation zone characterized by a rise of the water surface, and of a deviation of the near-surface flow towards the outer bank. Interestingly, part of the flow progresses into the post-

confluence channel near the inner bank by plunging below the near-surface flow originating from the tributary (Figure 5-9b).

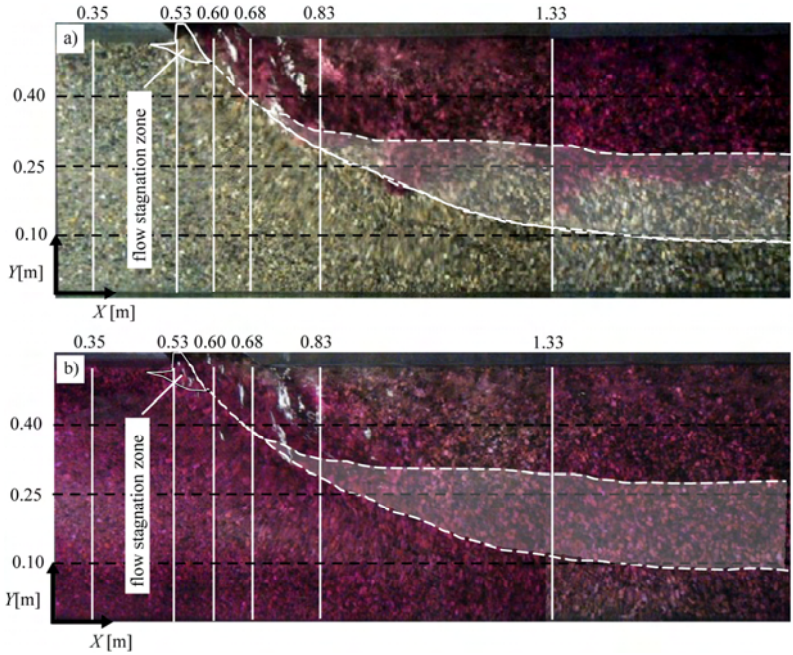

Figure 5-9 : Flow visualization of the main and post-confluence channels with dye colour injected at the tributary (a), and at the main channel (b). The vertical lines correspond to the location of the cross-sections where flow velocities have been measured. The location of the shear layer varies between the two dashed lines in the shadow zone.

We postulate that this two-layer flow near the inner bank is characteristic of confluences with marked bed discordance and a relatively low discharge ratio (~0.1) and momentum flux ratio (~0.2). This two-layer flow leaves a strong footprint on the 3D flow field in the confluence zone. The relatively strong flow near the bed originating from the main channel prevents the formation of a flow recirculation zone over the shallow sediment deposition zone near the inner bank. The absence of the flow recirculation zone differs from the conceptual model of bed concordant confluences (Best, 1987), Figure 5-1. However, the present results are in accordance with the description of Biron et al. (1996b) concerning bed discordant confluences, where flow upwelling from the main channel to the post-confluence channel in the outer bank is described.

Differences in magnitude and direction between the upper and lower layers of the flow lead to a skewing of the velocity profiles. This is clearly seen in Figure 5-10, which shows a zoom of the bed topography in the confluence zone as well as the near-bed and the near-surface average flow velocities at $Z/h = 0.2$ (dashed vectors) and $Z/h = 0.7$ (full vectors), respectively. At the tributary mouth, the near-bed flow from the main channel follows a rather straight path and it is directed upslope the bar (most left near-bed vector in $X = 0.60$ and $X = 0.83$; Figure 5-11). The presence of the tributary flow in this zone can be easily recognized by the near surface velocities that are outwards directed and, which deviate the flow originating from the main channel to the outer bank (full ellipse). Outside of the zone occupied by the bar (dashed ellipse), the near-bed flow is about parallel to the deposition bar contours while the near-surface flow is slightly less outwards skewed. These observations are in accordance with the measurements in a natural bed discordant confluence with a similar momentum flux ratio but a higher discharge ratio ($Q_t/Q_m = 0.68$) presented by De Serres et al. (1999). The vertical skewing of the velocity profile does not lead to the formation of helical flow cells, however, since no upward/downward vertical velocities occur that are of similar magnitude to the variation of the transverse velocity component over the flow depth (Figure 5-11).

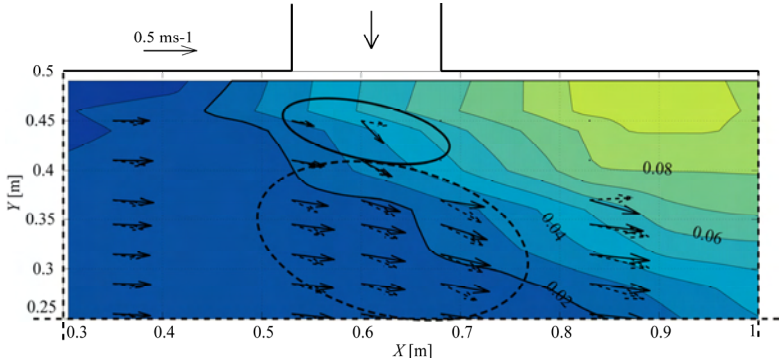

Figure 5-10: Zoom of the final bed topography in the confluence zone with the vectors (u_x,u_y) near the bed at Z/h= 0.2 (dashed vectors) and near the surface at Z/h= 0.70 (full vectors).

Figure 5-11 shows the vectors of the cross-sectional velocities (u_y,u_z) superimposed on the contours of the streamwise velocity u_x. The flow upstream of the confluence (X = 0.13 m and $X = 0.35$ m) shows a pattern that is typical for open-channel flow in a relatively narrow rectangular cross-section ($B/H = 5$) with a rough bed (Tominaga et al., 1989; Nezu and Nakagawa, 1993; Rodriguez and Garcia, 2008; Blanckaert et al., 2010). The flow distribution

is about symmetrical over the width of the channel, but shows significant transverse variations with amplitude of about 10-15% in the streamwise velocities. Moreover, the maximum streamwise velocities are found below the water surface, a phenomenon commonly called the velocity dip. This velocity distribution is the result of advective transport of momentum by helical flow cells. These cells are induced by turbulence, reach maximum cross-stream velocities of about $0.02U$ and scale with the flow depth, which explains the existence of four cells over the width of the channel (Blanckaert et al., 2010). These four cells are schematically indicated in Figure 5-11a. Regions of downward vertical velocities (Y = 0.1 m and Y = 0.4 m; Figure 11a) advect high near-surface velocities towards the bed and cause an increase in streamwise velocity in the water column, whereas regions of upward vertical velocities (Y = 0.25 m; Figure 11a) advect low near-bed velocities towards the water surface and cause a decrease in streamwise velocity in the water column.

The cross-section at X = 0.35 m (Figure 5-11b) is characterized by a slight rise of the water surface near the inner bank, an outwards mass flux in the inner part of the cross-section, and a weak outwards shift of the streamwise velocity pattern. This slight asymmetry can be attributed to the effect of the entrance of the tributary flow which perturbs the flow upstream of the confluence where flow is subcritical.

According to the flow visualization in Figure 5-9a, flow in the cross-section located at the upstream corner of the confluence (X = 0.53 m, Figure 5-11c) uniquely originates from the main channel and is not yet affected by momentum input from the tributary. But it is strongly conditioned by the confluence and shows considerable outwards velocities that are accompanied by a global decrease/increase of velocities in the inner/outer part of the cross-section. Different processes contribute to this velocity redistribution. The most important is probably topographic steering due to the presence of the bar just downstream that directs the flow outwards. As shown by the flow visualization, the flow coming perpendicularly from the tributary acts as an obstacle that causes a stagnation zone characterized by a rise in the water level near the inner bank, and a flow deceleration and flow deflection in the outwards direction. The effect of the obstruction by the tributary inflow is especially strong near the water surface, as visible in the bulging of the u_x-contours. These processes originate at the confluence and weaken with distance from the inner bank. The vertical u_x-contours near the water surface at the inner bank and the quite important velocity gradient suggest the development of a shear layer.

The pronounced transverse velocities near the inner bank in the cross-sections situated in the confluence zone ($X = 0.60$ m at the axis of the tributary and $X = 0.68$ m at the downstream corner of the confluence) represent the transverse inflow from the tributary. They follow the bed topography and weaken with distance from the inner bank, which is due to the change in the direction of flow (see visualization in Figure 5-9a). These transverse velocities are higher at $X = 0.68$ m than at $X = 0.60$ m, indicating that the flow in the tributary is asymmetrical with higher velocities towards the downstream confluence corner. This can be explained by the presence of the stagnation zone at the upstream confluence corner (Figure 5-9). These results are in agreement with the measurements presented by Weber et al. (2001b). The momentum input by the tributary increases the magnitude of the velocity vector near the inner bank (Figure 5-10) and causes the core of highest velocity magnitudes to occur near the inner bank close to the bed. This core of highest velocities is of particular importance for the transport of sediment originating from the tributary (see further in section 5.5). The outward velocities lead to an outward shift of the location of the shear layer (at about $Y = 0.37$ m/0.32 m in the cross-sections at $X = 0.60$ m/0.68 m). Velocities near the inner bank are smallest at the water surface and increase considerably towards the bed, confirming the two-layer structure of the flow at this location. Other flow processes are similar to those in the cross-section at $X = 0.53$ m.

The confluence-induced flow processes persist in the cross-section downstream of the confluence at $X = 0.83$ m. The transverse velocities near the inner bank have weakened, but the two-layer flow structure and the core of highest velocities close to the bed near the inner bank are still pronounced. This cross-section is characterized by considerable acceleration of the flow, especially on the slope of the sediment deposition zone near the inner bank. This flow acceleration, which plays an important role in the transport of sediment (see further in section 5.5), can be attributed to two effects. First, the sediment deposition zone near the inner bank reaches its maximum height, which leads to a considerable reduction of the flow cross-section in the post-confluent channel. Second, the near-surface flow originating from the tributary occupies about half of the width (see dye visualization in Figure 5-9a) which leads to a contraction and a further reduction of the flow area. The shear layer, located around $Y = 0.25$ m according to the dye visualization in Figure 5-9, has considerably weakened as indicated by the attenuated gradient in the near-surface velocities.

Velocities are rather low in the shallowest part ($Y > 0.4$ m) of the cross-section at $X = 1.33$ m. Outwards mass and momentum transport between the cross-sections at

X = 0.83 m and X = 1.33 m has shifted the core of maximum velocities to the central zone of the channel. Interestingly, it occurs over the sediment deposition zone and not over the deepest part of the cross-section. Inwards mass transport is observed in the inner part of the cross-section, which is due to the decreasing transverse bed slope (Figure 5-5a). This cross-section is marked by considerable global flow acceleration accompanied by an increase of the post-confluence water surface slope (Figure 5-5b).

It is interesting to note that the signature of the helical flow cells observed in the cross-sections at X = 0.13 m and X = 0.35 m remain visible onto the last measured cross-section at X = 1.33 m, in the form of the bulging of the u_x-isolines and the two cores with increased streamwise velocities. These features are shifted outwards, however, by the flow originating from the tributary, and they only occur in the confluence zone at the outside of the shear layer. Moreover, the transverse velocities of these turbulence induced helical flow cell of about $0.02U \approx 0.01$ ms^{-1} are more than an order-of-magnitude smaller than the transverse velocities generated by lateral inflow from the tributary. These observations indicate that these helical cells do not modify considerably the 3D flow processes induced by the channel confluence.

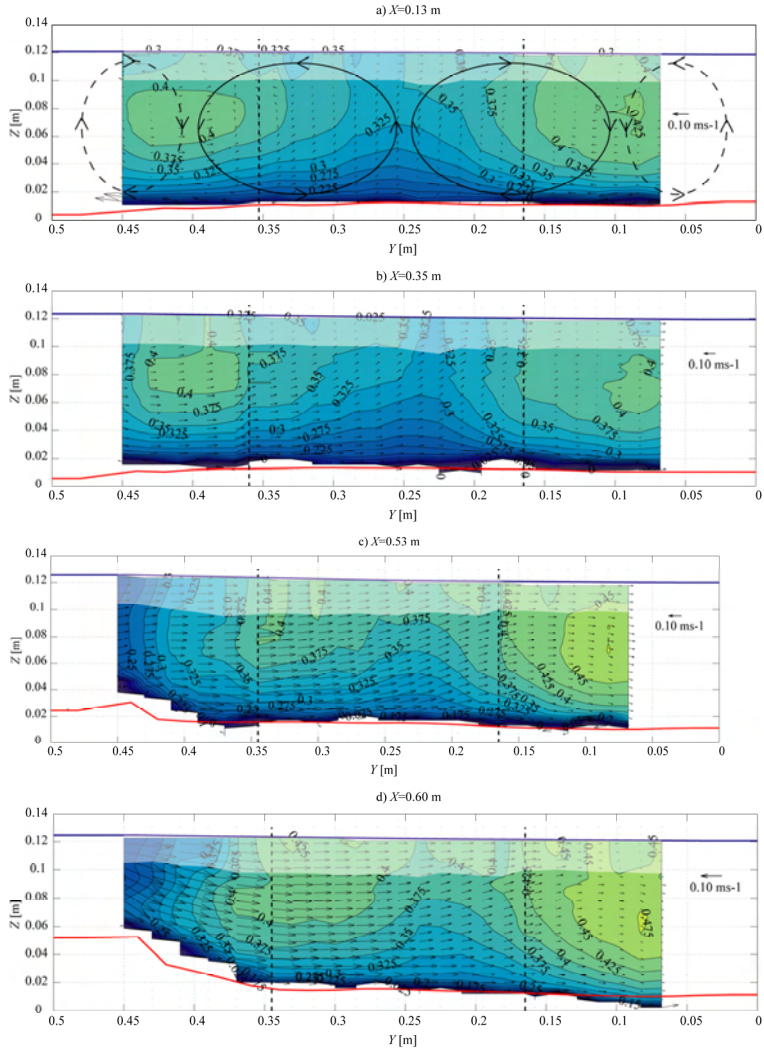

Figure 5-11 : Mean streamwise flow velocities u_x (contours) and cross-sectional velocities, u_y,u_y (vectors) at the seven measured cross-sections indicated in Figure 5-3. The two vertical dashed lines represent the boundaries between measurements performed with the asymmetrical and symmetrical ADVP configurations, whereas the shaded areas indicate regions where the flow measurements are perturbed by the ADVP housing that touches the water surface (more details in Blanckaert, 2010).

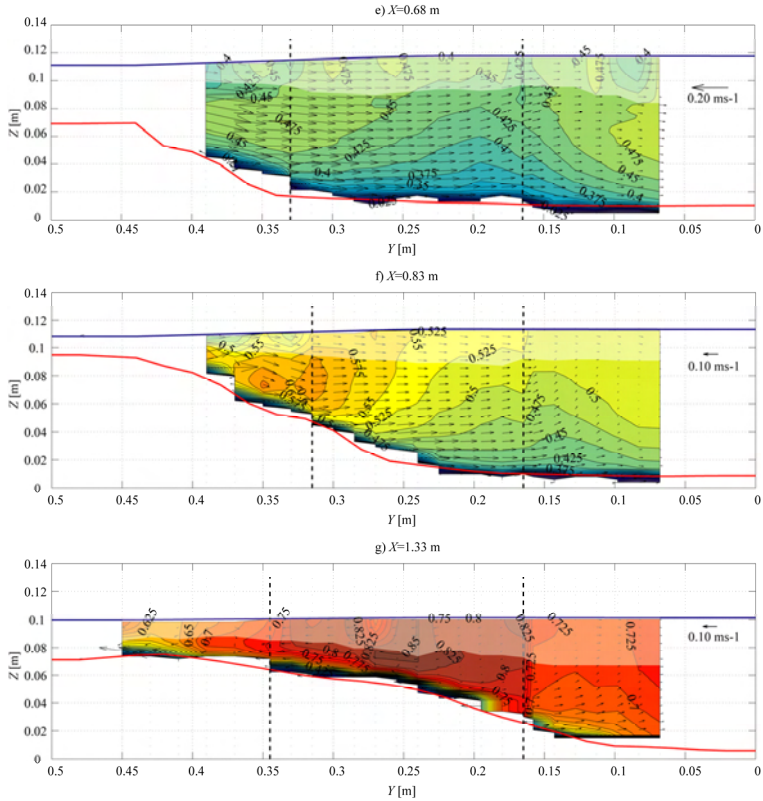

Figure 5-11: (continued).

5.4.3 Turbulent flow structure

The confluence enhances turbulence activity, which is relevant with respect to the mixing of the mass, the momentum, the heat, the suspended matter and the sediment coming from the main channel and the tributary. Figure 5-12 shows the normalized turbulent kinetic energy, tke/u_*^2, in the cross-sections at X = 0.13 m, X = 0.68 m and X = 0.83 m. These cross-sections were chosen because of their representativeness in terms of turbulent structure in a confluence zone. The characteristic shear velocity u_* used for the normalization is calculated between X = 0.13 m to X = 1.33 m and is equal to 0.04 ms^{-1}. As mentioned in section 5.2, only turbulence measurements with the symmetrical ADVP configuration are discussed.

The pattern of *tke* in the cross-section at $X = 0.13$ m is typical of straight channel flows in narrow rectangular cross-sections. The turbulence is mainly induced by bottom friction and redistributed in the cross-section by the turbulence-induced helical flow cells (Figure 5-12a) that cause transverse variations in the *tke* (Blanckaert et al., 2010). These patterns subsist in the central parts of the cross-sections at $X = 0.68$ m and $X = 0.83$ m, but they are slightly advected outwards by the transverse velocities associated with the tributary inflow (Figure 5-12). The most noticeable features in the cross-sections at $X = 0.68$ m and $X = 0.83$ m are the increased and pronounced gradients in *tke* near the inner edge of the measuring grid. These gradients correspond to the position of the shear layer as identified by means of dye flow visualisation (Figure 5-9) and in the mean velocity patterns (Figure 5-11). Also the momentum input by the tributary flow contributes considerably to the *tke* increase: it increases the magnitude of the velocities in the confluence zone (Figure 5-11) and hence also the turbulence activity, since *tke* scales with the square of the mean velocity magnitude. In the cross-section at $X = 0.68$ m, the pronounced *tke* gradient is only apparent near the water surface, which is in agreement with the pronounced vertical two-layer flow structure in this zone (Figure 5-11). Interestingly, the core of pronounced *tke* increase in the shear layer about coincides with the preferential corridors of sediment transport (Figure 5-6b).

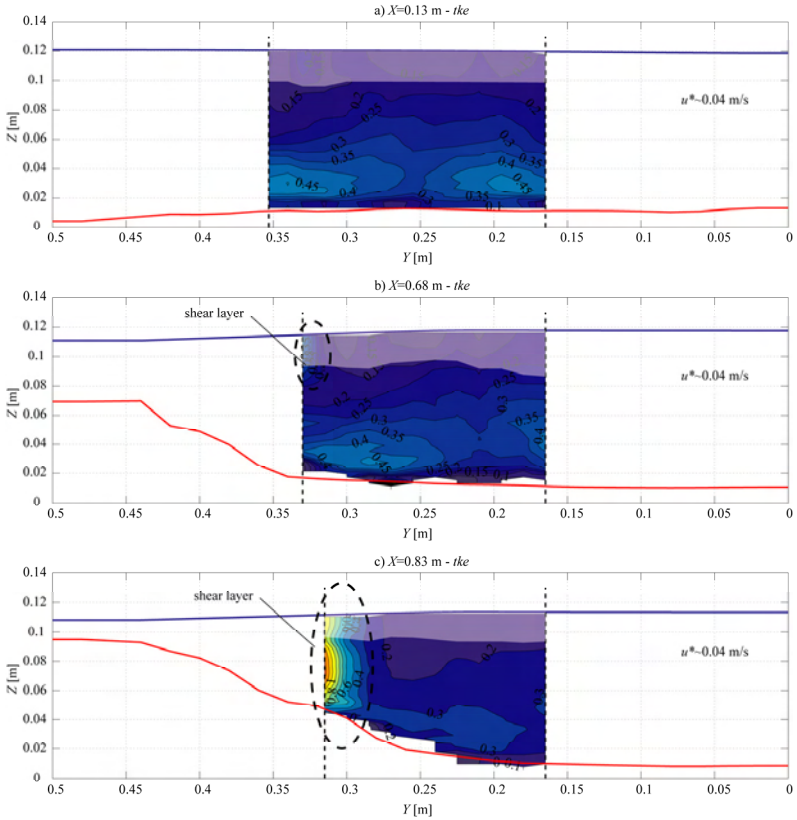

Figure 5-12 : Patterns of normalized turbulent kinetic energy tke/u_*^2 *in the cross sections at X = 0.13 m (a), X = 0.68 m (b), X = 0.83 m (c). The shaded areas indicate regions where the flow measurements are perturbed by the ADVP housing that touches the water surface (more details in Blanckaert, 2010).*

Figure 5-13 presents the relative contributions to the *tke* of the streamwise, transverse and vertical velocity fluctuations at a relative depth of $Z/h = 0.7$ in the cross-sections at $X = 0.13$ m, $X = 0.68$ m and $X = 0.83$ m. Upstream of the confluence in the cross-section at $X = 0.13$ m, the contribution of $\overline{u_x'^2}$, $\overline{u_y'^2}$ and $\overline{u_z'^2}$ are about 58%, 30% and 12%, respectively, which is in agreement with Nezu and Nakagawa's (1993) semi-theoretical values for straight open-channel flows. In the cross-section at $X = 0.68$ m, the tributary input of transverse momentum causes an increased relative contribution of $\overline{u_y'^2}$ at the expense of $\overline{u_x'^2}$, which weakens with transverse distance from the confluence mouth. Interestingly, although the mean flow reorients in the streamwise direction between the cross-sections at $X = 0.68$ m and $X = 0.83$ m (Figure 5-11 and Figure 5-12), $\overline{u_y'^2}$ continues to grow at the expense of $\overline{u_x'^2}$ in the inner part of the cross-section where the transverse fluctuations form the dominant contribution to *tke*. Similar behaviour has been measured by Sukhodolov and Rhoads (2001) in small natural bed concordant confluences.

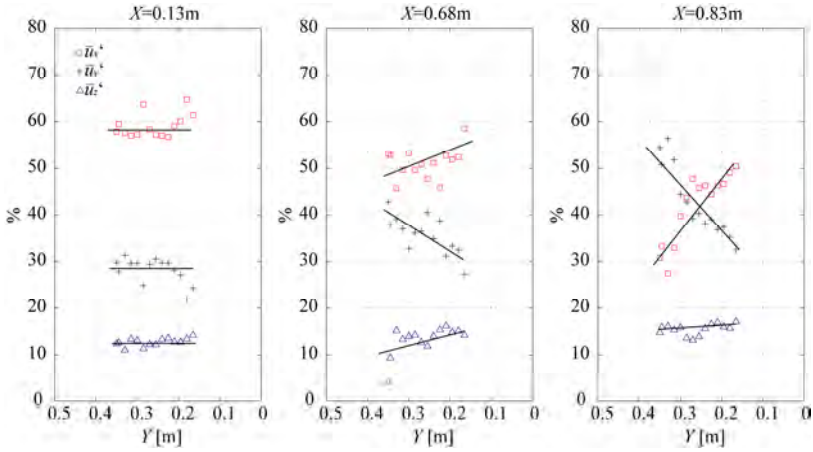

Figure 5-13 : Relative contributions of $\overline{u_x'^2}$, $\overline{u_y'^2}$ and $\overline{u_z'^2}$ on the turbulent kinetic energy in the cross-sections X = 0.13 m, X = 0.68 m and X = 0.83 m near the water surface (Z/h= 0.70).

5.5 Hydro-morpho-sedimentary processes and interactions

The previous sections reported and analysed separately the bed morphology and the sediment transport on the one hand and the flow dynamics on the other hand. Results indicated important differences between confluences such as found in alpine environments that are characterized by pronounced bed discordances and the conceptual model of Best (1988) presented in Figure 2, which was based on observations in confluences with concordant beds.

In order to facilitate the discussion, Figure 5-14 attempts to integrate the foregoing observations in a (speculative) conceptual framework for the hydro-morpho-sedimentary processes that would characterize confluences with low discharge and momentum flux ratios, such as confluences found in the Upper Rhone River. This section describes the dominant processes and interactions and explains the differences with Best's (1988) model.

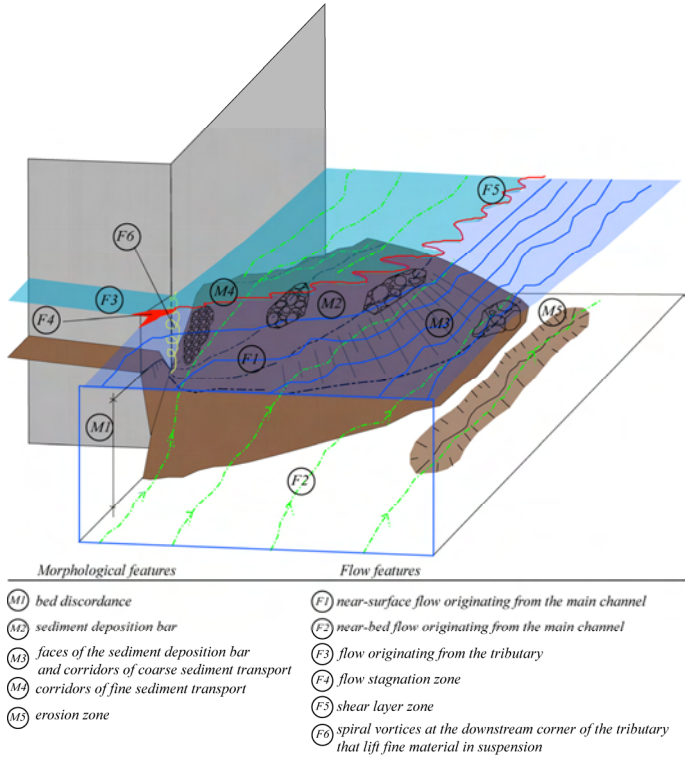

Figure 5-14 : Conceptual framework of hydro-morpho-sedimentary processes in channel confluences such as found in alpine environments.

5.5.1 Representativeness of the experimental results

The first important point to discuss is the representativeness of the morphodynamic processes observed in the laboratory set-up. Figure 5-15 illustrates the confluence of the Lonza and the Upper Rhone Rivers for which the main parameters are presented in Table 5-3. It is important to note that the aerial view and the cross-sections (Figure 5-15a) and the pictures taken at the confluence (Figure 5-15b and Figure 5-15c) do not represent the same time and discharges.

Table 5-3 : Main geometric and hydraulic parameters of the confluence of the Upper Rhone and the Lonza Rivers in Switzerland.

	Angle [°]	B_t/B_m	$B_m/B_{p\text{-}c}$	*Tributary bed slope [%]*	$Q2_t/Q2_m$	Fr_{tQ2}	M_{r_Q2}
Lonza	65	0.11	1.06	1.1%	0.1	~1	0.1

Although the main geometrical and hydraulic parameters are not exactly the same, the main morphological features described in the experiment can be observed in the field. The Lonza-Rhone confluence is marked by a significant discordance at the mouth of the tributary, which is responsible for the disconnection between the waters during low flow periods. The confluence promotes the formation of a deposition zone that occupies around 75% of the channel width in the cross-section at Km 99.384 (Figure 5-15a). The deposition zone deviates the main flow towards the left bank; generating flow acceleration and consequently creating a small erosion zone near the left bank (Figure 5-15b). As for the present experiment, the erosion is considerably smaller than the deposition. The sediment bar is characterized by significant grain sorting, where fine and coarse materials regions can be recognized in Figure 5-15c. During low flows, the bar is exposed and the flow is redistributed to the left bank. A well marked shear layer is formed between the confluent flows (Figure 5-15c).

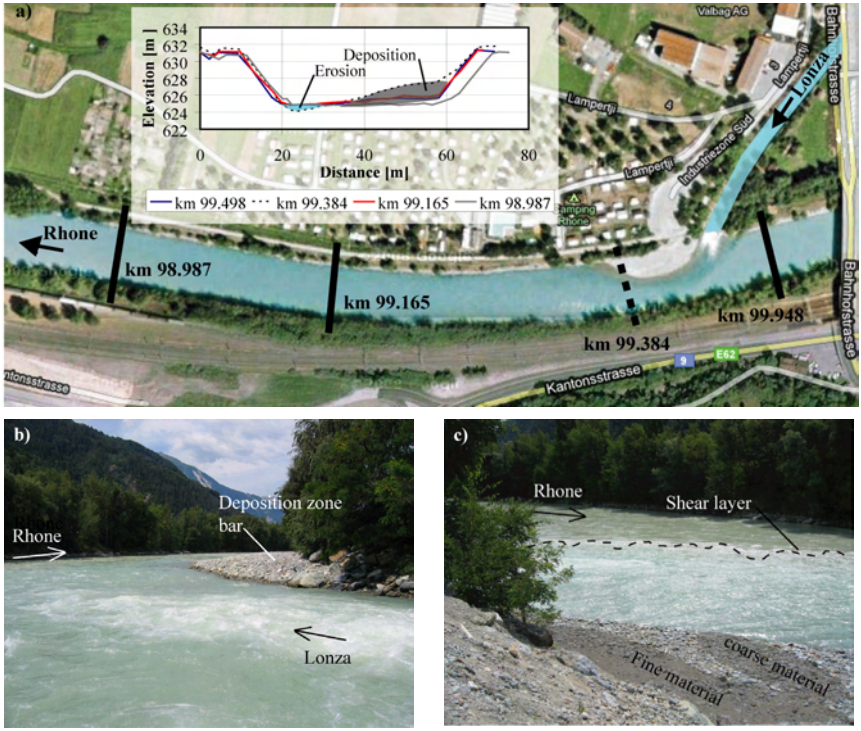

Figure 5-15: Confluence of the Lonza and Upper Rhone Rivers in Switzerland during low flow conditions. a) Aerial view (source: www.maps.google.com) showing 4 cross-sections. b) Picture taken from the mouth of the tributary towards downstream and c) picture taken from the right bank at the deposition zone from upstream. The confluence is characterized by a junction angle of 65° and the parameters $B_t/B_m = 0.11$, $Q_t/Q_m = 0.1$, $Fr_t \sim 1.0$ and $Mr = 0.1$.

5.5.2 Deposition dominated vs. scour dominated confluence zones

For the present experiment, no scour occurs in the confluence zone and only a very slight scour develops near the outer bank in the post-confluence channel (Figure 5). These observations do not agree with the results described by Mosley (1976), Best (1988) or Ashmore and Parker (1983), where well-defined scour zones were found. The equilibrium bathymetry is more in line with the model of discordant sand-bed confluences proposed by Leclair and Roy (1997), which describes the formation of the tributary mouth bar in response to changes in the momentum flux ratio. However, their model cannot be directly applied to the present experiment since it concerns momentum flux ratios $Mr \geq 1$ that are much higher

than those of the present case (Mr= 0.21). Moreover, although the dominant sediment input in the model proposed by Leclair and Roy (1997) comes from the tributary, there was hardly any bedload transport in their measurements in contrast to the significant bedload transport in the experiments reported here.

The bed topography and the dominance of deposition or scour are determined by the requirements of sediment continuity in the equilibrium configuration. The bed topography depends essentially on the flow discharges, the sediment particle characteristics and sediment supplies in the main channel and the tributary. In cases where there is no bedload supply or the dominant sediment supply originates from the main channel (Mosley, 1976; Ashmore, 1982; Ashmore and Parker, 1983; Rhoads and Kenworthy, 1995; Rhoads and Kenworthy, 1998; Rhoads and Sukhodolov, 2001), the tributary flow locally enhances the sediment transport capacity, which leads to the development of scour until the sediment transport and the sediment supply are re-equilibrated. In these confluences, there is hardly any formation of bed discordance and the model proposed by (*Best*, 1988) is applicable (Figure 5-2).

In cases where the dominant sediment supply originates from the tributary, such as in the Upper Rhone River or also in the Bayonne-Berthier confluence (investigated by Biron et al., 1993; Biron et al., 1996a; Biron et al., 1996b; Leclair and Roy, 1997; Biron et al., 2002; Boyer et al., 2006), there is formation of significant deposition bar at the inner bank reducing the flow area and inducing flow acceleration. This adjustment provides the increase in sediment transport capacity required to transfer the additional sediment supply from the tributary. This increase in flow velocity is accompanied by an increase in the energy gradient (which scales with the square of the velocity) as illustrated by the marked increase in the water surface slope in the reported experiment (Figure 5-5c).

In natural cases with intermittent sediment supply from the tributaries only during floods, the sediment deposition bar can be expected to grow during the flood event when the sediment supply exceeds the sediment transport capacity. After the flood when the sediment supply has vanished, however, the bar can be expected to attenuate through the evacuation of sediment until equilibrium is established. Averaged in time over multiple flood events, however, the sediment transport capacity downstream of the confluence needs to be higher than in the main channel upstream of the confluence. This is in agreement with experimental evidence of flow acceleration downstream of confluences in natural rivers as well as in the reported experiment (Roy and Roy, 1988; Roy et al., 1988).

5.5.3 Bed discordance vs. bed concordance at the confluence mouth

The most typical feature of the bed morphology in alpine confluences is the marked discordance in the bed elevations at the mouth of the main and tributary channels (Figure 5-5b). These confluences are typically characterized by a subcritical flow ($Fr_{p\text{-}c}$ <1) in the post-confluence channel and transcritical flow (Fr_t~1) in the tributary, and a low discharge ratio Q_t/Q_m. These different flow regimes play a crucial role in the formation of the bed discordance.

Flow in the post-confluence channel is subcritical, and hence by definition conditioned by the downstream boundary conditions for the water surface elevation and the bed level. The total discharge, Q_m+Q_t, and sediment supply, $Q_{s,m}$ + $Q_{s,t}$, originating from the main channel and the tributary determine the (cross-sectional-averaged) flow depth and the bed slope in the post-confluence channel, and hence also the absolute elevations of the bed and the water surface at the confluence mouth, $Z_{b,m}$ and $Z_{w,m}$, respectively (Figure 5-16). These considerations did not take into account the three-dimensionality of the bed topography in the post-confluence channel. This three-dimensionality, however, mainly occurs downstream of the confluence due to the sediment supply by the tributary, and it is much less pronounced in the confluence zone where the bed discordance is observed (Figure 5-5a).

At the confluence mouth, the water levels in the main channel, the tributary and the post-confluence channel are about equal. For the reported experiment, a hydraulic jump has to occur to accommodate the transition from the supercritical flow in the tributary to the subcritical flow in the post-confluence channel. The characteristics of a hydraulic jump are mainly determined by Fr_m and Fr_t. The values in the experiment of Fr_m = 0.9 and Fr_t = 1.3, lead to the formation of a weak undulated hydraulic jump that only induces a very small difference in water level elevations at the confluence mouth, $Z_{w,m} \approx Z_{w,t}$. This behaviour is similar to what is observed at confluences of the Upper Rhone River, where the transition from the transcritical flow (Fr~1) in the tributary to the subcritical main channel flow does not require a hydraulic jump.

The discharge Q_t, the sediment supply $Q_{s,t}$ and the sediment characteristics in the tributary determine the flow depth, H_t, and the bed slope S_t. The absolute elevations of bed and the water surface are determined by the downstream boundary conditions at the confluence mouth. The absolute elevation of the bed level is determined by $Z_{b,t} = Z_{s,t}$-H_t. The bed discordance is readily obtained as $Z_{b,t}$ - $Z_{b,m} \approx H_m$-H_t. The bed discordance is pronounced in alpine confluences due to the different flow regimes in the tributary and main channels.

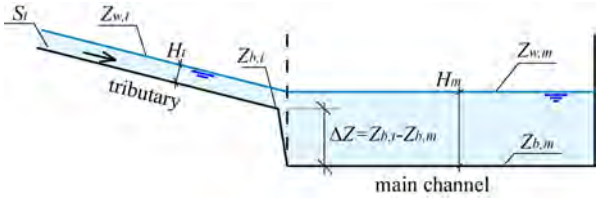

Figure 5-16 : Conceptual model for bed discordance.

5.5.4 Two-layer flow structure vs. flow recirculation zone

In the case of concordant beds as described in Best (1988) conceptual model, the tributary flow obstructs the main-channel flow over the entire flow depth and deviates it in outwards direction. The directional change of the tributary creates a zone of horizontal flow recirculation at the inner bank (Best and Reid, 1984) where mainly fine sediment tends to settle and to build a separation zone bar (Figure 5-2). As mentioned in section 5.3, a morphological depression that coincides with a corridor of deposition and transport of fine sediment was observed in the flume at the inner bank. However, this corridor of fine-sediment transport is much narrower than the bank-attached lateral bars associated with a region of flow recirculation in Best's (1987) conceptual model.

Processes in alpine confluences are fundamentally modified by the presence of pronounced bed discordance, which is at the origin of the formation of a two-layer flow structure. Flow originating from the tributary mainly protrudes in the upper part of the water column of the main channel, where it forms an obstruction for flow originating from the main channel and deviates the latter outwards. The bed discordance protects the flow in the lower part of the water column from the obstruction by the tributary inflow, and allows it to go straight on (Figure 5-9, Figure 5-10, Figure 5-11 and Figure 5-14), which prevents the formation of a zone of horizontal flow recirculation. The near-bed flow originating from the main channel plays an important role in the morphological development, since it encounters at the confluence mouth coarse sediment supplied by the tributary. Initially, the near-bed flow has insufficient sediment transport capacity, leading to the deposition of the sediment and the development of the deposition bar. This causes, however, a reduction in the local flow depth, an acceleration of the near-bed flow, and its outwards deviation by topographic steering. At equilibrium, the near-bed flow is mainly found on the sloping face of the sediment deposition bar. It accelerates by moving upslope on the face of the sediment deposition bar. As described in section 5.3, its upslope component equilibrates the downslope gravitational pull on the

sediment particles and thereby conditions the slope of the face of the sediment deposition bar and the sediment sorting on the bar's face.

5.6 Conclusions

Alpine confluences are characterized by steep tributaries with high supply of poorly sorted sediment, relatively low discharge and momentum flux ratios, and a pronounced bed discordance at the tributary mouth. These characteristics condition the hydro-morpho-sedimentary processes, which differ fundamentally from existing conceptual models (Mosley, 1976; Ashmore and Parker, 1983; Best, 1988). The paper reports results from measurements of the three-dimensional velocity field, turbulence, sediment transport, sediment granulometry and morphology in a laboratory confluence that is representative of the Upper-Rhone River, Switzerland, under channel-forming conditions.

The marked bed discordance at the confluence mouth is mainly determined by the different flow regimes in the main channel and the tributary. The flow depth in the subcritical main channel is considerably higher than in the transcritical steep tributary. This difference in flow depth is materialized in a pronounced bed discordance, whereas the water surface elevation only shows weak variations in the confluence zone. Due to this bed discordance, the tributary flow penetrates into the main channel mainly in the upper part of the water column, whereas the main-channel flow moves beneath the tributary in the lower part of the water column.

The sediment transfer between the tributary and the post-confluence channels mainly occurs near the downstream corner of the confluence due to the formation of a stagnation zone at the upstream confluence corner that causes an asymmetric distribution of the flow and sediment transport. Sediment provided by the tributary to the post-confluence channel is mainly transported by the near-bed flow on the face of the sediment bar, which originates from the main channel. Three hydro-morphological interactions provide the sediment transport capacity required. First, the development of the sediment bar causes a reduction in the local flow depth, an acceleration of the near-bed flow, and its outwards deviation by topographic steering. Second, the bed discordance gives rise to a two-layer flow structure and to highly three-dimensional flow patterns that are characterized by near-bed cores of high velocity with increased sediment transport capacity. The near-bed flow prevents the formation of a zone of flow recirculation and deposition of fine sediment at the inner-bank. Third,

considerable turbulence is generated in the shear layer at the junction of the flows originating from the main channel and the tributary. The coincidence of the shear layer with the location of the preferential corridors of coarse sediment transport indicates that the increased turbulence levels contribute substantially to the required increase in sediment transport capacity.

6. Hydro-morphological implications of local tributary widening for river rehabilitation

6.1 Introduction

During the past centuries, many rivers have been channelized and regulated, often with the aim of reclaiming land for urbanization and agriculture. These river training works typically resulted in linear river systems with quasi homogeneous flow and morphologic conditions, which are characterized by considerably reduced natural dynamics, impoverished ecological value and deficiency in flood safety. The Upper Rhone River in Switzerland (Figure 6-1) is an example of such a regulated river.

River confluences are the nodes of the fluvial network. They are typically characterized by high variability in flow, sediment load, sediment size and water quality (Rice and Church, 2001), which is a requisite for a sound fluvial ecosystem. Tributary regulations can be largely responsible for ecological changes (Rice et al., 2001; Rice et al., 2006) and can have dramatic impacts on the flood safety (Sloan et al., 2001; Roca et al., 2009).

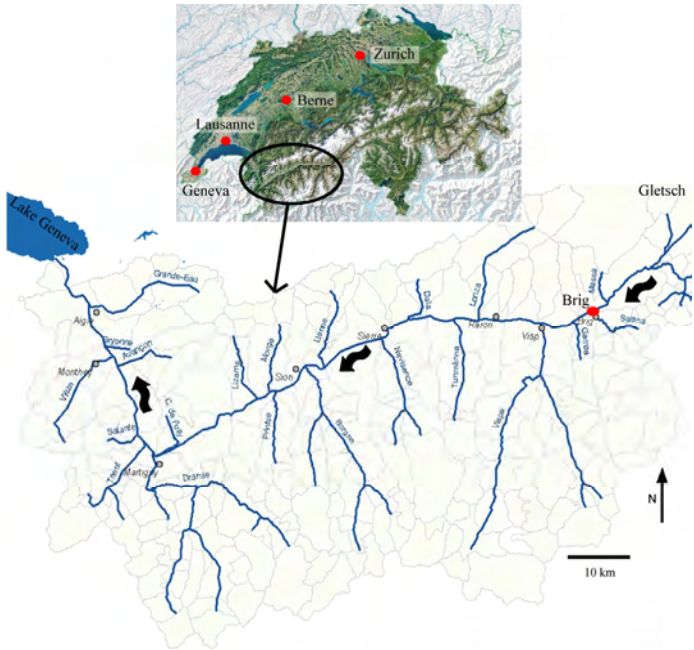

Figure 6-1: Upper Rhone River basin showing the twenty main confluences between Brig (upstream, at the right in the figure) and the lake of Geneva (downstream, at the left in the figure).

This paper investigates the hydro-morphological implications of a local tributary widening in river systems such as the Upper Rhone. Two main river training works have been performed on this river since 1850 and presently, less than 1% of the basin can be considered truly natural (Bourgeois, 2006). The main channel is embanked at a width varying between 30 and 60 m, and also the tributaries are channelized. The confluences are characterized by pronounced bed discordances, which have often been stabilized by means of weirs or block ramps. At present, a major river rehabilitation project is in progress (SRCE, 2008) in the Upper Rhone basin, which aims at conciliating improved flood protection and enhanced ecological value. The rehabilitation of confluence zones, which is critical component of the overall rehabilitation project, is hindered by a lack of understanding of the relevant hydro-morpho-sedimentary processes.

River widening, which allows the river to adjust to its natural dynamics, has become a common concept in river rehabilitation (Rohde et al., 2005; Nakamura et al., 2006; Formann et al., 2007; Weber et al., 2009). Surprisingly, the local widening of the tributary at confluences (Figure 6-2) has not yet been investigated. Such a local tributary widening aims to increase the heterogeneity in sediment substrate, flow depth and flow velocity, which is favourable for in-stream habitat (e.g. aquatic invertebrates, fish, and vegetation) and for the connectivity between the main river and the tributary. Especially zones of quiescent water (flow stagnation or flow recirculation zones) may play an important role as refuges during flood events or during the hydropeaking (Meile et al., 2010). Moreover, a local tributary widening aims to create a riparian zone which favours the diversity of plants and animals (e.g. birds, mammals, insects, amphibians). A local tributary widening may constitute a local hotspot for biodiversity along confined, channelized and regulated river systems. Obviously, river rehabilitation by means of local tributary widening is only feasible if it has negligible adverse effects on the flood safety.

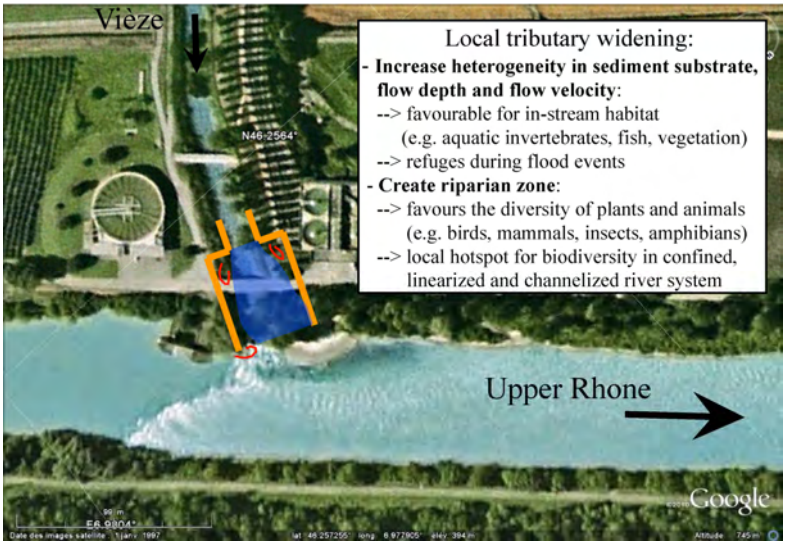

Figure 6-2: Confluence of the channelized Upper Rhone and Vièze Rivers. Local widening is schematic illustrated and its main objectives are listed.

Although the flow characteristics of river confluences are well documented in the literature (Best and Reid, 1984; Best, 1987; Best and Roy, 1991; Lane et al., 1994; Biron et al., 1996b; McLelland et al., 1996; Bradbrook et al., 1998; Lane et al., 1998; Lane et al., 1999a; Bradbrook et al., 2000a; Lane et al., 2000; Biron et al., 2004), the presence of sediment transport and its influence on the morphodynamic are still poorly understood. The few existing laboratory studies on confluence morphology (Mosley, 1976; Ashmore and Parker, 1983; Best, 1988) and the field investigation on flow and morphological features of bed concordant (Roy and Bergeron, 1990; Rhoads and Kenworthy, 1995; Rhoads and Sukhodolov, 2008, Rhoads et al., 2009) and bed discordant (Biron et al., 1993; Leclair and Roy, 1997; Boyer et al., 2006) confluences show that the hydrodynamics of confluence zones are highly responsive to the changes in the morphology.

Chapter 5 has shown that the current knowledge provided by these previous contributions is not directly applicable to alpine river confluences. Alpine confluences are characterized by relatively low ratios of tributary discharge to main channel discharge, Q_t/Q_m, dominant sediment supply from the tributary, steep bed slopes in the tributary, and a pronounced difference in bed elevation between the main channel and the tributary, which is called bed discordance. Based on detailed measurements of the morphology, the sediment

size, and the three-dimensional flow field in a laboratory flume, Chapter 5 has proposed an enhanced conceptual model (Figure 6-3) for the hydro-morpho-sedimentary processes in channelized alpine confluences. The model has been validated by observations of the confluences of the Upper Rhone.

The pronounced bed discordance (*M1*) at the confluence mouth is due to the important difference between the flow depths in the steep tributary and in the main channel. The formation of a stagnation zone (*F4*) at the upstream confluence corner causes an asymmetric distribution of the flow and sediment transport, whereby the sediment transfer between the tributary and the main channel mainly occurs near the downstream corner of the confluence. The presence of a large sediment bar at the inner bank (*M2*) and the absence of a marked scour hole at the outer bank (*M5*) are typical for confluences characterized by a dominant sediment supply originating from the tributary and low discharge and momentum flux ratios. The sediment bar lead to a reduction in cross-sectional area and a corresponding acceleration of the flow that provides the increase in sediment transport capacity required to transfer the additional sediment supply from the tributary. The pronounced bed discordance leads to the formation of a two-layer flow structure in the confluence zone (*F1, F2, F3*). Flow originating from the tributary mainly protrudes in the upper part of the water column of the main channel, where it forms an obstruction for flow originating from the main channel and deviates the latter outwards. The bed discordance protects the flow in the lower part of the water column from the obstruction by the tributary inflow, and allows it to go straight on. The two-layer flow structure does not lead to the formation of secondary flow circulation cells. The near-bed flow originating from the main channel encounters at the confluence mouth coarse sediment supplied by the tributary. This near near-bed flow is mainly found on the sloping avalanche faces of the sediment deposition bar (*M3*). It accelerates by moving upslope on the face of the sediment bar. Its upslope component equilibrates the downslope gravitational pull on the sediment particles and thereby conditions the slope of the avalanche faces and the sediment sorting occurring on them. A shear layer (*F5*) develops where flows originating from the tributary and from the main channel collide. It is characterized by increased turbulence and its outer limit coincides closely with the toe of the sediment bar (*M2*). In the downstream confluence corner, spiral vortices (*F6*) lift fine material into suspension. Fine materials are then transported near the inner bank (*M4*) while the coarse ones are transported on the face of the sediment bar (*M3*).

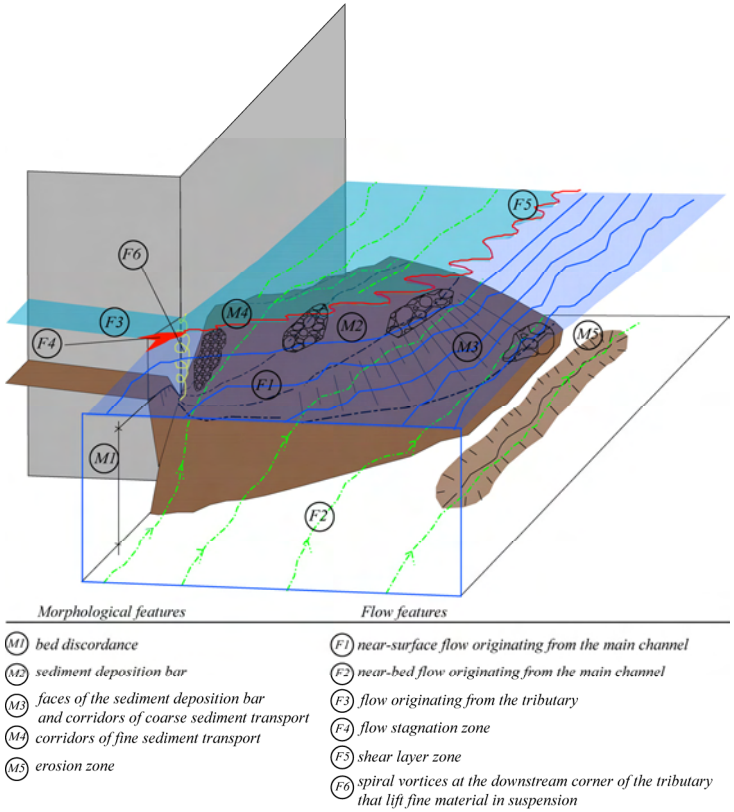

Figure 6-3: Conceptual model for hydro-morpho-sedimentary processes in confluences such as found in alpine environments (Chapter 5).

By means of laboratory experiments, this paper compare a reference configuration that represents a channelized confluence (reported in detail in Chapter 5) to a configuration with a local tributary widening, with the aim of:

- Investigating the influence of a local tributary widening on the hydro-morpho-sedimentary processes in the confluence zone;
- Assessing the potential of local tributary widening in the framework of river rehabilitation, and in particular to assess its effect on the flood safety.

6.2 The experiments

A laboratory investigation was performed under geometric and hydraulic conditions that are representative of the confluences of the Upper Rhone River (Table 6-1). The confluence flume with smooth vertical banks was composed of a 8.5 m long and 0.50 m wide main channel and a 4.9 m long and 0.15 m wide tributary, connected an angle of 90°at a distance of 3.60 m downstream of the inlet of the main channel (Figure 6-4). The ratios of the tributary width to the main channel width of B_t/B_m = 0.3 and of the main channel width to the post-confluence channel width of $B_m/B_{p\text{-}c}$ = 1 are typical of river channel confluences in the Upper Rhone River (Table 6-1). The choice of 90° confluence angle is based on the fact that the lateral valleys of the basin are almost perpendicular. The present state of the Rhone confluences zones is the result of the river training works. Consequently the current angles are not truly natural. Moreover, with the local widening, a self-natural dynamic is expected in the confluence zone, which includes the adjustment of a natural angle.

Table 6-1: Geometric and hydraulic characteristics of the main confluences on the Upper Rhone River

	Angle [°]	B_t/B_m	$B_m/B_{p\text{-}c}$	*Tributary bed slope [%]*	$Q2_t/Q2_m$	$Q5_t/Q5_m$	Fr_{tQ2}	Fr_{tQ5}	M_r_Q2	M_r_Q5
Average	62	0.22	1.02	1.1%	0.10	0.09	0.83	0.83	0.12	0.08
Max	90	0.54	1.27	4.0%	0.32	0.31	1.29	1.30	0.45	0.30
Min	30	0.07	0.71	0.0%	0.01	0.01	0.03	0.03	0.00	0.00

The width of the tributary was symmetrically doubled (B_w=0.30 m) in the confluence zone, over a distance from the tributary channel mouth that is three times the reference tributary channel width (L_w= $3B_t$ = 0.45 m). Figure 6-4 shows the experimental set-up including the geometry of the locally widened tributary channel and the reference configuration (Chapter 5). The present paper adopts an orthogonal (*X*, *Y*, *Z*) reference system, where the *X*-axis is along the main channel in streamwise direction, the *Y*-axis points towards the left and has its origin at the right bank of the main channel (outer bank), and the Z-axis is vertically upwards.

The flow discharges of the main and tributary channels were Q_m = 18 ls^{-1} and Q_t = 2 ls^{-1}, respectively, leading to a discharge ratio Q_t/Q_m = 0.11 that is typical for the Rhone basin under morphogenic conditions corresponding to floods with return periods of about 2-5 years (Chapter 5). Constant flow discharges were supplied by two independent pumps, connected upstream of the main channel and the tributary. An adjustable tailgate at the end of the main channel fixed the downstream flow depth at 0.07 m. Initial flow depths in the main channel and in the tributary were 0.09 m and 0.06 m, respectively.

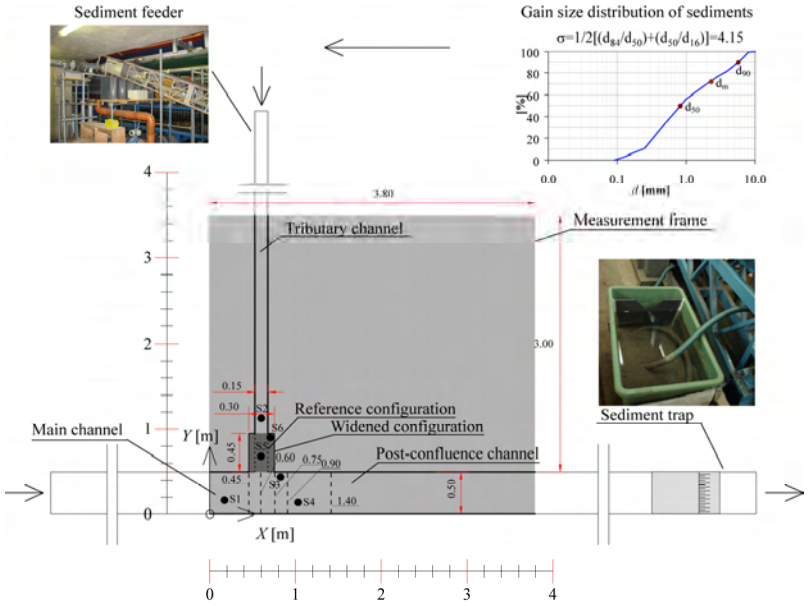

Figure 6-4: Experimental set-up, (X,Y,Z) reference system and grain size distribution of the sediment. The cross sections where velocity measurements were performed are indicated by the dashed lines and the locations of the bed samples by the dark circles. The limit between the main channel and the post-confluence channel is the tributary axis at X = 0.60 m.

The movable bed was initially flat in the main channel and consisted of a sediment mixture characterized by d_{50} = 0.82 mm; d_m = 2.3 mm and d_{90} = 5.7 mm with a gradation coefficient σ = 4.15, where $\sigma = 0.5*(d_{84}/d_{50} + d_{50}/d_{16})$. A constant sediment discharge of 0.30 kg/min from the same sediment mixture was supplied by a conveyor belt at the tributary inlet only. The sediment characteristics and the sediment discharge adopted for the experiments satisfy two requirements:

- The gradation of the sediment mixture is representative of the Upper Rhone River, as indicated by the dimensionless grain size distribution in Figure 3-17.
- The sediment discharge yields a longitudinal slope in the tributary that are in the range of those of the Upper Rhone tributaries (Table 6-1).

A sediment trap at the downstream end of the main channel recovered the sediment transported. Equilibrium conditions, defined by a steady level of the bed topography, were reached after 22 h.

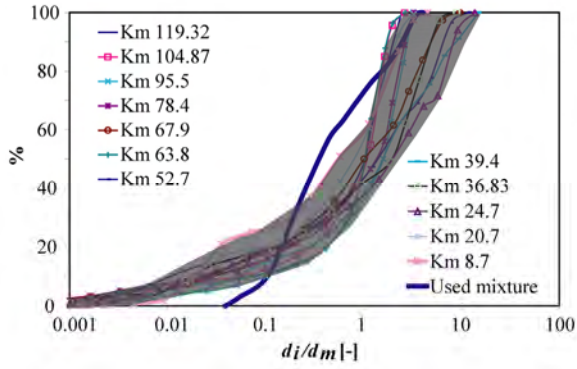

Figure 6-5: Distributions of the grain size normalized with the average grain diameter of the bed surface for the sediment mixture used in the laboratory experiments and for different locations on the Upper Rhone River (upstream distances with respect to the Lake Geneva, see Figure 6-1).

Water surface elevations were measured with echosounders during 10 s with a frequency of 128 Hz, providing an average value with an accuracy of ±1 mm. The bed topography was measured with a Mini EchoSounder with an accuracy of ±1 mm. Both instruments were installed on a movable frame that covers part of the experimental set-up (3.80 m in the main and post-confluence channels and 3.00 m in the tributary, see Figure 6-4). Table 6-2 summarizes information on the measuring grids. The bed topography maps reported hereafter are obtained by linear interpolation between the measured points.

Table 6-2: Measuring grids for the water surface elevation and the bed topography.

Location	Water level	Bed topography
Main channel and post-confluence channel	Three transverse points (Y=0.05, Y= 0.25 and Y=0.45 m) in nine cross-sections (X=0.03, X=0.44, X=0.50, X=0.60, X=0.72, X=0.74, X=1.18, X=2.18 and X=3.18m).	Thirteen longitudinal profiles (measuring grid of ΔX =0.009m in the domain X= 0 to 3.80 m) spaced by ΔY=0.04m from Y=0.04 to Y=0.46 and additional profile at Y=0.48m.
Tributary upstream of the local widening	Eight points on the tributary axis spaced by ΔY=0.20m between Y=1.04 and Y=3.44m.	Points on the tributary axis with a spaced by ΔY=0.20 m between Y=1.13 and Y=1.33m.
Local tributary widening	Three transverse points (X =0.50, X=0.60 and X=0.72m) in five cross-sections (Y= 0.54, Y=0.64, Y=0.74, Y=0.84 and Y=0.90m).	Nine cross-sections (measuring grid of ΔX=0.009m in the domain X =0.475 to X=0.725 m) spaced by ΔY=0.05m from Y=0.54 to Y=0.84 and additional profile at Y=0.90m.

Once the equilibrium bed morphology was established, non-intrusive measurements of velocity profiles were made with an Acoustic Doppler Velocity Profiler (ADVP) developed at École Polytechnique Fédérale Lausanne (Switzerland). The working principle of the ADVP

has been described by Lemmin and Rolland (1997), Hurther and Lemmin (1998), Blanckaert and Graf (2001) and Blanckaert and Lemmin (2006). Blanckaert (2010) describes in detail the data treatment procedures and quantified the uncertainty in the measurement as follows: about 4% in the time-averaged longitudinal velocity u_x, about 10 % in the cross-stream velocities (u_y,u_z), about 20% in the turbulent kinetic energy (*tke*). More details about the application of the ADVP in the confluence flume are reported in Chapter 5.

Flow velocities were measured in five cross-sections in the main and post-confluence channels. The positions of the cross-sections were chosen in order to facilitate the comparison with the results of the velocity field in the confluence zone presented in Chapter 5, i.e, upstream corner of the confluence (X = 0.45 m), axis of the tributary (X = 0.60 m), downstream corner of the confluence (X = 0.75 m), a distance that corresponds to a tributary width (0.15 m) downstream of the confluence (X = 0.90 m) and 0.65 m downstream (X = 1.4 m).

Samples of the surface bed material under equilibrium conditions were collected at different locations and grain size analysis by means of hand sieving was performed. In the reference configuration, samples were collected in the main channel upstream of the confluence (S1), the tributary (S2), the avalanche faces (S3) and the sediment bar (S4). In the widened configuration additional samples were collected in the centre (S5) and the downstream corner (S6) of the widened zone (Figure 6-4).

6.3 Water surface elevation, bed morphology and sediment transport at equilibrium

This section presents the water surface elevation, the bed morphology and the sediment transport at equilibrium conditions for the configuration with locally widened tributary and compares them to their counterparts in the reference configuration.

The main morphological features (Figure 6-6) in the configuration with the locally widened tributary are the same as those described for the reference configuration in section 6.1, i.e (*i*) the formation of a pronounced bed discordance between the tributary and the main channel; (*ii*) the presence of a large sediment deposition bar downstream of the confluence at the inner bank; (*iii*) slight erosion near the outer bank. The local tributary widening does, however, provoke systematic morphological changes, as highlighted in Figure 6-7 for the tributary and in Figure 6-8 for the main and post-confluence channels.

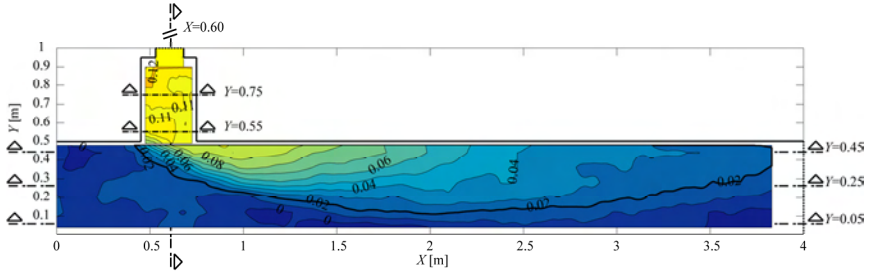

Figure 6-6: Equilibrium bed morphology for the main and post-confluence channels and the local tributary widening with indication of the 2 cross-sections in the tributary widening, 1 longitudinal profile along the tributary axis and the 3 longitudinal profiles in the main and post-confluence channels shown in Figure 6-7 and Figure 6-8. The reference level corresponds to the level of the initially horizontal bed and is situated at Z = 0.02 m.

Water surface elevations in the widening are similar to those in the reference configuration. However, there is a considerable overall rise in bed elevation in the local tributary widening compared to the reference configuration. The widened zone is constituted by a high variability in water depths (Figure 6-7). The flow depth in the axis is reduced to about 0.01 m, which corresponds to approximately half of the flow depth in the reference tributary (Figure 6-7), whereas the maximum flow depth in the thalweg of 0.018 m is still smaller than the reference flow depth in the tributary. The main-channel flow causes a deviation of the thalweg towards the inner bank of the widened zone (Figure 6-7 b, c). Moreover, it creates dry zones and zones of flow stagnation near the outer bank (Figure 6-7 b). As a surprising result, the local widening of the tributary leads to a reduction of about 15% in effective cross-sectional flow area measured at Y= 0.55 m as compared to the reference configuration. This leads to an increase of the tributary velocities and a corresponding increase in the transverse momentum flux provided to the main channel, which can be expected to enhance the hydro-morpho-sedimentary processes in the confluence zone. This is confirmed by the increase in the bed discordance height and the deeper penetration of the tributary into the main channel (Figure 6-7a, Figure 6-8a). The bed discordance is oblique with respect to the main channel and about perpendicular to the thalweg at the tributary mouth (Figure 6-6, Figure 6-8a). The local tributary widening does not affect the average flow depth of about 0.02 m and the average bed slopes of about 1.9% in the tributary upstream of the widening. Moreover, the local tributary widening does not noticeably affect the water surface and bed elevations in the tributary upstream of the widening (Figure 6-7). This implies that the local tributary widening does not have adverse effects on flood safety in the tributary.

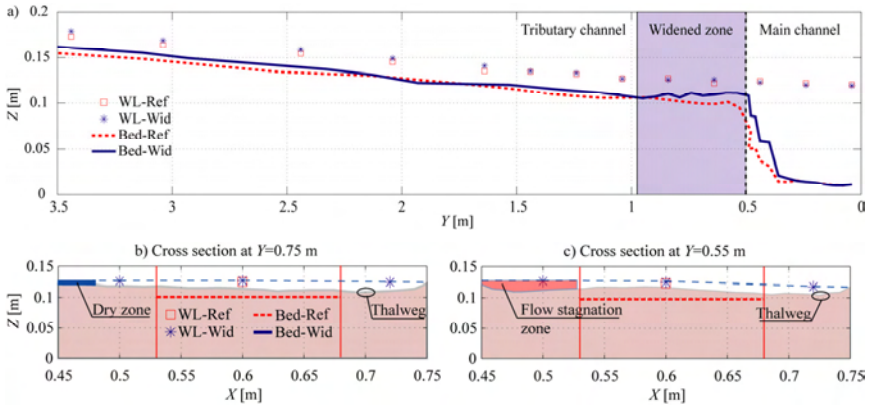

Figure 6-7: Comparison in the tributary of the water surface and bed elevations in the reference configuration and the configuration with local tributary widening. a) Longitudinal profile along the axis of the tributary, b) Cross-sections situated in the middle of the local tributary widening (Y=0.75 m) and at the tributary mouth (Y=0.55 m).

Figure 6-8 illustrates systematic morphological changes in the main and post-confluence channels induced by the local tributary widening. The increased discordance height and tributary penetration (Figure 6-7a) lead to a general rise in the bed level in the confluence zone (Figure 6-8). Downstream of the confluence zone, however, it does not lead to a change in the cross-sectional averaged bed levels (Figure 6-8b) but merely to morphological redistribution (Figure 6-8a). This could have been expected, since the flow and sediment discharge in the post-confluence channel are not modified by the local tributary widening. The morphological redistribution occurs by means of increased bed gradients. Increased deposition on the sediment bar leads to the occurrence of a dry zone at the inner bank just downstream of the confluence. This zone is about 0.65 m long (*X*-axis) and 0.08 m wide (*Y*-axis) and is constituted by fine sand. The increased deposition at the inner bank is about compensated by slightly increased erosion at the outer bank. The slope of the upstream face of the deposition bar along the *X*-axis increases considerably from about 20% in the reference configuration to about 27% in the configuration with local tributary widening (Figure 6-8c). The local tributary widening does not noticeably affect the water surface elevation in the main and post-confluence channels (Figure 6-8b-e). This implies that the local tributary widening does not have adverse effects on flood safety in the main and post-confluence channels.

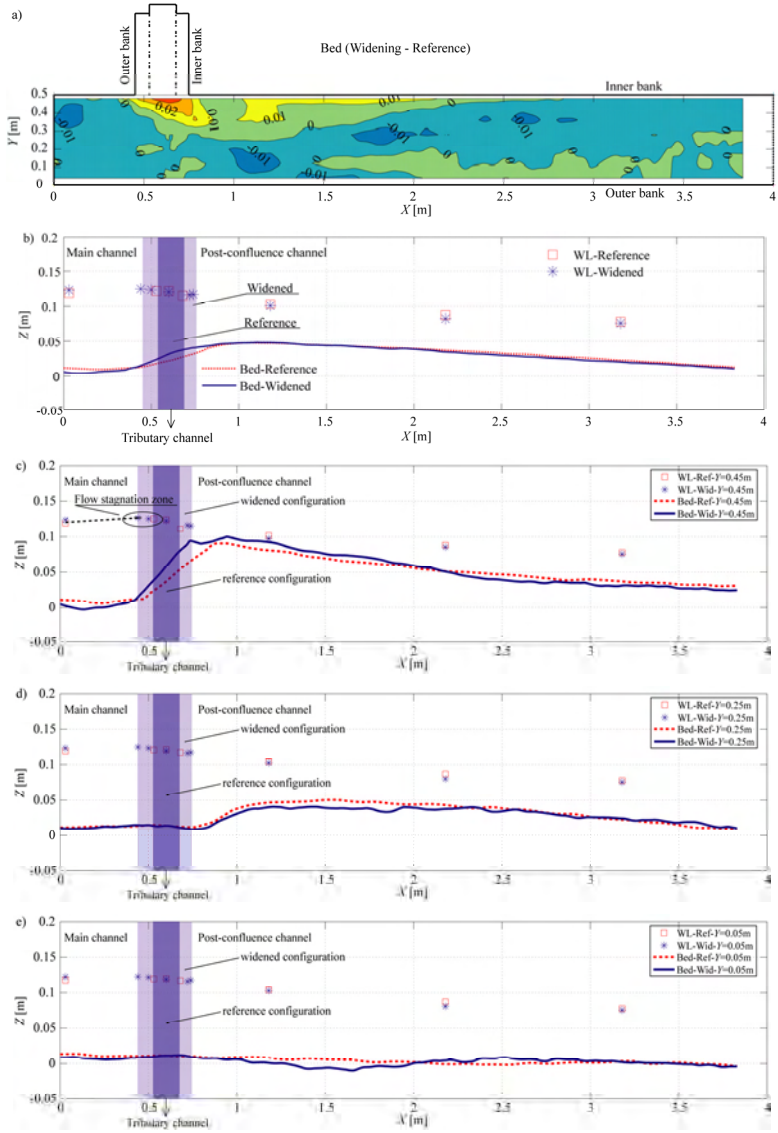

Figure 6-8. Comparison in the main and post-confluence channels of the water surface and bed elevations in the reference configuration and the configuration with local tributary widening. a) Differences in bed topography; b) Longitudinal profile of the cross-sectional averaged water-surface and bed elevations; c), d), e) Longitudinal profiles near the inner bank (Y = 0.45 m), on the channel axis (Y = 25m) and near the outer bank (Y = 0.05 m), respectively.

Visual observations of the local tributary widening and the confluence zone show that the sediment transport corridors also deviate towards the inner bank (Figure 6-9a). In addition, two dry zones constituted of fine sediments are formed at the entrance of the local tributary widening. The presence of a third dry zone at the inner bank in the post-confluence channel shifts the flow and sediment transport corridors in outside direction (Figure 6-9). As qualitatively indicated in Figure 6-9b, the size of the transported sediment increases from the top of the deposition bar towards the toe of the avalanche faces. This sediment sorting on the avalanche face is quantified by means of the grain size distributions in the sampling locations S3 and S4on the top and near the toe of the deposition bar, respectively (Figure 6-10).

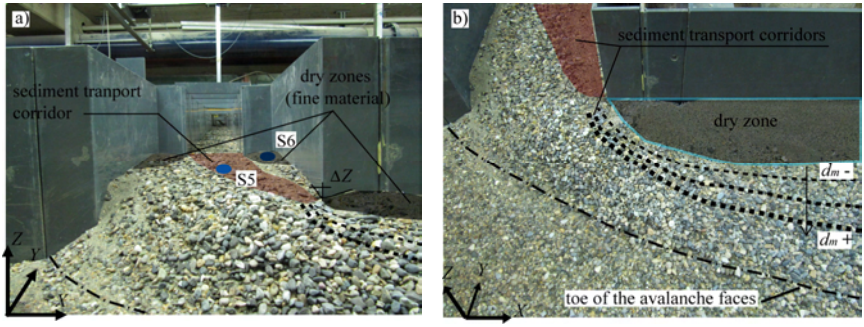

Figure 6-9: Sediment transport corridors, dry zones and avalanche faces based on visual observations in the local tributary widening and the confluence zone. The view is from the outer bank into the tributary.

Figure 6-10 compares the grain size distributions in corresponding locations in the reference configuration and the configuration with local tributary widening. The grain size distributions upstream of the confluence zone in the main channel (S1) and upstream of the local tributary widening (S2) should not be affected by the local tributary widening. Differences between the grain size distributions in both configurations therefore give an indication on the uncertainty in the bed surface sampling procedure. The grain size distribution on the axis of the local tributary widening (S5) is considerably coarser than in the reference tributary (S2). This is consistent with the reduced effective flow area and increased velocities in the local tributary widening. The local tributary widening is characterized by a high heterogeneity in grain sizes, as indicated by the considerable differences in the grain size distributions in the locations S5 (d_m= 5.4 mm) and S6 (d_m= 0.6 mm).

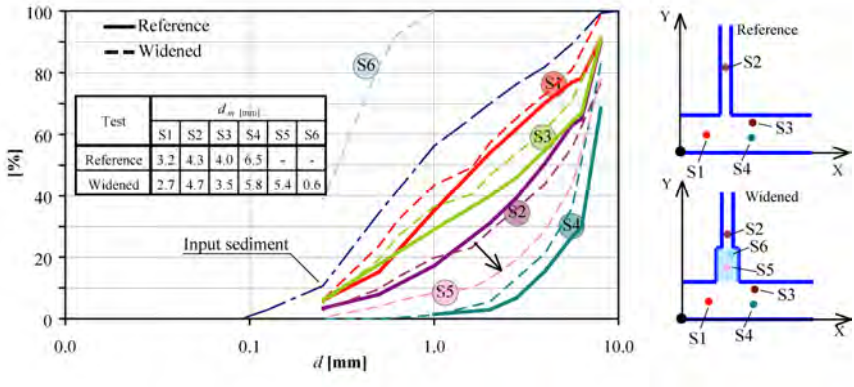

Figure 6-10: Grain size distributions in the sampled locations for the reference configuration (full lines) and the configuration with local tributary widening (dashed lines).

6.4 Flow dynamics

6.4.1 Flow visualization

Flow expands upon entering the local tributary widening (Figure 6-11). The influence of the flow in the main channel induces an asymmetry of the flow expansion, which is deviated towards the inner (downstream) bank of the widened zone. At a distance of 0.27 m from the entrance of the widened zone, the tributary flow is reattached to the inner bank. The flow deviation, however, does not allow the flow to reattach to the outer bank. As a result of this deviation, the tributary flow enters the main channel at an angle of around 65° (Figure 6-11).

At the upstream corner of the confluence, flow originating from the main channel protrudes into the local tributary widening and creates a zone of flow stagnation (Figure 6-11), which is characterized by a slight rise in the water surface elevation. This stagnation zone confines the effective width of the tributary flow, which is not larger at the tributary mouth than in the reference case (Figure 6-11). As aforementioned, this reduced effective width and the reduced flow depth lead to increased tributary velocities and an increased tributary momentum flux into the main channel.

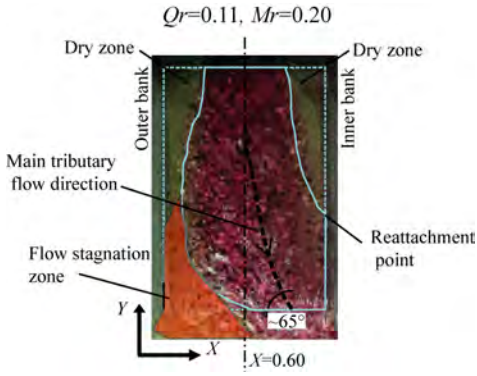

Figure 6-11: Flow visualisation in the local tributary widening using colour dye indicating the main flow features.

The local tributary widening considerably modifies the flow field in the confluence zone (Figure 6-12). The increased height of the deposition bar leads to the formation of a dry zone at the inner bank just downstream of the confluence. This dry zone has a length of about 0.65 m and a width of about 0.08 m. This dry zone and the increased tributary velocities shift the flow field further towards the outer bank of the main channel as compared to the reference configuration. This is well visualized by the position of the shear layer generated by the collision of flow originating from the main channel and the tributary (Figure 6-12).

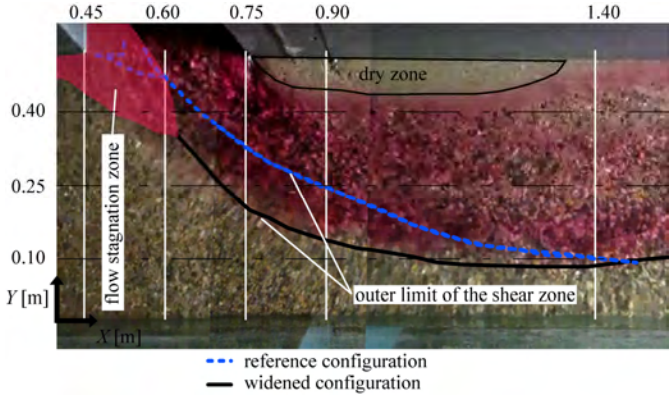

Figure 6-12: Flow visualisation with colour dye introduced in the tributary. Vertical white lines indicate the cross-sections where velocity measurements were performed. The location of the outer limit of the shear layers at the water surface is indicated by the full black line (configuration with local tributary widening) and by the dashed blue line (reference configuration).

6.4.2 The depth-averaged flow field

Figure 6-13 shows the measured patterns of the unit discharges $(q_x, q_y)=(U_xh,U_yh)$ (h is the local flow depth) and the depth-averaged velocities (U_x,U_y) superimposed on a contourplot of the bed morphology in the confluence zone for the configuration with local tributary widening. The local increase in depth-averaged velocity confirms the result of the flow visualization that the tributary flow is mainly conveyed to the main channel near the downstream corner of the confluence. The depth-averaged flow vectors are about parallel to the contourlines of the bed morphology, indicating the important role played by topographic steering: the flow steers around the shallow zones and concentrates in the deepest zones, which is in agreement with the requirements of mass conservation. This leads to considerable outwards mass transport in the confluence zone, accompanied by flow acceleration/deceleration in the outer/inner half of the cross-section. Downstream of the cross-section at X = 1.2 m (Figure 6-13), topographic steering leads to inwards mass transport, as illustrated by the flow vectors measured in the cross-section at X = 1.4 m. The pronounced transverse variations in the flow depth h cause a pronounced non-uniformity of the unit discharge U_xh over the width of the post-confluence channel.

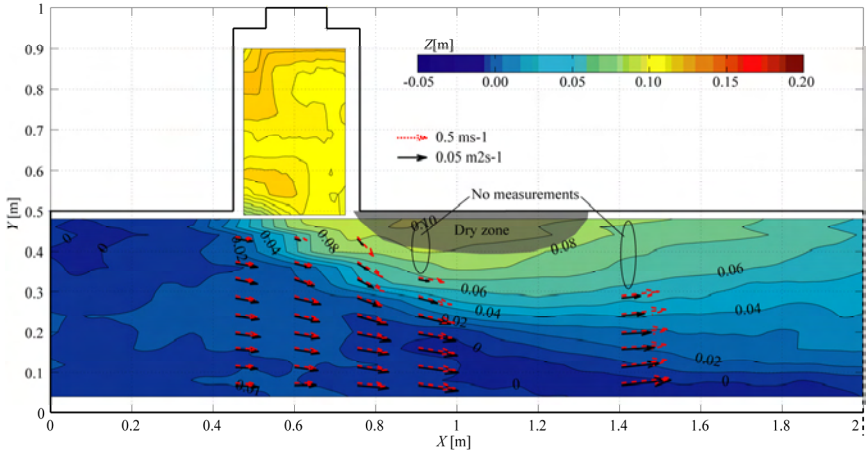

Figure 6-13: Contours of the bed morphology and vector representations of the depth-averaged unit discharges $(q_x, q_y)=(U_xh,U_yh)$ (full vectors) and the depth-averaged velocities (U_x,U_y) (dashed vectors). The dry zone is indicated by the shadow region.

The local tributary widening leads to an amplification of the bed gradients (Figure 6-8a), which also amplifies the topographic steering of the flow. This is illustrated in Figure 6-14,

which assesses the influence of the local tributary widening on the bed morphology and the streamwise unit discharge by comparison of corresponding cross-sections in the reference configuration and the configuration with local tributary widening.

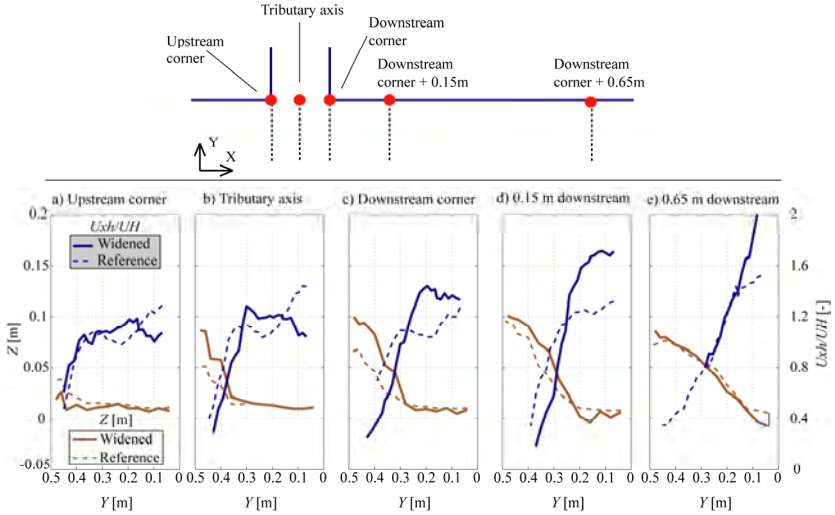

Figure 6-14: Comparison of the normalized streamwise specific discharge, $U_x h/UH$, and the bed morphology in the reference configuration (dashed lines) and the configuration with local tributary widening (full lines). a) At the upstream confluence corner; b) At the tributary axis, c) At the downstream confluence corner, d) 0.15 downstream of the confluence, e) 0.65m downstream of the confluence.

The bed morphology and the unit discharge in the cross-section measured at the upstream corners of the confluences (X=0.53 m for the reference configuration and X=0.45 m for the widened test) are rather similar. The bed morphology and unit discharge are already slightly outwards skewed, which is in agreement with the outwards velocities observed in Figure 6-13. This can be attributed to topographic steering due to the presence of the bar just downstream as well as to the obstruction by the inflow originating from the tributary. The local tributary widening has a marked influence on the bed morphology and the streamwise unit discharge from the cross-section located at the tributary axis on. In the cross-section located at the axis of the tributary (Figure 6-14b), bed elevations are higher for the widened case due to the higher bed discordance and the increased tributary penetration into the post-confluence channel (Figure 6-7 and Figure 6-8). This leads to reduced streamwise unit discharges in the inner part of the cross-section. Outwards deflection of the flow increases the

unit discharge in the outer part of the cross-section. In the reference configuration, the maximum unit discharge is found at the outer bank. In the configuration with local tributary widening, the outward flow deflection has not yet reached the outer bank and the maximum unit discharge is found in the central part of the cross-section. In the cross-section located at the downstream corner of the confluence, the local tributary widening causes a global decrease/increase of the unit discharge in the inner/outer part of the cross-section. The occurrence of a dry zone at the inner bank in the configuration with local tributary widening (Figure 6-12 and Figure 6-13) considerably affects the distribution of the unit discharge in the cross-section situated 0.15m downstream of the confluence. It amplifies the decrease/increase of the unit discharge in the inner/outer part of the cross-section and leads to an increased unit discharge at the outer bank. Morphological differences between both configurations have about died out in the cross-section 0.65 m downstream of the confluence (Figure 6-8, Figure 6-14), which corresponds to the downstream limit of the dry zone in the configuration with local tributary widening (Figure 6-12). The unit discharge at the outer bank is still considerably higher, however, in the configuration with local tributary widening. Due to the increased erosion (maximum about 0.015 m or about 15% of the flow depth) and the increased unit discharge near the outer bank, the local tributary widening may increase the flow attack on the outer bank.

6.4.3 The 3D flow field

The local tributary widening does not fundamentally modify the hydrodynamic processes shwon in Figure 6-3. The three-dimensional flow patterns in the confluence zone in the configuration with local tributary widening are illustrated in Figure 6-15 by means of the patterns of the three mean velocity components (u_x,u_y,u_z) measured in five cross-sections along the main and post-confluence channels. The contour lines correspond to the streamwise velocities (u_x) whereas the vectors represent the transverse and vertical (u_y,u_z) velocities.

The influence of the tributary is already discernable at the upstream corner of the confluence (X = 0.45 m) where considerable outwards velocities occur. Different processes contribute to this transverse mass redistribution. The most important is probably topographic steering due to the presence of the bar just downstream that directs the flow outwards. As shown by the flow visualization, the flow input from the tributary acts as an obstacle (Figure 6-12) that causes a stagnation zone characterized by a rise in the water level near the inner

bank (Figure 6-11). These processes originate at the confluence and weaken with distance from the inner bank.

Flow from the tributary protrudes into the confluence zone and post-confluence channel and thereby changes its direction in a zone about 1.5 m long (Figure 6-13). This tributary inflow mainly remains near the water surface, which is due to the pronounced bed discordance (Figure 6-7 and Figure 6-15b, c). This near-surface flow originating from the tributary occupies at maximum about two thirds of the width of the post-confluence channel (Figure 6-15d). A considerable two-layer flow structure exists near the confluence mouth: flow in the upper part of the water column originating from the tributary is considerably more outwards directed than flow in the lower part of the water column originating from the main channel. This effect is most pronounced near the downstream corner of the confluence (Figure 6-15c) where the main tributary inflow occurs. The skewing of both flow layers, however, does not lead to the generation of secondary flow cells. A shear layer is generated where both skewed flow layers collide (Figure 6-15b-d). The position of this shear layer at the water surface deduced from the velocity patterns (Figure 6-15b- d) is in good agreement with the position indicated by the flow visualization (Figure 6-12). The momentum input by the tributary increases the magnitude of the velocity vector near the inner bank (Figure 6-13, and compare Figure 6-15b and Figure 6-15c). The core of maximum streamwise velocities occurs in the lower part of the water column near the toe of the avalanche face (Figure 6-15b-d). Its coincidence with the transport corridors of the coarsest sediment (Figure 6-9) indicates its importance with respect to sediment transport. In the cross-section situated at $X = 0.90$ m, i.e. 0.15 m downstream of the confluence (Figure 6-15d), the transverse velocities near the inner bank have weakened, but the two-layer flow structure and the core of highest velocities close to the bed near the inner bank are still discernable. This cross-section is characterized by considerable acceleration of the flow, especially on the slope of the sediment deposition bar near the inner bank. This flow acceleration, which plays an important role in the transport of sediment supplied by the tributary, can be attributed to two effects. First, the deposition bar near the inner bank reaches its maximum height (Figure 6-6), which leads to a considerable reduction of the flow area. Second, the near-surface flow originating from the tributary occupies about two thirds of the width (see dye visualization in Figure 6-12) which leads to a contraction of the flow originating from the main channel. The 3D flow patterns confirm the topographic steering of the flow which was identified in the depth-averaged flow patterns (Figure 6-13): flow goes outwards over the entire flow depth in regions where the transverse

bed slope increases in streamwise direction (around X = 1.1 m according to Figure 6-6) and inwards further downstream where the transverse bed slope decreases (Figure 6-15e).

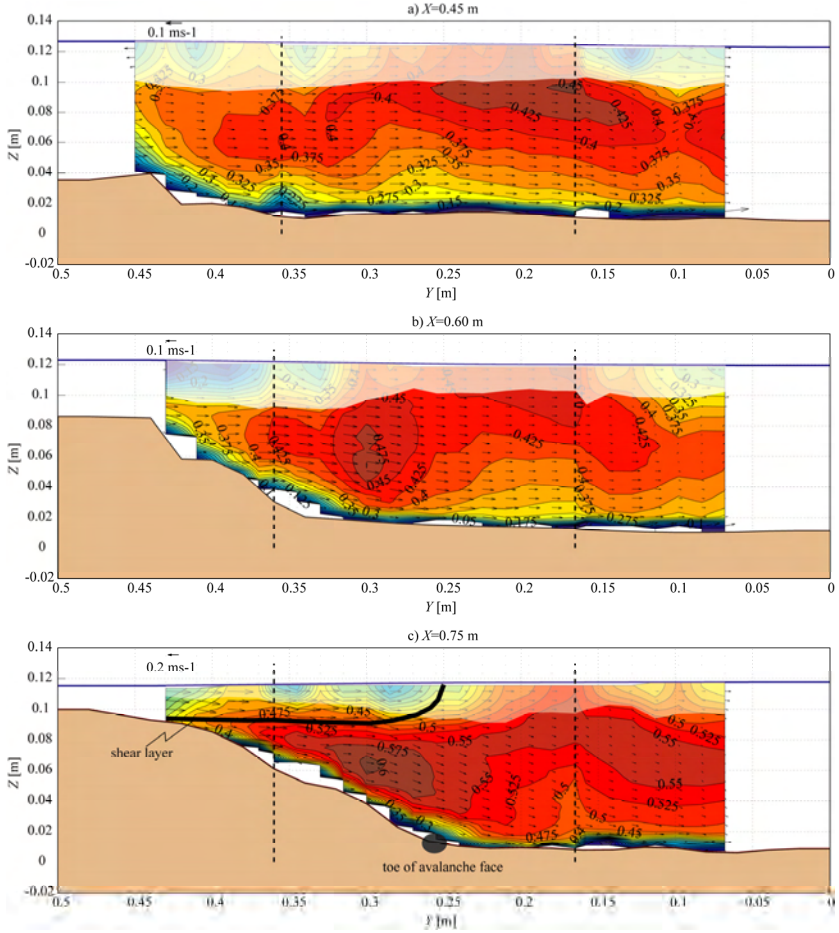

Figure 6-15: Mean streamwise flow velocities u_x (contourlines) and cross-sectional flow vectors (u_y,u_z) measured in the five cross-sections in the main and post-confluence channels indicated in Figure 6-4. The two vertical dashed lines represent the boundaries between measurements performed with the asymmetrical and symmetrical ADVP configurations, whereas the shaded areas indicate regions where the flow measurements are perturbed by the ADVP housing that touches the water surface (more information is provided in Chapter 5). The thick black line indicates the position of the shear layer as inferred from the velocity patterns (present figures), the patterns of the turbulent kinetic energy (Figure 6-18) and the flow visualization (Figure 6-12). The approximated position of the toe of the avalanche faces are indicated by the shadow ellipses.

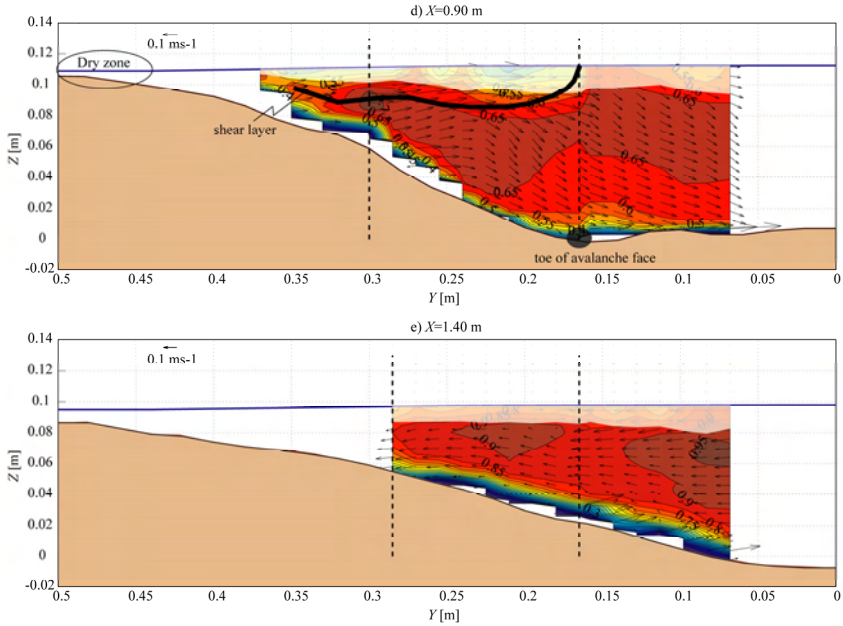

Figure 6-15: (continued).

The key element explaining the differences in the hydro-morpho-sedimentary processes due to the local tributary widening is the amplification of the tributary velocities. The effects of the local tributary widening on the transverse velocities in the main and post-confluence channels are assessed in Figure 6-16. At the downstream corner of the confluence, where the dominant tributary inflow occurs (Figure 6-12 and Figure 6-13), the increased bed discordance and tributary penetration (Figure 6-7 and Figure 6-8) considerably increase the transverse velocities (Figure 6-16a, b). Moreover, these transverse velocities penetrate further outwards in the main channel. This increased transverse tributary input amplifies the two-layer flow structure and its delimiting shear layer generated by the collision of the flows originating from the tributary and the main channel. Non-negligible transverse velocities directed towards the outer bank occur close to the outer bank, and may enhance the flow attack on that bank. These differences induced by the local tributary widening persist in the cross-section 0.15m downstream of the tributary widening (Figure 6-16c, d).

The amplification of the hydrodynamic processes in the confluence induced by the local tributary widening are well illustrated in Figure 6-17, which compares the near bed (Z/h = 0.2) and near-surface (Z/h = 0.7) velocities in both configurations.

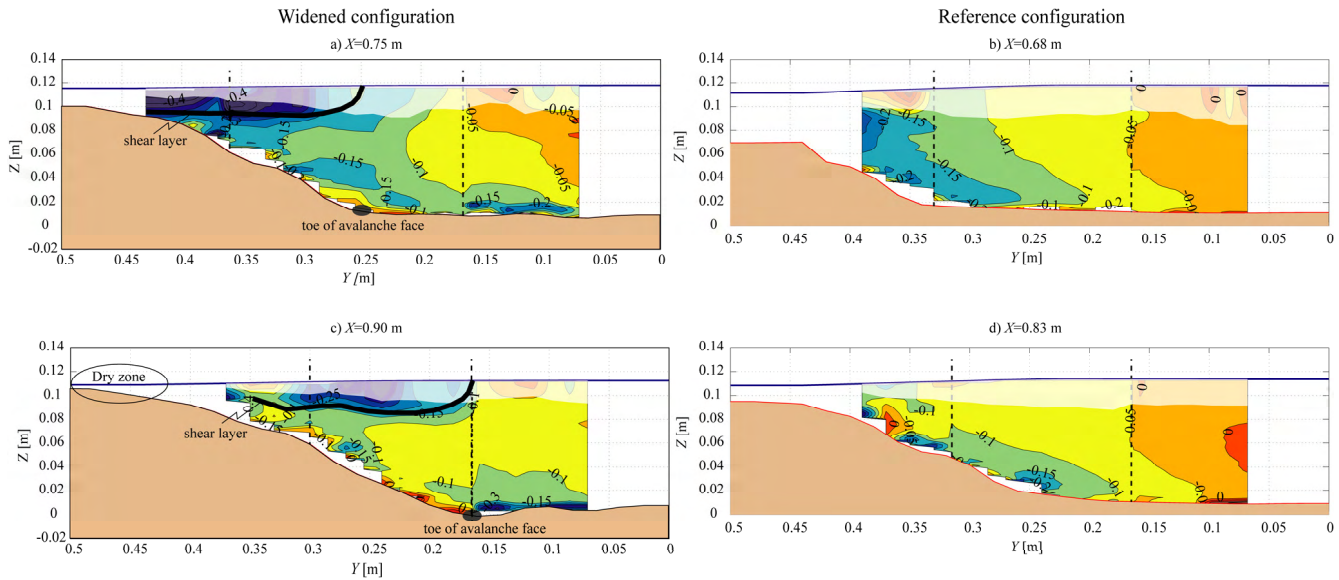

Figure 6-16: Comparison between the patterns of the transverse velocity, u_y, in the confluence zone measured in the configuration with local tributary widening (left column) and the reference configuration (right column). The thick black line indicates the position of the shear layer as inferred from the velocity patterns (Figure 6-15), the patterns of the turbulent kinetic energy (Figure 6-18) and the flow visualization (Figure 6-12). The approximated position of the toe of the avalanche faces are indicated by the shadow ellipses.

Near the inner bank, the near-bed flow from the main channel follows a rather straight path and it is directed upslope the bar (most left near-bed vectors in X = 0.45 m and X = 0.60 m in the widened configuration and in X = 0.53 m and X = 0.60 m in the reference configuration). This upslope flow component conditions the slope of the avalanche faces. The dominant tributary inflow (in X = 0.75 m in the widened configuration and in X = 0.60 m in the reference configuration) can easily be recognized by the near surface velocities that are outwards directed. Their skewing with respect to the near-bed velocities illustrates the two-layer flow structure. The two-layer structure mainly occurs in the region confined by the shear layer, which about coincides with the toe of the avalanche faces. This region is considerably wider in the configuration with local tributary widening than in the reference configuration (Figure 6-16 and Figure 6-17).

The presence of the stagnation zone where the tributary and main-channel flows collide is clearly discernable in the low near surface velocities, occurring near the tributary axis in the widened configuration and near the upstream confluence corner in the reference configuration (Figure 6-17).

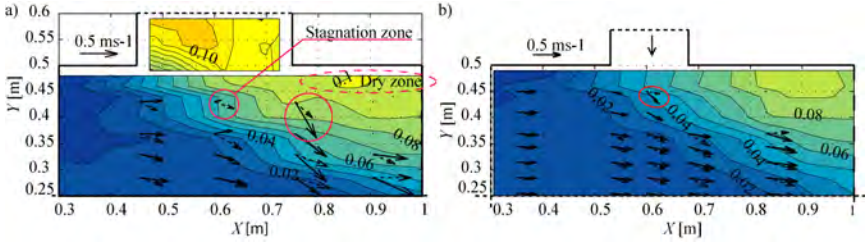

Figure 6-17: Velocity vectors (u_x,u_y) near the bed (Z/h=0.; dashed vectors) and near the surface (Z/h=0.70, full vectors) superimposed on the local bed morphology. (a) configuration with local tributary widening, (b) reference configuration. The dashed circle in (a) indicates the dry zone.

6.4.4 Turbulent flow structure

Confluences locally enhance the turbulence activity, which is relevant with respect to the mixing of mass, momentum, heat, suspended matter and sediment coming from the main channel and the tributary. The patterns of the normalized *tke* measured in the configuration with local tributary widening are displayed in Figure 6-18 for the cross-sections at the downstream corner of the confluence (X=0.75 m) and 0.15 m downstream of the confluence (X = 0.90 m). Turbulence measurements were only performed in the central part of the cross-section (as explained in Chapter 5). The most noticeable features are the zones of pronounced

tke increase. They occur in the upper part of the water column inside the shear layer and further accentuate the two-layer flow structure in the confluence zone. The increased turbulence activity may be attributed to two processes. First the collision of the flows originating from the main channel and the tributary creates a shear layer (indicated in Figure 6-18) that is characterized by increased turbulence activity. Second, the momentum input by the tributary flow increases the magnitude of the velocities in the confluence zone (Figure 6-13 and Figure 6-17) and hence also the turbulence activity, since *tke* scales with the square of the mean velocity magnitude. In line with observations in the reference configuration (Chapter 5), the core of pronounced *tke* increase in the shear layer about coincides with the preferential corridors of sediment transport (Figure 6-9).

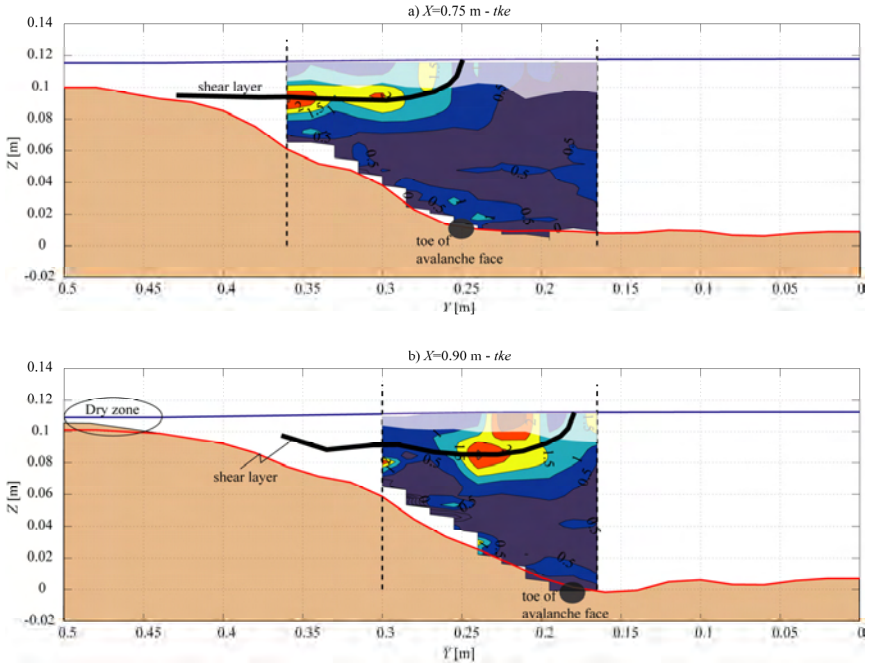

Figure 6-18: Patterns of the normalized turbulent kinetic energy (tke/u_*^2) in the cross-sections at (a) X=0.75 m, (b) and X=.0.90 m in the configuration with local tributary widening. The characteristic shear velocity $u_* = 0.04\ ms^{-1}$ used for the normalization is the same as for the reference case (see Chapter 5).The shaded areas indicate regions where the flow measurements are perturbed by the ADVP housing that touches the water surface (more details in Chapter 5). The thick black line indicates the position of the shear layer as inferred from the velocity patterns (Figure 6-15), the patterns of the turbulent kinetic energy (present figure) and the flow visualization (Figure 6-12).

6.5 Conclusions

Alpine river systems are often channelized and characterized by a high linearity and a high homogeneity in flow, sediment and morphology characteristics. Laboratory experiments indicate that the local widening of tributaries can locally improve the ecological potential of the river system. In the local widening, the heterogeneity of the sediment substrate, the flow velocities and the flow depths is considerably increased and includes such features as dry zones and flow stagnation zones. The local tributary widening does not have adverse effects on flood safety, neither in the post-confluence channel, nor in the tributary upstream of the local widening. Nevertheless the local tributary widening considerably affects the hydro-morpho-sedimentary processes in the confluence zone.

Although the local tributary widening allows a realignment of the tributary flow and a corresponding reduction in the confluence angle, it leads to an amplification of the hydro-morpho-sedimentary processes in the confluence zone. This somewhat counterintuitive result is due to the reduction of the effective flow area in the local tributary widening and the corresponding increase in the tributary velocities and the tributary momentum flux. The reduction in effective flow area allows satisfying the requirements of sediment transport continuity in the local tributary widening. It occurs by means of a general rise in the bed elevation and by a lateral constriction of the flow induced by a zone of flow stagnation at the upstream confluence corner.

The increased tributary velocities accentuate and amplify the two-layer flow structure in the confluence zone. Flow originating from the tributary remains in the upper part of the water column and is strongly outwards directed. Flow originating from the main channel remains in the lower part of the water column and is considerably less outwards directed. This two-layer flow structure does not, however, evolve to secondary flow cells. A pronounced shear layer characterized by increased turbulence activity develops at the interface between flows originating from the main channel and the tributary.

The increased tributary momentum flux due to the local tributary widening leads to an increased bed discordance and a deeper tributary penetration in the confluence zone for the studied discharge scenario. Downstream of the confluence zone, higher deposition/erosion in the inner/outer part of the cross-section amplifies the bed morphology gradients. This represents mainly morphological redistribution, however, because the cross-sectional flow area and the water surface elevation remain unchanged. This morphological redistribution amplifies the topographic steering of the flow and the corresponding transverse fluxes of mass and momentum. It leads to an increased flow attack on the outer bank just downstream of the confluence zone.

7. Influence of the discharge ratio and local tributary widening on the morphodynamics of channel confluences

7.1 Introduction

In alpine regions of Europe, river training works were typically responsible for the transformation of wide and braided rivers into straight channels exhibiting monotonous linear profiles with a lack of structural diversity, i.e. gravel banks, islands, woody debris, riffles or pools. These interventions have impoverished river ecosystems (Dynesius and Nilsson, 1994; Lorenz et al., 1997; Dynesius et al., 2004; Formann et al., 2007; Gurnell et al., 2009). Currently, only about 10% of the most important rivers of the entire European Alpine region are still in a "near-natural" condition (Rohde, 2004).

From the end of the 20th century, "river rehabilitation" has been a concept heavily used by environmental professionals and river management authorities (Bernhardt et al., 2005; Reichert et al., 2007). The purpose of rehabilitation is to recover the vital space required for the rivers which were degraded by human interventions and to link the sustainable use of rivers and wetlands with human well-being (Nakamura et al., 2006). In river systems, the vital space ensures the fluvial dynamics and the interface favourable to the river's fauna and flora. Vital space is necessary to maintain the quantity and quality of the water in the natural water system in order to safeguard its role in the ecosystem over time (Havinga et al., 2005). Thus, rehabilitation projects can be considered as complex processes in which fluvial dynamics, environment and flood protection play an important role (Peter, 2006). No adverse impacts on flood safety resulting from rehabilitation projects can be tolerated. The insufficient understanding of natural conditions may be responsible for the fact that a high proportion of rehabilitation projects fail (Lockwood and Pimm, 1999).

One of the most common solutions used in fluvial rehabilitation schemes is "river widening", which allows the self re-establishment of the natural morphodynamics of a river reach (Hunziger, 1999; Nakamura et al., 2006; Formann et al., 2007). Consequently, it provides a potential to restore some elements of riparian ecosystems by increasing the amount of the in-stream habitat heterogeneity. These solutions have been applied as small-scale restoration measures. However, the success of a rehabilitation project depends on the intervention effects at the catchment scale (Rohde et al., 2004; Rohde et al., 2005; Weber et al., 2009).

In fluvial networks, river channel confluences are the sites of significant changes in flow, bed morphology and sediment transport. Their presence is important notably for the

ecological connectivity, flood control, water quality etc (Sloan et al., 2001; Rice et al., 2008; Wallis et al., 2009). A good understanding of the flow dynamics, of sediment transport patterns and of the development of bed morphology is essential to successfully accomplish river rehabilitation projects in these zones.

Alpine confluences are typically characterized by mountain gravel-bed torrents carrying large sediment loads often connecting asymmetrically at large angles with the main river. As described in Chapter 5, current knowledge on river channel confluences (Mosley, 1976; Best, 1987; Best, 1988; Fujita and Komura, 1989; Best and Roy, 1991; Biron et al., 1993; Rhoads and Kenworthy, 1995; De Serres et al., 1999; Lane et al., 1999b; Rhoads and Kenworthy, 1999; Lane et al., 2000; Biron et al., 2002; Boyer et al., 2006) may not be applicable to these situations. In Chapter 5, an enhanced conceptual framework for the hydro-morpho-sedimentary processes in confluences with low discharge and momentum flux ratio and high sediment delivery ratio was developed through a laboratory flume experiment of a 90º confluence between a small stream and a large channel. These confluences are typical of alpine environments. As shown in Figure 7-1, bed morphology is characterized by the deposition of a bar downstream from the confluence. Differences between the water depths in the tributary and in the main channel are linked to the formation of large bed discordance between the confluent channels. Moreover, there is an absence of a marked scour hole. Concerning the flow, the tributary momentum input, associated with the presence of the deposition bar lead to a considerable mass redistribution in the confluence zone as the main flow is pushed towards the outer bank. Bed discordance is responsible for the presence of a two-layer flow, which plays an important role in dampening the formation of a flow recirculation zone downstream of the confluence. The model has been validated by field observations and contributed in gaining insight on the morphodynamics processes of alpine confluences, which were not yet been considered in previous studies.

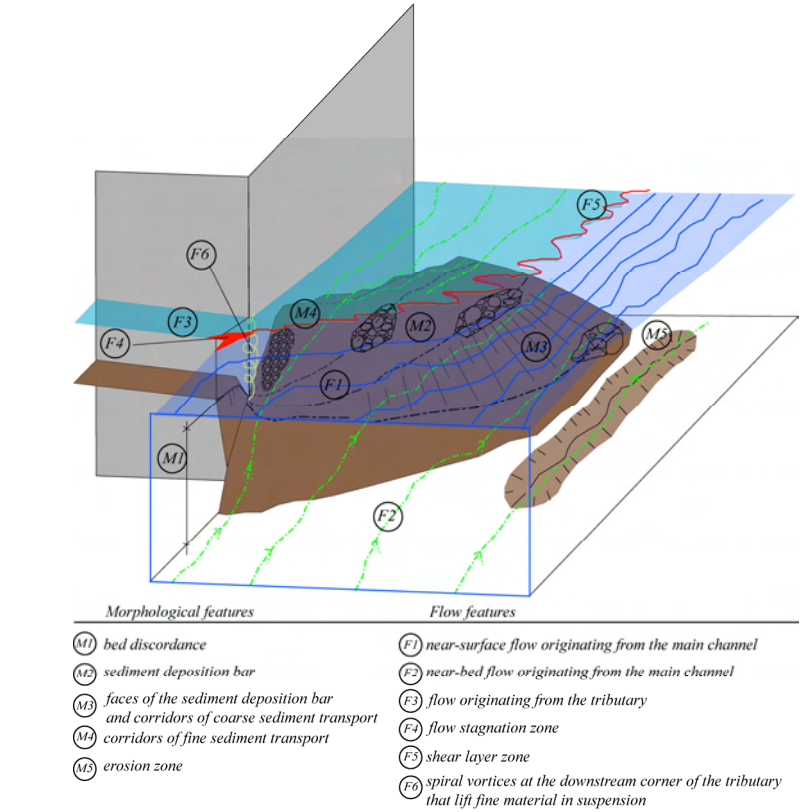

Figure 7-1: Conceptual framework representing the main morphological and flow features of a channel confluence found in alpine regions (Chapter 5).

The water and sediment supply from tributaries can produce important geomorphological adjustments in the main channel, thus increasing the physical heterogeneity in the recipient channel (Rice et al., 2006; Benda, 2008). Bourgeois (2006) performed an extensive analysis of the increase of the "ecological potential" of the Upper Rhone River by an optimal connection of its tributaries in order to guarantee the lateral connectivity of the fluvial system. The analysis is based on four different domains: ecomorphology, flow, water quality and connectivity and it was applied at 20 important confluences of this river. It was concluded that the Upper Rhone basin is currently in an ecological poor state not only because of the channelization main river but also the regulation of it tributaries, as well as the presence of fixed weirs in some confluence zones (Figure 7-2). Increasing the ecological value of most

regulated confluences in the Upper Rhone Valley, however, can be achieved with a relatively small investment (Bourgeois, 2006).

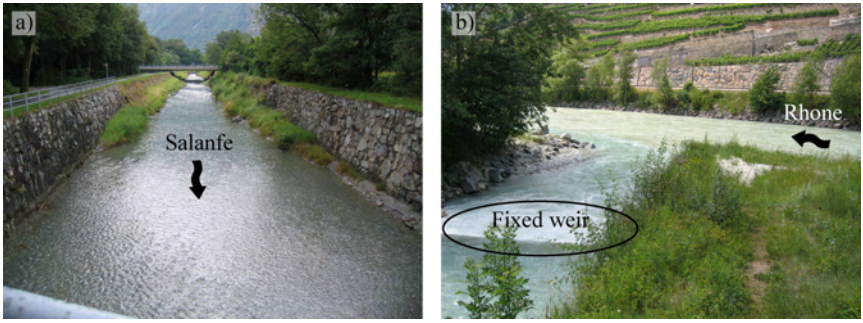

Figure 7-2: a) Upper view of the channelized Salanfe River (tributary of the Upper Rhone) and b) view of the Borgne River showing the fixed weir upstream of the confluence with the Upper Rhone.

In Chapter 6, the possibility to rehabilitate river confluences by means of a local widening of the tributary near its mouth was investigated. The results of the laboratory flume experiment indicated that such a procedure would induce localized changes in the hydro-morpho-sedimentary processes. Globally, it has been suggested that local tributary widening of a 90º confluence such as found in alpine environments would enhance its ecological potential by increasing of the spatial variation of the flow widths, flow depth and flow velocities in the widened zones. It provides a potential local hotspot for biodiversity along confined, channelized and regulated river systems. Furthermore, it does not create noticeable adverse effects on the flood safety in the tributary and the main channel. Due to the influence of the main channel flow, the existing stochastic models developed to predict the morphological and hydraulic consequences of river widening (Stewardson and McMahon, 2002; Schweizer et al., 2007a; Schweizer et al., 2007b) are not applicable for confluence cases.

This paper further investigates the local widening of tributary channels near the confluence with a main channel; in the perspective of river rehabilitation. The influence of changes in discharge ratio and in the shape of the widened area on the morphodynamics of confluence zones is examined by means of systematic laboratory experiments. It aims to answer four important questions:

- What is the influence of the discharge and momentum flux ratios on the morphology of channelized confluences?

- Does a local tributary widening have adverse effects on flood safety of confluence zones?
- How robust/stable is the resulting morphology with respect to changes in the geometric configuration of the tributary widening?
- What is the ecological potential of a local tributary widening in confluence zones?

The analysis is divided in three parts. First, the results of laboratory experiments performed with a reference configuration (without widening) are described (section 7.3). In the second part, the influence of different tributary widening is investigated for different discharge scenarios (section 7.4). The last topic of the paper (section 7.5) discusses the application of local tributary widening in the framework of river rehabilitation projects.

7.2 Experimental investigation

In order to design the experimental set-up and the conditions for the research project, a detailed analysis of the Upper Rhone River basin (Switzerland) and its twenty main confluences between Brig and Lake Geneva was conducted. The analysis is based on the last reach of the tributaries in the floodplain before its junction with the Rhone. This basin was chosen because of its representativeness of regulated alpine river systems. Furthermore, rehabilitation projects are planned in this basin and their design suffers from a lack of knowledge about the morphodynamic processes involving the confluences zones.

The main hydraulic and geometrical characteristics of the Upper Rhone confluences used for designing the experimental set-up and the experimental conditions are summarized in Table 7-1.

Table 7-1: Hydraulic and geometrical characteristics of the main confluences of the Upper Rhone basin.

	Angle [°]	B_t/B_m	$B_m/B_{p\text{-}c}$	*Tributary bed slope [%]*	$Q2_t/Q2_m$	$Q5_t/Q5_m$	Fr_{tQ2}	Fr_{tQ5}	M_r_Q2	M_r_Q5
Average	62	0.22	1.02	1.1%	0.10	0.09	0.83	0.83	0.11	0.08
Max	90	0.54	1.27	4.0%	0.32	0.31	1.29	1.30	0.45	0.30
Min	30	0.07	0.71	0.0%	0.01	0.01	0.03	0.03	0.01	0.01

Generally, the Upper Rhone confluences are characterized small steep tributaries (average tributary slope of 1.1%). During channel-forming events (Q_2 and Q_5), the discharge and momentum flux ratios are relative low ($0.01<Qr<0.32$ and $0.01<Mr<0.45$ respectively). From the analyses of the existing literature (Figure 7-3), it is possible to see that the couples

Mr versus Qr characterizing the Upper Rhone confluences are considerably lower and out of the range than those already investigated in river confluence studies.

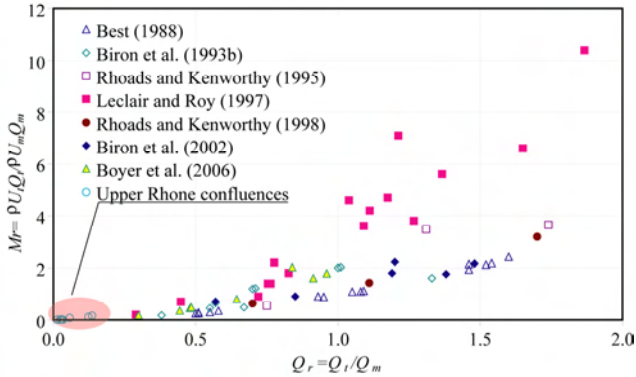

Figure 7-3: Couples of the momentum flux ratios (Mr) versus the discharge ratios (Qr) studied in literature and those characterizing the Upper Rhone confluences. With the exception of Best (1988), who investigated laboratory confluence, all the other works considered field measurements.

The experimental facility was built from an existing straight glass sided flume 8.5 m long and 0.50 m wide located at the École Polytechnique Fédérale de Lausanne (EPFL, Switzerland). The width of this channel, assumed as the main channel ($B_m/B_{p\text{-}c} = 1$) was used to determine the width of the tributary channel, which was made in PVC. From Table 7-1, the average value of B_t/B_m is equal to 0.22 for the Rhone River thus resulting in a very small tributary (~0.10 cm) if scaled exactly. In order to avoid laboratory scale effects, the tributary width was chosen to be equal to 0.15 cm corresponding to a ratio $B_t/B_m = 0.30$. Although higher than the average found along the Upper Rhone, this value is still representative for the studied area.

The tributary (4.9 m long) and the main channel are connected at a right angle (90°), 3.60 m downstream of the inlet of the main channel. The angle corresponds to the maximum value observed at the confluences in the Upper Rhone valley (Table 7-1). The choice of 90° confluence angle is based on the fact that the lateral valleys along the Upper Rhone corridor are almost perpendicular to the main channel. The present state of the confluences zones has been reconstructed during the river training works and consequently the current angles are not natural. Furthermore, the local widening should allow the tributary channel to adjust freely its confluence angle.

The experimental set-up is schematically shown in Figure 7-4. All the results presented in this paper are related to the reference axes (*X, Y, Z)*.

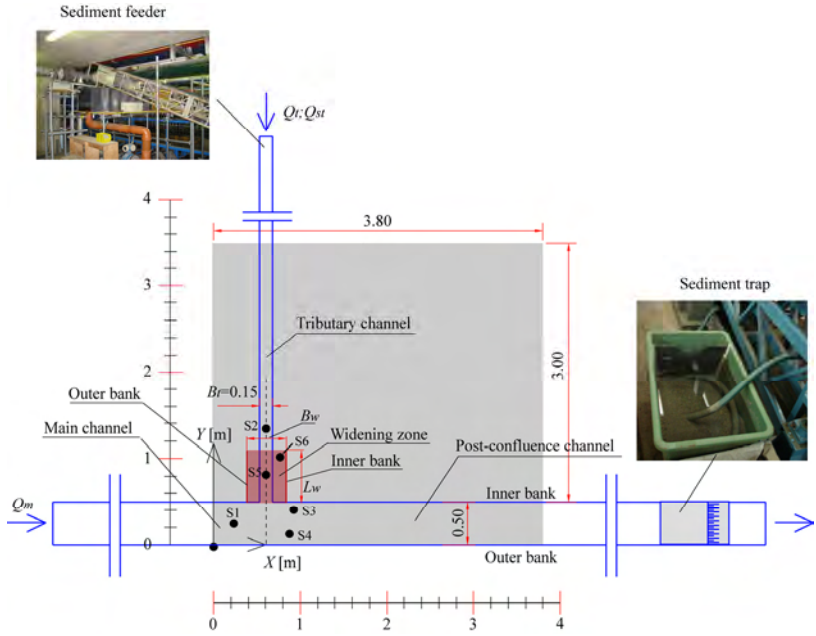

Figure 7-4: Experimental set-up. The locations of the bed samples are indicated by the dark circles.

In the present experimental investigation, the long-term averaged state of a dynamic equilibrium is investigated and therefore, an approach based on steady flows and sediment discharge was adopted. Sediments are only introduced in the tributary and there is no sediment transport in the main channel upstream of the confluence. This procedure aims at reproducing the situation of river confluences during tributary flood events where the amount of the tributary bed load discharge is relatively more important than that of the main channel. In fluvial systems, however, the constant variation of discharges are fundamental elements of river ecosystems (Schweizer et al., 2007b; Tal and Paola, 2010), guarantying for example the dynamics of the channel morphology, the remobilization of the bed subtract and the supply of the organic matter (Rice et al., 2008; Wallis et al., 2009).

Three water discharge scenarios were chosen in the range of the discharge ratios Q_t/Q_m presented in Table 7-1: a "low discharge scenario", where Q_t=2 l/s and Q_m=18 l/s (Q_t/Q_m=0.11), an "intermediate discharge scenario" with Q_t=2.6 l/s and Q_m=17.4 l/s (Q_t/Q_m=0.15) and a "high discharge scenario" where Q_t=3.7 l/s and Q_m=16.3 l/s (Q_t/Q_m=0.23).

The magnitude of the discharges was primarily based on the analyses of width-to-depth ratios (B/h). The criterion was to have $B/h \geq 5$ in the main and post-confluence channels.

Figure 7-5a shows the particle size distribution of the poorly-sorted sediments used in the experiments, which consists of a mixture of 80% sand (0 - 4 mm) and 20% gravel (4-8 mm). A picture of the mixture is depicted in Figure 7-5b. The sediments of the bed material and the solid discharge have a d_{50} = 0.82 mm, d_m = 2.3 mm and d_{90} = 5.7 mm. The sediment characteristics and the solid discharge adopted for all experiments satisfy two requirements:

- The grain size distribution, characterized by the dimensionless grain size distribution with respect to the average diameter (d_m) is representative of the Upper Rhone River. The gradation coefficient of the used mixture is σ = 4.15, which is representative for the grain size distributions found in the Upper Rhone (Figure 7-5a).
- The solid discharge in the tributary channel was set at $Q_{s,t}$=0.30 kg/min for all tests. This sediment input led to longitudinal channel slopes that are representative of the Upper Rhone tributaries (Table 7-1).

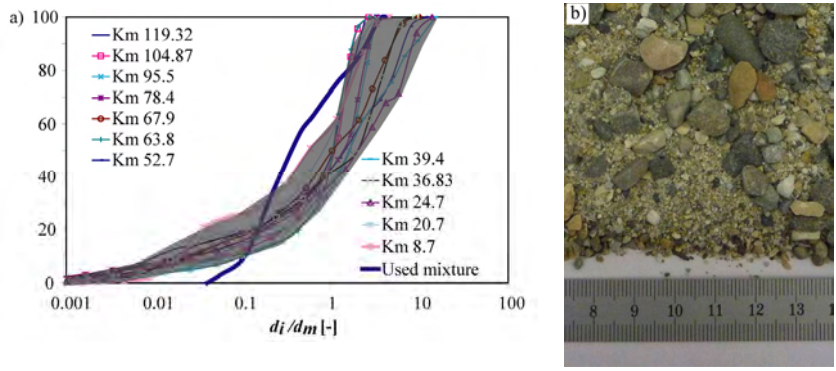

Figure 7-5: a) Dimensionless grain size distribution of the bed surface of the Upper Rhone River at different locations and that of the sediment mixture used for the experiments and b) a picture of the adopted sediments mixture.

Four geometric configurations of the confluence zone (Figure 7-6) including the reference case (no widening) and three local tributary widening are analysed. For the "Small" configuration, the tributary width has been symmetrically doubled (B_w = 0.30 m) over a length (L_w) of 45 cm while the "Medium" configuration considers a tributary three times wider (B_w = 0.45 m) within the same length (L_w = 0.45 m). The "Large" configuration is composed by a tributary also three times wider (B_w = 0.45 m) over a length L_w = 0.60 m.

The choice of the widening configurations is based on two criteria: (*i*) the maximum width of the enlarged zone is limited by the width of the main channel, as wider configurations could result in a local main channel widening and (*ii*) the length of the widened zone is limited by the fact that for longer widenings, the flow reattachment downstream of the entrance of the enlarged zone would occur symmetrically and thus the effect of a local widening in the confluence zone would be lost.

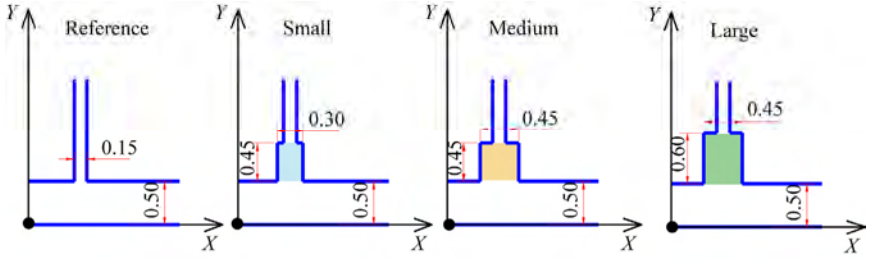

Figure 7-6: Configurations of the confluence zone.
The reference axis is the same as presented in Figure 7-4.

For all experiments, the beds of the main channel and of the tributary were initially covered with the poorly sorted sediment mixture. At the beginning of the experiment, the bed of the main and post-confluence channels was flat and the longitudinal slope of the tributary at its mouth was approximately 0.05%. An adjustable tailgate at the end of the post-confluence channel controlled the flow depth within the entire flume. The water level at the end of the channel was kept constant at 0.07 m. At the beginning of the test, it leads to flow depths of 0.09 m in the main channel and 0.06 m in the tributary.

Due to the initial deficit of sediment transport capacity, all experiments are characterized by aggradation in the tributary. The achievement of equilibrium was mainly assessed on the basis of changes in the bed morphology. The duration of the tests varied from 22 and 24 hours.

Several campaigns of topographic surveys were performed during each run. Bed elevations are measured using a Mini EchoSounder probe (UltraLab UWS) that works with an ultrasonic-impulse-run time procedure with a precision of ±1 mm (Kantoush et al., 2008). The instrumentation is installed on a movable frame that covers part of the experimental set-up, 3.80 m in the main and post-confluence channels and 3.00 m in the tributary (Figure 7-4). For each series of measurement, 12 longitudinal profiles laterally spaced by 4 cm are measured in the main and post-confluence channels. The distance between measured points of each profile

is 9 mm. In the tributary, measurements are done in cross-sections spaced by 5 cm near the confluence zone ($0.5<Y<0.95$ m) and 20 cm in the upstream reach. For the reference configuration, the cross-sections of the tributary are rectangular and for this reason, only one point at the middle of the section is measured. In the enlarged zones, several cross sections (X-axis) spaced by 5 cm are measured. As for the main and post-confluence channels, the distance of the measured points in each cross-section is 9 mm. The point topographic data are then linearly interpolated to obtain the bathymetric maps.

Water elevations are measured in three points ($Y = 0.05$, $Y = 0.25$ and $Y = 0.45$ m) of seven cross-sections in the main and post-confluence channels and in eight points of the tributary upstream of the widening. In the enlarged zone, cross-sections (X-direction) distanced by 5 cm are measured and in each section, three points are recorded. Each point is recorded during 10 s with a frequency of 128 Hz. and an average value is considered for the analyses.

7.3 Reference configuration

Equilibrium bed morphologies of the confluence zones ($0<X<2$ m and $0<Y<1.2$ m) as well as the position of selected cross and longitudinal sections for all tests are shown Figure 7-7. All the longitudinal sections analysed in this paper consider the entire domain of measurements ($0<X<4$ m and $0<Y<3.5$ m). This section analyses the influence of the different discharge scenarios on the morphodynamics of the reference configuration (first line of the Figure 7-7).

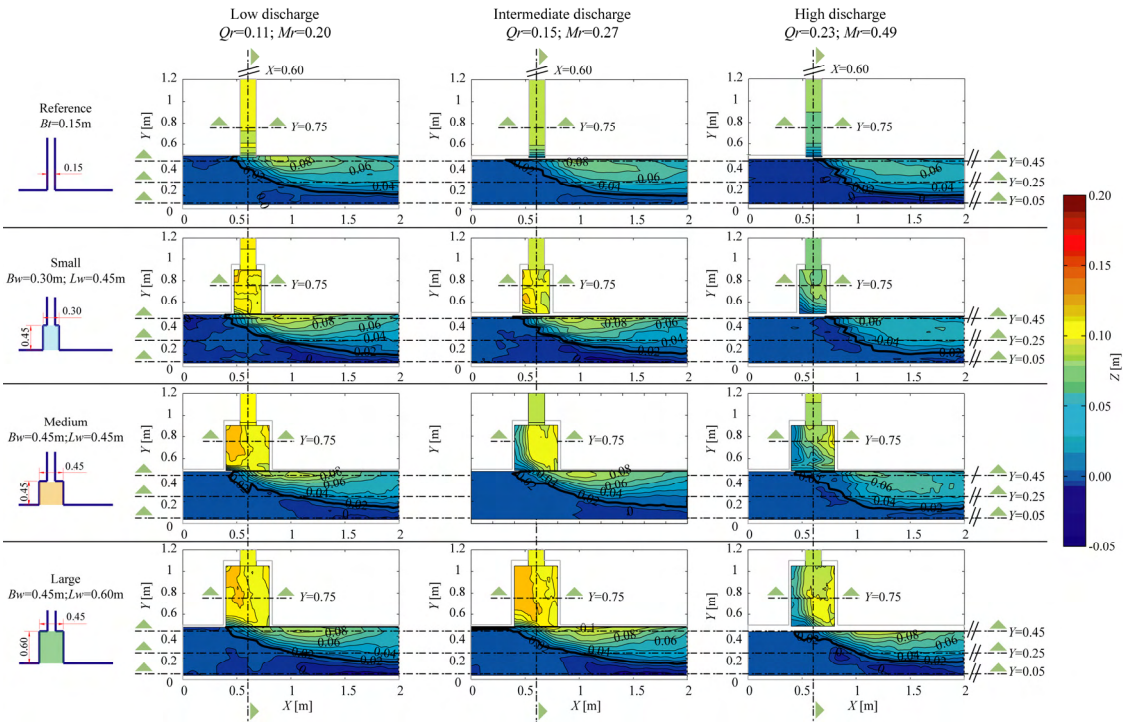

Figure 7-7: Equilibrium bathymetry of the main, post-confluence and part of the tributary channels for the three discharge scenarios and the reference and widened configurations. Contour lines denote the bed elevation, Z[m]. The limit of the sediment bar corresponds to the main channel bed elevation (elevation Z=0.02 m) and is marked by thick black line. The location of the cross and longitudinal sections are represented by the dashed lines.

7.3.1 Hydraulic characteristics

For all experiments, the flow is subcritical in the main and post-confluence channels (Table 7-2). The flows in the tributary for the tests *Low-Reference* and *Intermediate-Reference* are characterized by a supercritical regime with Froude Numbers Fr = 1.30 and 1.20 respectively. Froude Number is defined as $Fr = U / \sqrt{gH}$, where U denotes the mean velocity [ms^{-1}], g, the acceleration due to the gravity [ms^{-2}] and H the flow depth [m]. This leads to a change of flow regime in the confluence zone by means of a weak undulated hydraulic jump (Chow, 1959). The test *High-Reference* is characterized by a transcritical flow (Fr~1) in the tributary.

The hydraulic conditions of the experiments performed with the reference configuration are shown in Table 7-2. At equilibrium conditions, momentum flux ratios Mr resulting from the reference tests are equal to 0.20, 0.27 and 0.49, respectively for the runs *Low-Reference*, *Intermediate-Reference* and *High-Reference*. These values are in the range of those found in the Upper Rhone valley (Table 7-1).

Table 7-2: Hydraulic characteristics of the investigated discharge scenarios

Scenario	Q_m [l/s]	Q_t [l/s]	Q_t/Q_m	Qs_t [kg/min]	Fr_m	Fr_t	Fr_{p-c}	*Mr*
Low	18.0	2.0	0.11	0.3	0.34	1.30	0.70	0.20
Intermediate	17.4	2.6	0.15	0.3	0.31	1.20	0.70	0.27
High	16.3	3.7	0.23	0.3	0.25	1.00	0.70	0.49

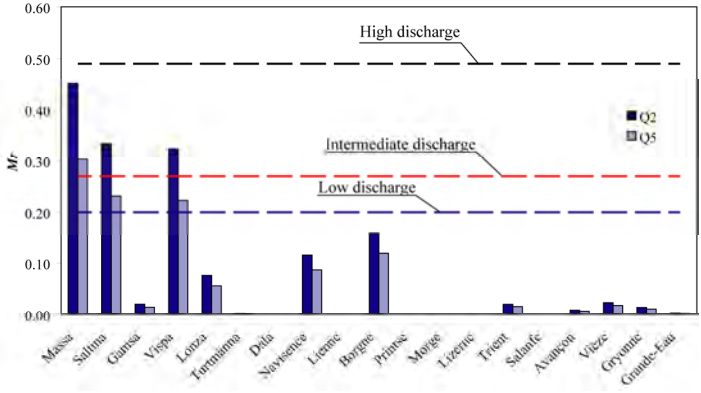

Figure 7-8: Momentum flux ratios estimated for the Upper Rhone confluences and resulting from the experiments.

7.3.2 Equilibrium water surfaces and bed morphologies

The main morphological features resulting from the different discharge scenarios tested with the reference configuration (first line of the Figure 7-7) are quite similar. This is in agreement with the conceptual framework proposed in Chapter 5 based on the low discharge scenario. However, differences concerning the magnitude of the bed discordance, tributary penetration, deposition bar and erosion zone can be highlighted.

The equilibrium bed morphologies in the post-confluence channels are characterized by the formation of a substantial deposition bar near the inner bank which attains its maximum height just downstream of the confluence (Figure 7-9a) and then, decreases with a width-averaged slope of 1.1% towards downstream. A corridor of fine sediment transport near the inner bank is associated with a small depression in the post-confluence channel (Figure 7-9).

With the increase of the discharge ratio, the volume of the sediment bar reduces and the deposits are shifted towards downstream. For the run *Low-Reference,* the sediment bar attains its maximum elevation of 0.09 m at $X = 0.85$ m, while for the runs *Intermediate-Reference* and *High-Reference* the highest points are at the elevations 0.082 m ($X = 0.97$ m) respectively 0.07 m ($X = 1.07$ m). At the centre of the main and post-confluence channels the longitudinal profile of the deposit is the same for all tests (Figure 7-9b).

The presence of the deposition bar causes a reduction of the cross-sectional area downstream of the confluence. As the flow upstream of the confluence is subcritical, this reduction in area leads to the increase of energy in the main channel and subsequently the acceleration of the flow, which is responsible for the slight erosion along to the sediment bar (Figure 7-9c). The erosion slightly increases with the increase of the discharge ratio.

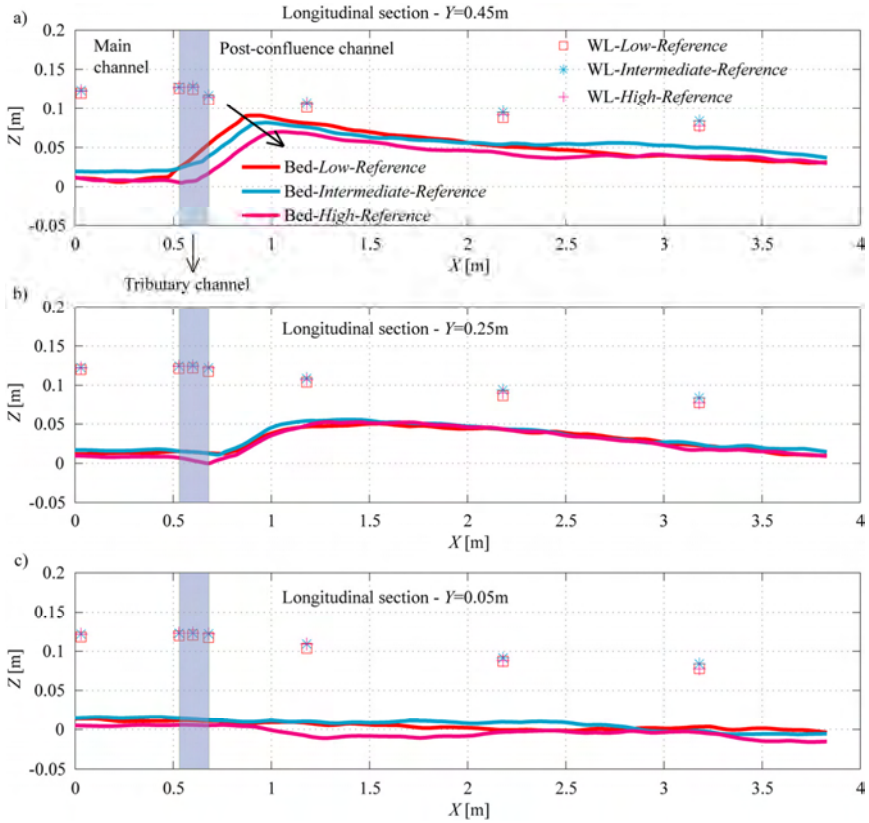

Figure 7-9: Longitudinal sections of the main and post-confluence channels at a) Y=0.45 m, b) Y=0.25 m and c) Y=0.05 m showing the water levels and bed elevations for the three tests performed with the reference configuration (B_t=0.15 m).

As the solid discharge and the composition of the sediment input material are constant for all tests, the increase of the tributary discharge leads to an increase of the tributary flow depth (H_t=0.02 m, 0.026 m and 0.04 m respectively for the low, intermediate and high discharges) and a reduction of the equilibrium tributary bed slope (S_t~1.9%, 1.5% and 1.2% respectively for the low, intermediate and high discharges). Therefore, bed discordance decreases with the discharge ratio, which is in accordance with the conceptual model describing bed discordances in Chapter 5. Differences in bed elevation of 0.09 m, 0.078 m and 0.072 m are observed for the runs *Low-Reference*, *Intermediate-Reference* and *High-Reference* respectively. Another important observation is related to the tributary penetration into the

main channel. As shown in Figure 7-10 (dashed ellipse), it decreases from the *Low-Reference* test to the *High-Reference* tests.

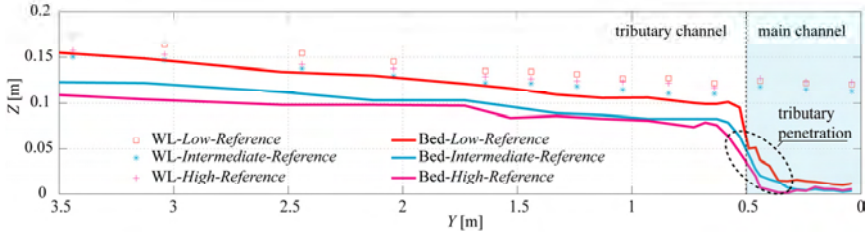

Figure 7-10: Longitudinal profiles of the tributary channel at X=0.60 m showing the final water and bed elevations for the tests performed with the reference configuration. The dashed ellipse indicates the tributary penetration into the main channel.

7.3.3 Influence of the discharge ratio and the momentum flux ratio on the hydro-morpho-sedimentary processes in the reference case

The imposed hydraulic (constant water discharges and fixed water level at the downstream end of the post-confluence channel) and sediment supply conditions (constant solid discharges and sediment characteristics) lead to equilibrium morphodynamic situations, which can be parameterized by the momentum flux ratio $Mr=(\rho QU_t/\rho QU_m)$ between the tributary and the main channel. Here, ρ is the water density [kgm^{-3}], Q the discharge [m^3s^{-1}], U the mean velocity [ms^{-1}] and the subscripts t and m represent respectively the tributary and the main channels. Since this parameter takes into account the ratio between the upstream discharges and also the ratio between the flow velocities and considering that in uniform conditions flow velocity is a function of the bed slope, it is the most appropriate control variable for describing the hydro-morpho-sedimentary processes in confluences (Biron et al., 1993; Rhoads and Kenworthy, 1995; Biron et al., 1996a; Rhoads and Kenworthy, 1998; Biron et al., 2002; Boyer et al., 2006).

Increasing the discharge ratio leads to an increase of the discharge that is confined near the inner bank by the main channel flow and also indirectly increases the sediment transport capacity in the tributary. This explains the reduction of the tributary penetration and of the sediment volume in the bar observed with the increase of the tributary flow.

Visual observations of the surface flow indicate that the lateral expansion and intensity of the shear zone increases slightly with the increase of the momentum flux ratio (Figure 7-11). As described in Chapters 5 and 6, the lateral expansion of the bar (here delineated by

the elevation curve 0.02 m, see Figure 7-7) is directly linked to the outer limits of the shear layer as seen from the above. The greater lateral expansion of the shear layer is associated with a decrease of the intensity of the two-layer flow and to a greater deflection of the main flow towards the outer bank. The lateral expansion of the shear layer induces a greater acceleration of the main flow which in turn generates more erosion of the bar side (Figure 7-9c).

These results are interesting because one could expect that an increase in tributary discharge would cause a shift of the shear layer towards the outer bank of the post-confluence channel. This is not the case and the outside edge of the shear layer is found at about the same position for the three flow conditions. This indicates that the system is mainly determined by the sediment input, which conditions the morphology in the confluence zone and the post-confluence channel (where the solid and water discharges are the same for all configurations). And this morphology determines the position of the shear layer (it seems to occur above the toe of the avalanche faces) and the global flow distribution.

The behaviour of the two-layer flow due to the presence of the bed discordance in confluence zone described in Chapter 5 is also modified with the increasing discharge ratios. The low discharge scenario leads to low momentum flux ratio and higher bed discordance. Consequently, near-bed flow coming from the inner bank of the main channel is not deflected completely and part of the main channel flow slips underneath of the tributary flow towards and/or along the inner bank of the post-confluent channel. The increase of the tributary flow (and decrease of the main channel flow) leads to smaller bed discordance and a higher momentum flux ratio. Therefore, the main channel near-bed flow is more influenced by the tributary momentum input and its deflection towards the outer bank of the post-confluence channel increases.

The second line of the Figure 7-11 illustrates the confluence zone for the three runs with colour dye introduced only in the main channel. It shows that for the test *Low-Reference*, water coming from the main channel is found in the inner bank downstream of the confluence. The portion of the water originating from the main flow that passes through to the inner bank decreases with the increase of the discharge ratio.

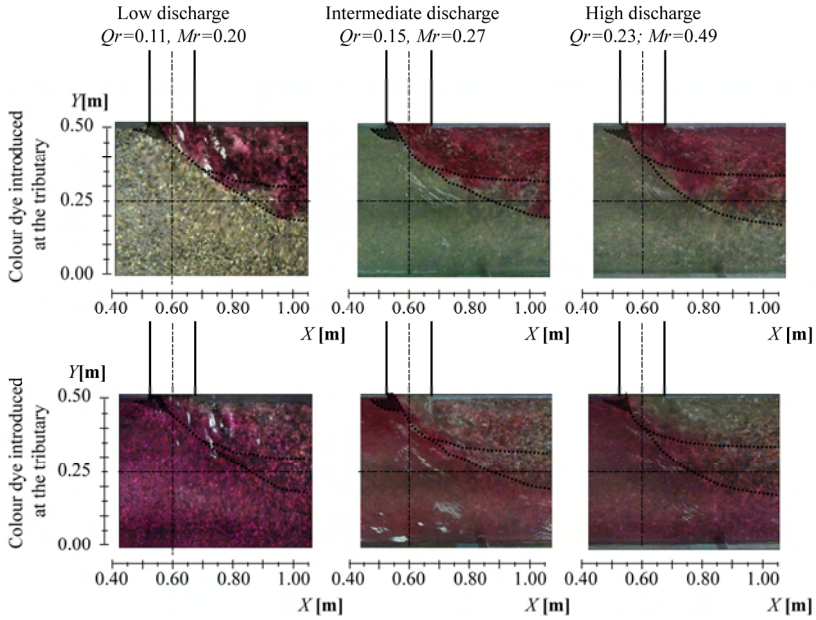

Figure 7-11: Flow visualisation of the confluence zone for the three investigated discharge ratios with the reference configuration. First line: colour dye is injected only in the tributary. Second line: colour dye is injected only in the main channel. The approximate flow stagnation zone and the limits of the shear layer zone are shown by the dashed lines.

The above observations suggest that the near-bed flow has an important influence on the construction and elevation of the bar and on the slope of the avalanche face along the bar. The slope of the avalanche faces decreases with increasing tributary discharge. This means that less upslope flow is required to maintain this slope in equilibrium. And hence a less pronounced two-layer structure of the shear layer is generated.

As described in Chapters 5 and 6, the confluence zones induces a significant sorting of grain sizes. Despite the small magnitude of the differences in sediment size sampled at the same location for different discharge scenarios, some important observations can be highlighted. It can be explained in first approximation by the pseudo-equation proposed by (*Lane*, 1955):

$$Q, Es \sim Q_s, d \qquad \textit{Eq. 7.1}$$

where Q_s and d are the flux and characteristic grain size of bed material load supplied and Q and E_s denote the water discharge and energy gradient respectively.

- In the main channel upstream of the confluence, the reduction of the main flow discharge (Q_m) due to the increase of the discharge ratio is responsible for the reduction of the fine material transported. Therefore, the average diameters of the material constituting the bed surface decrease.
- In the tributary channel, the term on the right-hand side of the Eq. 7.1 remains constant for all tests. It explains the small changes in the sediment size constitution (d) measured at the flume.
- As described in section 7.3.2, the increase of the discharge ratio is associated with the reduction of the sediment deposition on the bar. Generally, higher depositions are associated to fine sediments.
- In the avalanche faces, higher discharge ratios lead to a coarsening of the bed material and it is explained by the increase of the discharge and consequently the shear stress over the avalanche faces.

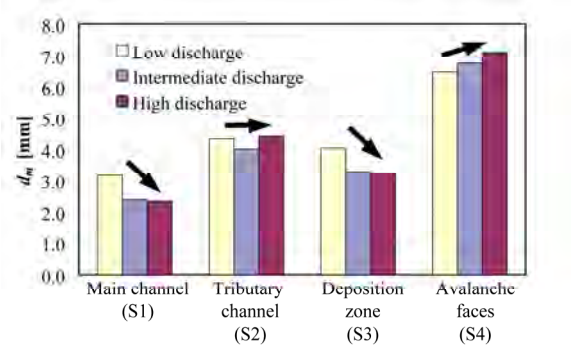

Figure 7-12: Average diameters (d_m) of the bed surface sampled at the different locations.

7.4 Widened configurations

In this section, the three investigated widened tributary geometries are presented for the three discharge scenarios and their changes in comparison with the reference cases are discussed. The bathymetries including the main channel, part of the post-confluence channel, the widened zones and part of the tributaries for all configurations are presented in Figure 7-7.

As illustrated by the cross-sections in the enlarged zones at Y= 0.75 m shown in Figure 7-13, the new equilibrium situations in the widening zones are characterized by higher bed elevations compared to the reference configurations. The adjustments of new bed elevations

are generally associated with the decrease of flow depths and the consequent increase of flow velocities. The examination of Figure 7-13 reveals two important morphologic behaviours in the enlarged zones. For the low and intermediate *Qr*, sediment deposition occurs near the outer bank of the widened zone where bed elevations increase and as a result the talwegs are found near the inner bank of the widened zone. The only exception concerns the test *Intermediate-Medium*, where the bed elevations of the centre of the widening are similar of those measured for the test *Intermediate-Small* but the outer bank of the widening was not filled by the sediments. At high discharge ratios (higher *Mr*), no sediments transported by the tributary reach the outer bank. Consequently, no deposition occurs in this part of the widened zone. Sediments transported by the tributary are mainly deposited near the inner bank and therefore the cross-sections are characterized by a lateral slope towards the outer bank.

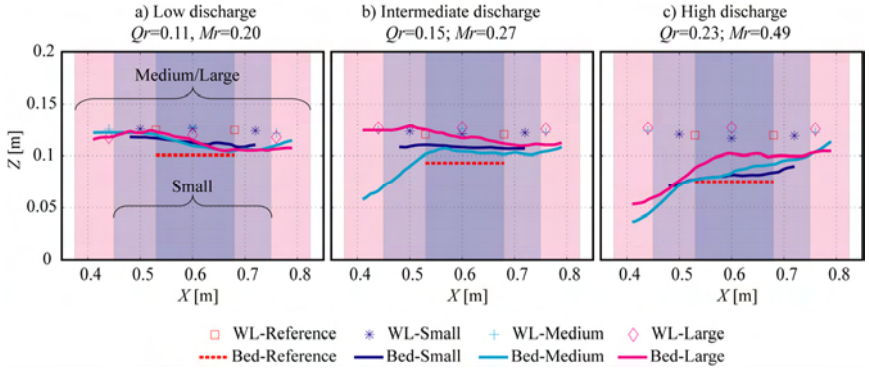

Figure 7-13: Cross-sections at Y=0.75 m in the tributary mouth showing the water levels and bed elevations of all tests. a) Low discharge ratios (Qr=0.11, Mr=0.20), b) Intermediate discharge ratios (Qr=0.15, Mr=0.27) and c) High discharge ratios (Qr=0.23, Mr=0.49). See Figure 7-7 for the location of the cross-sections.

7.4.1 *Influence of the widening on the morphodynamics of the main and post-confluence channels*

Local tributary widening leads to important morphological development of the enlarged zones. However, it is only responsible for local alterations in morphodynamics of post-confluence channels. As described in Chapter 6 for the *Low-Small* test, there is a local increase of the maximum height of the deposition bar which influences the behaviour of the two-layer flow discussed in Chapter 5. The near-bed flow coming from the inner bank of the

main channel is more deflected towards the outer bank. In addition, there is a re-fining of the sediments deposed to the deposition bar.

The analysis of the width-averaged values of water levels and bed elevations in the main and post-confluence channels of the entire dataset (Figure 7-14) reveals that there are no important differences between the investigated configurations tested with the same discharge ratio. The variations of the deposited volume of sediments are limited to the confluence zone and the differences in water levels upstream of the confluence are negligible, being less than 5 mm. These results confirm the findings described in Chapter 6 for different discharge scenarios and tributary configurations.

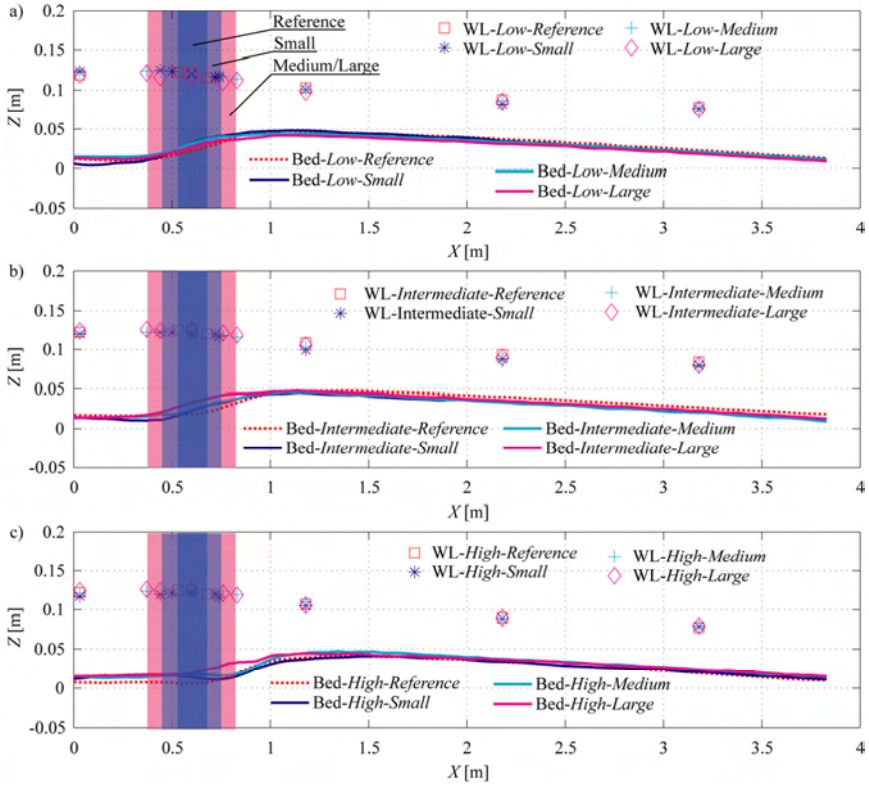

Figure 7-14: Width-averaged water levels and bed elevations at the main and post-confluence channels for all tests. a) Low discharge ratios (Qr=0.11, Mr=0.20), b) Intermediate discharge ratios (Qr=0.15, Mr=0.27) and c) High discharge ratios (Qr=0.23, Mr=0.49).

7.4.2 Influence of the widening on the upstream reach of the tributary

Figure 7-15 illustrates the longitudinal profiles of the tributary (X = 0.60 m) showing the water levels and bed elevations for each of the discharge scenarios and tributary configurations. For all tests, the global differences in water level and bed elevation related to the reference configuration have been calculated for the reach upstream of the widened zones. The mean deviations ($Z_{Widened}$- $Z_{Reference}$) of the entire dataset are typically smaller than the d_{90} of the sediments used in the experiment and therefore, the differences can be considered to be negligible.

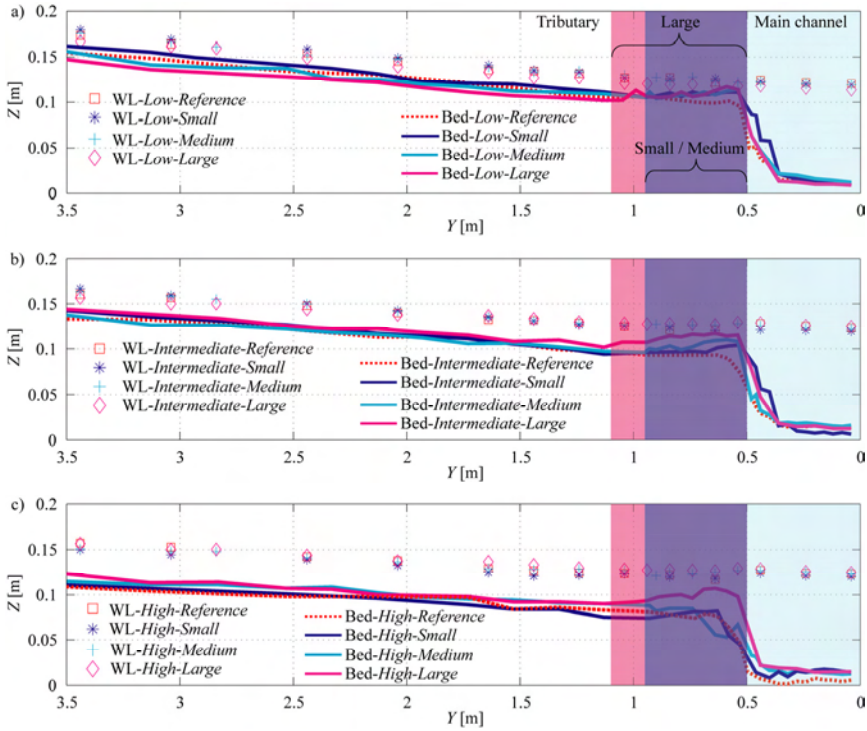

Figure 7-15: Longitudinal profiles along the tributary mid-channel axis (X=0.60 m) showing the water level and bed elevations for the different geometric configuration for a) the Low discharge ratios (Qr=0.11, Mr=0.20), b) the Intermediate discharge ratios (Qr=0.15, Mr=0.27) and c) the High discharge ratios (Qr=0.23, Mr=0.49).

Although there are small differences in the absolute bed and water elevations in the tributary channel upstream of the widened zone, the overall bed and water slopes do not change between the runs performed under the same discharge conditions for the different geometries. These important results indicate that the local widening of the tributary does not affect the upstream hydraulic and morphological behaviour of the tributary channel.

7.4.3 Morphodynamics at the widened zone

The interaction between flow dynamics and sediment transport in the widened zones creates complex three-dimensional bed morphologies, without modifying the water levels. Grain sorting and aggradation are the two dominant morphological processes responsible for the development of equilibrium beds.

Different morphodynamic responses are associated with the different shapes of the enlarged zone and hydraulic conditions. Figure 7-16 shows the flow behaviour in the enlarged zone of the nine tests performed with the widening configurations. For all cases, the flow limits indicated are based on the observation of the surface flow using colour dye. Three important flow features can be distinguished in the enlarged zones. (i) The main flow corridors (*mfc*) recognized by the presence of the colour dye in the flow and the coarse material at the bed surface. It is usually oriented towards the inner bank of the widened zone. (ii) The dry zones (*dz*), where the sediment deposition of quite fine material generally attains the flow surface. (iii) The flow stagnation zones (*fsz*), where the flow depths are relatively high and some recirculation is observed.

The main tributary flow detaches from the confining lateral walls and expands laterally as it enters the widened zone. Due to the relatively short length of the widened zone (L_w), the tributary flow appears to be influenced by the main channel flow well upstream from the tributary mouth. Consequently, the global lateral expansion of the tributary flow does not occur symmetrically on both sides of the widened zone, as is typically the situation in straight channels without the influence of lateral inputs (Hunziger, 1999). For the present experiments, flow reattachment only occurs at the inner bank of the tributary.

The difference between the dry zones and the flow stagnation zones is remarkable. On the one hand, the flow detachment at the entrance of the widened zone creates flow recirculation zones at both upstream corners of the enlarged areas that are mainly supplied by the tributary flow. In the case where fine sediments carried by the tributary are transported

into these zones, it tends to settle, filling up this part of the channel and forming the dry zones (Figure 7-16a). On the other hand, visual observations show that the flow stagnation zones are supplied by the main flow (Figure 7-16g). Therefore, no fine sediments reach these zones and consequently there is no deposition.

For the low discharge ratio scenarios (Figure 7-16a-c), the morphologies on the enlarged zones are quite similar, characterized by a complete filling up of the widened area. The formation of both the upstream dry zones occurs for all tests. The inner dry zones are confined while the outer dry zones extend along borders of the main flow corridors.

The intermediate discharge scenarios (Figure 7-16d-f) show the most important difference between the widened configurations. The small (Figure 7-16d) and large (Figure 7-16e) geometries are characterized by the presence of two dry zones, similar to those encountered for all geometries of the low discharge scenario. The morphodynamic behaviour observed for the medium widening (Figure 7-16e) is marked by the presence of a flow stagnation zone on the outer bank of the widening and a confined dry zone on the inner bank. The outer bank is not completely filled by the sediments.

The presence of flow stagnation zones (*fsz*) at the outer bank of the widening for the high discharge scenarios is the most important characteristic of these tests. As explained above, there is no sedimentation in these zones. Therefore, the final bathymetry of the enlarged zones is characterized by a lateral slope towards the outer bank (Figure 7-13).

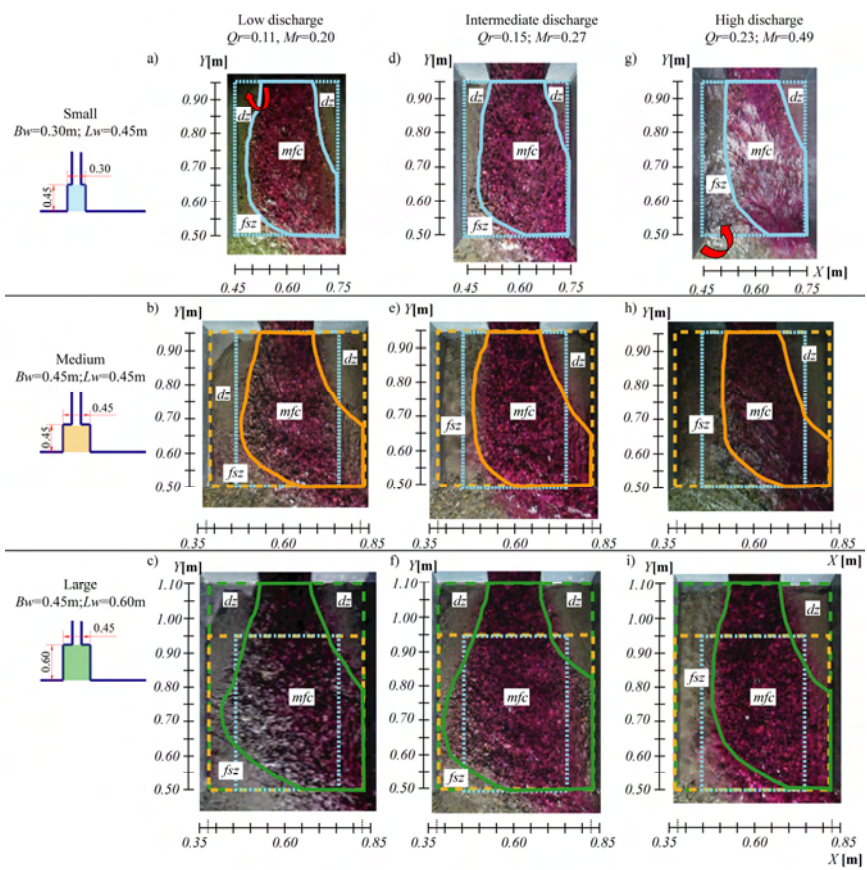

Figure 7-16: Flow visualization of the widened zones for the nine runs using colour dye. "dz" denotes the dry zones, "mfc" the tributary main flow corridors and "fsz" the flow stagnation zones.

The superposition of the main flow zones of different widening configurations illustrated in Figure 7-17 shows important similarities between the different configurations. For all discharge scenarios tested with the same widening length (Small and Medium, L_w = 0.45 m), the outer limits of the main flow corridor do not change substantially.

The efficiency of the widening on the lateral expansion of the main flow increases for the tests performed with the large configurations, for both the inner and outer flow limits. As the distances from the entrance of the widening zone to the confluence increases, main flow corridors have more freedom to widen before being influenced by the main channel flow. For

the investigated configurations, the increased length of the widened zone, however, does not influence the asymmetry of the flow expansion. Even for the large widening, none of the discharges scenarios conduced to outer flow reattachment.

As shown in Figure 7-17, the main flow expansion towards the outer bank as measured from the central axis of the tributary channel is influenced by the length of the widening. For all discharge scenarios, there are no differences between the outer expansions of the tributary main flow for the widening with the same length (Small and Medium). For these cases, the maximum outer widths are around 0.12 m for the low discharges, 0.10 m for the intermediate and 0.075 m (no expansion) for the high discharges. However, a significant flow widening towards the outer bank is observed when the length of the widening increases from 0.45 m ($3*B_t$) to 0.60 m ($4*B_t$). For the Large widening case, the outer flow width reaches 0.17 m for the low and intermediate discharge scenarios while it reaches around 0.11 m for the high discharge test. This behaviour is due to the increased distance from the widened zone entrance to the moment where the tributary flow starts being influenced by the main channel flow due to the confluence.

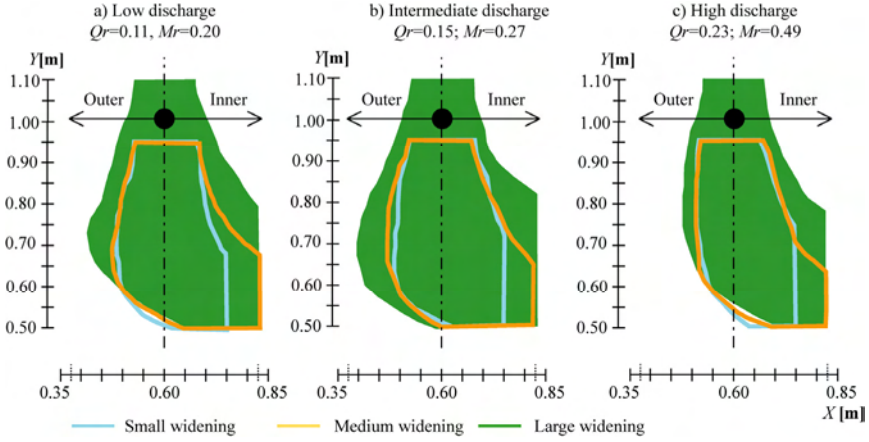

Figure 7-17: Tributary main flow corridors observed in the widened zones. a) Tests with low discharge ratio, b) tests with the intermediate discharge ratios and c) tests with the high discharge ratios.

In all the tests with a widened zone, the presence of the inner bank in the constrained the lateral flow expansion as the flow always reattaches to the inner wall. The distances of reattachment measured from the entrance of the widening (L_r) are, however, different and they depend upon the momentum flux ratios and the width of the widening. As shown in

Figure 7-18, the values of L_r differ only by ±2 cm between the Medium and Large configurations for each discharge scenario. Some similarity in the initial flow expansion angles can also be observed between the different tests. For the low and intermediate discharge scenarios and for all widening configurations, the flow expansion begins symmetric, before being influenced by the flow in the main channel. In these cases, an approximate angle of 15° (referred to the *Y*-axis) is observed. The situation is quite different for the high discharge tests. Flow expansion is asymmetric very early after the tributary flow becomes unconstrained with the outer part showing an angle of 5° and the inner part an angle of 15°. This can be explained by the presence of the flow stagnation zone on the outer part of the widened region, which avoids the outer tributary flow expansion.

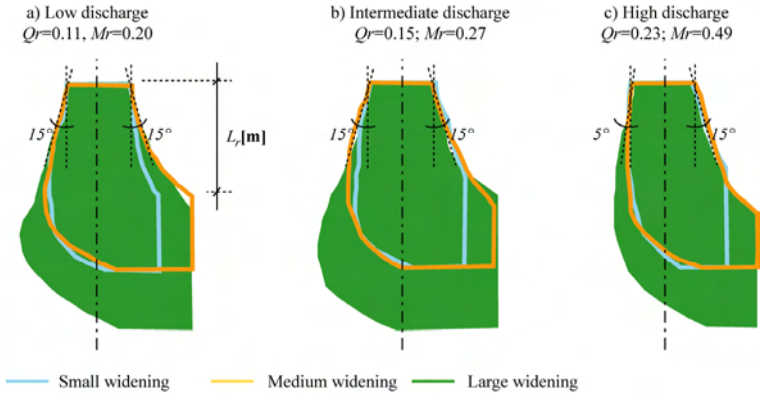

Figure 7-18: Tributary main flow corridors observed in the widened zones. a) Tests with low discharge ratio, b) tests with the intermediate discharge ratios and c) tests with the high discharge ratios. The tributary flow corridors are overlaid with reference to the entrance of the widened zones.

As depicted in Figure 7-19, the main tributary flow corridor (*mfc*) can be divided in three phases in the widening zone. The expansion phase occurs just after the entrance of the widening zone and for the low and intermediate discharges, it does not seem to depend on the main channel. In this part, the flow expands and is at the same time deflected towards the inner bank (Figure 7-16). Contrary to what is observed at rivers with straight reaches that have been widened, the contraction phase of the flow is not due to the channel narrowing downstream of the widening. Instead, it is due to the presence of the confluence, which induces the formation of the flow stagnation zone that consequently causes the deviation of the tributary flow. Between the expansion and the contraction phases, there is an

"intermediate zone" which depends on the widening shape and on the hydro-sedimentary conditions.

The efficiency of each geometry configuration to enhance the expansion of the tributary flow decreases with the increase of the discharge ratio. Different responses are, however, related to the geometric variations of the widening zone. As illustrated by Figure 7-19, the maximum width of the tributary main flow corridor is around 0.26 m (1.75*B_t) for the *Low-Small* test while it is only 0.22 m (1.5*B_t) for the *High-Small* test. It corresponds approximately to 88% and 73% respectively of the total available width. For the medium configuration, the situation is the same. The main flow corridor widens to 0.35 m (2.3*B_t) for the *Low-Medium* test and to 0.30 m (2.0*B_t) for the *High-Medium* test, corresponding respectively to 77% and 67% of the available width. The efficiency of the widening increases for the large configuration, compared to the medium and small ones. Maximum width reaches 0.40 m (2.7*B_t) for the *Low-Large* test and 0.34 m (2.3*B_t) for the *High-Large* test thus corresponding to the best performance in terms of percentage of available area, being 89% and 76% for the *Low-Large* and the *High-Large* tests respectively.

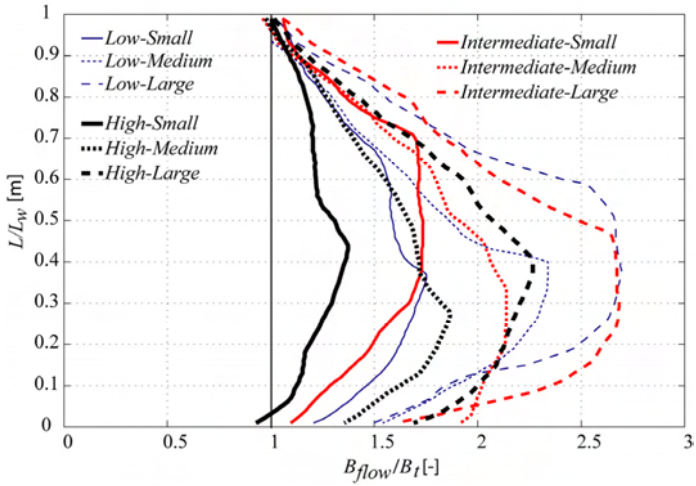

Figure 7-19: Dimensionless total main flow width versus dimensionless widening length. On the ordinate axis, 1 denotes the entrance of the widening zone (Y=0.95 m for the small and medium configurations and Y=1.10 m for the large configuration) and 0 the location of the confluence (Y=0.50 m for all configurations).

The lateral expansion of the tributary flow seems to be directly associated to the length of the widened reach. As illustrated in Figure 7-20a, the maximum percentage of the occupation of

the tributary flow in the widened zone is about 75%. It decreases considerably when the width of the widened area increases for the same length of widening (dashed lines). This behaviour is due to the interaction of the tributary main flow and the flow stagnation zones with the sediment transport, which creates different morphological zones.

The increase of the flow expansion is obtained with the increase of the widening length (L_w), as denoted by the full lines in Figure 7-20a. For the low and intermediate scenarios, the increase is supported in part by the outer expansion of the flow whereas in the high discharge case, the investigated length is not sufficient to provoke an outer expansion.

The ratio L_w/B_w also plays an important role in terms of efficiency of the tributary flow expansion. As illustrated in Figure 7-20b, higher efficiencies of the percentage of the flow occupation increase with the ratio L_w/B_w for the low and intermediate runs. However, for the high discharge scenarios, the increase from L_w/B_w=1.3 (Small) to L_w/B_w=1.5 (Large) seems not to influence the flow occupation, but in both cases, it is considerable higher than that observed for the ratio L_w/B_w=1.0.

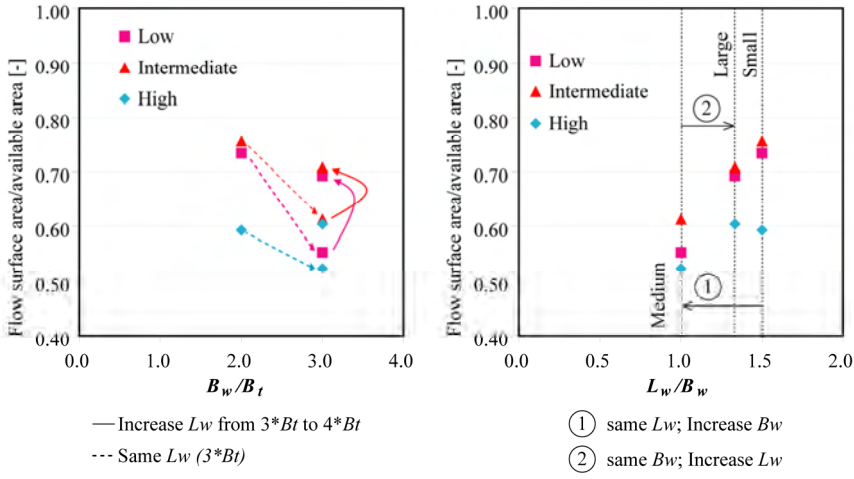

*Figure 7-20: Percentage of the total available surface at the widening zone (Bw*Lw) occupied by the flow as a function of the ratios B_w/B_t (a) and L_w/B_t (b).*

Visual observations during the experiment reveal that the tributary main flow corridors are directly associated with the sediment transport corridors, which are responsible for the development of the bed morphology in the widened zones and for the transfer between the sediment coming from the tributary to the post-confluence channels. Figure 7-21 shows

pictures of the widened area at the end of the Low-Small and the High-Large tests. The two pictures are representative of the main morphological processes described for all experiments. The equilibrium condition is marked by an important narrowing and deviation of the sediment transport corridors as the discharge ratio increases. It precludes a sediment supply to the outer bank of the widened zone, which explains the absence of deposition on the outer bank of the zone. The re-confinement of the flow due to the presence of the confluence also influences the sediment transport corridors, which entrains the narrowing of the corridor near the downstream confluence corner.

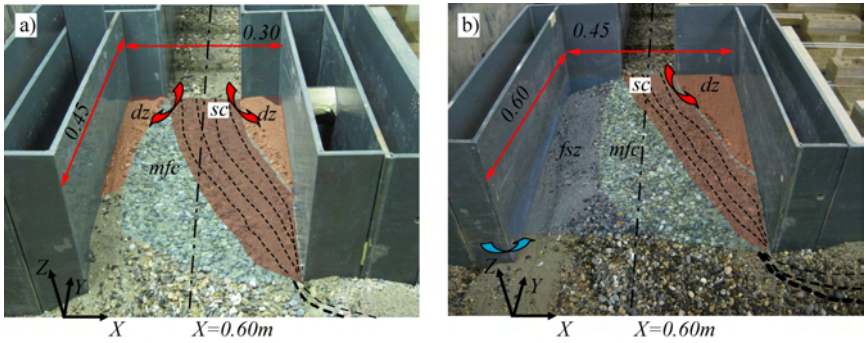

Figure 7-21: Images of the widened zone in equilibrium conditions for the test (a) Low-Reference and (b) High-Large. "dz" denotes the dry zones, "mfc" the tributary main flow corridors, "fsz" the flow stagnation zones and "sc" the sediment corridors.

The increase of available space in the confluence zone due to the local tributary widening seems to facilitate the development of a natural connection between the tributary and main channel flows. The definition of the junction angle between the flows is not straightforward, however. For the present tests, an angle is defined between the centrelines of each main flow corridor shown in Figure 7-16 and the *X*-axis. As illustrated in Figure 7-22, it appears that the confluence angle increases with the discharge ratio and momentum flux ratio. The deflection angle downstream is rather similar for a given discharge and does not seem to depend on the configuration of the widening.

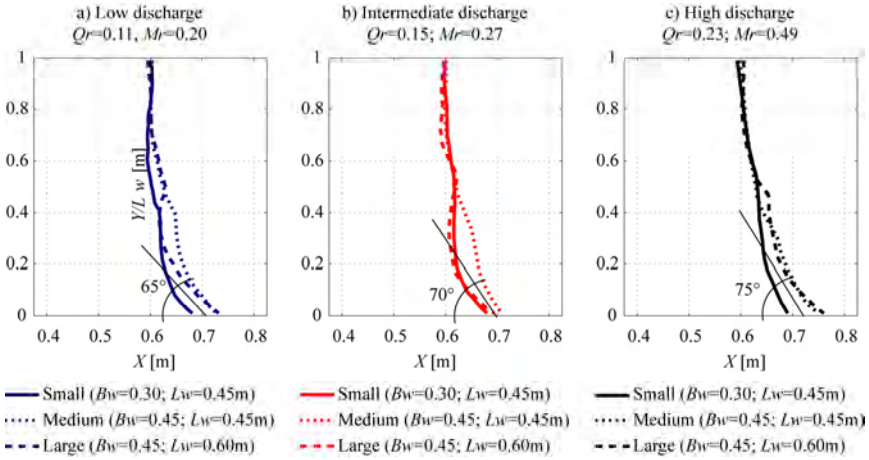

Figure 7-22: Angles of the confluence resulting from the investigated geometric and hydraulic conditions.

7.5 Ecological potential of local tributary widening in the framework of rehabilitation of confluences zones

As discussed in previous sections, the local tributary widenings are responsible for the development of regions characterized by a combination of flow corridors with dry and flow stagnation zones. In fluvial systems the presence of such as zones are extremely important for the habitat suitability. Dry zones are request for example for the development of the riparian vegetation and are common associated to the habitat of micro invertebrates (Singer and Dunne, 2006; Schweizer et al., 2007a; Weber et al., 2009) whereas flow stagnation zone can become refuge areas during flood events. Moreover, it was demonstrated that there are no adverse impacts due to local tributary widening on the tributary and main channel water levels. This is extremely important because water level raises can be catastrophic for the flood safety of confluence zones, putting in risk confluence rehabilitation projects.

In fluvial systems, flow depths characteristics strongly influence the quality of habitat for aquatic biota (Schweizer et al., 2007b). As illustrated in Figure 7-23, the relative low variability of the flow depths of the channelized tributaries (reference cases) measured in the tributary main corridors (Figure 7-16) increases considerably with the local widening.

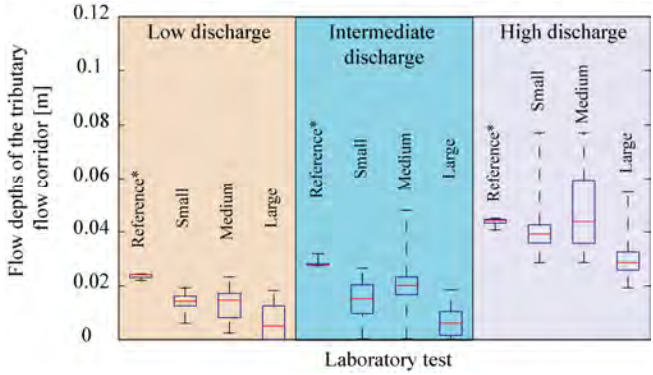

Figure 7-23: Boxplots of the flow depths measured in the tributary main flow corridors in the widening zone showing the median values (mid-lines), 25th and 75th percentiles (box) and the maximum and minimum values (extreme limits). Flow depths in the tributary between 0.60 m<Y<1.10 m in the reference cases are used for comparison.

The analyses of the water depths variability can also be done over the entire widening zone, where the dry zones and the flow stagnation zones also are taken into account. From Figure 7-24, it is possible to see that the variability in water depths further increase when the zones out of the tributary main flow corridor are included.

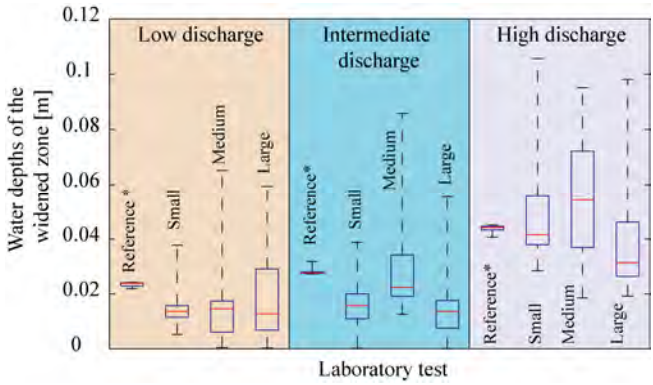

Figure 7-24: Boxplots of the water depths in the widening zone showing the median values (mid-lines), 25th and 75th percentiles (box) and the maximum and minimum values (extreme limits). Flow depths in the tributary between 0.60 m<Y<1.10 m in the reference cases are used for comparison matter.

The increased variation of the flow depths, associated to the higher variability of flow velocities and bed substrate discussed in section 7.4.3 show the ecological potential of a local tributary widening in confluence zones.

It is important to notice that the present experiments have been performed under constant water and solid discharge conditions which represents the bed-forming events of the tributary channel. In fluvial systems, however, the constant variations of discharges are fundamental elements of river ecosystems. For that reason, the lateral freedom obtained by the local widening and the different combinations of the main and tributary flood events further contributes for increasing the dynamics of confluence zones, which can be important for enhancing the lateral connectivity of regulated fluvial systems, such as the Upper Rhone basin.

7.6 Conclusions

Systematic experimental tests are carried out in the perspective of a research project related to the rehabilitation of regulated confluences found in alpine regions. Experimental conditions as dimensions, sediments and scenarios are based on an analysis of the main confluences of the Upper Rhone River, in Switzerland. This basin is currently in a poor ecological state due to past river training works and is being subject of a major rehabilitation project.

In the first part of the paper, the effects of the momentum flux ratio resulting from three different discharge ratios were investigated for a reference configuration of a 90º confluence without a widening of the tributary mouth. With the increase of the momentum flux ratio, the following morphological behaviours can be highlighted: 1) the discordance between the tributary and main channel decreases; 2) the penetration of the tributary into the main channel decreases and 3) and the volume of the deposition bar is smaller. Moreover, a significant grain sorting can be observed at the confluence zone. Coarse material is found on the avalanche faces, while finer one are encountered at the separation zone.

Although the morphology of the confluence zone is highly responsive to changes in the discharge and momentum flux ratios, the results presented in this work allows the validation of the conceptual model concerning the main hydro-morpho-sedimentary processes of confluences with relative low discharge and momentum flux ratios and high sediment delivery ratio proposed in Chapter 5.

In the second part of the paper, the influence of different three local tributary widening for three discharge scenarios has been investigated in the framework of confluence rehabilitation projects. It has been shown that these relative small interventions can increase the variability of water depths, flow velocities and bed material substrate in confluence zones.

These hydraulic and morphological conditions are potentially important for the re-establishment of diverse natural riparian ecosystems, and to restore the fluvial systems that were degraded by river training works. Results of this research demonstrate the complexity of the morphodynamic responses to a given widening configuration. It depends on the momentum flux ratio and on the shape and dimensions of the widening. For all cases, some parts of the widened space are not used by the flow at equilibrium conditions. These areas are either completely filled by fine sediments or occupied by stagnating flows.

Finally, the different tributary widening configurations tested in this research did not cause major consequences for the morphodynamics neither in the tributary channel upstream of the widening nor in the post-confluence channels for a given discharge scenario. It is important to notice that in the experiments, the solid discharge introduced in the tributary corresponds exactly to its transport capacity (equilibrium conditions) and the above statements only concern this situation. In these conditions, local tributary widening can be powerful in increasing the ecological potential of fluvial systems without reducing the conveyance capacity of a given network.

8. General conclusions and future research

8.1 Challenges of alpine confluences

Alpine confluences are characterized by small steep tributaries with a high supply of poorly sorted sediment during channel-forming flood events. Their morphology is characterized by pronounced bed discordance at the tributary mouth and the formation of a significant deposition bar downstream of the confluence. The current knowledge on the morphodynamics of river channel confluences, mainly based on lowland confluences is not applicable to these conditions. Low values of discharge and momentum flux ratios, associated to the important sediment loads supplied by the tributary can, in part, explain the non-applicability of the existing knowledge.

In regulated systems, the tributaries are often channelized and characterized by monotonous linear profiles with a lack of structural diversity, i.e. gravel banks, islands, woody debris, riffles or pools. River training works resulted in an impoverishment of the fluvial ecosystems. Confluences are the nodes of the river networks and hence they are critical points to be considered in rehabilitation projects. Regulated alpine confluences present important challenges, not only for rehabilitation projects but also because of the continuous increase of the flood risks due to urbanization.

In the present research project, the morphodynamics of confluences such as found in alpine environments were investigated for the first time. Laboratory investigation of the main hydro-morpho-sedimentary processes for different discharge and momentum flux ratios allowed gaining insight in the interactions and feedback mechanisms between these processes. Furthermore, the ecological potential of local tributary widening in the framework of confluence rehabilitation projects was investigated and its influence on the flow dynamics, sediment transport and bed morphology was examined. The reported study was based on systematic laboratory experiments performed under live bed conditions in a configuration that is representative of typical regulated alpine confluences as they can be found in the Upper Rhone River, Switzerland.

8.2 Main results

8.2.1 Hydro-morpho-sedimentary processes in channel confluences

Measurements of the three-dimensional velocity field, turbulence, sediment transport, bed material grain size and morphology in the confluence flume at equilibrium conditions revealed that the hydro-morpho-sedimentary processes occurring in confluences with alpine characteristics differ fundamentally from existing conceptual models of confluence morphodynamics. Therefore, a conceptual model for the main hydraulic and morphological processes in confluences with low discharge and momentum flux ratio and high sediment delivery ratio was proposed and validated by means of twelve experimental tests with different discharge ratios as well as field observations at the Rhone River confluences. The model can be considered as an extension of the Best's work to bed discordant confluences with hydro-sedimentary characteristics not yet considered.

The difference between the low flow depth in the steep tributary and the higher flow depth in the main channel explains the presence of bed discordance in channel confluences. Due to this bed discordance, the tributary flow penetrates into the main channel mainly in the upper part of the water column, whereas the main-channel flow moves beneath the tributary in the lower part of the water column, giving rise to a two-layer flow structure at the tributary mouth. In confluences with high sediment supply from the tributary, the development of a deposition bar downstream from the confluence reduces the flow area and causes a flow acceleration that contributes to the required increase in sediment transport capacity. The sediment supplied by the tributary is mainly sorted and transported on the face of the deposition bar. The sediment transport capacity is further increased by the three-dimensionality of the flow, which is characterized by maximum velocities occurring near the bed. Furthermore, a significant increase in turbulent kinetic energy is generated in the shear layer at the interface of the flows originating from the main channel and the tributary. With the increase of the momentum flux ratio, the following morphological behaviours can be highlighted: 1) the discordance between the tributary and main channel decreases; 2) the penetration of the tributary into the main channel decreases and 3) the volume of the deposition bar decreases.

8.2.2 Effects of tributary widening

The effects of local tributary widening in the framework of confluence rehabilitation projects was assessed by investigations of three different widening configurations under three different steady discharge scenarios. Local tributary widening considerably influences the morphodynamics in the confluence zone and increase the heterogeneity in bed topography, water depth, flow velocity and particle size distribution. These hydraulic and morphological conditions are potentially important for the re-establishment of diverse natural riparian ecosystems, and the restoration of fluvial systems that were degraded by river training works. The lateral freedom obtained by the local widening associated to the different combinations of the main and tributary discharge events further allows the formation of different bed forms, which contributes to the improvement of the lateral connectivity of regulated networks.

Local tributary widening was found to amplify the hydro-morpho-sedimentary processes in the confluence zone, but without altering them fundamentally. The local interventions represented by the tributary widening do not promote adverse effects in terms of the conveyance capacity and the flood safety in equilibrium conditions.

8.3 Future research

Laboratory experiments are inherently limited to a relatively small number of configurations that only partially cover the relevant parameter space. Moreover, they are limited to schematized and simplified conditions. The reported experiments, for example, only investigated tributaries that join the main channel at 90° angle. Furthermore, it only investigated equilibrium conditions under steady flow and sediment conditions. The performed laboratory experiments can be considered as the first important step in research on alpine confluences. Knowledge on the hydro-morpho-sedimentary processes in these settings may be further increased by means of a combination of laboratory, field and numerical investigations.

Laboratory investigations

Further laboratory investigations could have the purpose:

- To broaden the investigated parameter space, and especially the flow and sediment discharges in the main channel and the tributary, the sediment characteristics, the confluence angles, the channel widths;

- To investigate the hydro-morpho-sedimentary dynamics under time-variable conditions of flow and sediment discharges in order to mimic the effects of flood events occurring in the main channel and/or the tributary.
- To investigate different configurations of tributary widening. Preliminary tests in the present experimental set-up considering asymmetric widening have been done in the framework a Master project at LCH (Bidaud, 2010). However, in order to be conclusive, the investigation should be done systematically.
- To investigate the influence of main channel widening on the morphodynamics of confluence zones.

Numerical simulations

Currently, the available morphodynamic numerical codes are not able to simulate accurately the bed evolution of channel confluences (Bidaud, 2011). In addition, the application of numerical models to confluence zones still suffers of the lack of experimental data for model validation. The detailed experimental data on the three-dimensional flow field, turbulence, sediment transport, bed material grain size and morphology provided by the performed laboratory experiments constitute benchmark data for the validation of morphodynamic numerical models. Validated models may be useful for research (broadening of the parameter space) and river management (design of river rehabilitation schemes).

Field investigations

The existing knowledge on the morphodynamics of river confluences is mainly based on field investigations on two small lowland river confluences. In order to further validate the results presented in this research project, field investigations on channel confluences is required. In the choice of the site, the most important characteristics to be taken into account are: (*i*) low discharge and momentum flux ratios; (*ii*) important poorly-sorted sediment supply by the tributary during bed-forming events and (*iii*) bed discordance between the tributary and main channels. A first step could be the monitoring of the discharges and the morphological evolution in the confluence zone.

Concerning the application of the local tributary widening at confluence zones in the framework of river rehabilitation projects, the ecological evolution in addition to the morphological changes after the rehabilitation should be monitored.

References

Ashmore, P., and G. Parker (1983), Confluence scour in coarse braided streams, Water Resources Research, 19, 392-402.

Ashmore, P. E. (1982), Laboratory modelling of gravel braided stream morphology, Earth Surface Processes and Landforms, 7, 201-225.

Bajestan, M. S., and M. Hemmati (2008), Scour depth at river confluence of unequal bed level, Journal of Applied Sciences, 8, 1766-1770.

Baranya, S., and J. Józsa (2007a), Comparative CFD and Scale Model Analysis of the Flow Complexity at a River Confluence, paper presented at 32nd Congress of IAHR.

Baranya, S., and J. Józsa (2007b), Numerical and laboratory investigation of the hydrodynamic complexity of a river confluence, Periodica Polytechnica: Civil Engineering, 51, 3-8.

Benda, L. (2008), Confluence environments at the scale of river networks, in River Confluences, Tributaries and the Fluvial Network, edited by S. P. Rice, Roy, A.G. and Rhoads, B.L. , pp. 271-300, John Wiley & Sons, Ltd.

Benda, L., K. Andras, D. Miller, and P. Bigelow (2004), Confluence effects in rivers: Interactions of basin scale, network geometry, and disturbance regimes, Water Resources Research, 40.

Bernhardt, E. S., M. A. Palmer, J. D. Allan, G. Alexander, K. Barnas, S. Brooks, J. Carr, S. Clayton, C. Dahm, J. Follstad-Shah, D. Galat, S. Gloss, P. Goodwin, D. Hart, B. Hassett, R. Jenkinson, S. Katz, G. M. Kondolf, P. S. Lake, R. Lave, J. L. Meyer, T. K. O'Donnell, L. Pagano, B. Powell, and O. Sudduth (2005), Synthesizing U.S. river restoration efforts, Science, 308, 636-637.

Best, J. L. (1987), Flow dynamics at river channel confluences: Implications for sediment transport and bed morphology, Recent Developments in Fluvial Sedimentology, Spec. Publ. SEPM Soc. Sediment. Geol., 39, 27-35.

Best, J. L. (1988), Sediment transport and bed morphology at river channel confluences, Sedimentology, 35, 481-498.

Best, J. L., and I. Reid (1984), Separation zone at open-channel junctions, Journal of Hydraulic Engineering, 110, 1588-1594.

Best, J. L., and B. L. Rhoads (2008), Sediment transport, bed morphology and the sedimentology of river channel confluences, in River Confluences, Tributaries and the

Fluvial Network, edited by S. P. Rice, Roy, A.G. and Rhoads, B.L. , pp. 45-72, John Wiley & Sons, Ltd.

Best, J. L., and A. G. Roy (1991), Mixing-layer distortion at the confluence of channels of different depth, Nature, 350, 411-413.

Bidaud, L. (2010), Etude morphologique de confluences alpines. Application à la jonction du Rhône et de la Borgne, edited, p. 152, Master Project. LCH-EPFL.

Biron, P., J. L. Best, and A. G. Roy (1996a), Effects of Bed Discordance on Flow Dynamics at Open Channel Confluences, Journal of Hydraulic Engineering, 122, 676-682.

Biron, P., A. Roy, J. L. Best, and C. J. Boyer (1993), Bed morphology and sedimentology at the confluence of unequal depth channels, Geomorphology, 8, 115-129.

Biron, P., A. G. Roy, and J. L. Best (1996b), Turbulent flow structure at concordant and discordant open-channel confluences, Experiments in Fluids, 21, 437-446.

Biron, P. M., and S. N. Lane (2008), Modelling hydraulics and sediment transport at river confluences., in River Confluences, Tributaries and the Fluvial Network, edited by S. P. Rice, Roy, A.G. and Rhoads, B.L. , pp. 17-43, John Wiley & Sons, Ltd.

Biron, P. M., A. Ramamurthy, S., and S. Han (2004), Three-Dimensional Numerical Modeling of Mixing at River Confluences, Journal of Hydraulic Engineering, 130, 243-253.

Biron, P. M., A. Richer, A. D. Kirkbride, A. G. Roy, and S. Han (2002), Spatial patterns of water surface topography at a river confluence, Earth Surface Processes and Landforms, 27, 913-928.

Blanckaert, K. (2010), Topographic steering, flow recirculation, velocity redistribution, and bed topography in sharp meander bends, Water Resources Research., 46, W09506.

Blanckaert, K., A. Duarte, and A. J. Schleiss (2010), Influence of shallowness, bank inclination and bank roughness on the variability of flow patterns and boundary shear stress due to secondary currents in straight open-channels, Advances in Water Resources, In Press, Corrected Proof.

Blanckaert, K., and W. H. Graf (2001), Mean Flow and Turbulence in Open-Channel Bend, Journal of Hydraulic Engineering, 127, 835-847.

Blanckaert, K., and U. Lemmin (2006), Means of noise reduction in acoustic turbulence measurements, Journal of Hydraulic Research, 44, 3-17.

Boillat, J.-L., J. Dubois, and N. Nilipour (2006), Migration of a Dredging Pit in the Rhone River, paper presented at River Flow 2006, Ferreira, Alves, Leal and Cardoso, Lisbon, Portugal.

Borghei, S. M., and A. J. Sahebari (2010), Local scour at open-channel junctions, Journal of Hydraulic Research, 48, 538 - 542.

Bourgeois, M. (2006), Accroissement de la valeur naturelle de la vallée du Rhône par un raccordement optimal des affluents du Rhône, edited, p. 152, Master Project. LCH-EPFL.

Boyer, C., A. G. Roy, and J. L. Best (2006), Dynamics of a river channel confluence with discordant beds: Flow turbulence, bed load sediment transport, and bed morphology, Journal of Geophysical Research, 111, 1-22.

Bradbrook, K. F., P. M. Biron, S. N. Lane, K. S. Richards, and A. G. Roy (1998), Investigation of controls on secondary circulation in a simple confluence geometry using a three-dimensional numerical model, Hydrological Processes, 12, 1371-1396.

Bradbrook, K. F., S. N. Lane, and K. S. Richards (2000a), Numerical simulation of three-dimensional, time-averaged flow structure at river channel confluences, Water Resources Research, 36, 2731-2746.

Bradbrook, K. F., S. N. Lane, K. S. Richards, P. M. Biron, and A.G. Roy (2000b), Large Eddy Simulation of periodic flow characteristics at river channel confluences, Journal of Hydraulic Research, 38, 207-215.

Bradbrook, K. F., S. N. Lane, K. S. Richards, P. M. Biron, and A. G. Roy (2001), Role of bed discordance at asymmetrical river confluences, Journal of Hydraulic Engineering, 127, 351-368.

Brauchli, T. (2009), Hydro-economic analysis and simulation of extreme events in the Alpine Rhône basin, edited, p. 61, Master Project. LCH-EPFL.

Bryan, R. B., and N. J. Kuhn (2002), Hydraulic conditions in experimental rill confluences and scour in erodible soils, Water Resources Research, 38, 211-214.

Chow, V. T. (1959), Open-Channel Hydraulics, 680 pp., McGraw-Hill Book Singapore.

Coelho, M. M. L. P. (2003), Comportamento hidráulico em confluências de canais: Uma abordagem conceitual e experimental 273 pp, Universidade de São Paulo, São Paulo.

D'Oria, M., and T. M. Tanda (2007), Physical and Numerical Modeling of a River Confluence Reshaping, paper presented at 32nd Congress of IAHR, Venice.

De Serres, B., A. G. Roy, P. M. Biron, and J. L. Best (1999), Three-dimensional structure of flow at a confluence of river channels with discordant beds, Geomorphology, 26, 313-335.

Duan, J. G., and M. T. Schwar (2003), Modeling of Flow and Sediment Transport at a River Confluence with the EnSed2D model, paper presented at World Water and Environmental Resources Congress.

Dynesius, M., R. Jansson, M. E. Johansson, and C. Nilsson (2004), Intercontinental similarities in riparian-plant diversity and sensitivity to river regulation, Ecological Applications, 14, 173-191.

Dynesius, M., and C. Nilsson (1994), Fragmentation and flow regulation of river systems in the northern third of the world, Science, 266, 753-762.

Ferguson, R., and T. Hoey (2008), Effects of Tributaries on Main-Channel Geomorphology, 183-208 pp., John Wiley & Sons, Ltd.

Formann, E., H. M. Habersack, and S. Schober (2007), Morphodynamic river processes and techniques for assessment of channel evolution in Alpine gravel bed rivers, Geomorphology, 90, 340-355.

Fujita, I., and S. Komura (1989), Visualization of the flow at a confluence, in Refined Flow Modelling and Turbulence Measurements, edited by I. Universal Academy Press, International Association of Hydraulic Research, Tokyo, Japan.

Gaudet, J. M., and A. G. Roy (1995), Effect of bed morphology on flow mixing length at river confluences, Nature, 373, 138-139.

Ghobadian, R., and S. M. Bajestan (2007), Investigation of sediment patterns at river confluence, Journal of Applied Sciences, 7, 1372-1380.

Ghostine, R., G. Kesserwani, J. Vasquez, R. Mose, and A. Ghenaim (2007), Comparison of One and Two Dimensional Simulation of Subcritical Flow Through Combining Junction, paper presented at 32nd Congress of IAHR, Venice.

Guo, W., Yang, L. and Feng, Y. (2007), Numerical Simulation of Flow at "Y" Shaped Open-Channel Junctions, paper presented at 32nd Congress of IAHR.

Gurnell, A., N. Surian, and L. Zanoni (2009), Multi-thread river channels: A perspective on changing European alpine river systems, Aquatic Sciences, 71, 253-265.

Gurram, S. K., K. Karki, S. , and W. H. Hager (1997), Subcritical Junction Flow, Journal of Hydraulic Engineering, 123, 447-455.

Hager, W. H. (1989), Transitional flow in channel junctions, Journal of Hydraulic Engineering, 115, 243-259.

Havinga, H., H. R. A. Jagers, and C. J. Sloff (2005), Knowledge requirements for sustainable fairway management, paper presented at River, Coastal and Estuarine Morphodynamics.

Hsu, C.-C., W.-J. Lee, and C.-H. Chang (1998), Subcritical Open-Channel Junction Flow, Journal of Hydraulic Engineering, 124, 847-855.

Huang, J., L. J. Weber, and Y. G. Lai (2002), Three-Dimensional Numerical Study of Flows in Open-Channel Junctions, Journal of Hydraulic Engineering, 128, 268-280.

Hunziger, L. (1999), Morhology in river widenings of limited lenght, paper presented at 28th IAHR congress, IAHR, Graz, Austria, 22-27 August 1999.

Hurther, D., and U. Lemmin (1998), A constant-beam-width transducer for 3D acoustic Doppler profile measurements in open-channel flows, Meas. Sci. Technol., 9, 1706-1714.

Jenzer, J., S. C. Pereira, M. Federspiel, and J.-L. Boillat (2008), Multi-Purpose Modelling of the Rhone River in the Region of Visp (Switzerland), paper presented at Interpraevent 2008, Dornbirn - Austria.

Kantoush, S. A., G. De Cesare, J. L. Boillat, and A. J. Schleiss (2008), Flow field investigation in a rectangular shallow reservoir using UVP, LSPIV and numerical modelling, Flow Measurement and Instrumentation, 19, 139-144.

Kennedy, B. A. (1984), On Playfair's law of accordant junctions, Earth Surface Processes & Landforms, 9, 153-173.

Kenworthy, S. T., and B. L. Rhoads (1995), Hydrologic control of spatial patterns of suspended sediment concentration at a stream confluence, Journal of Hydrology, 168, 251-263.

Khan, A. A., R. Cadavid, and S. S. Y. Wang (2000), Simulation of channel confluence and bifurcation using the CCHE2D model, Proceedings of the Institution of Civil Engineers: Water and Maritime Engineering, 142, 97-102.

Knighton, A. D. (1980), Longitudinal changes in size and sorting of stream- bed material in four English rivers, Geological Society of America Bulletin, 91, 55-62.

Knighton, A. D. (1998), Fluvial Forms and Precesses. A new perspective, 383 pp., Arnold, London.

Lane, E. W. (1955), The design of stable channels, Trans. ASCE, 120, 1234-1279.

Lane, S. N., P. M. Biron, K. F. Bradbrook, J. B. Butler, J. H. Chandler, M. D. Crowell, S. J. McLelland, K. S. Richards, and A. G. Roy (1998), Three-dimensional measurement of river channel flow processes using acoustic doppler velocimetry, Earth Surface Processes and Landforms, 23, 1247-1267.

Lane, S. N., K. F. Bradbrook, K. S. Richards, P. Biron, and A. G. Roy (2000), Secondary circulation cells in river channel confluences: measurement artefacts or coherent flow structures?, Hydrological Processes, 14, 2047-2071.

Lane, S. N., K. F. Bradbrook, K. S. Richards, P. A. Biron, and A. G. Roy (1999a), The application of computational fluid dynamics to natural river channels: three-dimensional versus two-dimensional approaches, Geomorphology, 29, 1-20.

Lane, S. N., J. H. Chandler, and K. S. Richards (1994), Developments in monitoring and modelling small-scale river bed topography, Earth Surface Processes & Landforms, 19, 349-368.

Lane, S. N.,K. F. Bradbrook, K. S. Richards, P. M. Biron, and A. G. Roy (1999b), Time-averaged flow structure in the central region of a stream confluence: a discussion, Earth Surface Processes and Landforms, 24, 361-367.

Lane, S. N., and K. S. Richards (1998), High resolution, two-dimensional spatial modelling of flow processes in a multi-thread channel, Hydrological Processes, 12, 1279-1298.

Lane, S. N., K.S. Richards, and J.H. Chandler, (1995), Within-reach spatial patterns of process and channel adjustment. , in In: Hickin, E.J. Editor, 1995. River Geomorphology Wiley, edited, pp. 105-130., Wiley, Chichester, England.

Leclair, S., and A. G. Roy (1997), Variabilité de la morphologie et des structures sédimentaires du lit d'un confluent de cours d'eau discordant en periode d'étiage, Géographie physique et Quaternaire, 51, 125–139.

Lemmin, U., and T. Rolland (1997), Acoustic velocity profiler for laboratory and field studies, Journal of Hydraulic Engineering, 123, 1089-1098.

Lockwood, J. L., and S. L. Pimm (1999), When does restoration succeed?, in Ecological Assembly Rules: Perspectives, Advances, Retreats, edited, pp. pp. 363–392.

Lodina, R. V., and R. S. Chalov (1971), Effect of tributaries on the composition of river sediments and of deformations of the main river channel, Soviet Hydrology, Selected Papers, 4, 370-374.

Loizeau, J. L., and J. Dominik (2000), Evolution of the Upper Rhone River discharge and suspended sediment load during the last 80 years and some implications for Lake Geneva, Aquatic Sciences, 62, 54-67.

Lorenz, C. M., G. M. Van Dijk, A. G. M. Van Hattum, and W. P. Cofino (1997), Concepts in river ecology: Implications for indicator development, Regulated Rivers: Research and Management, 13, 501-516.

Masujin, K., Y. Shimizu, and K. Hoshi (2005), Study on flow at a river confluence, paper presented at River, Coastal and Estuarine Morphodynamics:RCEM 2005.

McLelland, S. J., J. L. Best, and P. J. Ashworth (1996), "The Origin and Downstream Development of Coherent Flow Structures at Channel Junctions", in Ashworth, P.J., Bennett, S.J., Best, J.L. and McLelland, S.J. (eds) Coherent Flow Structures in Open Channels, Wiley & Sons Ltd, Chichester, 459-490.

Meile, T. (2006), Hydropeaking on Watercourses, in EAWAG News, edited, pp. 28-29.

Meile, T., J. L. Boillat, and A. J. Schleiss (2010), Hydropeaking indicators for characterization of the Upper-Rhone River in Switzerland, Aquatic Sciences, 1-12.

Milano, V., and F. Sassoli (1977), Ricerca sperimentale sulle confluenze fluviali in regime permanente., Energia Elettrica, 54, 497-508.

Modi, P. N., P. D. Ariel, and M. M. Dandekar (1981), Conformal mapping for channel junction flow, Journal of the Hydraulics Division, ASCE, 107, 1713-1733.

Mosley, M. (1976), An experimental study of channel confluences, The journal of geology, 84, 535.

Nakamura, K., K. Tockner, and K. Amano (2006), River and wetland restoration: Lessons from Japan, BioScience, 56, 419-429.

Nezu, I., and H. Nakagawa (1993), Turbulence in open-channel flows, Turbulence in open-channel flows.

Nezu, I., A. Tominaga, and H. Nakagawa (1993), Field measurements of secondary currents in straight rivers, Journal of Hydraulic Engineering, 119, 598-614.

Olsen, N. R. B. (2006), A three-dimensional numerical model for simulation of sediment movements in water intakes with multiblock option. User's Manual, edited, Department of Hydraulic and Environmental Engineering. The Norwegian University of Science and Technology.

Parsons, D. R. (2003), Discussion of ``Three-Dimensional Numerical Study of Flows in Open-Channel Junctions" by Jianchun Huang, Larry J. Weber, and Yong G. Lai, Journal of Hydraulic Engineering, 129, 822-823.

Parsons, D. R., J. L. Best, S. N. Lane, O. Orfeo, R. J. Hardy, and R. Kostaschuk (2007), Form roughness and the absence of secondary flow in a large confluence-diffluence, Rio Paraná, Argentina, Earth Surface Processes and Landforms, 32, 155-162.

Peter, A. (2006), Rehabilitation – to What Extent, and Why?, in Eawag News, edited, pp. 4-8.

Qing-Yuan, Y., W. Xian-Ye, L. Wei-Zhen, and W. Xie-Kang (2009), Experimental study on characteristics of separation zone in confluence zones in rivers, Journal of Hydrologic Engineering, 14, 166-171.

Ramamurthy, A. S., L. B. Carballada, and D. M. Tran (1988), Combining open channel flow at right angled junctions, Journal of Hydraulic Engineering, 114, 1449-1460.

Reichert, P., M. Borsuk, M. Hostmann, S. Schweizer, C. Spörri, K. Tockner, and B. Truffer (2007), Concepts of decision support for river rehabilitation, Environmental Modelling and Software, 22, 188-201.

Rhoads, B. L. (1996), Mean structure of transport-effective flows at an asymmetrical confluence when the main stream is dominant, in Coherent Flow Structures in Open Channels: Origins, Scales and Interactions with Sediment Transport and Bed Morphology, edited by P. J. Ashworth, et al., pp. 491–517, Wiley, Chichester.

Rhoads, B. L., and S. T. Kenworthy (1995), Flow structure at an asymmetrical stream confluence, Geomorphology, 11, 273-293.

Rhoads, B. L., and S. T. Kenworthy (1998), Time-averaged flow structure in the central region of a stream confluence, Earth Surface Processes and Landforms, 23, 171-191.

Rhoads, B. L., and S. T. Kenworthy (1999), On secondary circulation, helical motion and Rozovskii-based analysis of time-averagedtwo-dimensional velocity fields at confluences, Earth Surface Processes and Landforms, 24, 369-375.

Rhoads, B. L., J. D. Riley, and D. R. Mayer (2009), Response of bed morphology and bed material texture to hydrological conditions at an asymmetrical stream confluence, Geomorphology, 109, 161-173.

Rhoads, B. L., and A. N. Sukhodolov (2001), Field investigation of three-dimensional flow structure at stream confluences: 1. Thermal mixing and time-averaged velocities, Water Resources Research, 37, 2393-2410.

Rhoads, B. L., and A. N. Sukhodolov (2004), Spatial and temporal structure of shear layer turbulence at a stream confluence, Water Resources Research, 40.

Rhoads, B. L., and A. N. Sukhodolov (2008), Lateral momentum flux and the spatial evolution of flow within a confluence mixing interface, Water Resources Research, 44.

Ribberink, J. S., and J. T. M. Van der Sande (1985), Aggradation in rivers due to overloading - Analytical approaches, Journal of Hydraulic Research, 23, 273-283.

Rice, S. P., and M. Church (2001), Longitudinal profiles in simple alluvial systems, Water Resources Research, 37, 417-426.

Rice, S. P., R. I. Ferguson, and T. B. Hoey (2006), Tributary control of physical heterogeneity and biological diversity at river confluences, Canadian Journal of Fisheries and Aquatic Sciences, 63, 2553-2566.

Rice, S. P., M. T. Greenwood, and C. B. Joyce (2001), Tributaries, sediment sources, and the longitudinal organisation of macroinvertebrate fauna along river systems, Canadian Journal of Fisheries and Aquatic Sciences, 58, 824-840.

Rice, S. P., P. Kiffney, C. Greene, and G. R. Pess (2008), The Ecological Importance of Tributaries and Confluences, 209-242 pp., John Wiley & Sons, Ltd.

Richards, K. S. (1980), A note on changes in channel geometry at tributary junctions, Water Resources Research, 16 , no.1, Feb. 1980, 241-244.

Roca, M., J. P. Marti?n-Vide, and P. J. M. Moreta (2009), Modelling a torrential event in a river confluence, Journal of Hydrology, 364, 207-215.

Rodriguez, J. F., and M. H. Garcia (2008), Laboratory measurements of 3-D flow patterns and turbulence in straight open channel with rough bed, Journal of Hydraulic Research, 46, 454-465.

Rohde, S. (2004), River Restoration: Potential and limitations to re-establish riparian landscapes. Assessment & Planning., 127 pp, Swiss Federal Institute of Technology, Zurich, Switzerland.

Rohde, S., F. Kienast, and M. BÃ¼rgi (2004), Assessing the restoration success of river widenings: A landscape approach, Environmental Management, 34, 574-589.

Rohde, S., M. Schutz, F. Kienast, and P. Englmaier (2005), River widening: An approach to restoring riparian habitats and plant species, River Research and Applications, 21, 1075-1094.

Rovina+Partner-AG (2008), Dienststelle für Strassen- und Flussbau, 172 pp, Varen, Switzerland.

Roy, A. G., and N. Bergeron (1990), Flow and particle paths at a natural river confluence with coarse bed material, Geomorphology, 3, 99-112.

Roy, A. G., and R. Roy (1988), Changes in channel size at river confluences with coarse- bed material, Earth Surface Processes & Landforms, 13, 77-84.

Roy, A. G., R. Roy, and N. Bergeron (1988), Hydraulic geometry and changes in flow velocity at a river confluence with coarse bed material, Earth Surface Processes and Landforms, 13, 583-598.

Schleiss, A. J. (2006), River Dynamics and Flood Protection: a Contradiction in Terms?, in EAWAG News, edited, pp. 18-20.

Schweizer, S., M. E. Borsuk, I. Jowett, and P. Reichert (2007a), Predicting joint frequency distributions of depth and velocity for instream habitat assessment, River Research and Applications, 23, 287-302.

Schweizer, S., M. E. Borsuk, and P. Reichert (2007b), Predicting the morphological and hydraulic consequences of river rehabilitation, River Research and Applications, 23, 303-322.

Seal, R., C. Paola, G. Parker, J. B. Southard, and P. R. Wilcock (1997), Experiments on downstream fining of gravel: I. Narrow-channel runs, Journal of Hydraulic Engineering, 123, 874-884.

Sekine, M., and G. Parker (1992), Bed-load transport on transverse slope. I, Journal of Hydraulic Engineering, 118, 513-535.

Shabayek, S., P. Steffler, and F. Hicks (2002), Dynamic Model for Subcritical Combining Flows in Channel Junctions, Journal of Hydraulic Engineering, 128, 821-828.

Shakibaeinia, A., A. R. Zaratti, and M. R. M. Tabatabaei (2007), Three-Dimensional Numerical Study of River Channel Confluence with Bed Changes, paper presented at 32nd Congress of IAHR, Venice, Italy.

Shakibainia, A., M. R. M. Tabatabai, and A. R. Zarrati (2010), Three-dimensional numerical study of flow structure in channel confluences, Canadian Journal of Civil Engineering, 37, 772-781.

Singer, M. B., and T. Dunne (2006), Modeling the influence of river rehabilitation scenarios on bed material sediment flux in a large river over decadal timescales, Water Resources Research, 42.

Sloan, J., J. R. Miller, and N. Lancaster (2001), Response and recovery of the Eel River, California, and its tributaries to floods in 1955, 1964, and 1997, Geomorphology, 36, 129-154.

SRCE (2008), Troisième Correction du Rhône. Sécurité pour le futur. Rapport de Synthèse du Plan d'aménagement. , 157 pp, Canton du Valais. Service de Routes et Cours d'Eaux.

Stewardson, M. J., and T. A. McMahon (2002), A stochastic model of hydraulic variations within stream channels, Water Resources Research, 38, 81-814.

Sukhodolov, A. N., and B. L. Rhoads (2001), Field investigation of three-dimensional flow structure at stream confluences 2. Turbulence, Water Resources Research, 37, 2411-2424.

Tal, M., and C. Paola (2010), Effects of vegetation on channel morphodynamics: Results and insights from laboratory experiments, Earth Surface Processes and Landforms, 35, 1014-1028.

Taylor, E. H. (1944), Flow characteristics at rectangular open-channel junctions, American Society of Civil Engineers -- Proceedings, 70, 119-121.

Tominaga, A., I. Nezu, K. Ezaki, and H. Nakagawa (1989), Three-dimensional turbulent structure in straight open channel flows, Journal of Hydraulic Research, 27, 149-173.

Toro-Escobar, C. M., C. Paola, G. Parker, P. R. Wilcock, and J. B. Southard (2000), Experiments on downstream fining of gravel: Wide and sandy runs, Journal of Hydraulic Engineering, 126, 198-208.

Wallis, E., R. Mac Nally, and S. Lake (2009), Do tributaries affect loads and fluxes of particulate organic matter, inorganic sediment and wood? Patterns in an upland river basin in south-eastern Australia, Hydrobiologia, 636, 307-317.

Wampfler, S. (2008), Morphologie des confuences naturellement aménagées, edited, p. 199, Master Project. LCH-EPFL.

Webber, N. B., and C. A. Greated (1966), An investigation of flow behavior at the junction of rectangular channels, Proc. Institute Civil Engineers, London, Vol. 34, 321–334.

Weber, C., E. Schager, and A. Peter (2009), Habitat diversity and fish assemblage structure in local river widenings: A case study on a Swiss River, River Research and Applications, 25, 687-701.

Weber, L. J., Y. G. Lai, and F. De Andrade (2001a), Three-Dimensional Numerical Model Validation: Issues and Directions, ASCE.

Weber, L. J., E. D. Schumate, and N. Mawer (2001b), Experiments on Flow at a 90° Open-Channel Junction, Journal of Hydraulic Engineering, 127, 340-350.

Wu, B., G. Wang, J. Xia, X. Fu, and Y. Zhang (2008), Response of bankfull discharge to discharge and sediment load in the Lower Yellow River, Geomorphology, 100, 366-376.

Xia, J., B. Wu, G. Wang, and Y. Wang (2010), Estimation of bankfull discharge in the Lower Yellow River using different approaches, Geomorphology, 117, 66-77.

Yalin, M. S. (1971), Theory of hydraulic models, 266 pp., The Macmillan Press LTD, London.

Yalin, M. S., and A. M. F. da Silva (2001), Fluvial Processes, 197 pp., IAHR, Delft, The Netherlands.

Notation

Roman lower cases

d	Characteristic grain size diameter	[mm]
d_{50}	Median grain size diameter	[mm]
d_m	Average grain size diameter	[mm]
d_s	Scour depth	[m]
g	Gravitational acceleration	[ms^{-2}]
h	Local flow depth	[m]
k_s	Characteristic particle size	[mm]
n	Manning coefficient	[$sm^{-1/3}$]
t	time	[h]
tke	Turbulent kinetic energy	[-]
$u*$	Characteristic shear velocity	[ms^{-1}]
u_j	time-averaged local velocity component along j-direction	[ms^{-1}]
$u'j$	velocity fluctuations	[ms^{-1}]

Roman capital

B	Channel width	[m]
B_w	Widening width	[m]
C_f	Chézy friction coefficient	[-]
E_s	Energy gradient	[-]
F_g	Densimetric Froude Number	[-]
F_r	Froude Number	[-]
G_s	Specific gravity	[-]
H	Width-averaged flow depth	[m]
L_r	Reattachment length	[m]
L_w	Tributary widening length	[m]
M_r	Momentum flux ratio	[-]
Q	Discharge	[m^3s^{-1}]
Q_r	Discharge ratio	[-]
Qs	Solid discharge	[kg min^{-1}]
Re_*	Particle Reynolds number	[-]
R_h	Hydraulic radius	[m]
S	Bed slope	[-]
U	Globally averaged velocity ($Q/(BH)$	[ms^{-1}]

Greek symbols

v	Kinematic viscosity	[m^2s^{-1}]
α	Confluence angle	[°]
ρ	Water density	[kg m^{-3}]
ρ_s	Sediment density	[kg m^{-3}]
σ	Gradation coefficient	[-]
τ_b	Bed shear stress	[Nm^{-2}]

Subscripts

t	tributary channel
m	main channel
p-c	post-confluence channel
2	Two years return period
5	5 years return period
x,y,z	Longitudinal, transversal and vertical directions

Acronyms

ADVP	Acoustic Doppler Velocity Profiler
EAWAG	Swiss Federal Institute of Aquatic Science and Technology
EPFL	Ecole Polytechnique Fédérale de Lausanne, Switzerland
ETHZ	Swiss Federal Institute of Technology Zurich
FOEN	Federal Office for the Environment
LCH	Laboratory of Hydraulic Constructions
SSIIM	Sediment Simulation in Intakes with Multiblock Option
VAW	Laboratory of Hydraulics, Hydrology and Glaciology
WSL	Swiss Federal Institute for Forest, Snow and Landscape
mfc	Main flow corridor
dz	Dry zone
fsz	Flow stagnation zone

Appendixes

A. Low-Reference

Appendix	Test	*Qr*	Windening		
			B_w	L_w	
A	***Low-Reference***	**0.11**	-	-	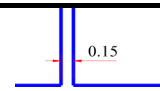
B	*Intermediate-Reference*	0.15			
C	*High-Reference*	0.20			
D	*Low-Small*	0.11	0.30	0.45	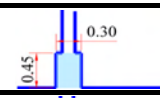
E	*Intermediate-Small*	0.15			
F	*High-Small*	0.20			
G	*Low-Medium*	0.11	0.45	0.45	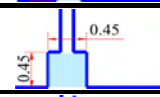
H	*Intermediate-Medium*	0.15			
I	*High-Medium*	0.20			
J	*Low-Large*	0.11	0.45	0.60	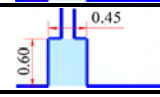
K	*Intermediate-Large*	0.15			
L	*High-Large*	0.20			

A.1 Summary

A.1.1 Initial hydraulic conditions

	Main (*m*)	Tributary (*t*)	*Qr* (Q_t/Q_m)
Q **[l/s]**	18	2	0.11
Qs **[kg/m^3]**	-	0.3	

A.1.2 Equilibrium flow depths

Main and post-confluence channels			
X\Y **[m]**	**0.05**	**0.25**	**0.45**
0	0.105	0.109	0.110
0.5	0.109	0.107	0.113
1.2	0.096	0.599	0.019
3.2	0.076	0.053	0.037
Tributary channel			
X **[m]**	**Average [0.5<*Y*<3.5m]**		
0.6	0.02		

A.1.3 Main morphological features

Bed discordance	0.090	[m]
Maximum deposition	0.096	[m]
Volume > elevation 0.02 m	0.024	[m^3]

A.2 Time-evolution of the bed elevations

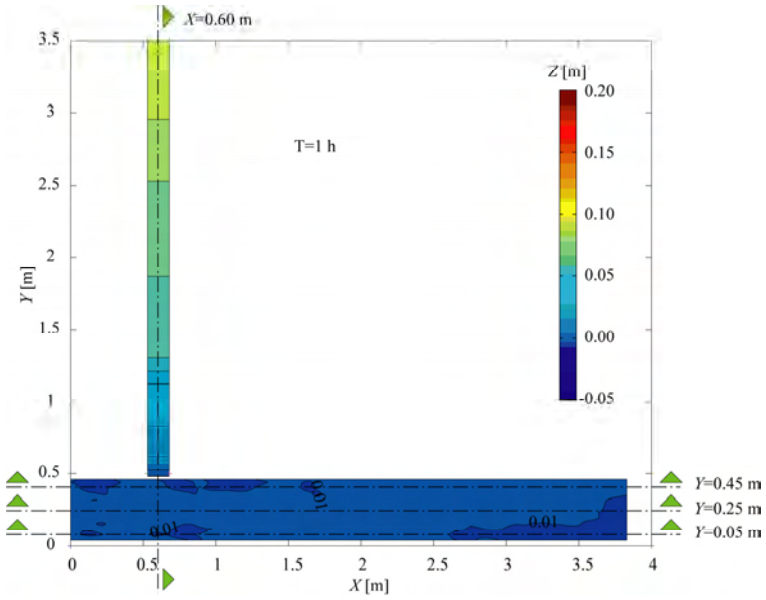

Figure 1: Bed elevations measured in the flume at t=1h

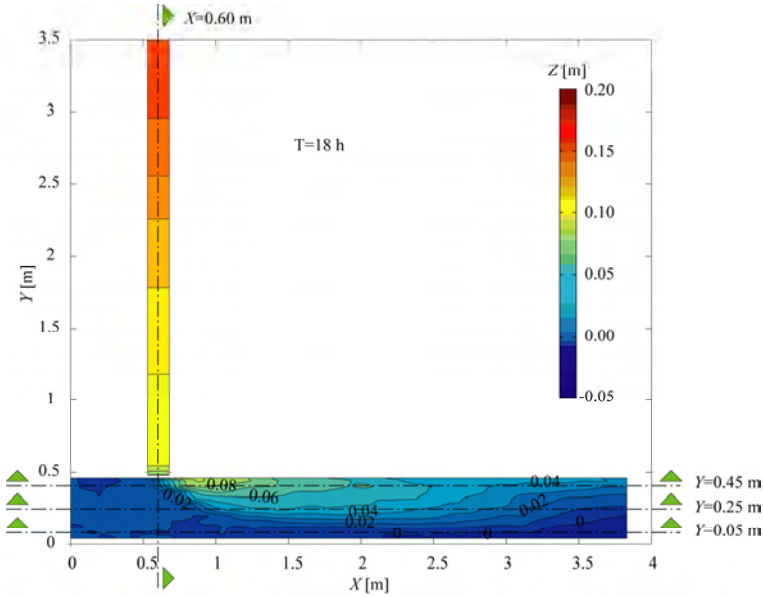

Figure 2: Bed elevations measured in the flume at t=18h

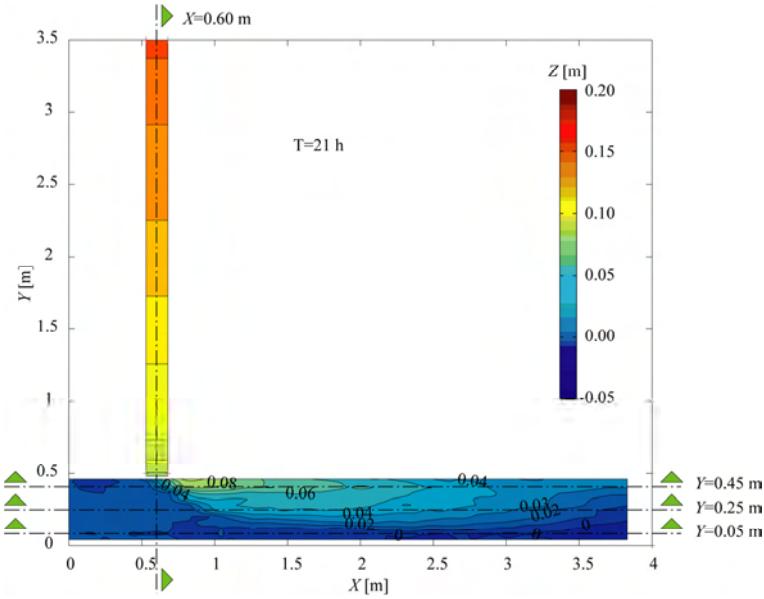

Figure 3: Bed elevations measured in the flume at t=21h

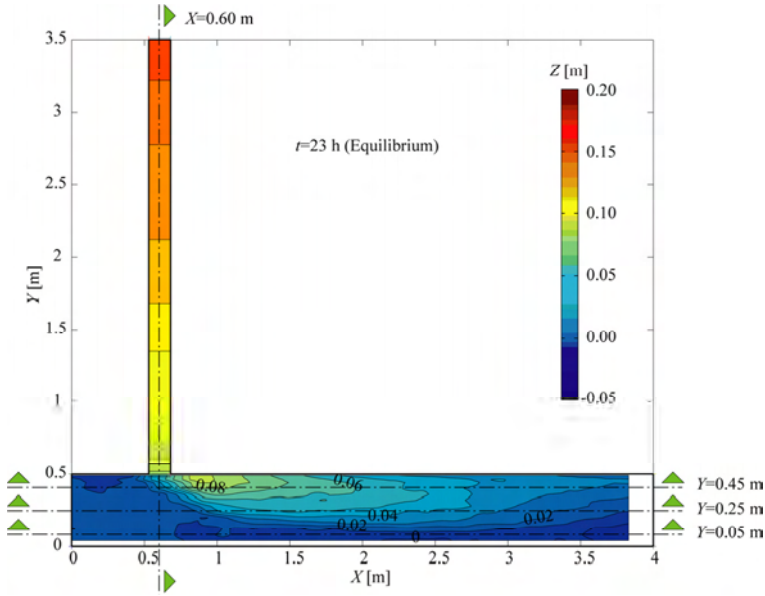

Figure 4: Bed elevations measured in the flume at t=23h

A.3 Longitudinal profiles

A.3.1 Main, post-confluence and tributary channels

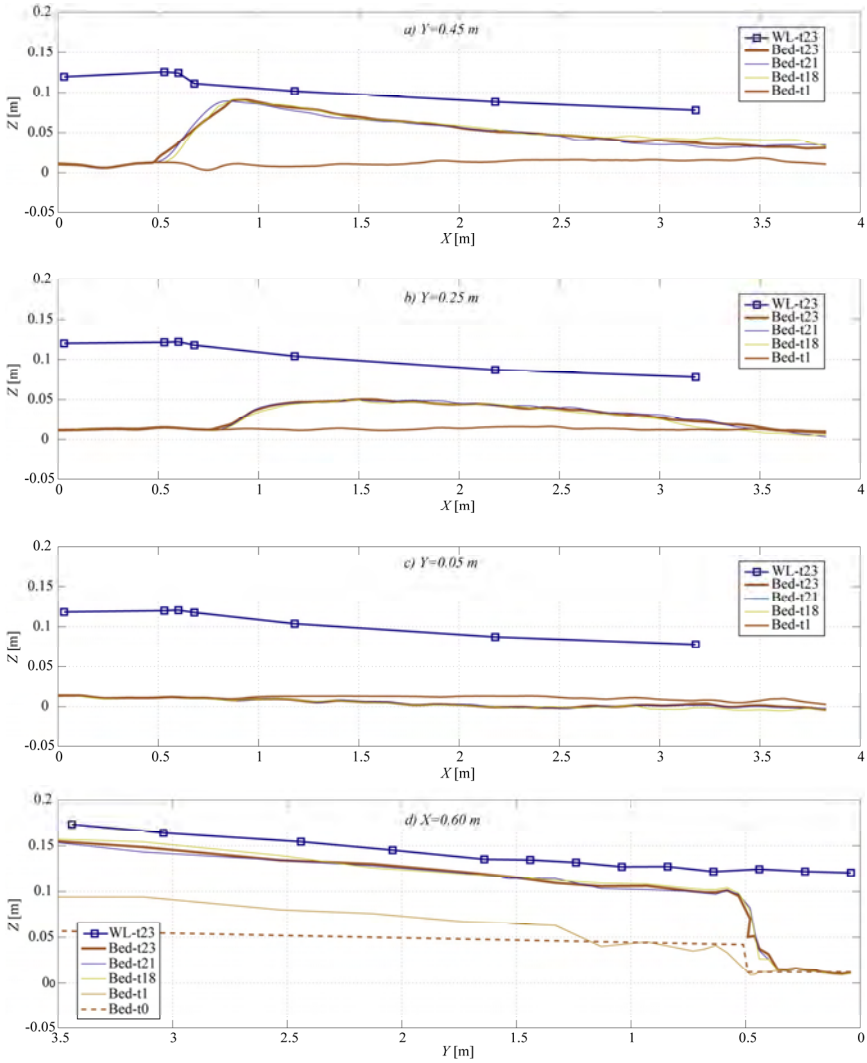

Figure 5: Longitudinal profiles along the main and post-confluence channels at Y*=0.05 m (a),* Y*=0.25 m (b) and* Y*=0.45 m (c) and longitudinal profile along the axis of the tributary (*X*=0.60 m) (d) showing the bed elevations and water levels measured in different time-steps*

A.4 Flow visualization of the main and post-confluence channels

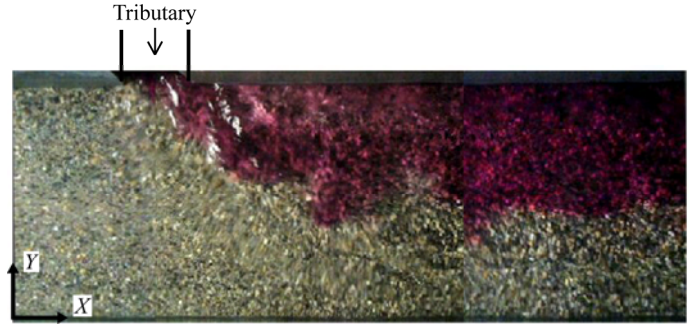

Figure 6: Upper view of the main and post-confluence channels with colour dye injected in the tributary

A.5 Pictures of the confluence zone

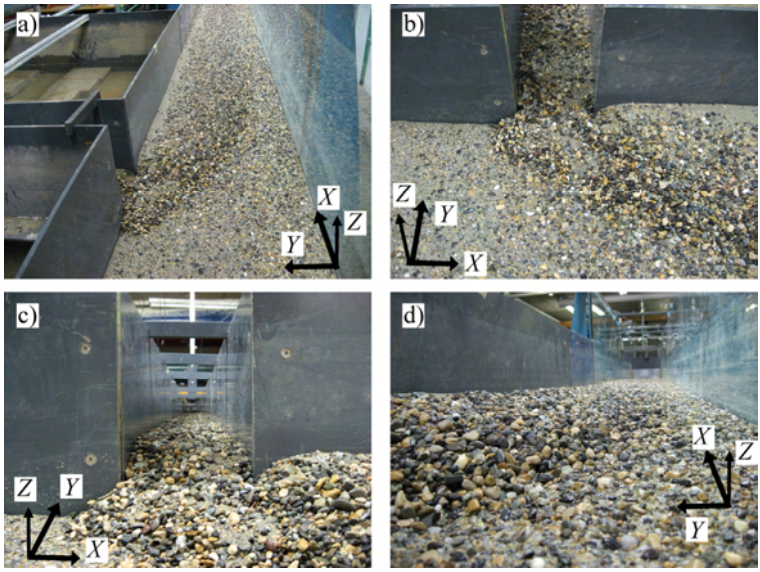

Figure 7: Pictures of the confluence zone. a) Upper view of the main and post-confluence channels. b) Upper view of the confluence zone, c) Upstream view of the tributary and d) Downstream view of the post- confluence channel

A.6 Grain size distributions

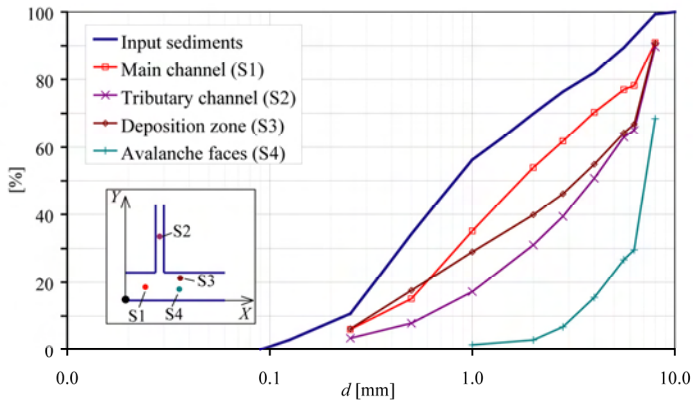

Figure 8: Sample locations and their respective grain size distributions

B. Intermediate-Reference

Appendix	Test	*Qr*	Windening		
			B_w	L_w	
A	*Low-Reference*	0.11	-	-	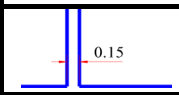
B	***Intermediate-Reference***	**0.15**			
C	*High-Reference*	0.20			
D	*Low-Small*	0.11	0.30	0.45	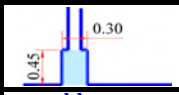
E	*Intermediate-Small*	0.15			
F	*High-Small*	0.20			
G	*Low-Medium*	0.11	0.45	0.45	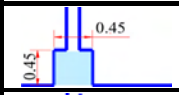
H	*Intermediate-Medium*	0.15			
I	*High-Medium*	0.20			
J	*Low-Large*	0.11	0.45	0.60	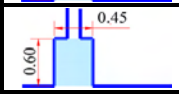
K	*Intermediate-Large*	0.15			
L	*High-Large*	0.20			

B.1 Summary

B.1.1 Initial hydraulic conditions

	Main (*m*)	Tributary (*t*)	*Qr* (Q_t/Q_m)
Q **[l/s]**	17.4	2.6	0.15
Qs **[kg/m^3]**	-	0.3	

B.1.2 Equilibrium flow depths

Main and post-confluence channels			
X\Y **[m]**	**0.05**	**0.25**	**0.45**
0	0.106	0.106	0.103
0.5	0.109	0.109	0.106
1.2	0.098	0.055	0.324
3.2	0.083	0.061	0.036
Tributary channel			
X **[m]**	**Average [0.5<*Y*<3.5m]**		
0.6	0.026		

B.1.3 Main morphological features

Bed discordance	0.078	[m]
Maximum deposition	0.082	[m]
Volume > elevation 0.02 m	0.026	[m^3]

B.2 Time-evolution of the bed elevations

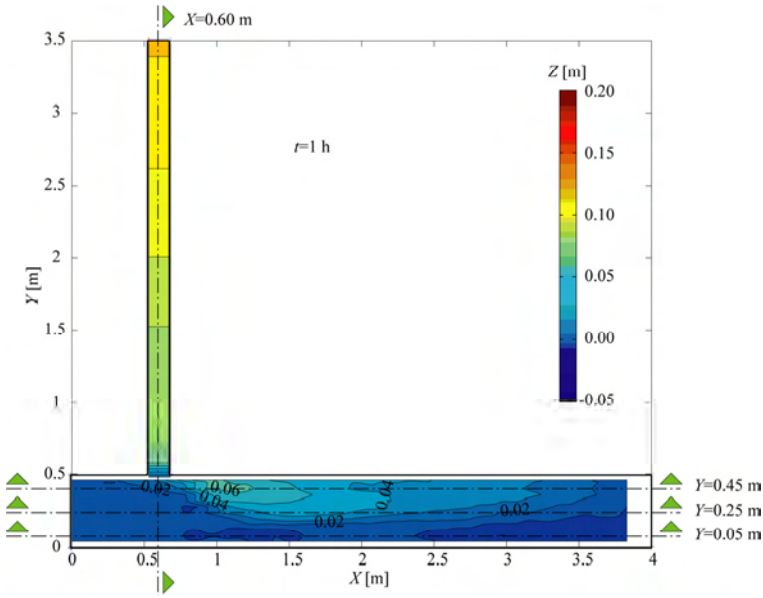

Figure 9: Bed elevations measured in the flume at t=1h

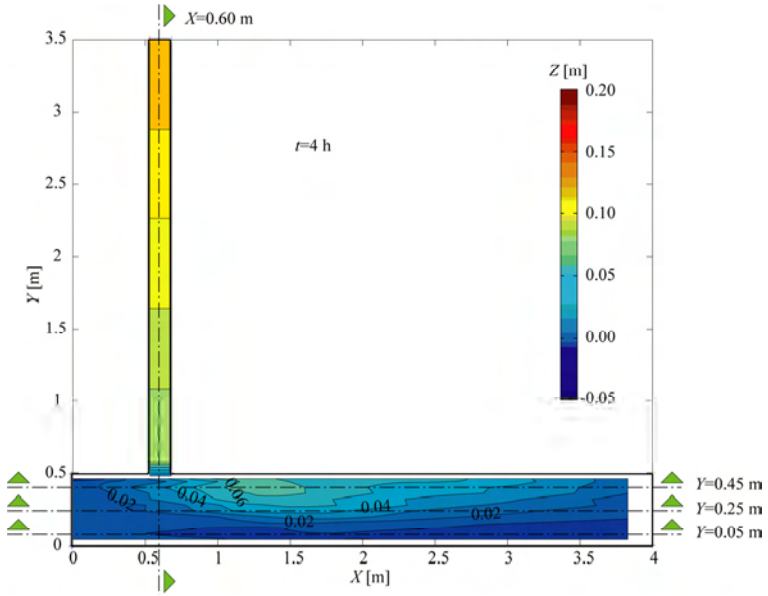

Figure 10: Bed elevations measured in the flume at t=4h

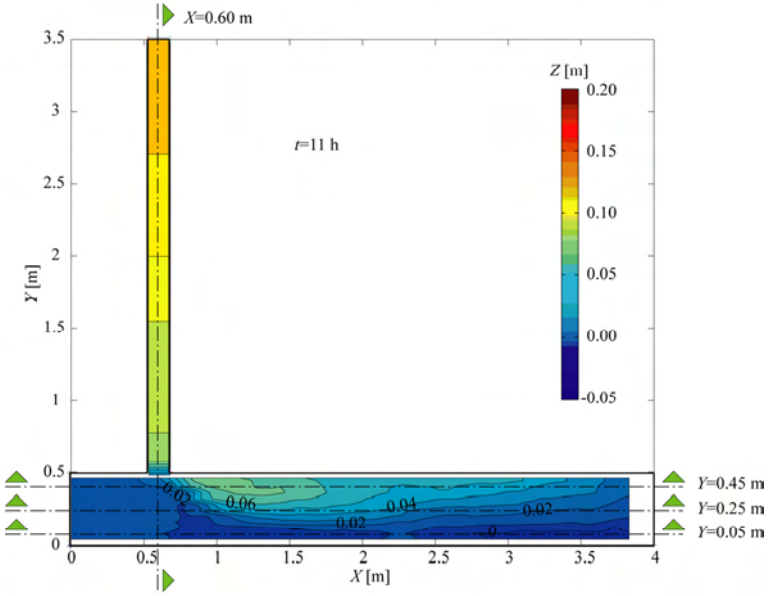

Figure 11: Bed elevations measured in the flume at t=11h

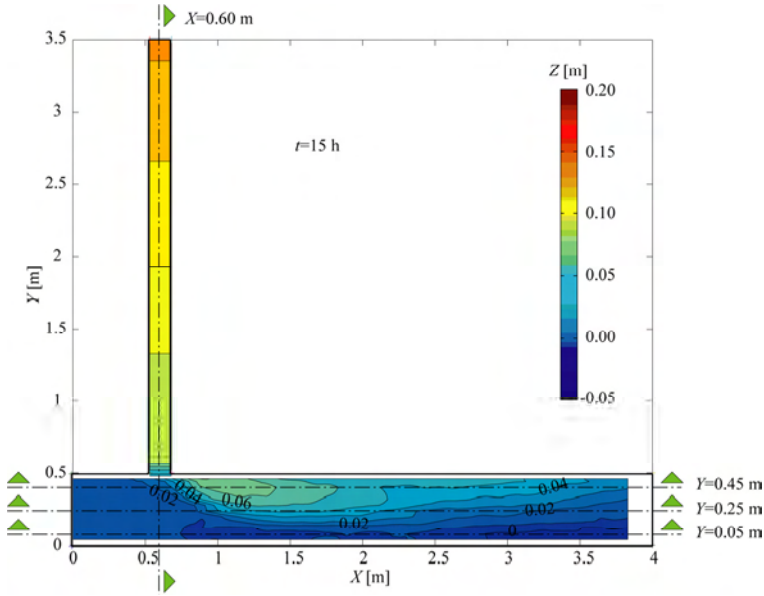

Figure 12: Bed elevations measured in the flume at t=15h

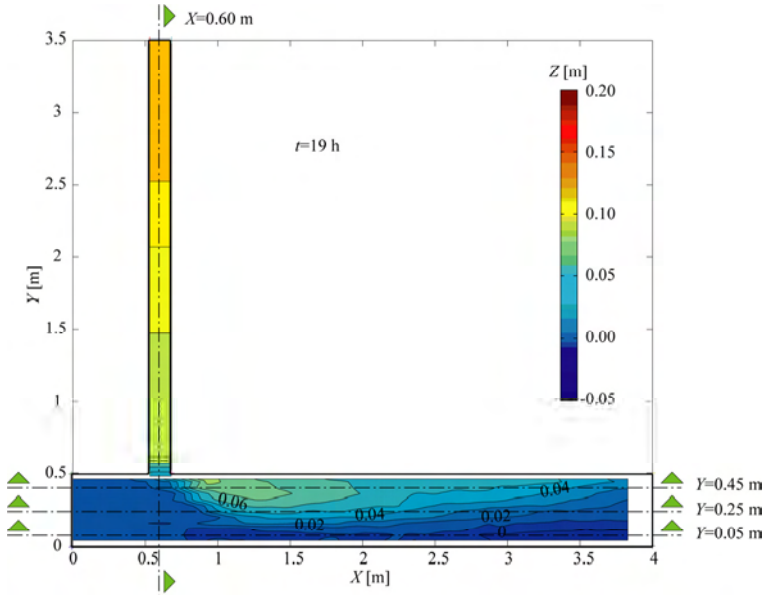

Figure 13: Bed elevations measured in the flume at t=19h

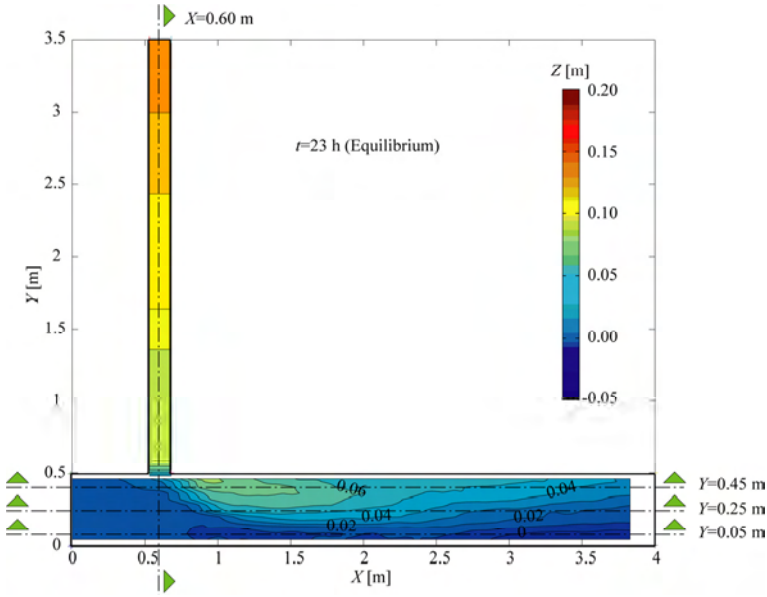

Figure 14: Bed elevations measured in the flume at t=23h

B.3 Longitudinal profiles

B.3.1 Main, post-confluence and tributary channels

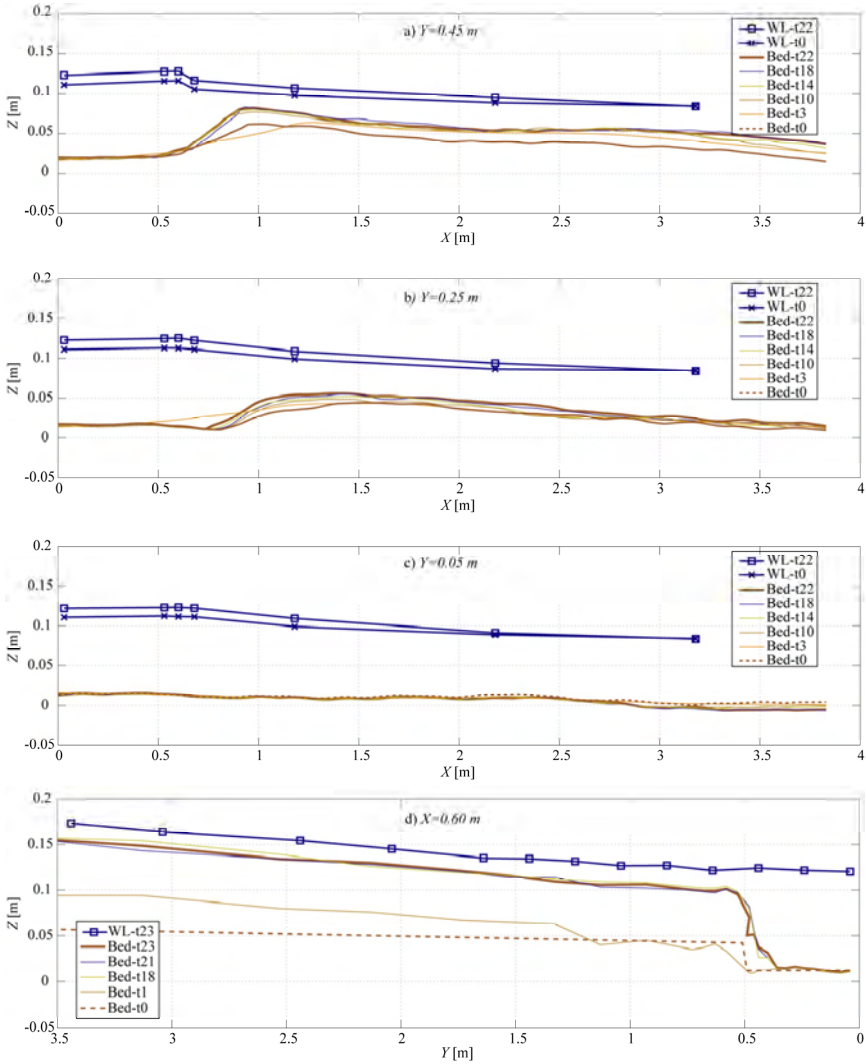

Figure 15: Longitudinal profiles along the main and post-confluence channels at Y*=0.05 m (a),* Y*=0.25 m (b) and* Y*=0.45 m (c) and longitudinal profile along the axis of the tributary (*X*=0.60 m) (d) showing the bed elevations and water levels measured in different time-steps*

B.4 Flow visualization of the main and post-confluence channels

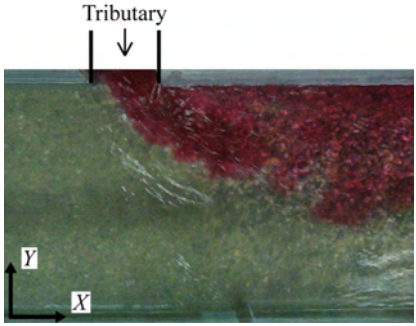

Figure 16: Upper view of the main and post-confluence channels with colour dye injected in the tributary

B.5 Pictures of the confluence zone

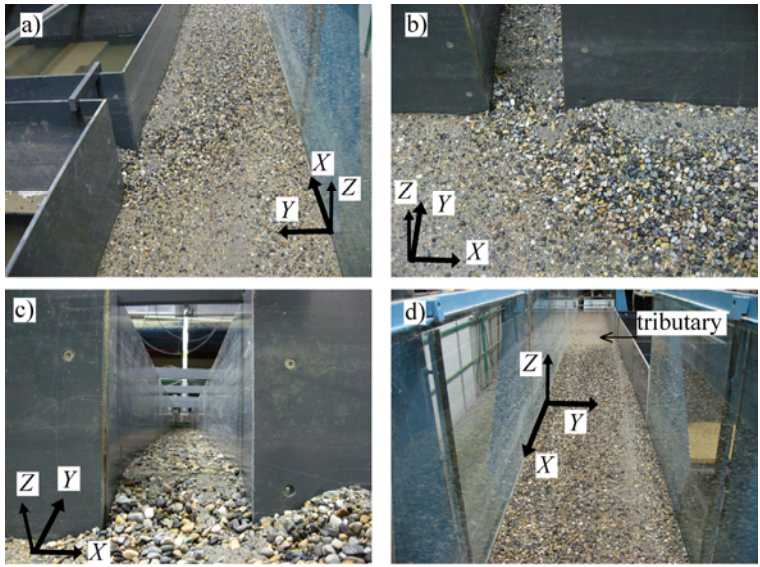

Figure 17: Pictures of the confluence zone. a) Upper view of the main and post-confluence channels. b) Upper view of the confluence zone, c) Upstream view of the tributary and d) Upstream view of the post- confluence channel

B.6 Grain size distributions

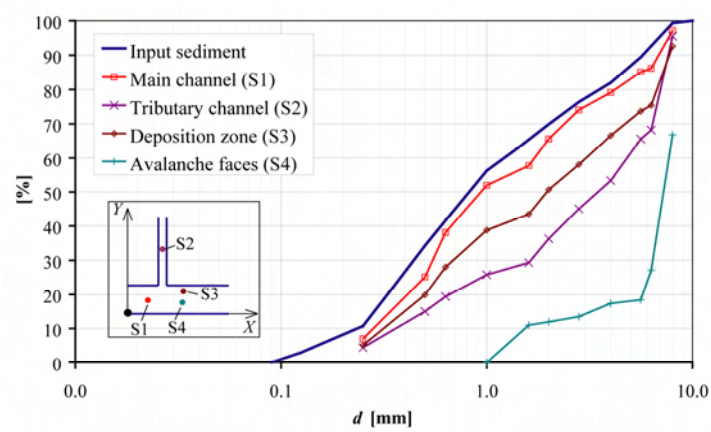

Figure 18: Sample locations and their respective grain size distributions

C. High-Reference

Appendix	Test	*Qr*	Windening		
			B_w	L_w	
A	*Low-Reference*	0.11	-	-	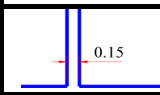
B	*Intermediate-Reference*	0.15			
C	***High-Reference***	**0.20**			
D	*Low-Small*	0.11	0.30	0.45	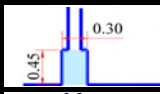
E	*Intermediate-Small*	0.15			
F	*High-Small*	0.20			
G	*Low-Medium*	0.11	0.45	0.45	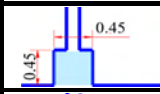
H	*Intermediate-Medium*	0.15			
I	*High-Medium*	0.20			
J	*Low-Large*	0.11	0.45	0.60	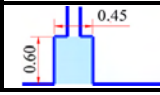
K	*Intermediate-Large*	0.15			
L	*High-Large*	0.20			

C.1 Summary

C.1.1 Initial hydraulic conditions

	Main (*m*)	Tributary (*t*)	*Qr* (Q_t/Q_m)
Q **[l/s]**	16.3	3.7	0.23
Qs **[kg/m^3]**	-	0.3	

C.1.2 Equilibrium flow depths

Main and post-confluence channels			
X\Y **[m]**	**0.05**	**0.25**	**0.45**
0	0.116	0.110	0.111
0.5	0.117	0.116	0.068
1.2	0.115	0.059	0.039
3	0.083	0.062	0.039
Tributary channel			
X **[m]**	**Average [0.5<*Y*<3.5m]**		
0.6	0.04		

C.1.3 Main morphological features

Bed discordance	0.072	[m]
Maximum deposition	0.070	[m]
Volume > elevation 0.02 m	0.019	[m^3]

C.2 Time-evolution of the bed elevations

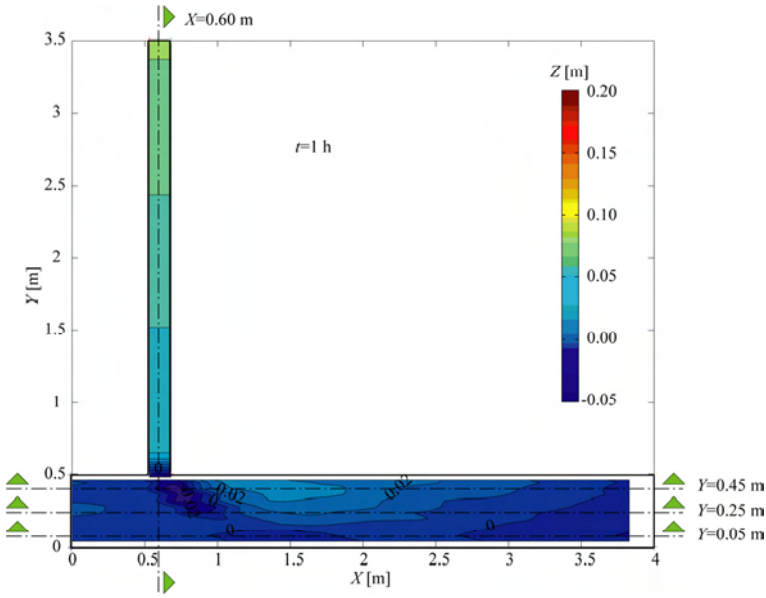

Figure 19: Bed elevations measured in the flume at t=1h

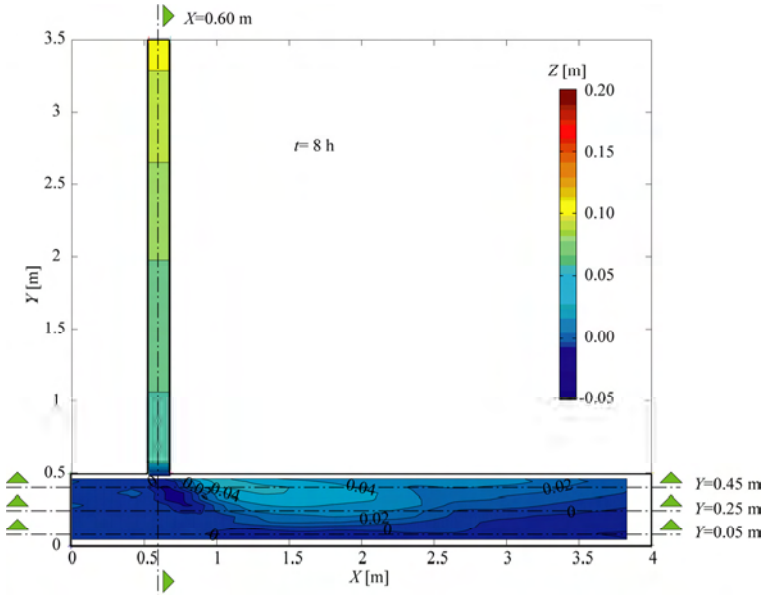

Figure 20: Bed elevations measured in the flume at t=8h

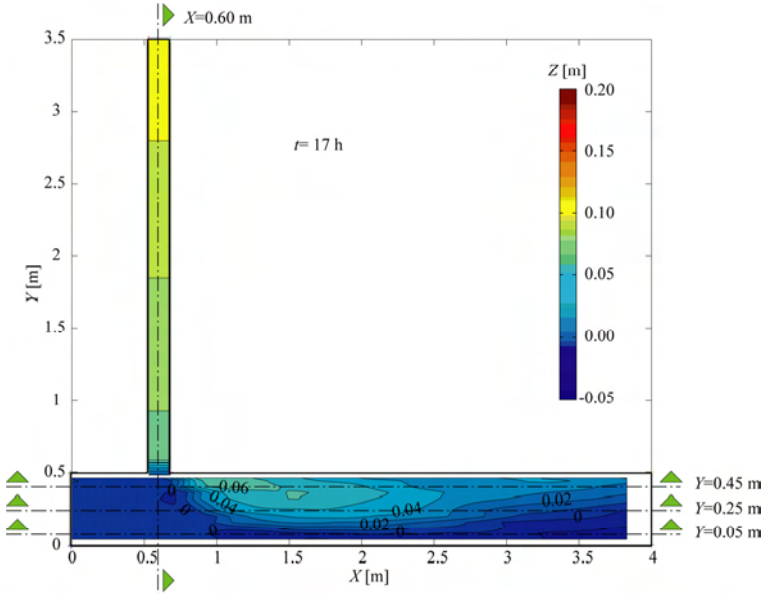

Figure 21: Bed elevations measured in the flume at t=17h

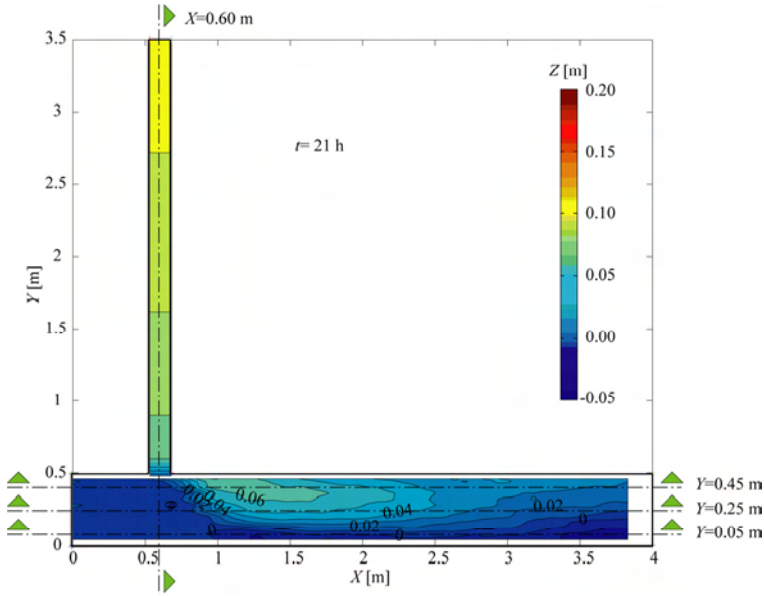

Figure 22: Bed elevations measured in the flume at t=21h

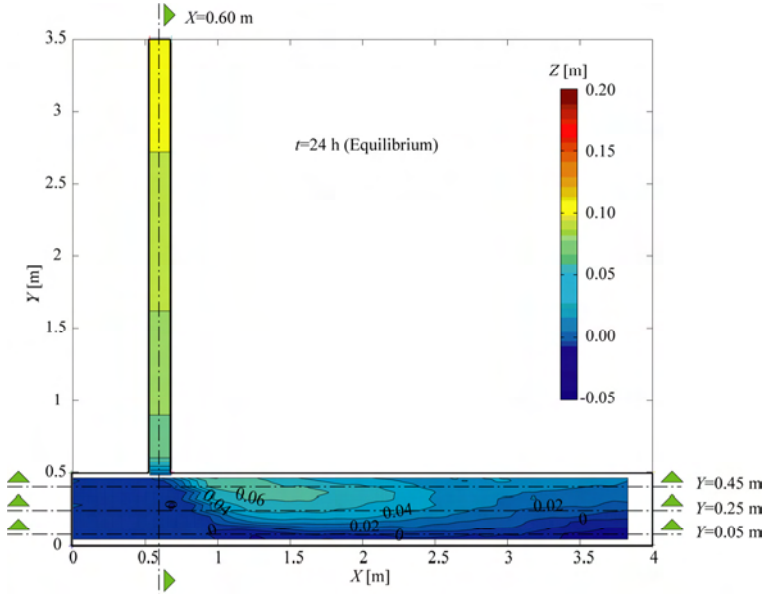

Figure 23: Bed elevations measured in the flume at t=24h

C.3 Longitudinal profiles

C.3.1 Main, post-confluence and tributary channels

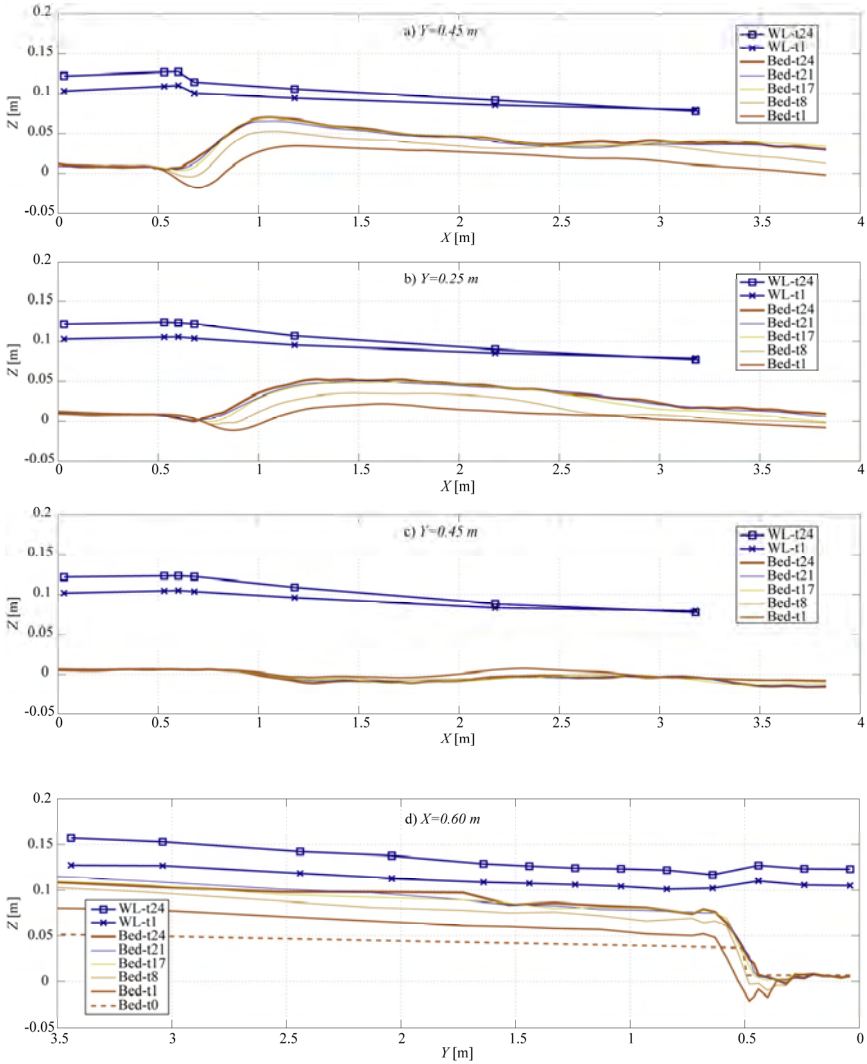

Figure 24: Longitudinal profiles along the main and post-confluence channels at Y*=0.05 m (a),* Y*=0.25 m (b) and* Y*=0.45 m (c) and longitudinal profile along the axis of the tributary (*X*=0.60 m) (d) showing the bed elevations and water levels measured in different time-steps*

C.4 Flow visualization of the main and post-confluence channels

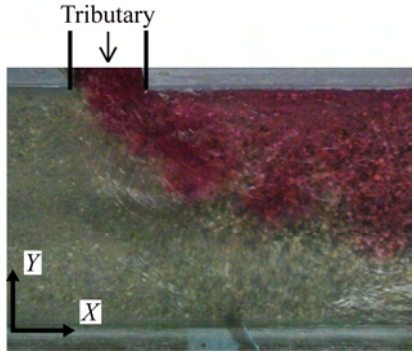

Figure 25: Upper view of the main and post-confluence channels with colour dye injected in the tributary

C.5 Pictures of the confluence zone

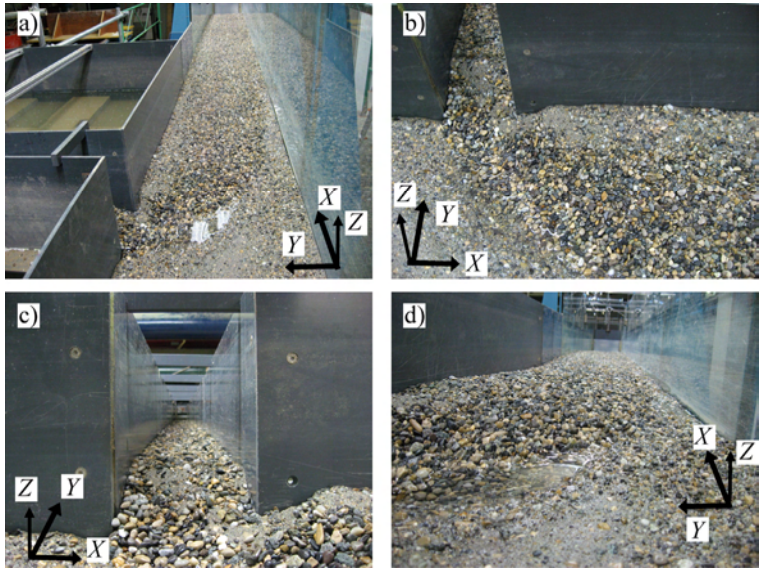

Figure 26: Pictures of the confluence zone. a) Upper view of the main and post-confluence channels. b) Upper view of the confluence zone, c) Upstream view of the tributary and d) Downstream view of the post- confluence channel

C.6 Grain size distributions

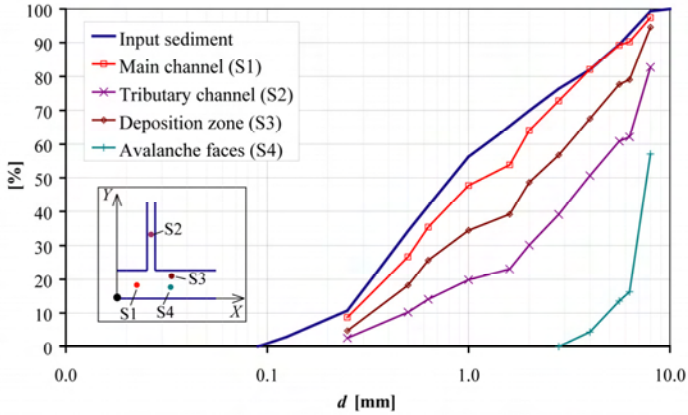

Figure 27: Sample locations and their respective grain size distributions

D. Low-Small

Appendix	Test	*Qr*	Windening B_w	Windening L_w	
A	*Low-Reference*	0.11	-	-	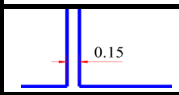
B	*Intermediate-Reference*	0.15			
C	*High-Reference*	0.20			
D	***Low-Small***	**0.11**	0.30	0.45	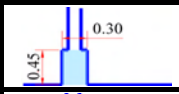
E	*Intermediate-Small*	0.15			
F	*High-Small*	0.20			
G	*Low-Medium*	0.11	0.45	0.45	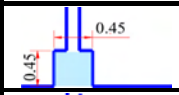
H	*Intermediate-Medium*	0.15			
I	*High-Medium*	0.20			
J	*Low-Large*	0.11	0.45	0.60	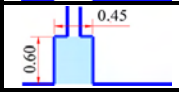
K	*Intermediate-Large*	0.15			
L	*High-Large*	0.20			

D.1 Summary

D.1.1 Initial hydraulic conditions

	Main (*m*)	Tributary (*t*)	*Qr* (Q_t/Q_m)
Q [l/s]	18	2	0.11
Qs [kg/m^3]	-	0.3	

D.1.2 Equilibrium flow depths

Main and post-confluence channels			
*X**Y* [m]	0.05	0.25	0.45
0	0.114	0.114	0.122
0.5	0.113	0.111	0.119
1.2	0.102	0.064	0.007
3	0.073	0.051	0.043
Tributary channel			
X [m]	Average [0.5<*Y*<0.90m] *		
0.6	0.014		

* only widened zone.

D.1.3 Main morphological features

Bed discordance	0.097	[m]
Maximum deposition	0.101	[m]
Volume > elevation 0.02 m	0.022	[m^3]

D.2 Time-evolution of the bed elevations

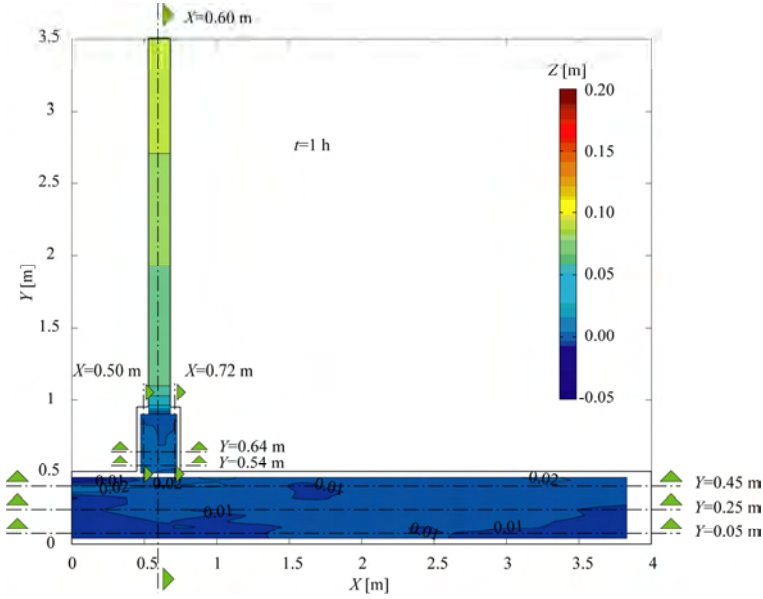

Figure 28: Bed elevations measured in the flume at t=1h

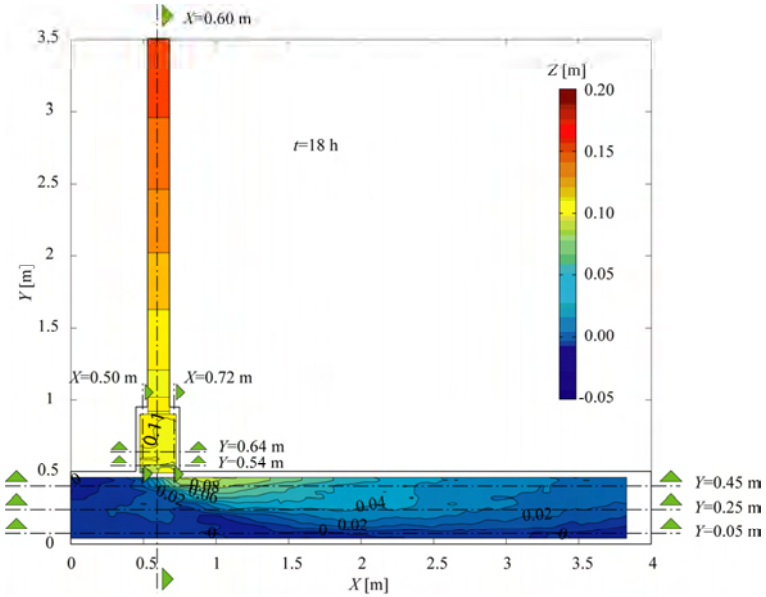

Figure 29: Bed elevations measured in the flume at t=18h

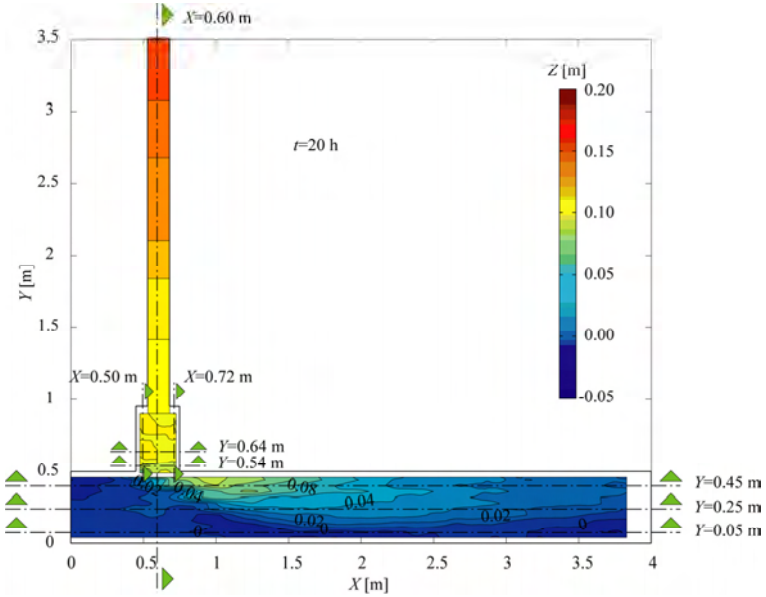

Figure 30: Bed elevations measured in the flume at t=20h

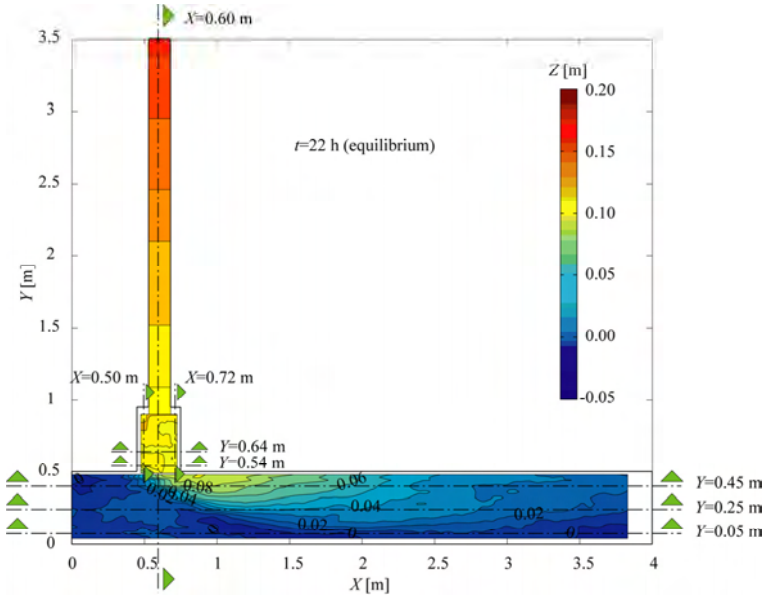

Figure 31: Bed elevations measured in the flume at t=22h

D.3 Longitudinal profiles and cross-sections

D.3.1 Main, post-confluence and tributary channels

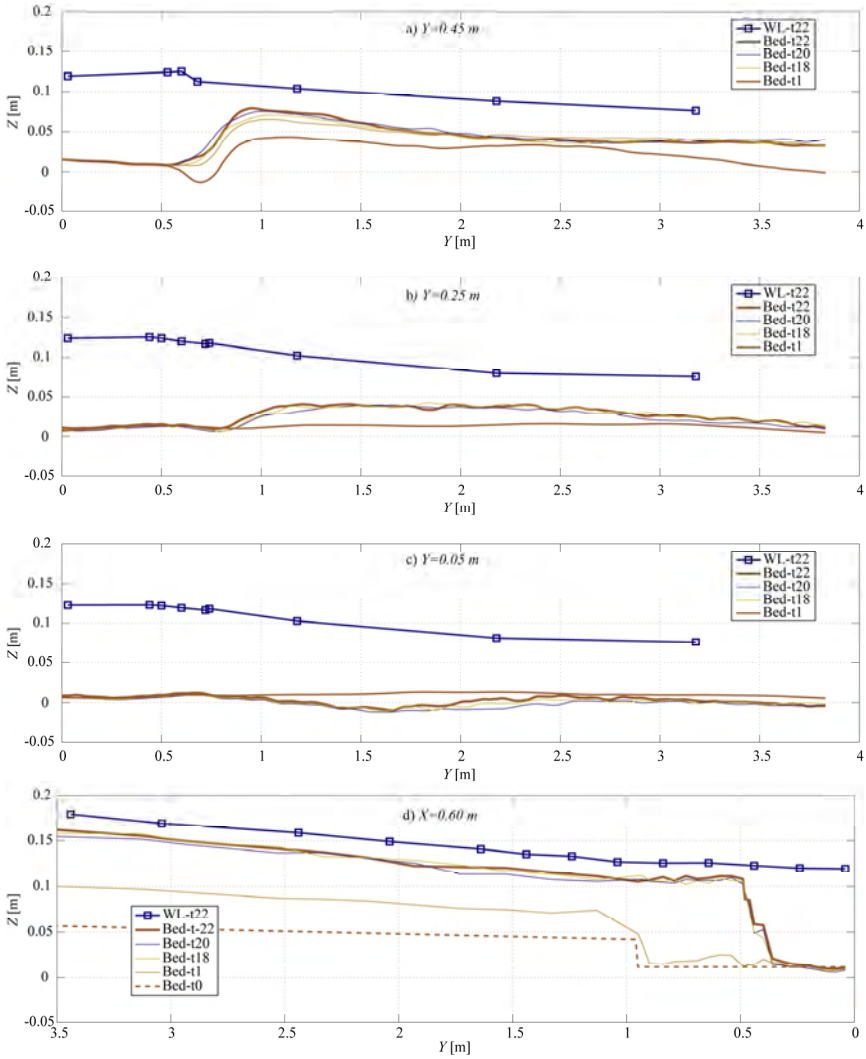

Figure 32: Longitudinal profiles along the main and post-confluence channels at Y=0.05 m (a), Y=0.25 m (b) and Y=0.45 m (c) and longitudinal profile along the axis of the tributary (X=0.60 m) (d) showing the bed elevations and water levels measured in different time-steps

D.3.2 Widened zone

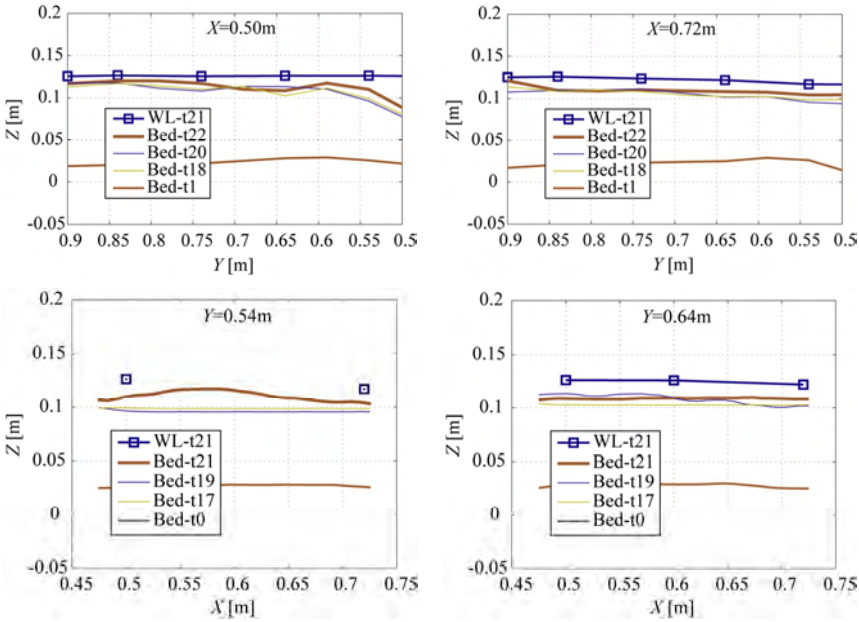

Figure 33: Cross-sections in the widened zone at: X=0.50 , X=0.72 m, Y=0.54 m and Y=0.64 m

D.4 Flow visualization of the main and post-confluence channels

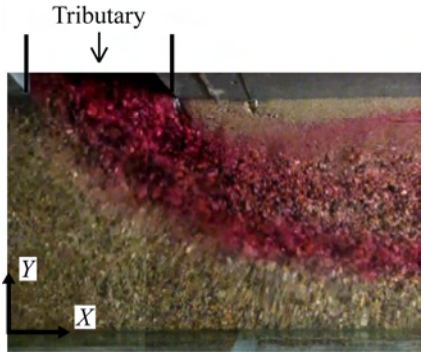

Figure 34: Upper view of the main and post-confluence channels with colour dye injected in the tributary

D.5 Pictures of the confluence zone

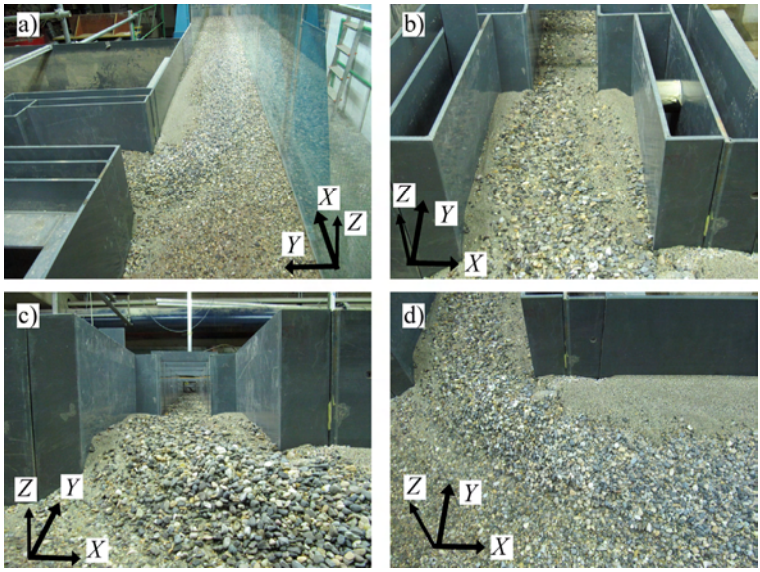

Figure 35: Pictures of the confluence zone. a) Upper view of the main and post-confluence channels. b) Upper view of the widened zone, c) Upstream view of the tributary and d) Upper view of the confluence zone

D.6 Grain size distributions

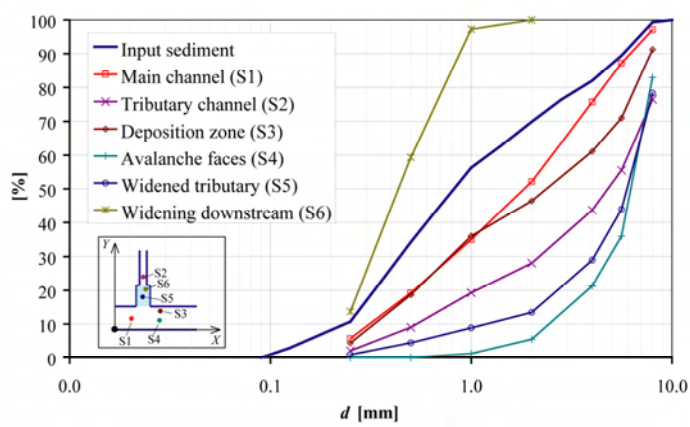

Figure 36: Sample locations and their respective grain size distributions

E. Intermediate-Small

Appendix	Test	*Qr*	Windening B_w	Windening L_w	
A	*Low-Reference*	0.11	-	-	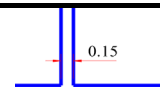
B	*Intermediate-Reference*	0.15			
C	*High-Reference*	0.20			
D	*Low-Small*	0.11	0.30	0.45	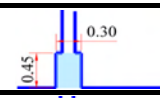
E	***Intermediate-Small***	**0.15**			
F	*High-Small*	0.20			
G	*Low-Medium*	0.11	0.45	0.45	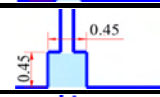
H	*Intermediate-Medium*	0.15			
I	*High-Medium*	0.20			
J	*Low-Large*	0.11	0.45	0.60	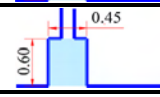
K	*Intermediate-Large*	0.15			
L	*High-Large*	0.20			

E.1 Summary

E.1.1 Initial hydraulic conditions

	Main (*m*)	Tributary (*t*)	*Qr* (Q_t/Q_m)
Q [l/s]	17.4	2.6	0.15
Qs [kg/m^3]	-	0.3	

E.1.2 Equilibrium flow depths

Main and post-confluence channels			
*X**Y* [m]	0.05	0.25	0.45
0	0.109	0.105	0.103
0.5	0.112	0.111	0.111
1.2	0.104	0.050	0.000
3	0.071	0.059	0.050
Tributary channel			
X [m]	Average [0.5<*Y*<0.90m] *		
0.6	0.015		

* only widened zone.

E.1.3 Main morphological features

Bed discordance	0.097	[m]
Maximum deposition	0.101	[m]
Volume > elevation 0.02 m	0.020	[m^3]

E.2 Time-evolution of the bed elevations

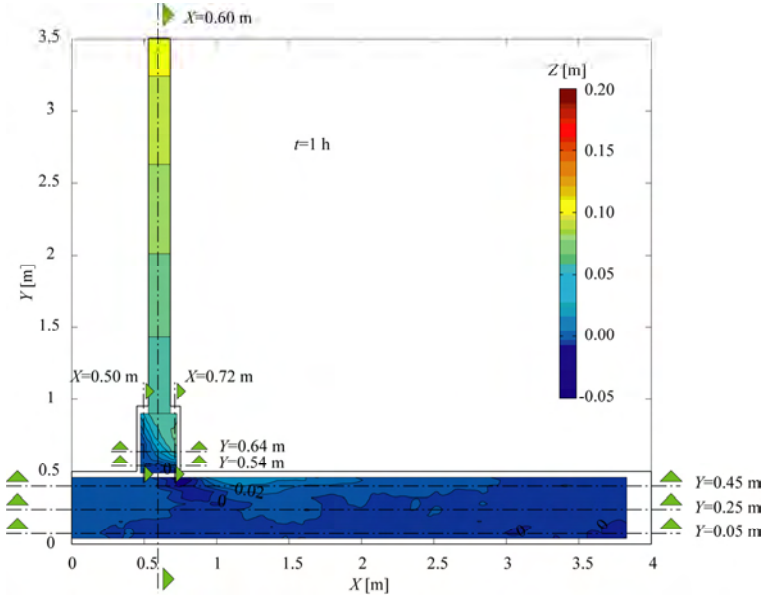

Figure 37: Bed elevations measured in the flume at t=1h

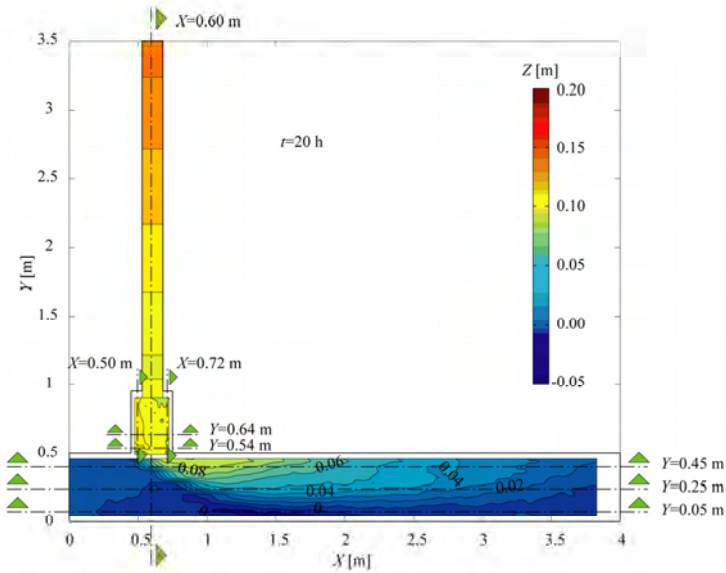

Figure 38: Bed elevations measured in the flume at t=20h

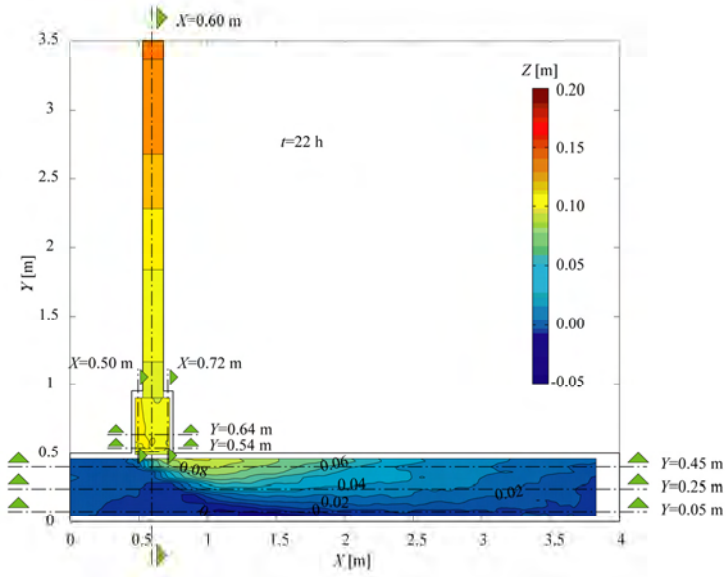

Figure 39: Bed elevations measured in the flume at t=22h

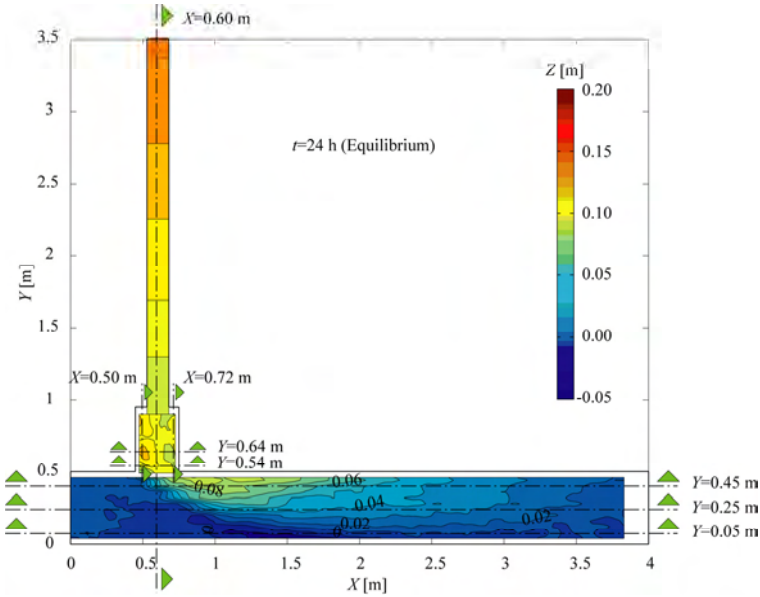

Figure 40: Bed elevations measured in the flume at t=24h

E.3 Longitudinal profiles and cross-sections

E.3.1 Main, post-confluence and tributary channels

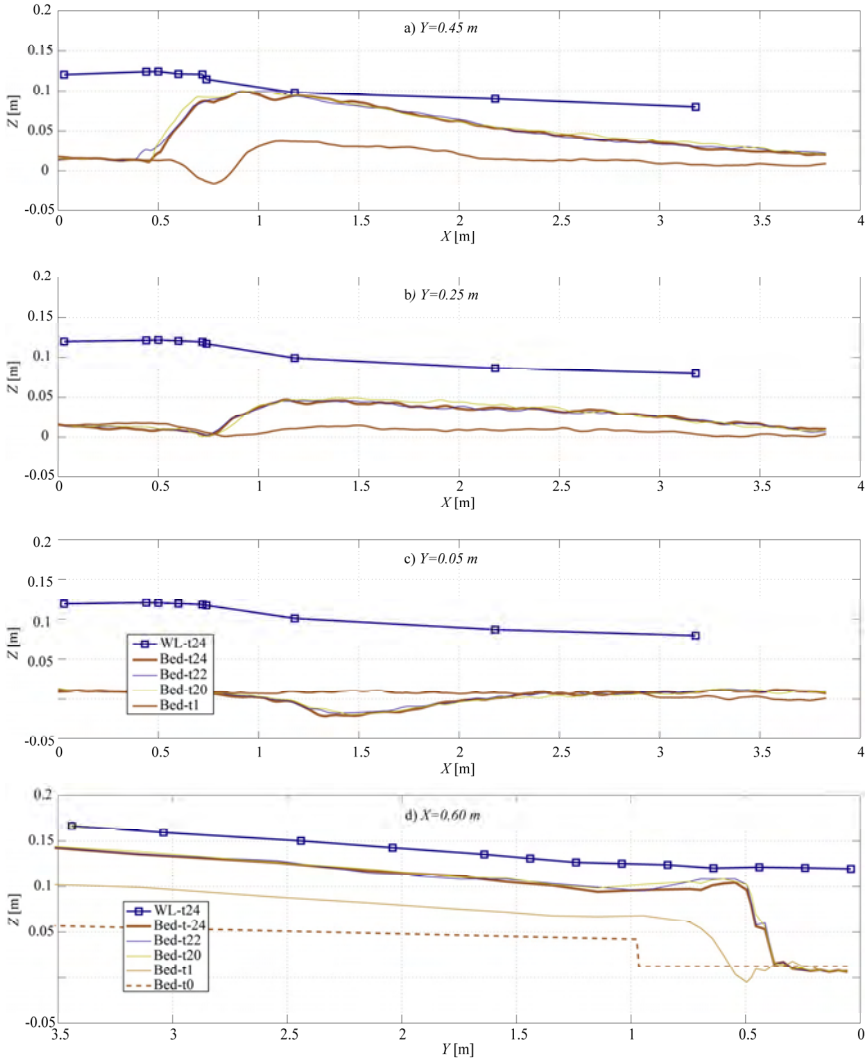

Figure 41: Longitudinal profiles along the main and post-confluence channels at Y=0.05 m (a), Y=0.25 m (b) and Y=0.45 m (c) and longitudinal profile along the axis of the tributary (X=0.60 m) (d) showing the bed elevations and water levels measured in different time-steps

E.3.2 Widened zone

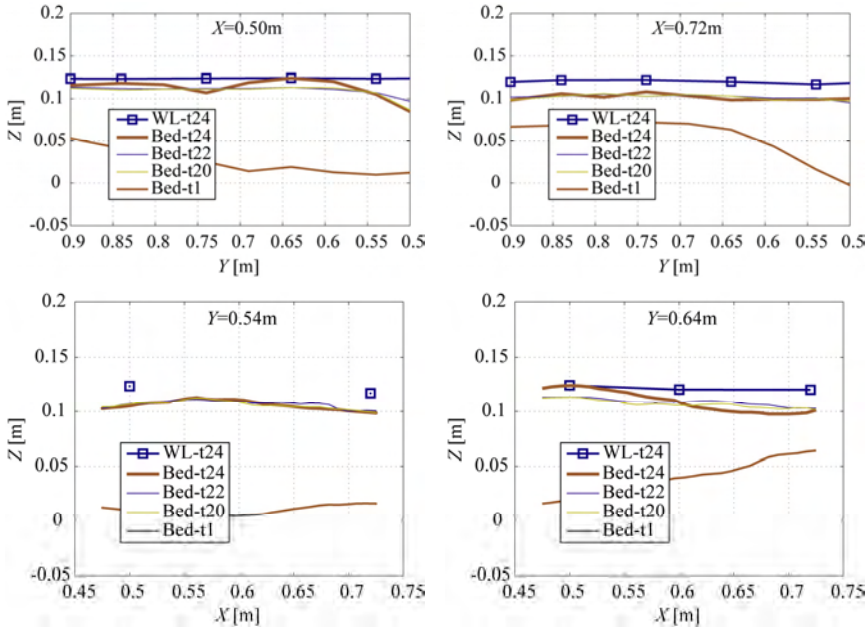

Figure 42: Cross-sections in the widened zone at: X=0.50 , X=0.72 m, Y=0.54 m and Y=0.64 m

E.4 Flow visualization of the main and post-confluence channels

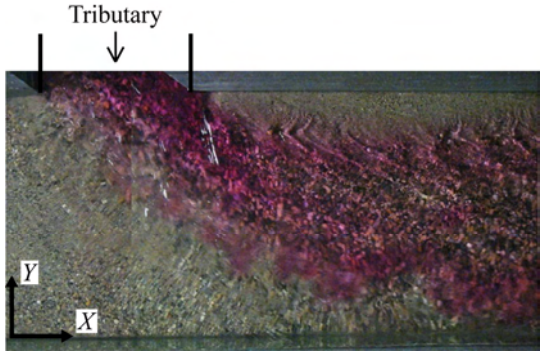

Figure 43: Upper view of the main and post-confluence channels with colour dye injected in the tributary

E.5 Pictures of the confluence zone

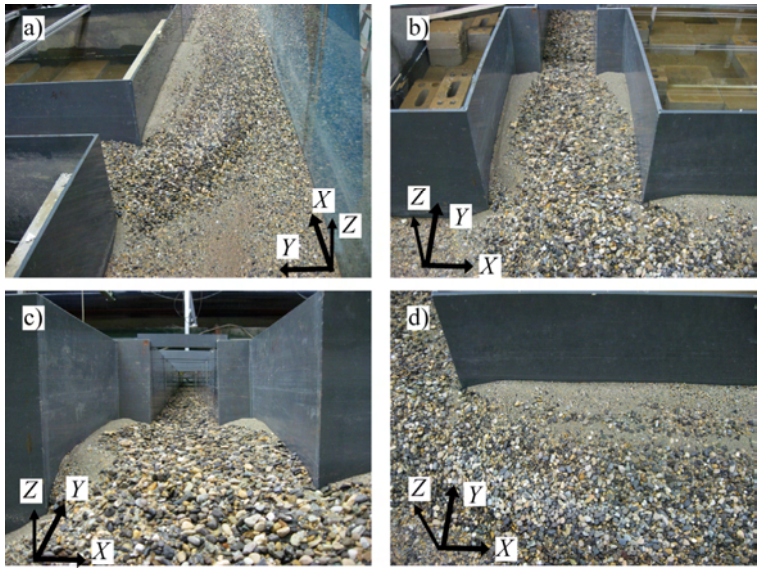

Figure 44: Pictures of the confluence zone. a) Upper view of the main and post-confluence channels. b) Upper view of the widened zone, c) Upstream view of the tributary and d) Upper view of the confluence zone

E.6 Grain size distributions

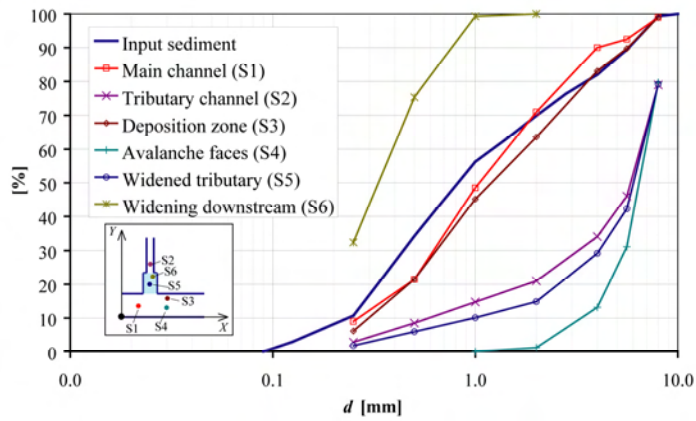

Figure 45: Sample locations and their respective grain size distributions

F. High-Small

			Windening		
Appendix	**Test**	***Qr***	B_w	L_w	
A	*Low-Reference*	0.11	-	-	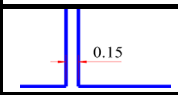
B	*Intermediate-Reference*	0.15			
C	*High-Reference*	0.20			
D	*Low-Small*	0.11	0.30	0.45	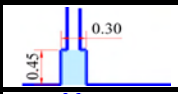
E	*Intermediate-Small*	0.15			
F	***High-Small***	**0.20**			
G	*Low-Medium*	0.11	0.45	0.45	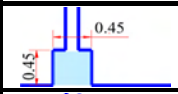
H	*Intermediate-Medium*	0.15			
I	*High-Medium*	0.20			
J	*Low-Large*	0.11	0.45	0.60	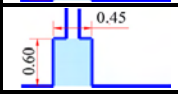
K	*Intermediate-Large*	0.15			
L	*High-Large*	0.20			

F.1 Summary

F.1.1 Initial hydraulic conditions

	Main (*m*)	Tributary (*t*)	*Qr* (Q_t/Q_m)
Q [l/s]	16.3	3.7	0.23
Qs [kg/m^3]	-	0.3	

F.1.2 Equilibrium flow depths

Main and post-confluence channels			
*X**Y* [m]	0.05	0.25	0.45
0	0.104	0.102	0.103
0.5	0.106	0.102	0.099
1.2	0.091	0.064	0.042
3	0.075	0.063	0.035
Tributary channel			
X [m]	Average [0.5<*Y*<0.90m] *		
0.6	0.039		

* only widened zone.

F.1.3 Main morphological features

Bed discordance	0.065	[m]
Maximum deposition	0.068	[m]
Volume > elevation 0.02 m	0.015	[m^3]

F.2 Time-evolution of the bed elevations

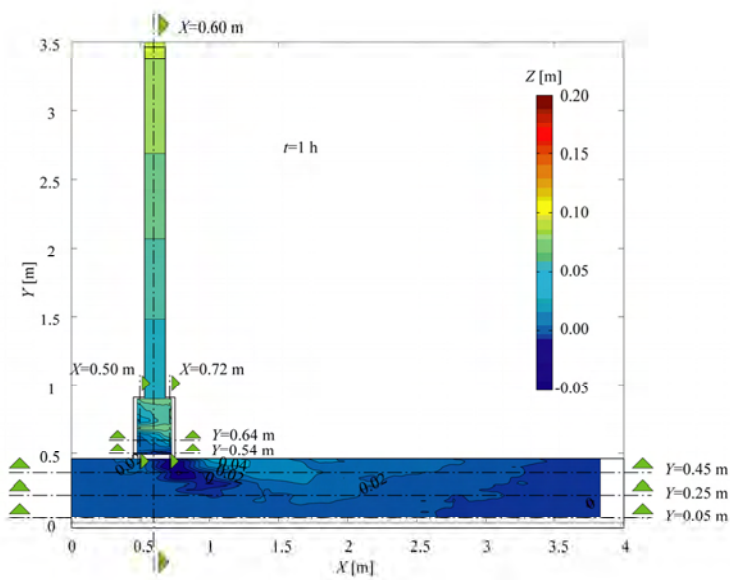

Figure 46: Bed elevations measured in the flume at t=1h

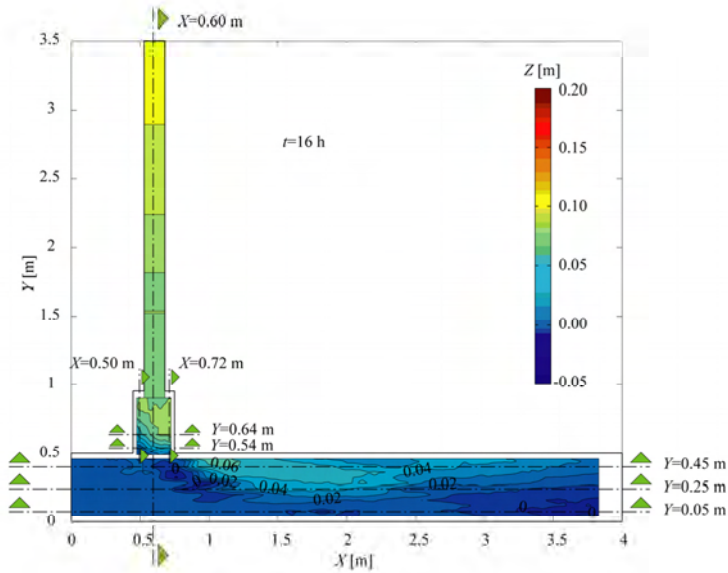

Figure 47: Bed elevations measured in the flume at t=16h

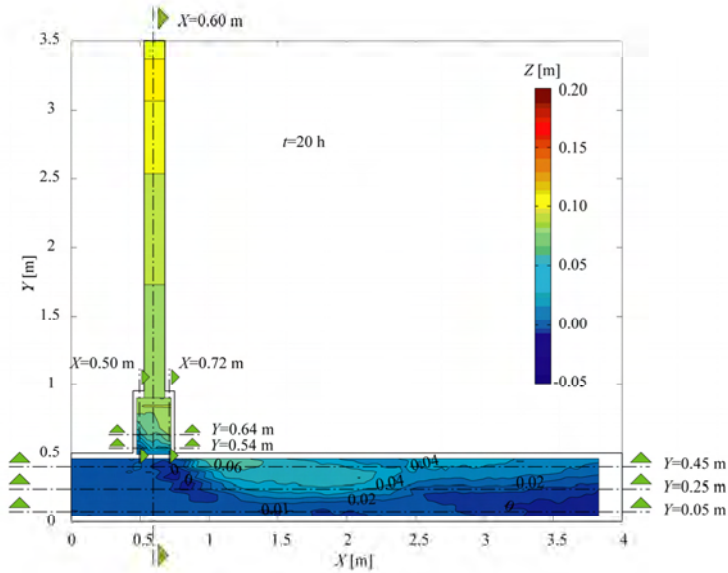

Figure 48: Bed elevations measured in the flume at t=20h

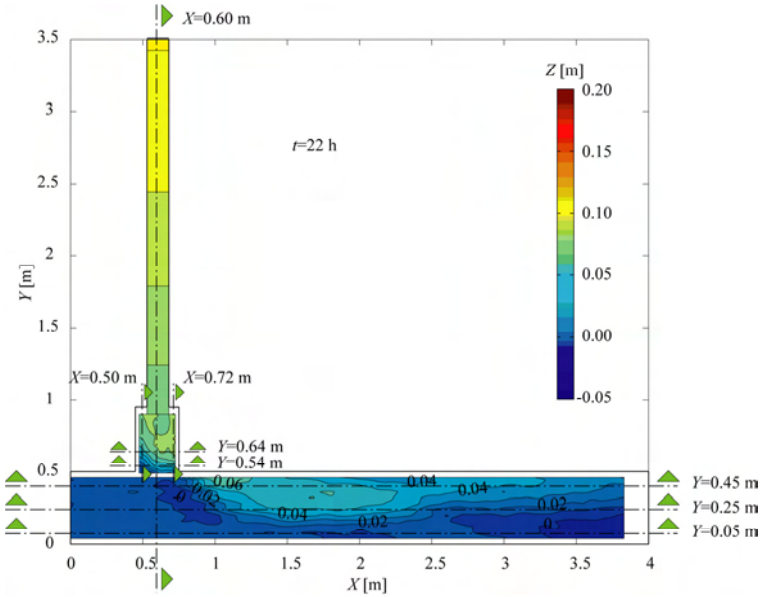

Figure 49: Bed elevations measured in the flume at t=22h

F.3 Longitudinal profiles and cross-sections

F.3.1 Main, post-confluence and tributary channels

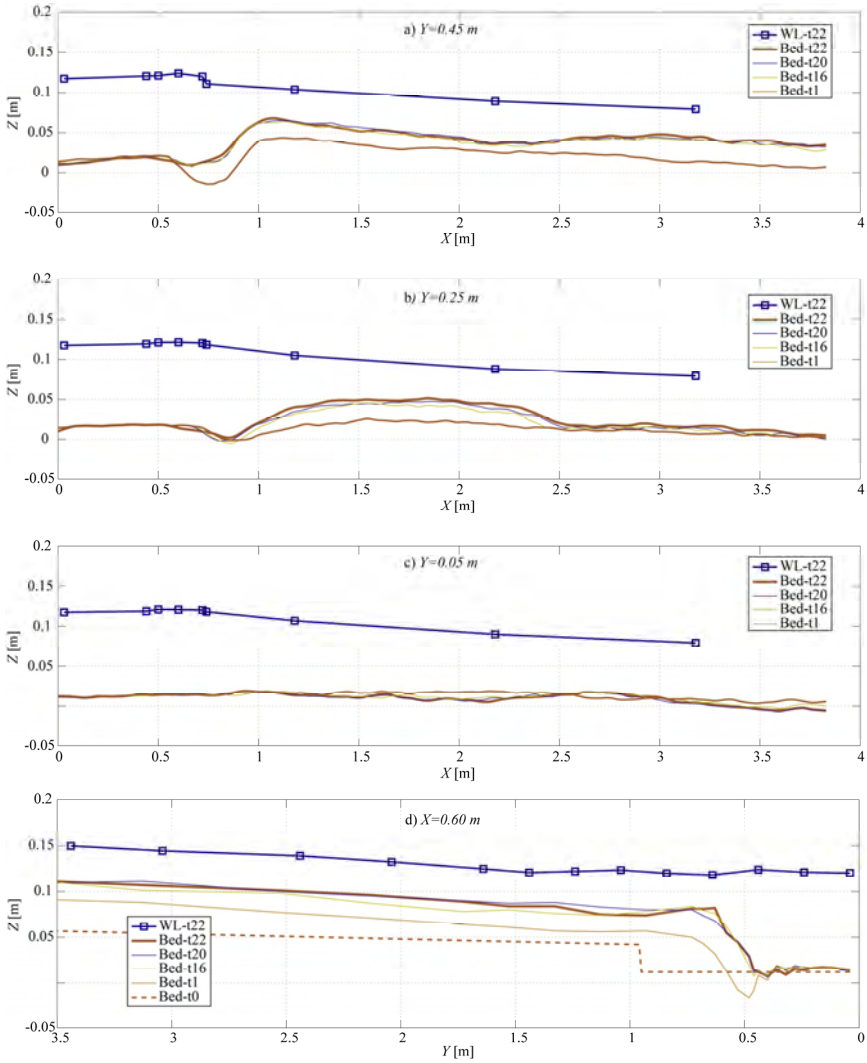

Figure 50: Longitudinal profiles along the main and post-confluence channels at Y=0.05 m (a), Y=0.25 m (b) and Y=0.45 m (c) and longitudinal profile along the axis of the tributary (X=0.60 m) (d) showing the bed elevations and water levels measured in different time-steps

F.3.2 Cross-sections in the widened zone

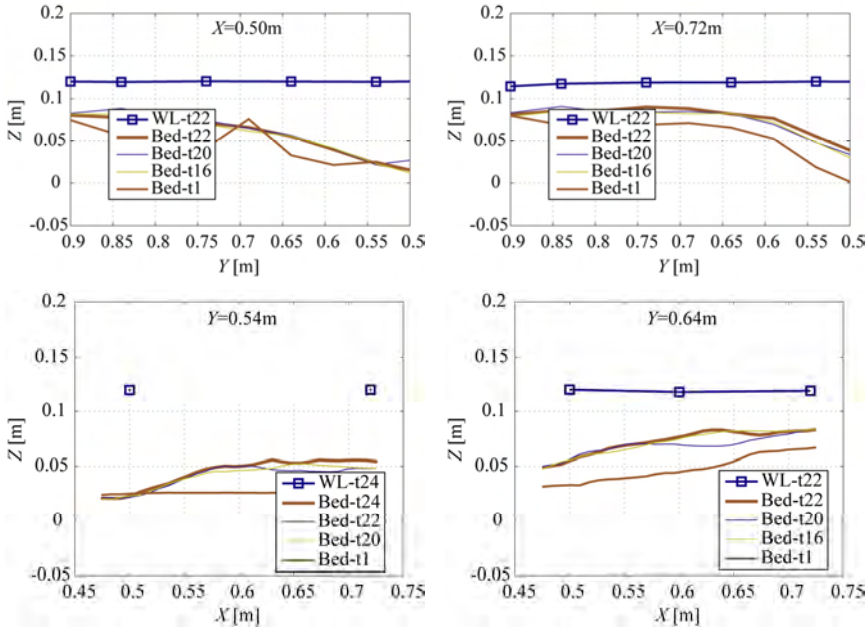

Figure 51: Cross-sections in the widened zone at: X=0.50 , X=0.72 m, Y=0.54 m and Y=0.64 m

F.4 Flow visualization of the main and post-confluence channels

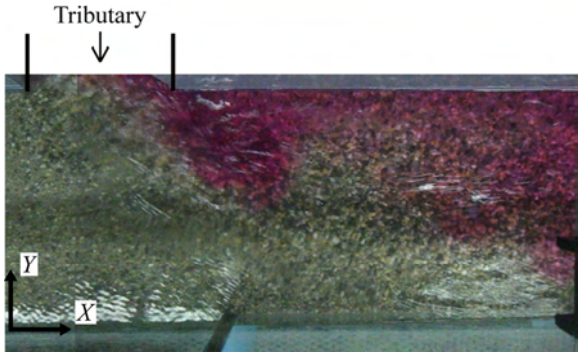

Figure 52: Upper view of the main and post-confluence channels with colour dye injected in the tributary

F.5 Pictures of the confluence zone

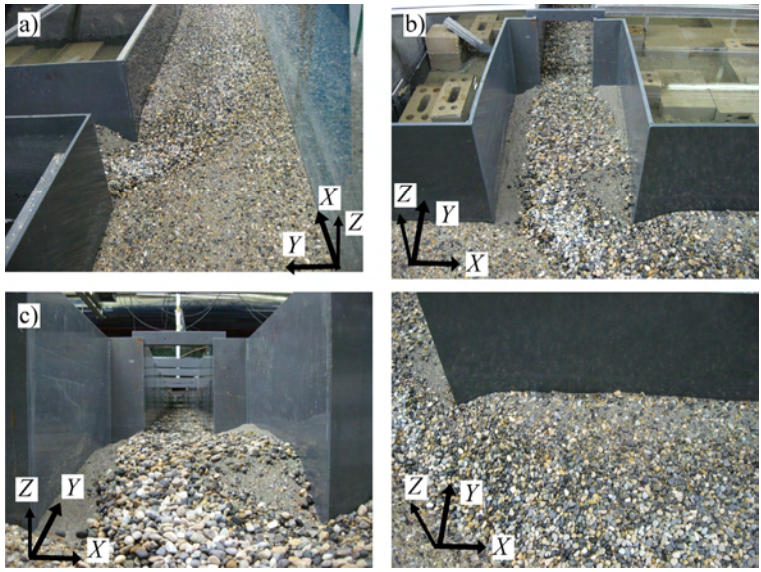

Figure 53: Pictures of the confluence zone. a) Upper view of the main and post-confluence channels. b) Upper view of the widened zone, c) Upstream view of the tributary and d) Upper view of the confluence zone

F.6 Grain size distributions

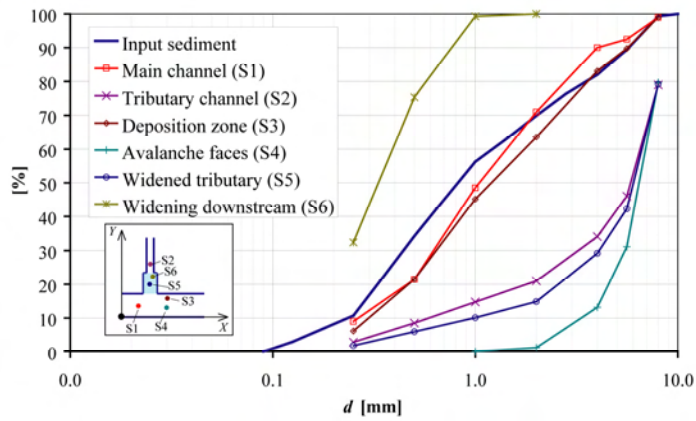

Figure 54: Sample locations and their respective grain size distributions

G. Low-Medium

Appendix	Test	*Qr*	Windening		
			B_w	L_w	
A	*Low-Reference*	0.11	-	-	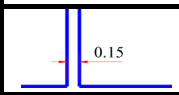
B	*Intermediate-Reference*	0.15			
C	*High-Reference*	0.20			
D	*Low-Small*	0.11	0.30	0.45	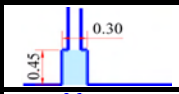
E	*Intermediate-Small*	0.15			
F	*High-Small*	0.20			
G	***Low-Medium***	**0.11**	0.45	0.45	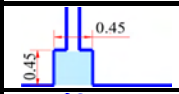
H	*Intermediate-Medium*	0.15			
I	*High-Medium*	0.20			
J	*Low-Large*	0.11	0.45	0.60	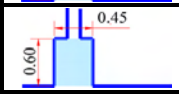
K	*Intermediate-Large*	0.15			
L	*High-Large*	0.20			

G.1 Summary

G.1.1 Initial hydraulic conditions

	Main (*m*)	Tributary (*t*)	*Qr* (Q_t/Q_m)
Q **[l/s]**	18	2	0.11
Qs **[kg/m^3]**	-	0.3	

G.1.2 Equilibrium flow depths

Main and post-confluence channels			
X\Y **[m]**	**0.05**	**0.25**	**0.45**
0	0.109	0.106	0.104
0.5	0.108	0.106	0.104
1.2	0.097	0.065	0.007
3	0.079	0.058	0.044
Tributary channel			
X **[m]**	**Average [0.5<*Y*<0.90m] ***		
0.6	0.015		

* only widened zone.

G.1.3 Main morphological features

Bed discordance	0.091	[m]
Maximum deposition	0.099	[m]
Volume > elevation 0.02 m	0.021	[m^3]

G.2 Time-evolution of the bed elevations

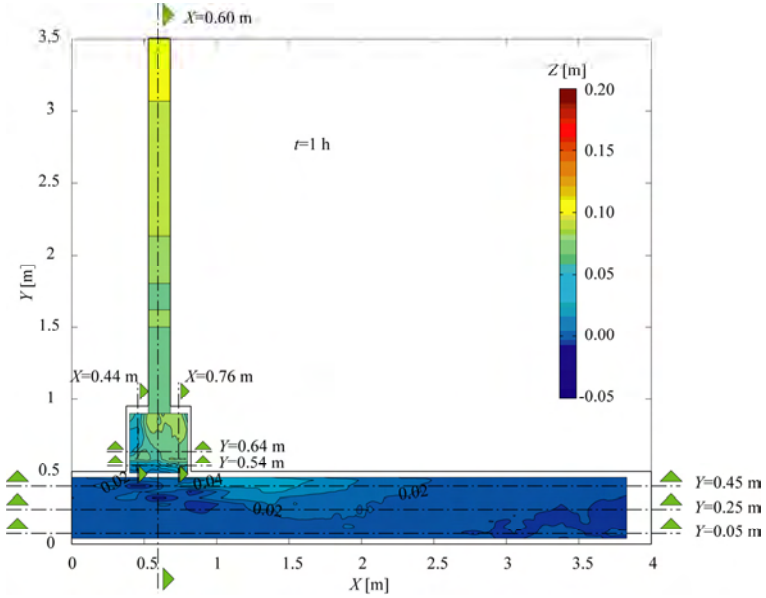

Figure 55: Bed elevations measured in the flume at t=1h

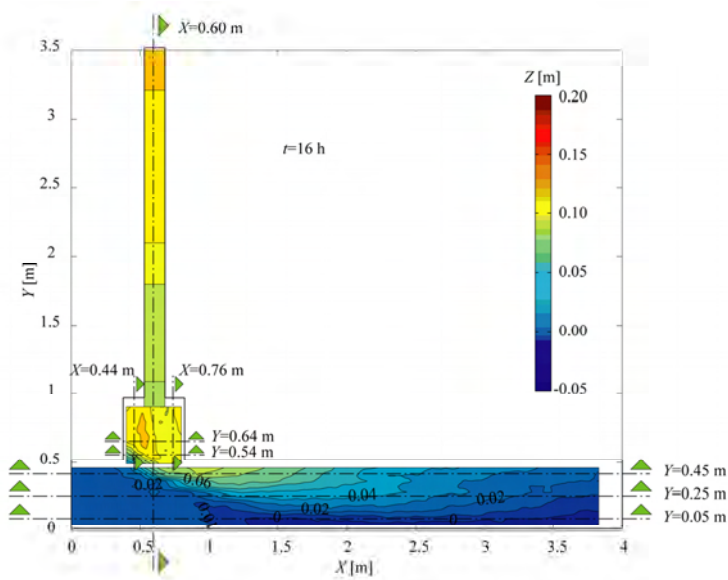

Figure 56: Bed elevations measured in the flume at t=16h

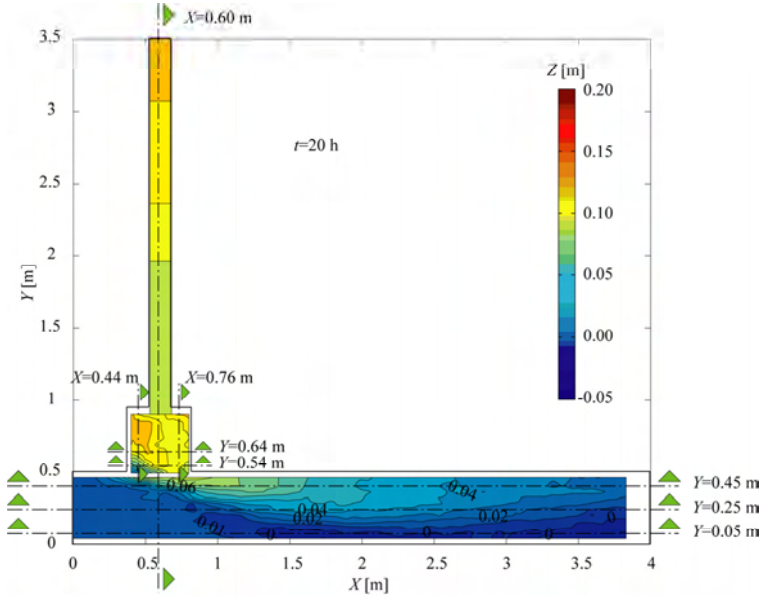

Figure 57: Bed elevations measured in the flume at t=20h

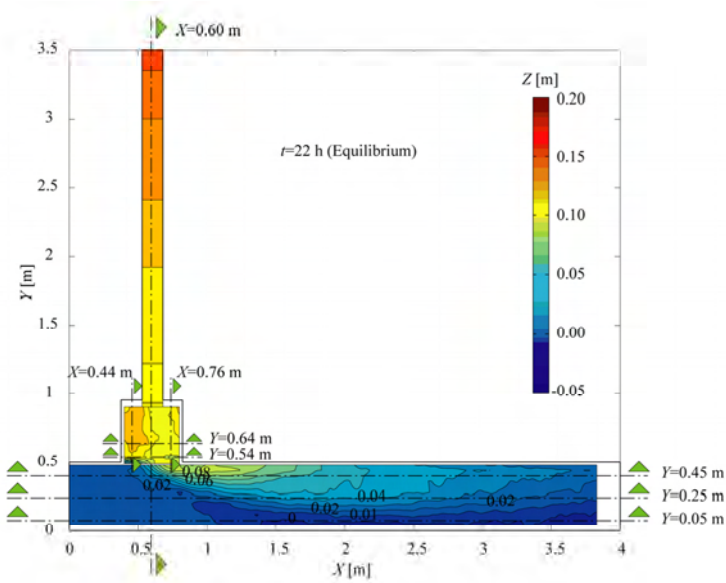

Figure 58: Bed elevations measured in the flume at t=22h

G.3 Longitudinal profiles and cross-sections

G.3.1 Main, post-confluence and tributary channels

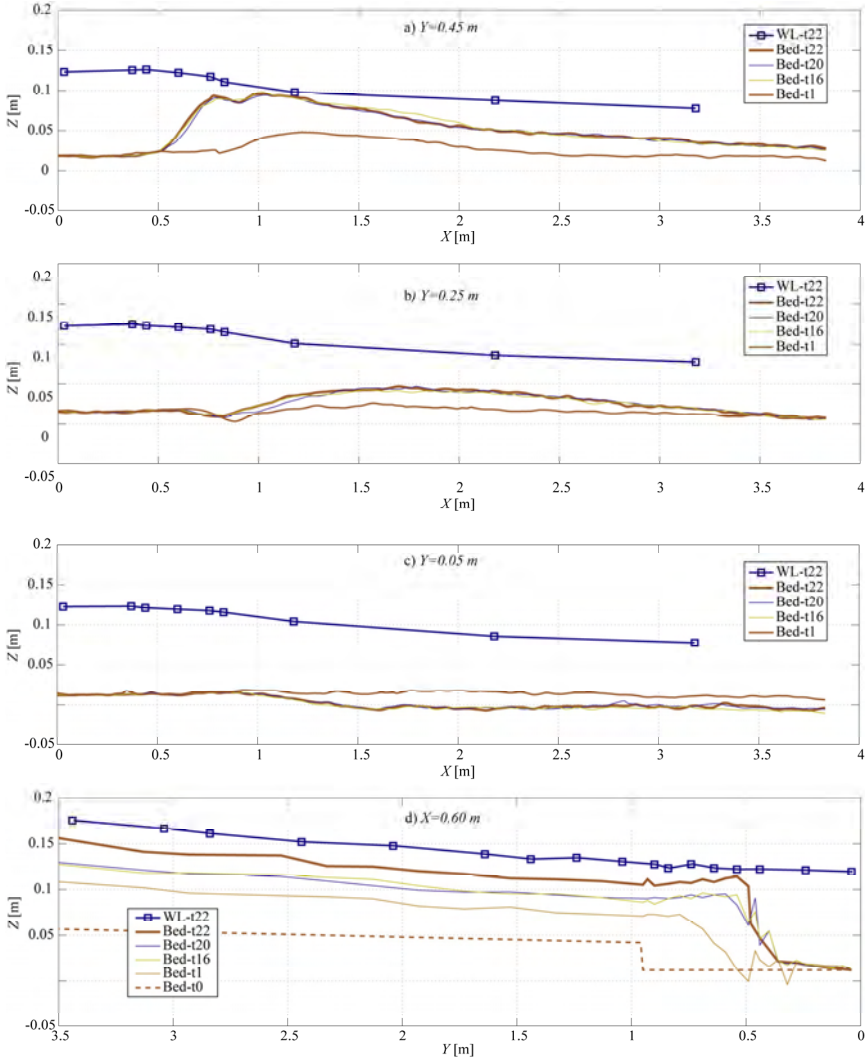

Figure 59: Longitudinal profiles along the main and post-confluence channels at Y=0.05 m (a), Y=0.25 m (b) and Y=0.45 m (c) and longitudinal profile along the axis of the tributary (X=0.60 m) (d) showing the bed elevations and water levels measured in different time-steps

G.3.2 Widened zone

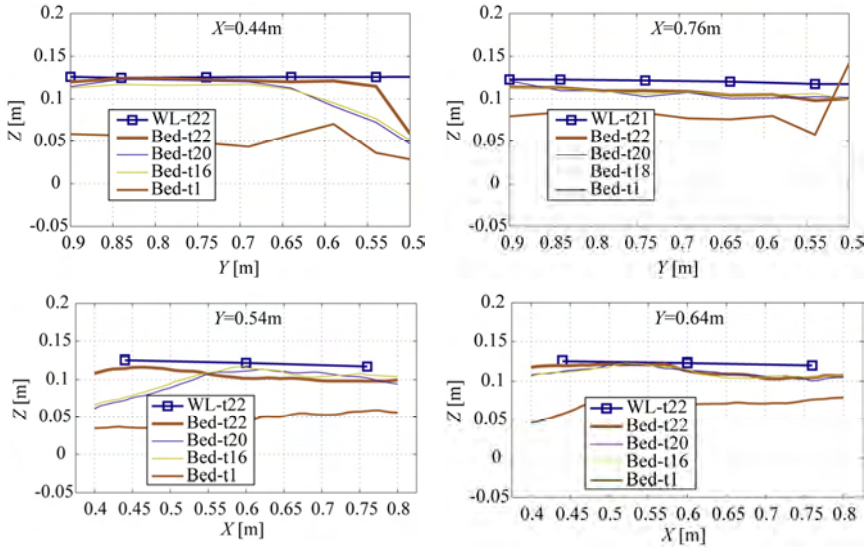

Figure 60: Cross-sections in the widened zone at: X=0.44 , X=0.76 m, Y=0.54 m and Y=0.64 m

G.4 Flow visualization of the main and post-confluence channels

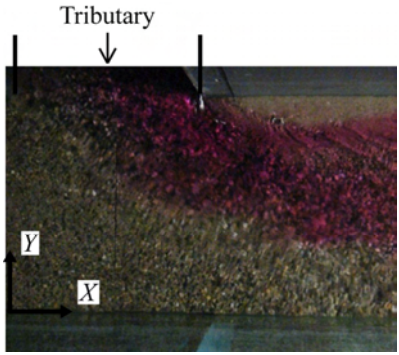

Figure 61: Upper view of the main and post-confluence channels with colour dye injected in the tributary

G.5 Pictures of the confluence zone

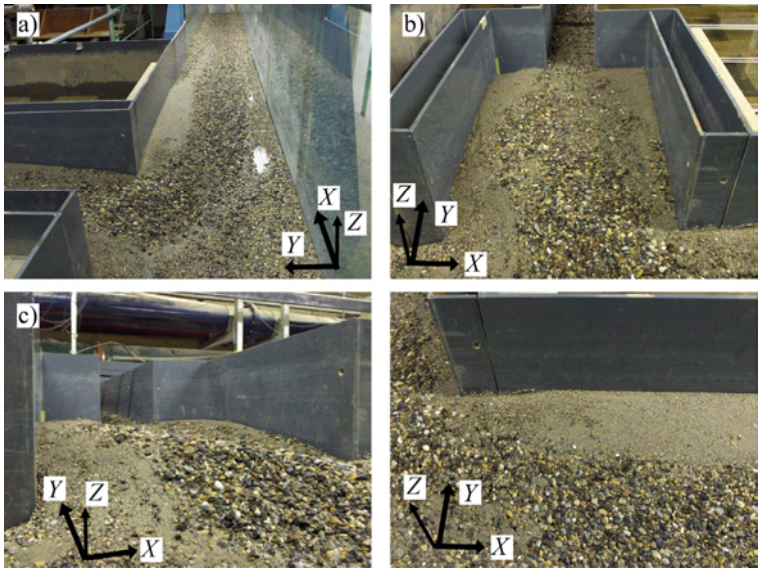

Figure 62: Pictures of the confluence zone. a) Upper view of the main and post-confluence channels. b) Upper view of the widened zone, c) View of the upstream avalanche faces and d) Upper view of the confluence zone

G.6 Grain size distributions

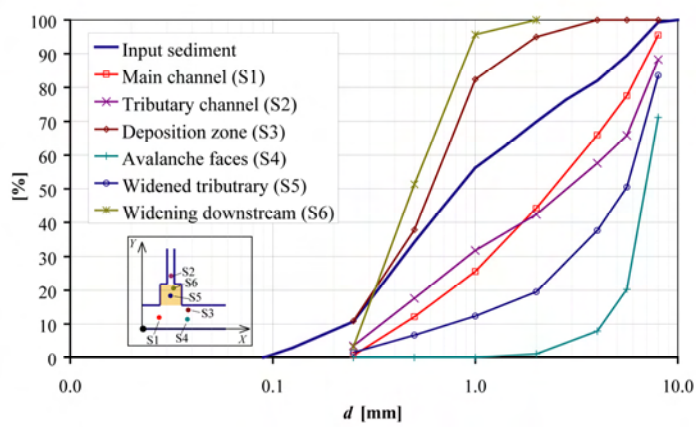

Figure 63: Sample locations and their respective grain size distributions

H. Intermediate - Medium

Appendix	Test	*Qr*	Windening B_w	Windening L_w	
A	*Low-Reference*	0.11	-	-	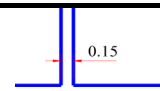
B	*Intermediate-Reference*	0.15			
C	*High-Reference*	0.20			
D	*Low-Small*	0.11	0.30	0.45	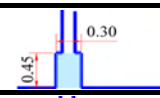
E	*Intermediate-Small*	0.15			
F	*High-Small*	0.20			
G	*Low-Medium*	0.11	0.45	0.45	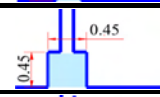
H	***Intermediate-Medium***	**0.15**			
I	*High-Medium*	0.20			
J	*Low-Large*	0.11	0.45	0.60	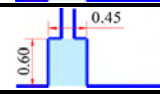
K	*Intermediate-Large*	0.15			
L	*High-Large*	0.20			

H.1 Summary

H.1.1 Initial hydraulic conditions

	Main (*m*)	Tributary (*t*)	*Qr* (Q_t/Q_m)
Q [l/s]	17.4	2.6	0.15
Qs [kg/m^3]	-	0.3	

H.1.2 Equilibrium flow depths

Main and post-confluence channels			
*X**Y* [m]	0.05	0.25	0.45
0	0.109	0.106	0.104
0.5	0.109	0.106	0.105
1.2	0.096	0.070	0.011
3	0.068	0.055	0.053
Tributary channel			
X [m]	Average [0.5<*Y*<0.90m] *		
0.6	0.02		

* only widened zone.

H.1.3 Main morphological features

Bed discordance	0.091	[m]
Maximum deposition	0.096	[m]
Volume > elevation 0.02 m	0.018	[m^3]

H.2 Time-evolution of the bed elevations

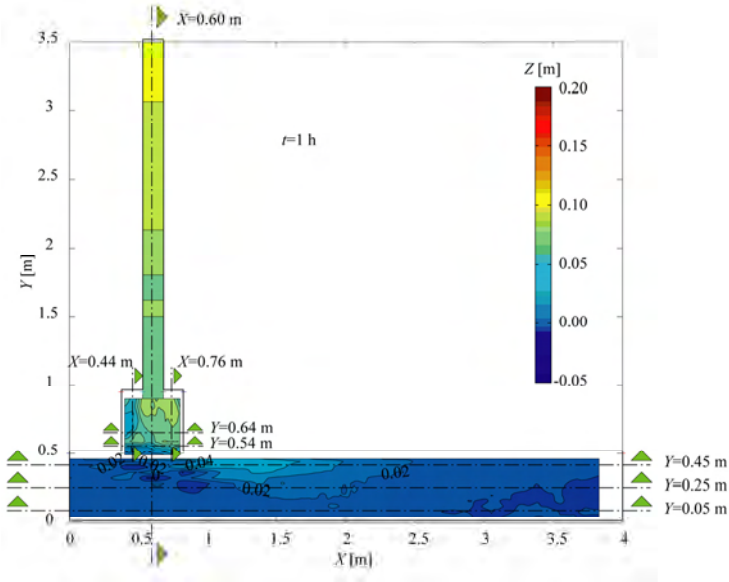

Figure 64: Bed elevations measured in the flume at t=1h

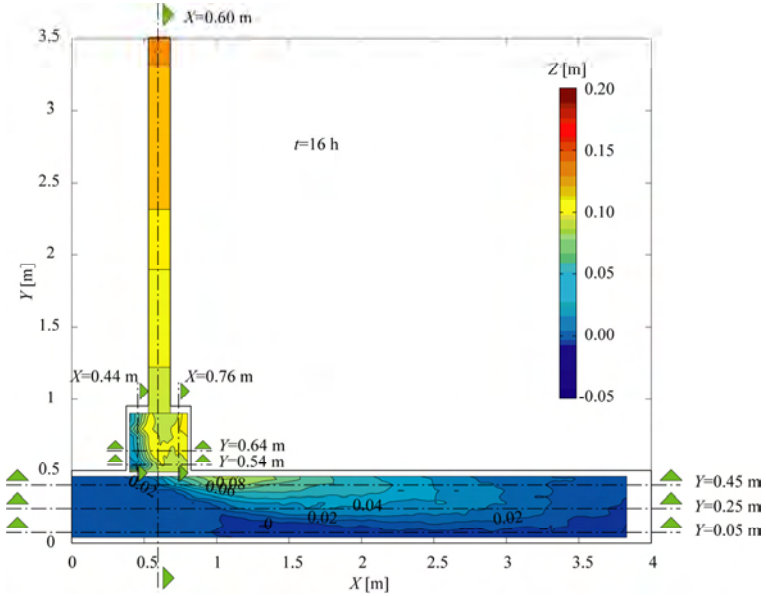

Figure 65: Bed elevations measured in the flume at t=16h

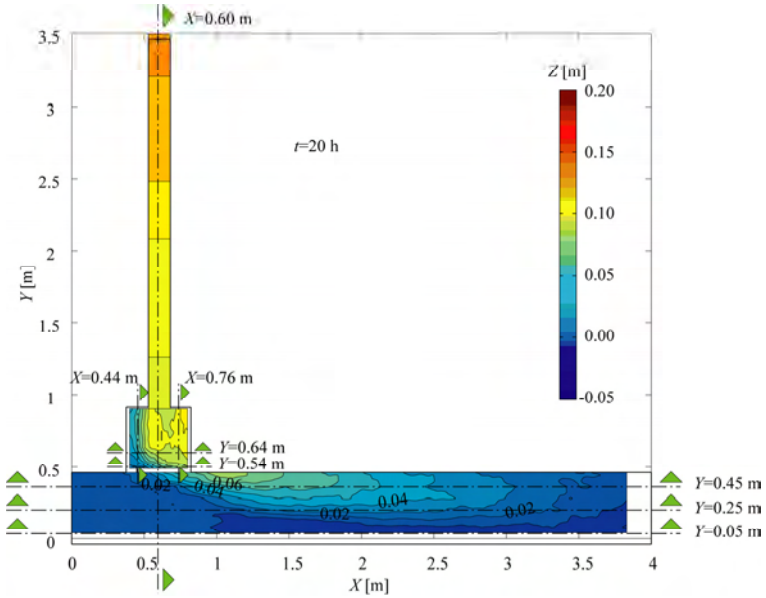

Figure 66: Bed elevations measured in the flume at t=20h

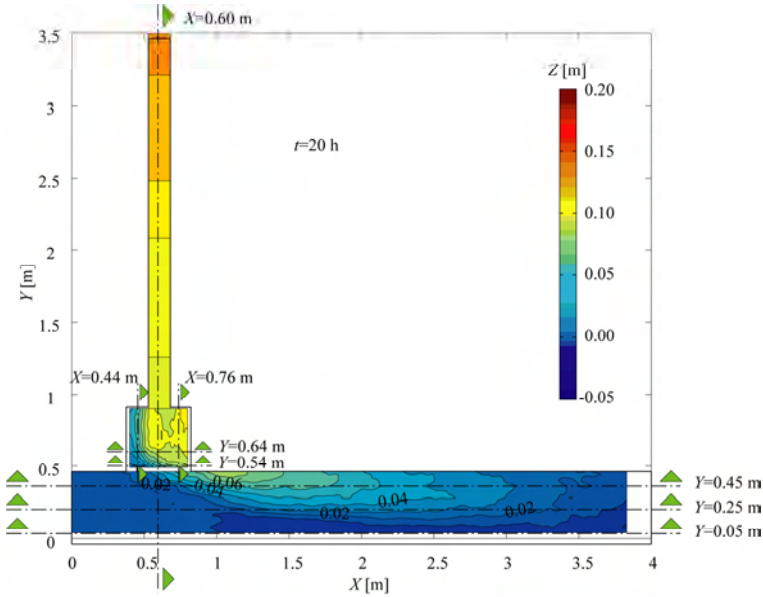

Figure 67: Bed elevations measured in the flume at t=22h

H.3 Longitudinal profiles and cross-sections

H.3.1 Main, post-confluence and tributary channels

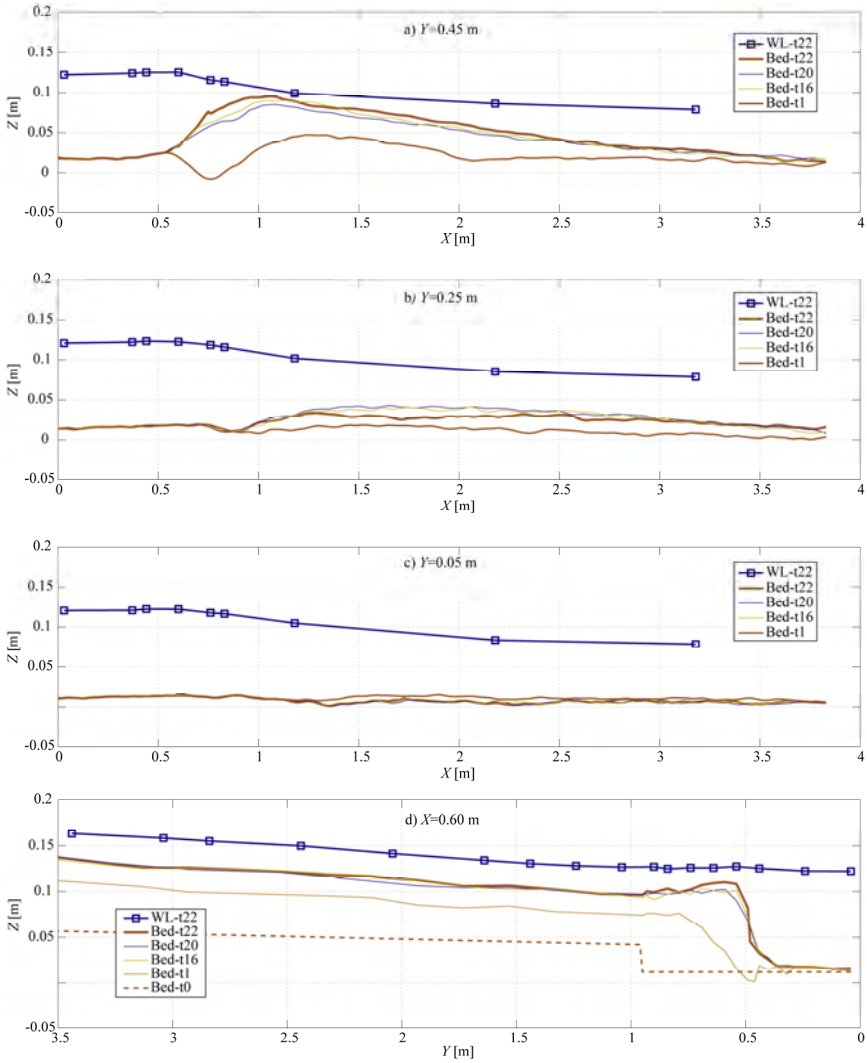

Figure 68: Longitudinal profiles along the main and post-confluence channels at Y=0.05 m (a), Y=0.25 m (b) and Y=0.45 m (c) and longitudinal profile along the axis of the tributary (X=0.60 m) (d) showing the bed elevations and water levels measured in different time-steps

H.3.2 Widened zone

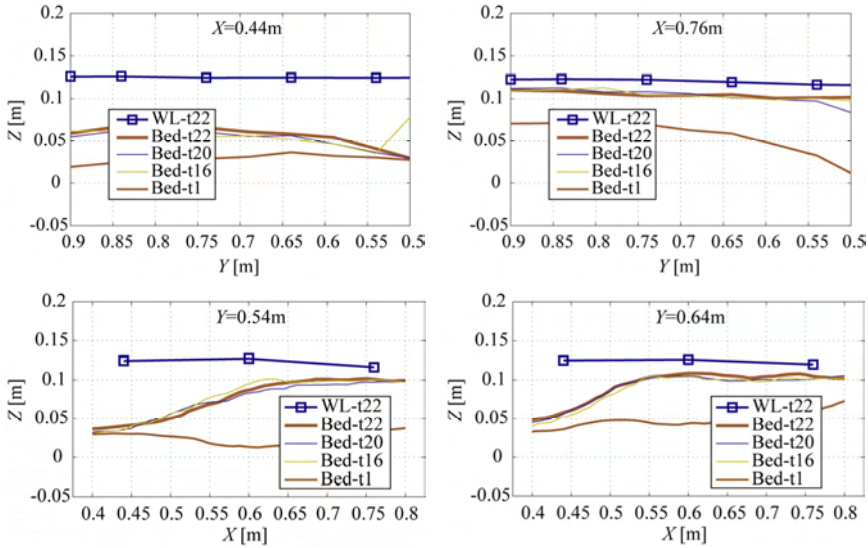

Figure 69: Cross-sections in the widened zone at: X=0.44 , X=0.76 m, Y=0.54 m and Y=0.64 m

H.4 Flow visualization of the main and post-confluence channels

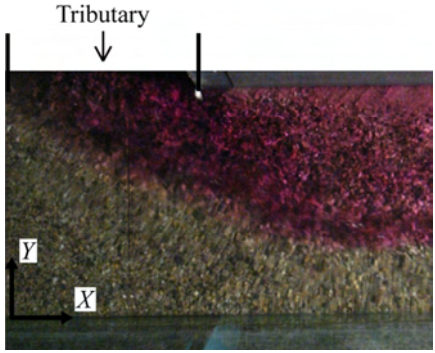

Figure 70: Upper view of the main and post-confluence channels with colour dye injected in the tributary

H.5 Pictures of the confluence zone

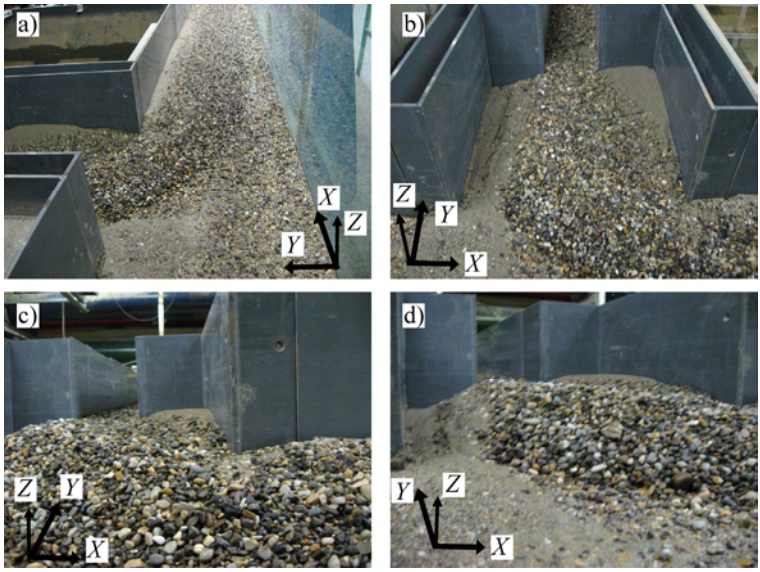

Figure 71: Pictures of the confluence zone. a) Upper view of the main and post-confluence channels. b) Upper view of the widened zone, c) View of the downstream corner of the confluence zone and d) View of the upstream avalanche faces

H.6 Grain size distributions

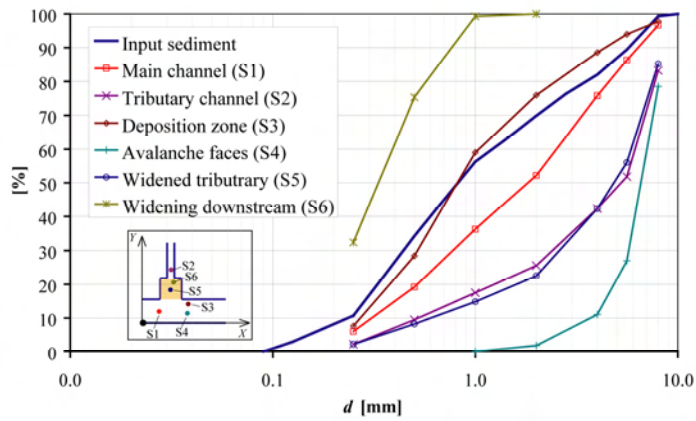

Figure 72: Sample locations and their respective grain size distributions

I. High-Medium

Appendix	Test	*Qr*	Windening B_w	Windening L_w	
A	*Low-Reference*	0.11	-	-	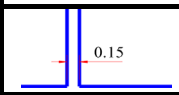
B	*Intermediate-Reference*	0.15			
C	*High-Reference*	0.20			
D	*Low-Small*	0.11	0.30	0.45	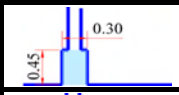
E	*Intermediate-Small*	0.15			
F	*High-Small*	0.20			
G	*Low-Medium*	0.11	0.45	0.45	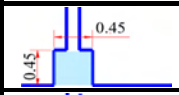
H	*Intermediate-Medium*	0.15			
I	***High-Medium***	**0.20**			
J	*Low-Large*	0.11	0.45	0.60	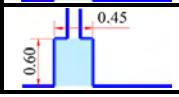
K	*Intermediate-Large*	0.15			
L	*High-Large*	0.20			

I.1 Summary

I.1.1 Initial hydraulic conditions

	Main (*m*)	Tributary (*t*)	*Qr* (Q_t/Q_m)
Q [l/s]	16.3	3.7	0.23
Qs [kg/m^3]	-	0.3	

I.1.2 Equilibrium flow depths

Main and post-confluence channels			
*X**Y* [m]	0.05	0.25	0.45
0	0.111	0.107	0.104
0.5	0.113	0.108	0.107
1.2	0.098	0.063	0.039
3	0.077	0.057	0.034
Tributary channel			
X [m]	Average [0.5<*Y*<0.90m] *		
0.6	0.044		

* only widened zone.

I.1.3 Main morphological features

Bed discordance	0.069	[m]
Maximum deposition	0.075	[m]
Volume > elevation 0.02 m	0.021	[m^3]

I.2 Time-evolution of the bed elevations

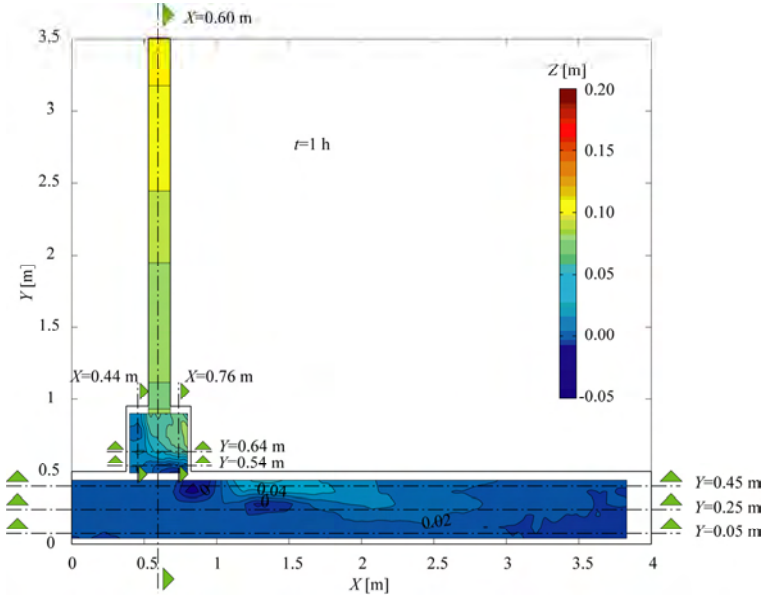

Figure 73: Bed elevations measured in the flume at t=1h

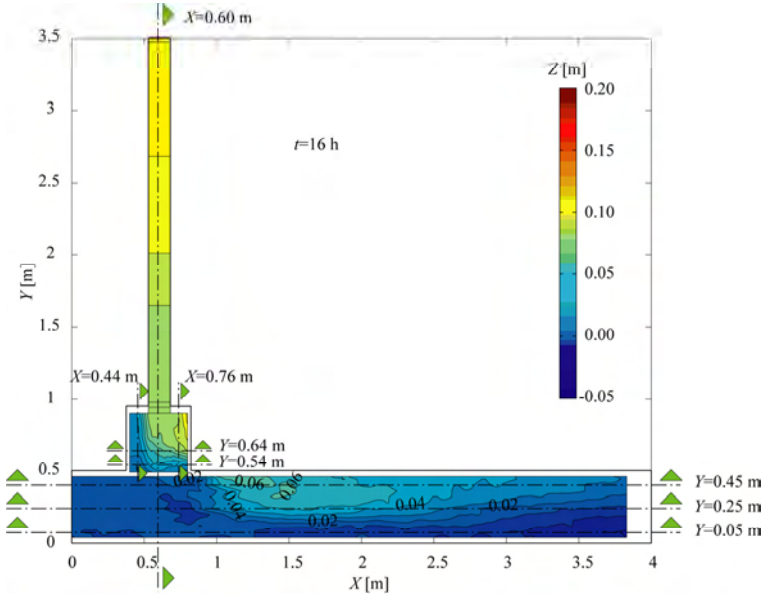

Figure 74: Bed elevations measured in the flume at t=16h

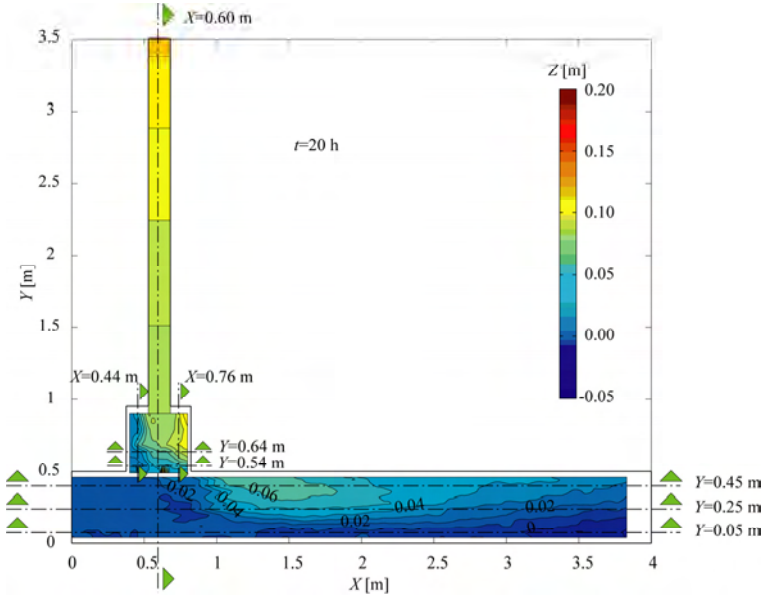

Figure 75: Bed elevations measured in the flume at t=20h

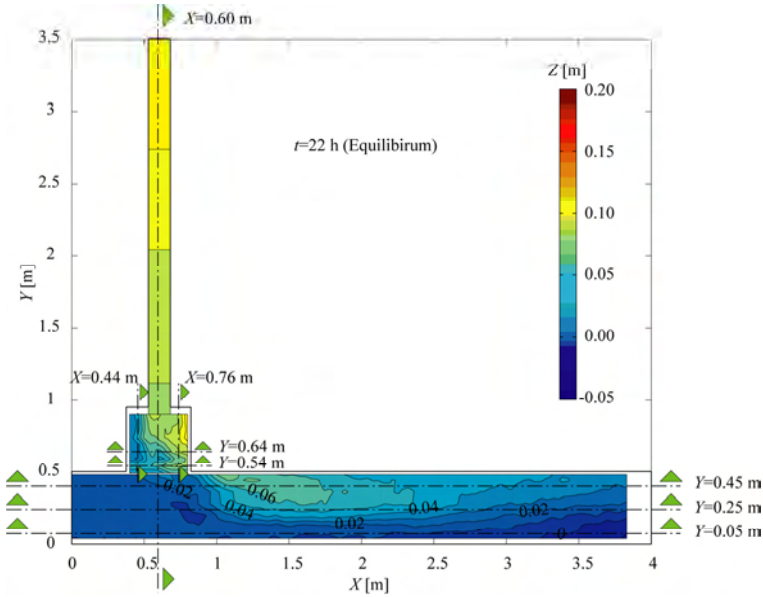

Figure 76: Bed elevations measured in the flume at t=22h

I.3 Longitudinal profiles and cross-sections

I.3.1 Main, post-confluence and tributary channels

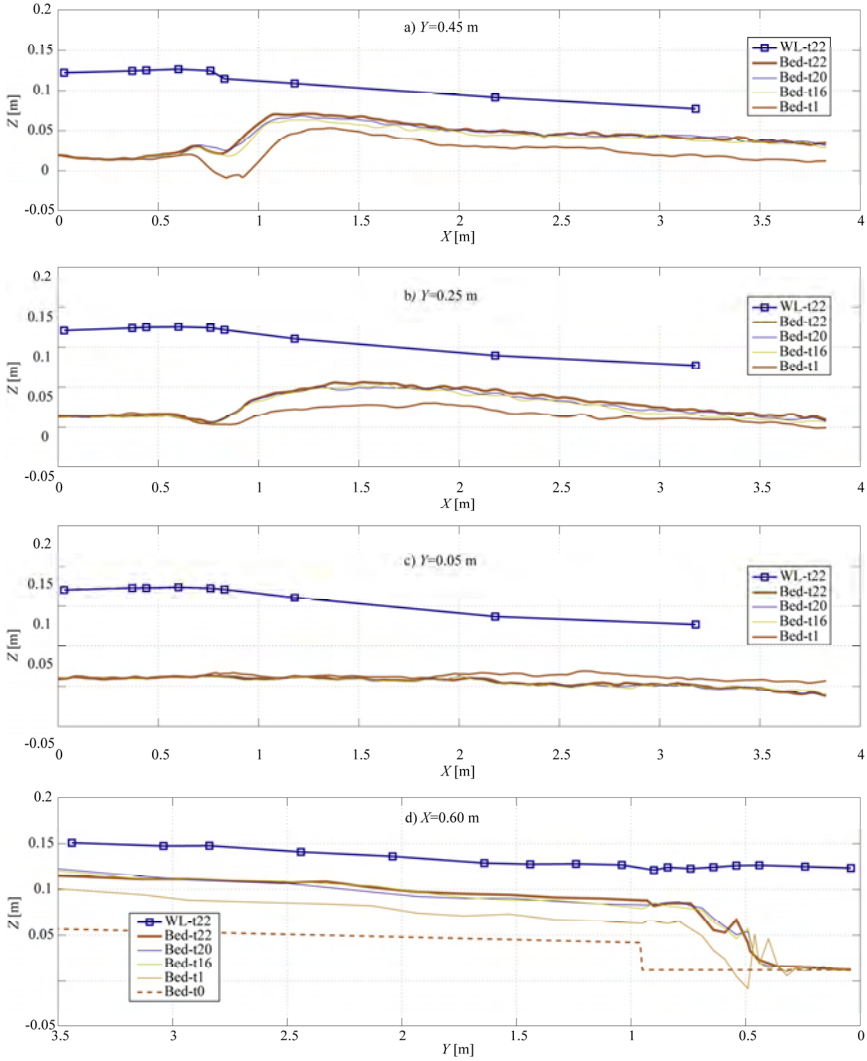

Figure 77: Longitudinal profiles along the main and post-confluence channels at Y=0.05 m (a), Y=0.25 m (b) and Y=0.45 m (c) and longitudinal profile along the axis of the tributary (X=0.60 m) (d) showing the bed elevations and water levels measured in different time-steps

I.3.2 Widened zone

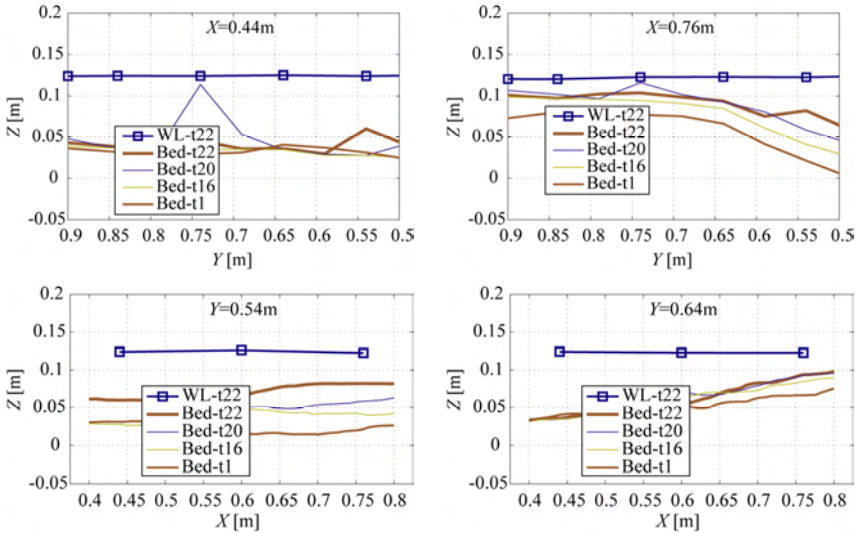

Figure 78: Cross-sections in the widened zone at: X=0.44 , X=0.76 m, Y=0.54 m and Y=0.64 m

I.4 Flow visualization of the main and post-confluence channels

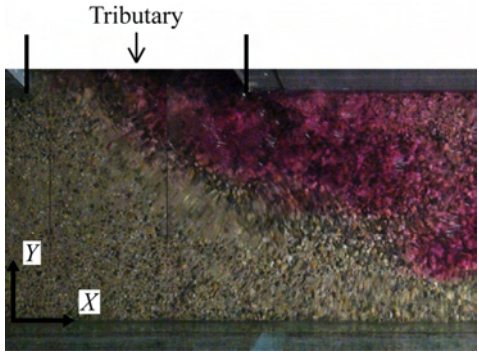

Figure 79: Upper view of the main and post-confluence channels with colour dye injected in the tributary

I.5 Pictures of the confluence zone

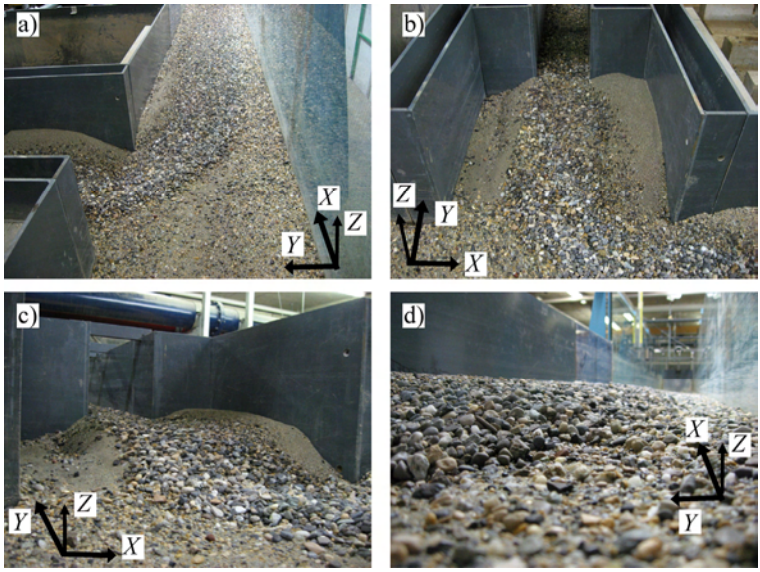

Figure 80: Pictures of the confluence zone. a) Upper view of the main and post-confluence channels. b) Upper view of the widened zone, c) Upstream view of the avalanche faces and d) Downstream view of the post-confluence channel

I.6 Grain size distributions

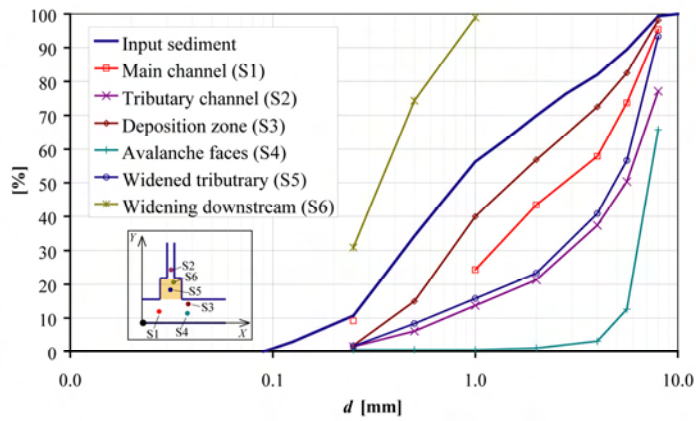

Figure 81: Sample locations and their respective grain size distributions

J. Low-Large

			Windening		
Appendix	**Test**	***Qr***	B_w	L_w	
A	*Low-Reference*	0.11	-	-	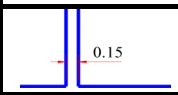
B	*Intermediate-Reference*	0.15			
C	*High-Reference*	0.20			
D	*Low-Small*	0.11	0.30	0.45	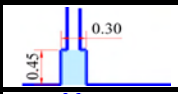
E	*Intermediate-Small*	0.15			
F	*High-Small*	0.20			
G	*Low-Medium*	0.11	0.45	0.45	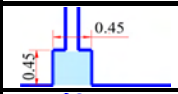
H	*Intermediate-Medium*	0.15			
I	*High-Medium*	0.20			
J	***Low-Large***	**0.11**	0.45	0.60	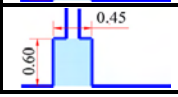
K	*Intermediate-Large*	0.15			
L	*High-Large*	0.20			

J.1 Summary

J.1.1 Initial hydraulic conditions

	Main (*m*)	Tributary (*t*)	*Qr* (Q_t/Q_m)
Q [l/s]	18	2	0.11
Qs [kg/m^3]	-	0.3	

J.1.2 Equilibrium flow depths

Main and post-confluence channels			
*X**Y* [m]	0.05	0.25	0.45
0	0.109	0.105	0.108
0.5	0.105	0.102	0.092
1.2	0.100	0.075	0.005
3	0.079	0.061	0.035
Tributary channel			
X [m]	Average [0.5<*Y*<1.10m] *		
0.6	0.005		

* only widened zone.

J.1.3 Main morphological features

Bed discordance	0.097	[m]
Maximum deposition	0.094	[m]
Volume > elevation 0.02 m	0.020	[m^3]

J.2 Time-evolution of the bed elevations

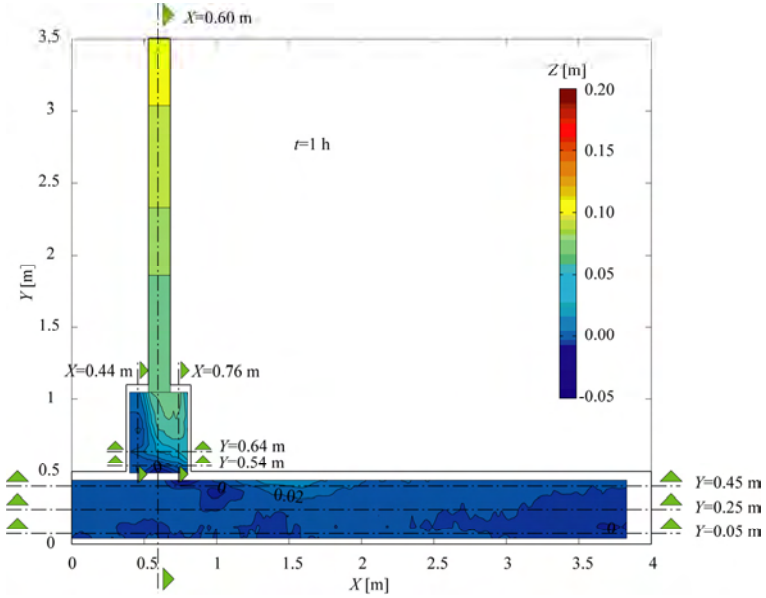

Figure 82: Bed elevations measured in the flume at t=1h

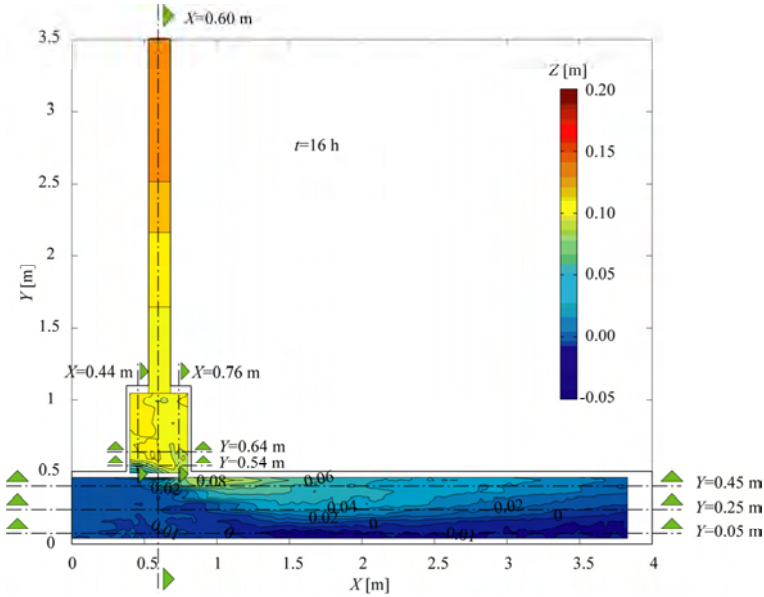

Figure 83: Bed elevations measured in the flume at t=16h

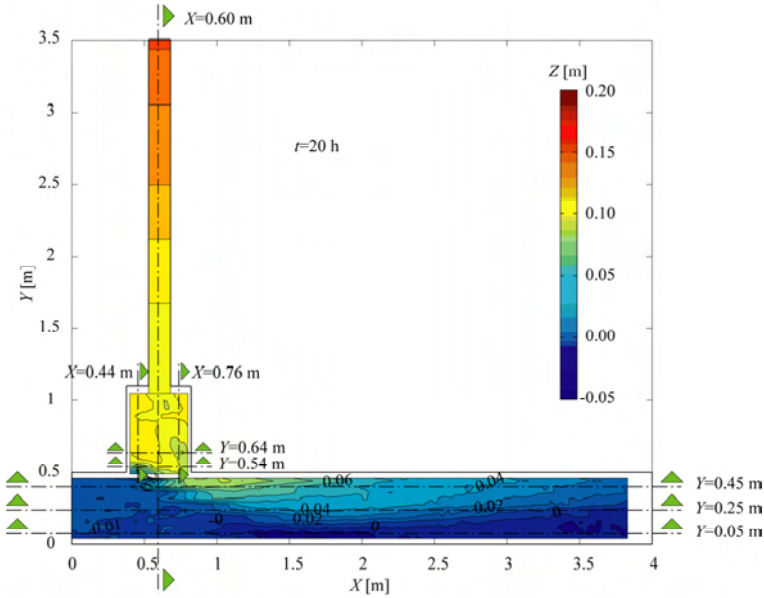

Figure 84: Bed elevations measured in the flume at t=20h

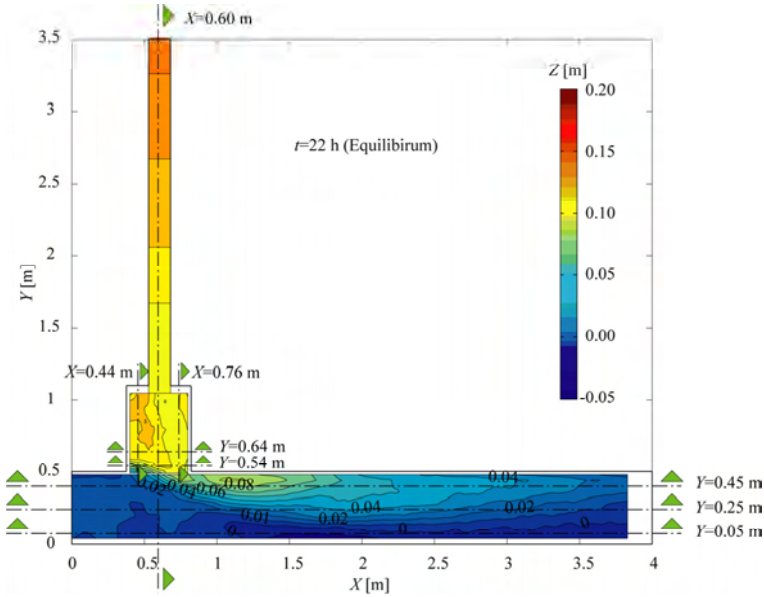

Figure 85: Bed elevations measured in the flume at t=22h

J.3 Longitudinal profiles and cross-sections

J.3.1 Main, post-confluence and tributary channels

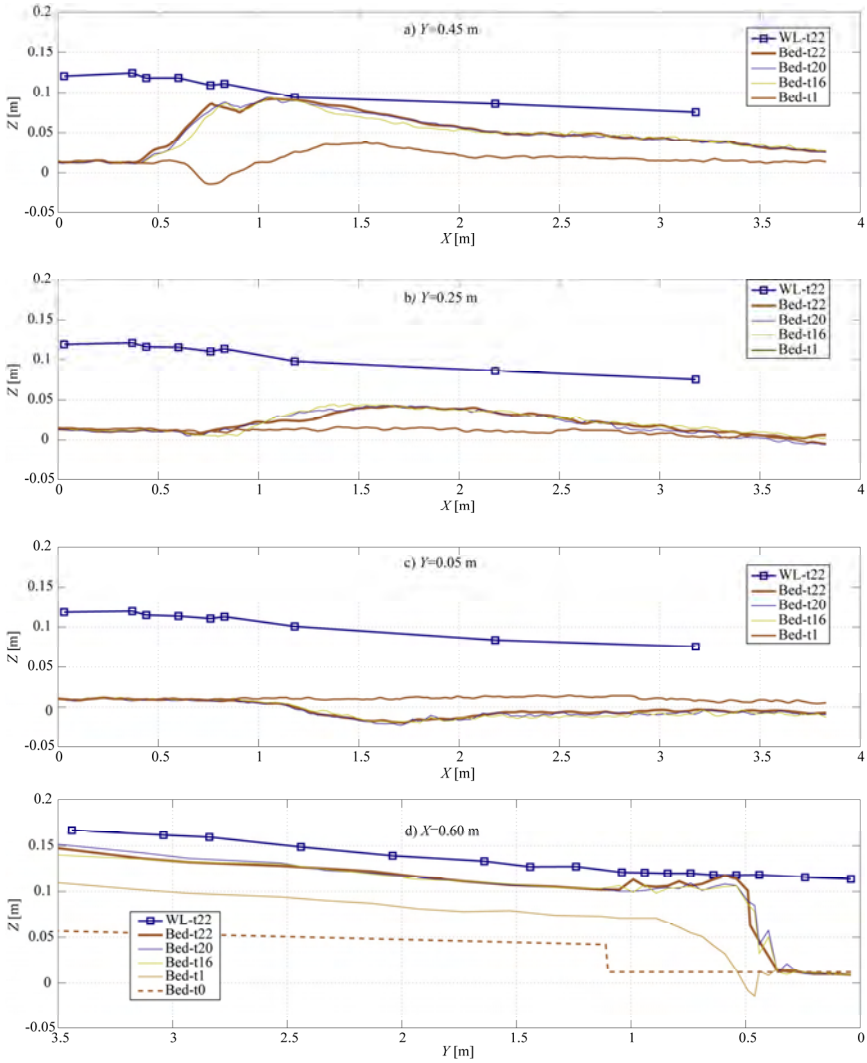

Figure 86: Longitudinal profiles along the main and post-confluence channels at Y=0.05 m (a), Y=0.25 m (b) and Y=0.45 m (c) and longitudinal profile along the axis of the tributary (X=0.60 m) (d) showing the bed elevations and water levels measured in different time-steps

J.3.2 Widened zone

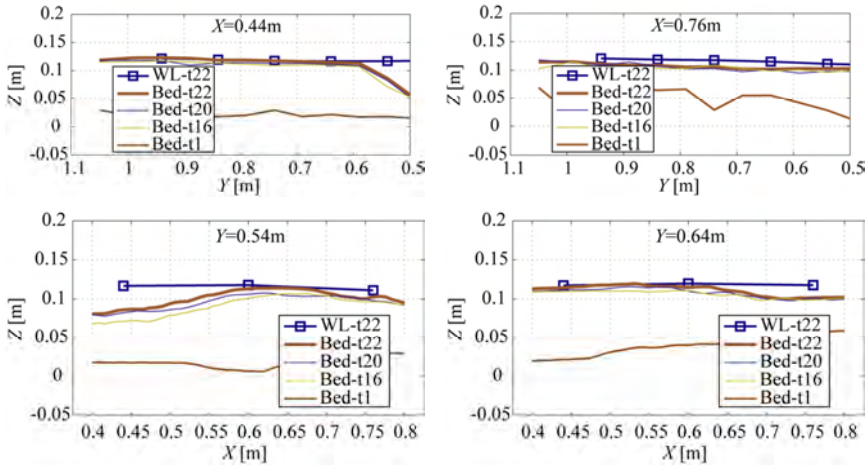

Figure 87: Cross-sections in the widened zone at: X=0.44 , X=0.76 m, Y=0.54 m and Y=0.64 m

J.4 Flow visualization of the main and post-confluence channels

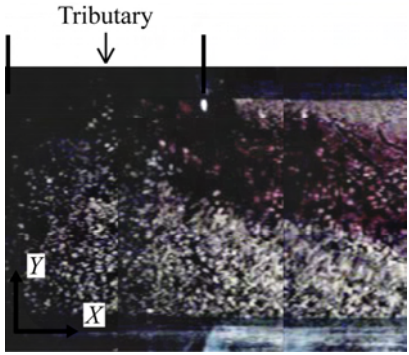

Figure 88: Upper view of the main and post-confluence channels with colour dye injected in the tributary

J.5 Pictures of the confluence zone

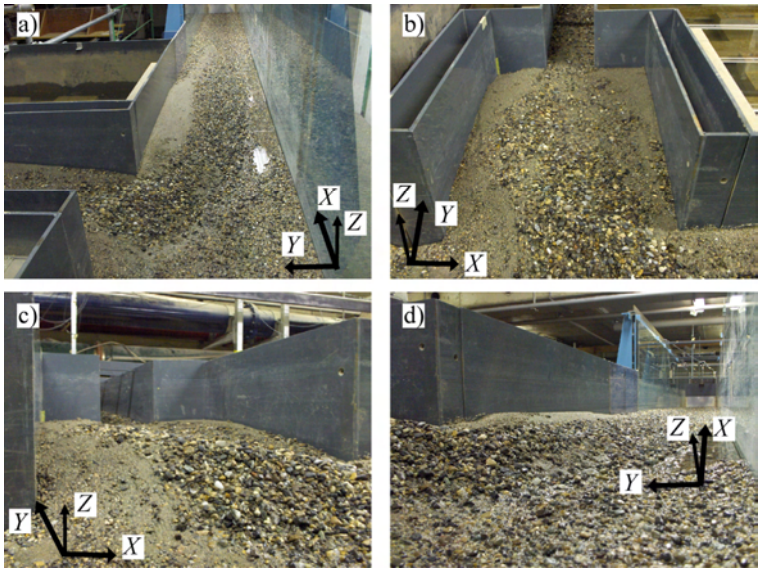

Figure 89: Pictures of the confluence zone. a) Upper view of the main and post-confluence channels. b) Upper view of the widened zone, c) Upstream view of the avalanche faces and d) Downstream view of the post-confluence channel

J.6 Grain size distributions

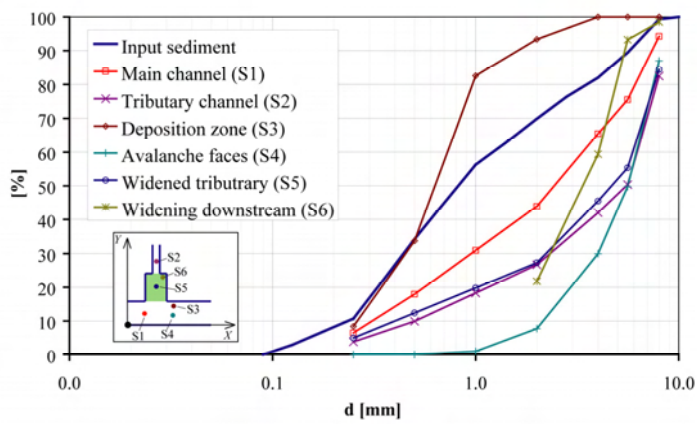

Figure 90: Sample locations and their respective grain size distributions

K. Intermediate-Large

Appendix	Test	*Qr*	Windening		
			B_w	L_w	
A	*Low-Reference*	0.11	-	-	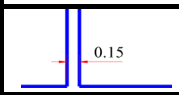
B	*Intermediate-Reference*	0.15			
C	*High-Reference*	0.20			
D	*Low-Small*	0.11	0.30	0.45	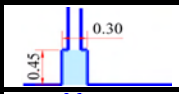
E	*Intermediate-Small*	0.15			
F	*High-Small*	0.20			
G	*Low-Medium*	0.11	0.45	0.45	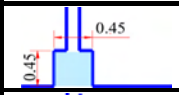
H	*Intermediate-Medium*	0.15			
I	*High-Medium*	0.20			
J	*Low-Large*	0.11	0.45	0.60	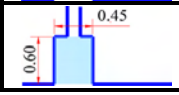
K	***Intermediate-Large***	**0.15**			
L	*High-Large*	0.20			

K.1 Summary

K.1.1 Initial hydraulic conditions

	Main (*m*)	Tributary (*t*)	*Qr* (Q_t/Q_m)
Q [l/s]	17.4	2.6	0.15
Qs [kg/m^3]	-	0.3	

K.1.2 Equilibrium flow depths

Main and post-confluence channels			
*X**Y* [m]	0.05	0.25	0.45
0	0.110	0.110	0.109
0.5	0.110	0.109	0.105
1.2	0.108	0.063	0.007
3	0.079	0.058	0.038
Tributary channel			
X [m]	Average [0.5<*Y*<1.10m] *		
0.6	0.0063		

* only widened zone.

K.1.3 Main morphological features

Bed discordance	0.100	[m]
Maximum deposition	0.110	[m]
Volume > elevation 0.02 m	0.024	[m^3]

K.2 Time-evolution of the bed elevations

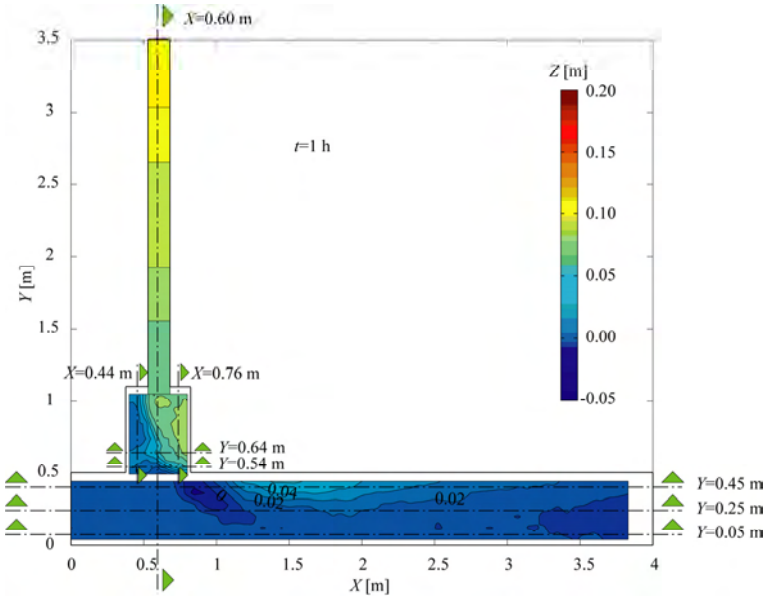

Figure 91: Bed elevations measured in the flume at t=1h

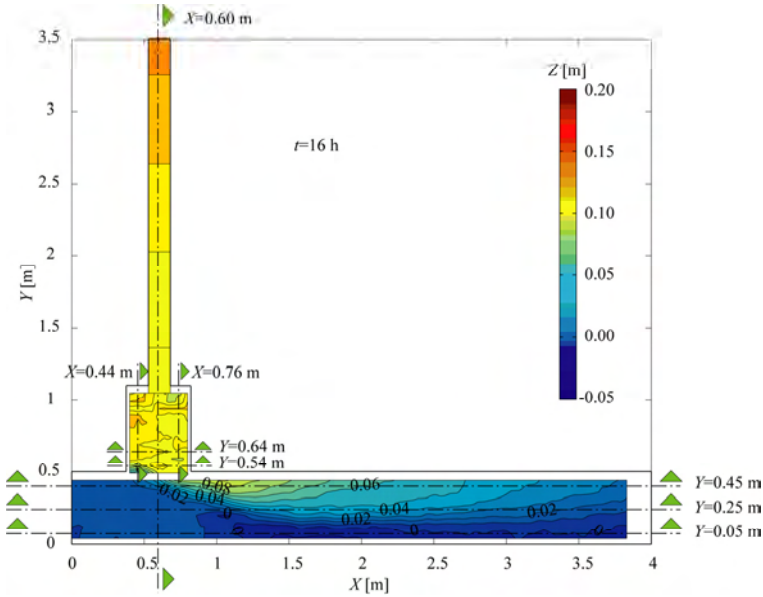

Figure 92: Bed elevations measured in the flume at t=16h

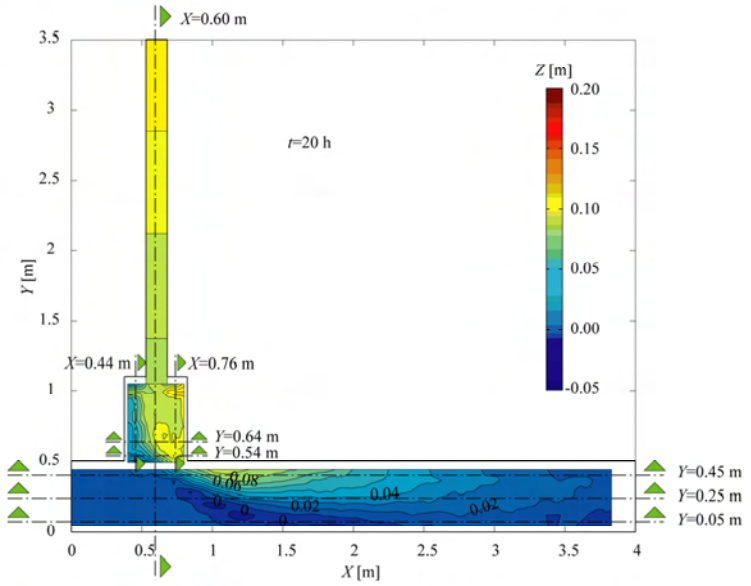

Figure 93: Bed elevations measured in the flume at t=20h

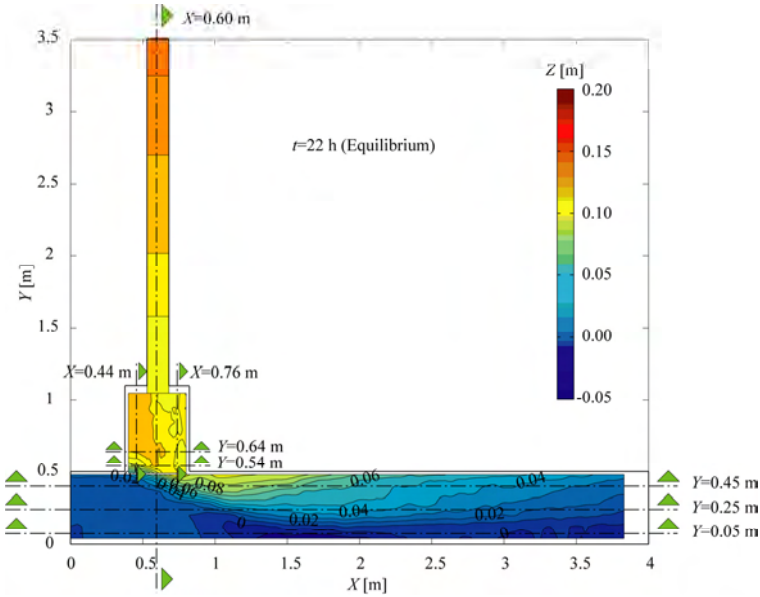

Figure 94: Bed elevations measured in the flume at t=22h

K.3 Longitudinal profiles and cross-sections

K.3.1 Main, post-confluence and tributary channels

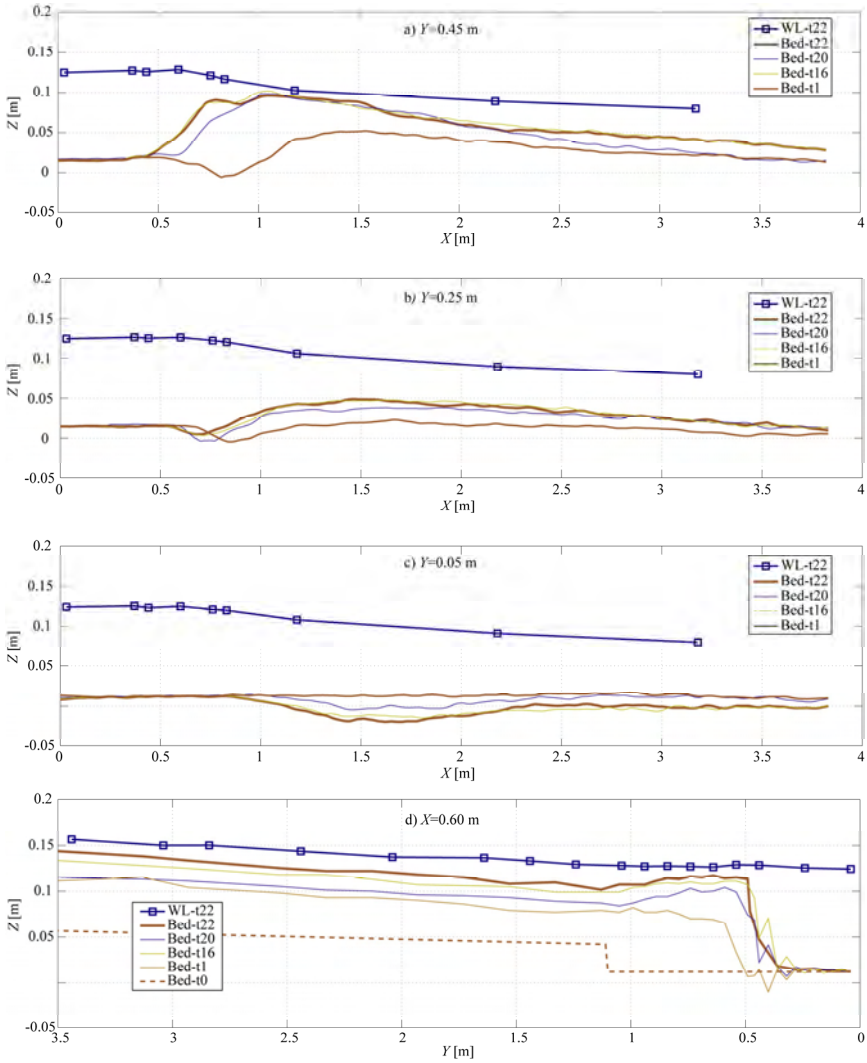

Figure 95: Longitudinal profiles along the main and post-confluence channels at Y=0.05 m (a), Y=0.25 m (b) and Y=0.45 m (c) and longitudinal profile along the axis of the tributary (X=0.60 m) (d) showing the bed elevations and water levels measured in different time-steps

K.3.2 Widened zone

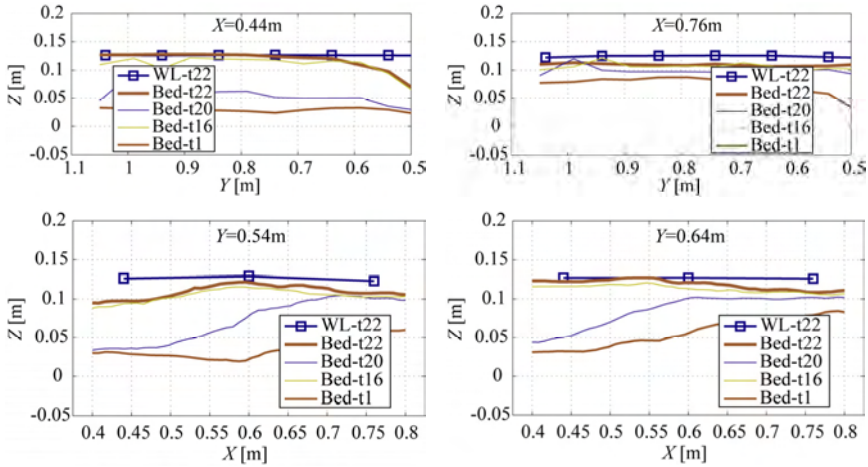

Figure 96: Cross-sections in the widened zone at: X=0.44 , X=0.76 m, Y=0.54 m and Y=0.64 m

K.4 Flow visualization of the main and post-confluence channels

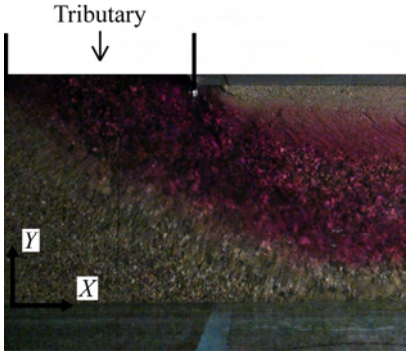

Figure 97: Upper view of the main and post-confluence channels with colour dye injected in the tributary

K.5 Pictures of the confluence zone

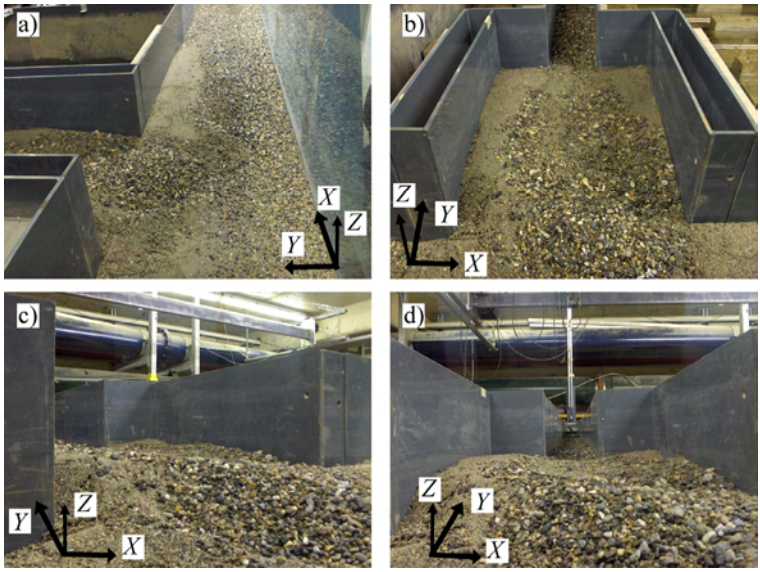

Figure 98: Pictures of the confluence zone. a) Upper view of the main and post-confluence channels. b) Upper view of the widened zone, c) Upstream view of the avalanche faces and d) Upstream view of the tributary

K.6 Grain size distributions

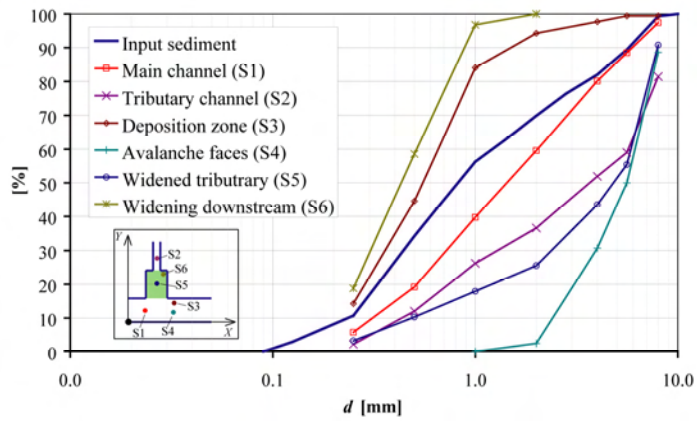

Figure 99: Sample locations and their respective grain size distributions

L. High-Large

			Windening		
Appendix	**Test**	***Qr***	B_w	L_w	
A	*Low-Reference*	0.11	-	-	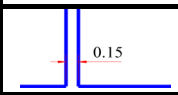
B	*Intermediate-Reference*	0.15			
C	*High-Reference*	0.20			
D	*Low-Small*	0.11	0.30	0.45	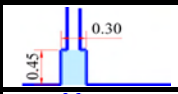
E	*Intermediate-Small*	0.15			
F	*High-Small*	0.20			
G	*Low-Medium*	0.11	0.45	0.45	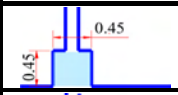
H	*Intermediate-Medium*	0.15			
I	*High-Medium*	0.20			
J	*Low-Large*	0.11	0.45	0.60	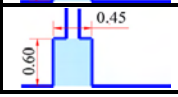
K	*Intermediate-Large*	0.15			
L	***High-Large***	**0.20**			

L.1 Summary

L.1.1 Initial hydraulic conditions

	Main (*m*)	Tributary (*t*)	*Qr* (Q_t/Q_m)
Q [l/s]	16.3	3.7	0.23
Qs [kg/m^3]	-	0.3	

L.1.2 Equilibrium flow depths

Main and post-confluence channels			
*X**Y* [m]	0.05	0.25	0.45
0	0.110	0.108	0.106
0.5	0.109	0.107	0.103
1.2	0.107	0.066	0.010
3	0.057	0.063	0.055
Tributary channel			
X [m]	Average [0.5<*Y*<1.10m] *		
0.6	0.028		

* only widened zone.

L.1.3 Main morphological features

Bed discordance	0.089	[m]
Maximum deposition	0.100	[m]
Volume > elevation 0.02 m	0.022	[m^3]

L.2 Time-evolution of the bed elevations

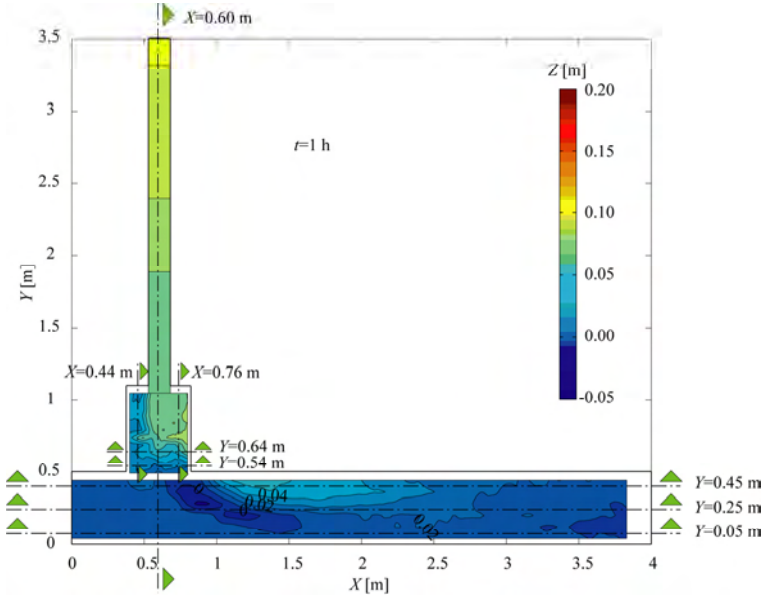

Figure 100: Bed elevations measured in the flume at t=1h

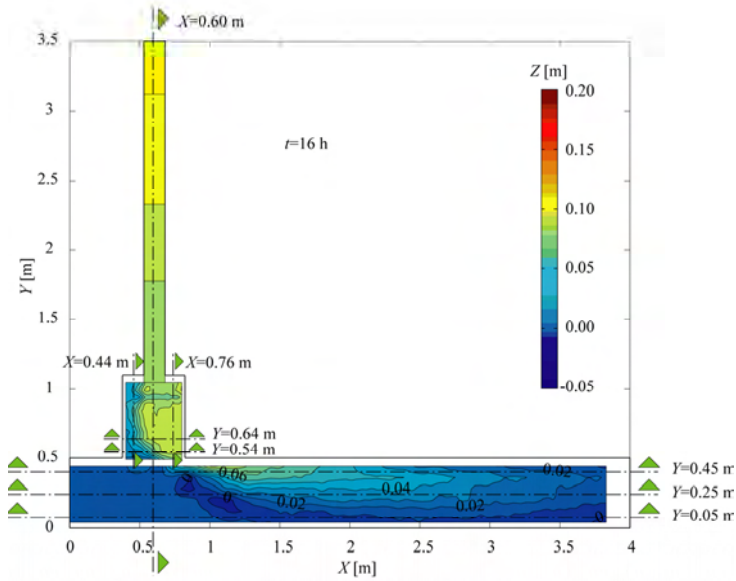

Figure 101: Bed elevations measured in the flume at t=16h

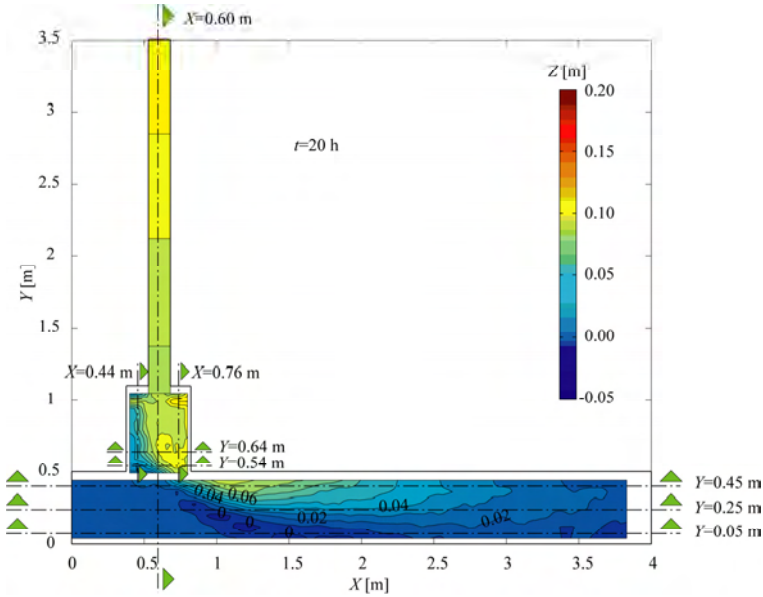

Figure 102: Bed elevations measured in the flume at t=20h

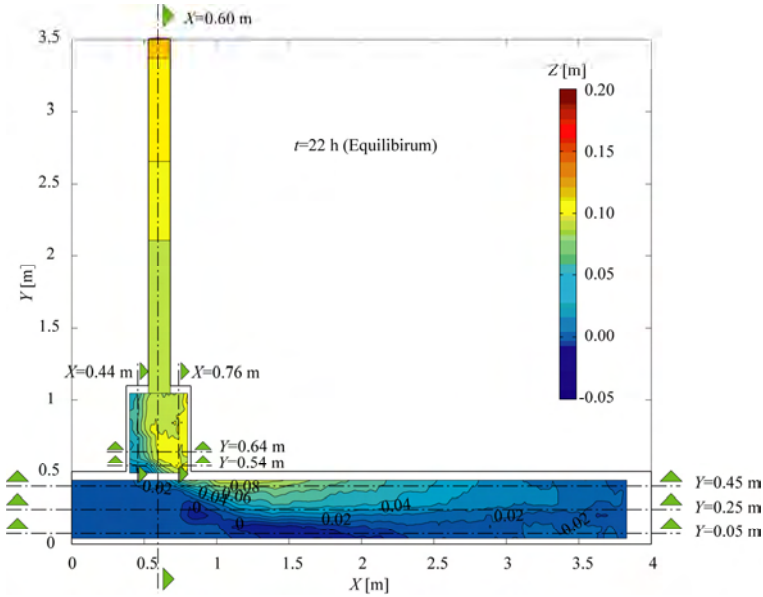

Figure 103: Bed elevations measured in the flume at t=22h

L.3 Longitudinal profiles and cross-sections

L.3.1 Main, post-confluence and tributary channels

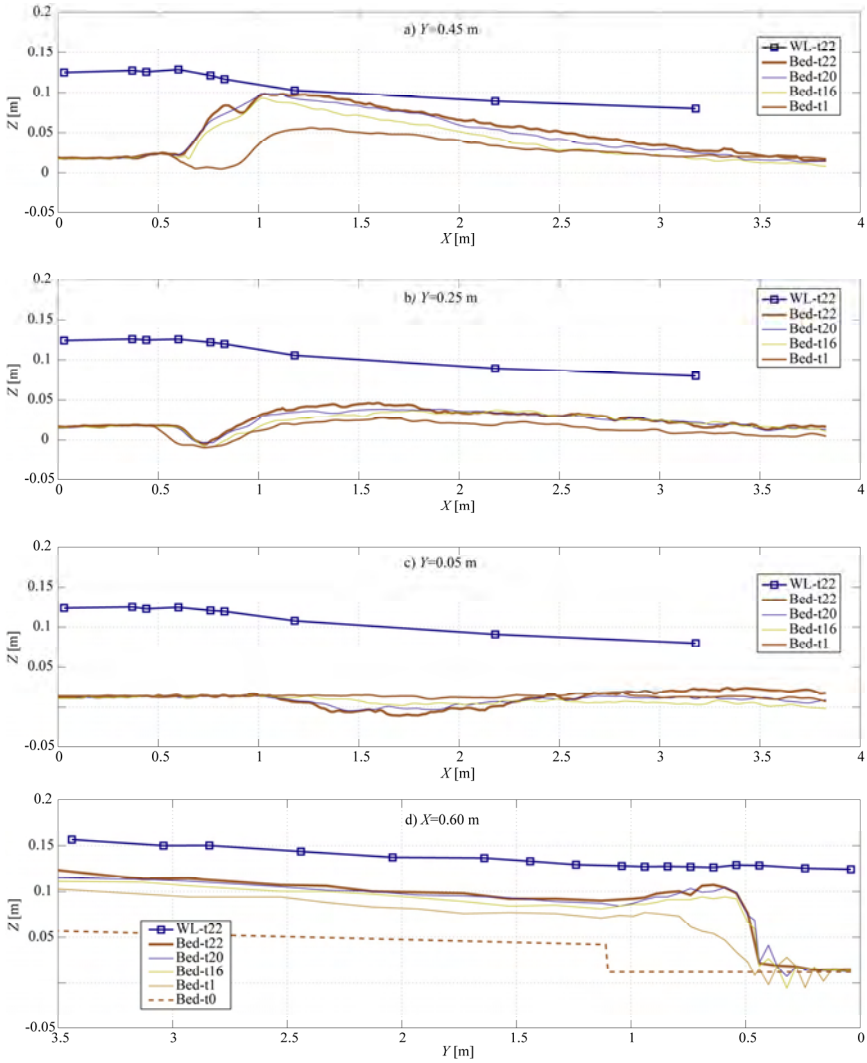

Figure 104: Longitudinal profiles along the main and post-confluence channels at Y=0.05 m (a), Y=0.25 m (b) and Y=0.45 m (c) and longitudinal profile along the axis of the tributary (X=0.60 m) (d) showing the bed elevations and water levels measured in different time-steps;

L.3.2 Widened zone

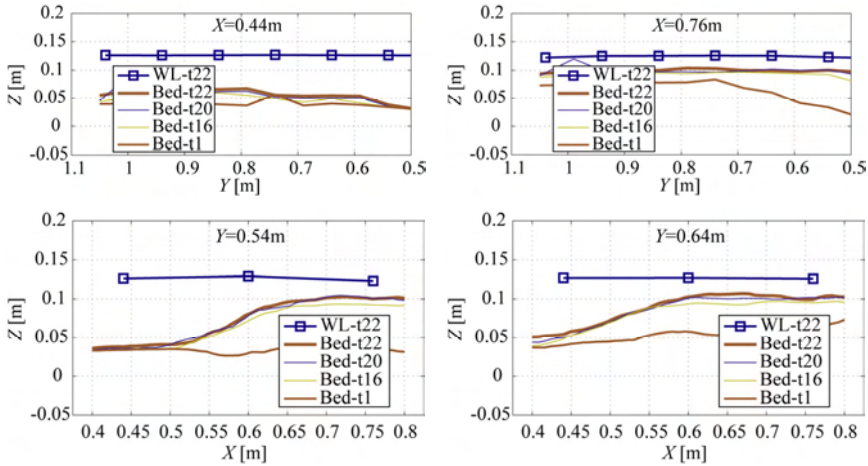

Figure 105: Cross-sections in the widened zone at: X=0.44 , X=0.76 m, Y=0.54 m and Y=0.64 m

L.4 Flow visualization of the main and post-confluence channels

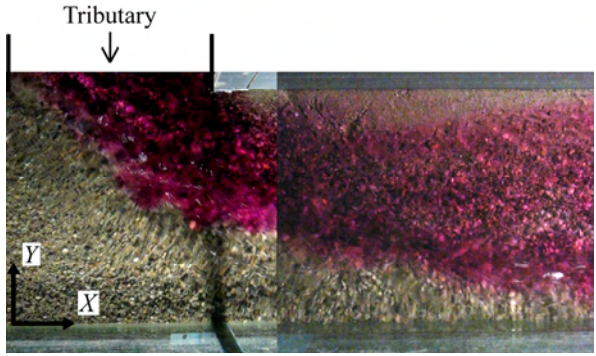

Figure 106: Upper view of the main and post-confluence channels with colour dye injected in the tributary

L.5 Pictures of the confluence zone

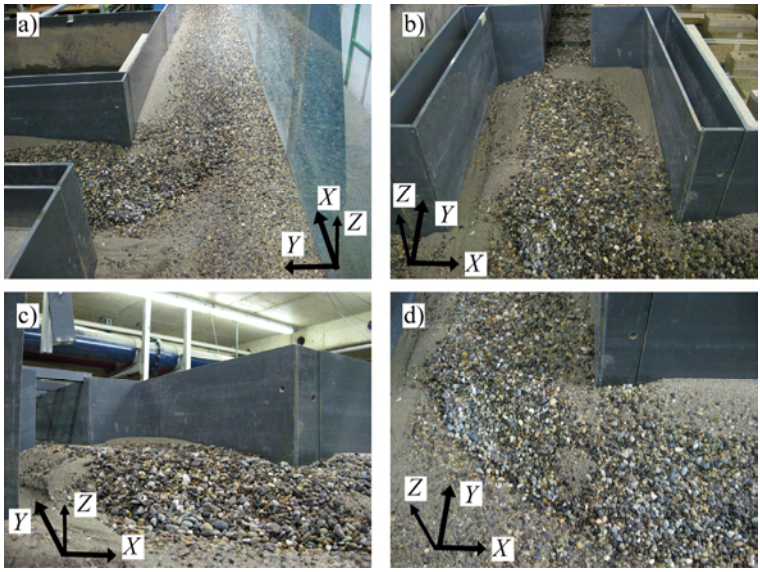

Figure 107: Pictures of the confluence zone. a) Upper view of the main and post-confluence channels. b) Upper view of the widened zone, c) Upstream view of the avalanche faces and d) Upper view of the confluence zone

L.6 Grain size distributions

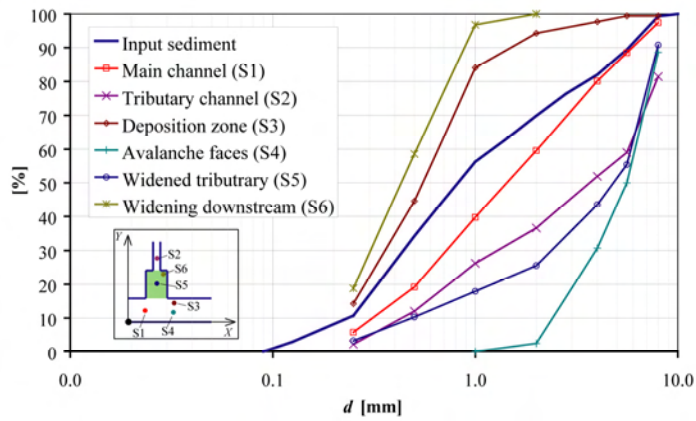

Figure 108: Sample locations and their respective grain size distributions

Communications du Laboratoire de Constructions Hydrauliques ISSN 1661-1179
Ecole Polytechnique Fédérale de Lausanne
Editeur: Prof. Dr A. Schleiss

ISSN 1661-1179

Prof. Dr A. Schleiss
Laboratoire de constructions hydrauliques - LCH
EPFL, Bât. GC, Station 18, CH-1015 Lausanne
http://lch.epfl.ch
e-mail: secretariat.lch@epfl.ch